

Metabolic and microenvironmental strategies to accelerate hematopoietic recovery post-aplasia

Thèse N° 9395

Présentée le 23 mai 2019

à la Faculté des sciences de la vie

Groupe Naveiras

Programme doctoral en biotechnologie et génie biologique

pour l'obtention du grade de Docteur ès Sciences

par

Vasco LEDEBUR DE ANTAS DE CAMPOS

Acceptée sur proposition du jury

Prof. A. C. Oates, président du jury

Prof. O. M. Naveiras Torres-Quiroga, directrice de thèse

Prof. T. Lapidot, rapporteur

Prof. L. Fajas, rapporteur

Prof. E. Oricchio, rapporteuse

2019

Acknowledgements

First and foremost, I would like to thank my supervisor, Prof. Olaia Naveiras, who allowed me to perform this work in her lab. Olaia, your continuous guidance and your ‘never-ending well-of-knowledge’ always helped me keep my motivation high and my eyes open to the bigger picture.

I would also like to thank the other hematopoietic experts, that came along with Olaia, namely Dr. Mukul Girotra and Dr. Nicola Vannini, who were essential in maintaining a relaxed atmosphere, while allowing me to perceive work and life from a different perspective. Thank you very much Nicola, for allowing me to work on the enormous NR-project, which I am confident will bring benefits to patients in the close future. All the *in vivo* experiments would also not be possible without the extensive help by Dr. Shanti Rojas-Sutterlin and Josefine Tratwal. Shanti, you are also a great well-of-knowledge and your patience always helpful in difficult decisions. Josefine, thanks for hanging in there with me throughout these years, and for all those days plating CFUs at 11pm. You are the next one, and I am sure you’ll do a great job! I would also like to thank Dr. Benoit von der Weid and all the students that I had the pleasure to work with, namely Jasmina Rubattel, Theophile Bian, Samuele Mercan and Michael Silverstein. Michael came all the way from America to work with me on a very ambitious engineering project, which resulted in an inter-cultural exchange and strong friendship – thank you for all the discussions! My acknowledgements also go to the students working with me in the final stages of my thesis: Manon Subilia, Ibrahim Bekri and Aaron Petruzzella – thanks for all your help! Also, Frederica Schyrr, thank you for helping out a finishing PhD student – I hope that this experience will be useful to you, when it will be your turn to finish. Finally, from our lab, I would also like to thank my experimental right arm and one of my best friends, Aurelien Oggier. Your motivation and helpfulness made it look like all of this would be impossible without you! Thanks a lot, and all the best for your future! Aurelien is the fourth in a line of technicians, which was preceded by Evangelos Panopoulos (‘the pope’) and Yannick Yersin, all great people that left a strong impact on my life and work.

My acknowledgements also go to the other collaborating professors, that made this project possible in the first place: Prof. Matthias Lutolf, Prof. Johan Auwerx and Prof. Bart Deplancke. From the Deplancke-Lab, I would like to thank Daniel Alpern and Pernille Rainer, for all the help with the RNA-seq on both projects. From the Lutolf Lab there are many people I would like to thank besides Matthias himself, who was together with Olaia, my stepping stone to EPFL. Samy Gobaa, Marta Roccio, Aline Roch, Sylke Höhnel, Nathalie Brandenburg, Sonja Giger, Steffen Cosson, Andrea Negro, Thibaut Cherbuin, and of course, Vincent Trachsel and Gena Nikitin. Besides the passionate science-related discussions, thanks to you two for all the ‘future-of-humanity’-type discussions, which were also always strongly based on scientific knowledge.

All this work would also not be possible without the core facilities at EPFL, especially the animal facility, flow cytometry facility and the Biomolecular Screening Facility (BSF). Within the flow cytometry facility, thanks to Miguel Garcia, Loïc Tauzin, André Mozes, Valérie Glutz and Telma Lopes for all the efforts put into the sorts! Within the BSF, I would also like to thank basically everybody, since they all play their own parts. First of all, Gerardo Turcatti, who allowed me to perform the screening in the facility and Benjamin Rappaz, who introduced me to the DHM and helped me start the project. Fabien Kuttler, thank you for your extensive help in image analysis and Jonathan Vesin and Julien Bortoli, for all your help in plating compounds and changing medias. In addition, I would like to thank Antoine Gibelin, Marc Chambon, Nathalie Ballanfat and Damiano Banfi for all their help.

I would also like to thank my industrial collaborators at both Nestlé Institute of Health Science (NIHS) and Endogena Therapeutics, for giving the opportunities and visions to implement the research in real life. At the NIHS, thank you to Federico Sizzano and his team, a true passionate of science and ‘the guru’ of flow cytometry. At Endogena thanks to Matthias Steger, for allowing this collaboration to happen and your commitment to it. Daphna Mokady and Alex Müller – I am truly looking forward to a fruitful collaboration.

Finally, I would like to thank all my friends including the ones I made during my time in Lausanne, since they all made an impact into this work, in one way or another. Thanks to Sat, for all the craft beers, and to the roof crew, for all their inspiration and incredible brotherhood. I would also like to thank Magda, for always being there for me and supporting me in the most difficult moments. And of course, my family, for always believing in me and their unconditional support.

Abstract

More than 50.000 bone marrow transplantations (BMT) are performed annually worldwide, however the procedure-associated mortality rate remains close to 25%. The BMT remains a risky procedure, only indicated for life-threatening diseases, while no replacement of this technology is to be expected in the foreseeable future. Modest improvements such as the use of G-CSF to accelerate hematopoietic recovery significantly reduce mortality. The main goal of this work is finding novel pharmacological approaches to accelerate hematopoietic recovery in the post-transplant period, and is addressed via two strategies: (i) by stimulating hematopoiesis using NAD⁺-boosters to promote mitochondrial clearance in the most primitive hematopoietic stem cells (HSC), and (ii) by pharmacologically modulating the differentiation of BMA, which are inhibitory to the expansion of fast proliferating hematopoietic progenitor cells (HPC).

HSCs reside in the bone marrow (BM) and are mostly quiescent. They cycle rarely, in order to give rise to their committed progeny as well as to self renew. A stable HSC pool is maintained via extracellular signals and interactions with other cell types of the BM (microenvironment) which result in symmetric or asymmetric self-renewing divisions. In turn, HPCs proliferate without sustained self-renewal, and differentiate to all mature blood cell types. Removing HSCs from their microenvironment increases oxidative phosphorylation, which, if combined with impairment of the mitochondrial stress response, can severely compromise the regenerative capacity of HSCs. Here we demonstrate that the NAD⁺-boosting agent Nicotinamide Riboside (NR) reduces mitochondrial activity within HSCs through increased mitophagy, the recycling mechanism of damaged mitochondria. We observed *in vitro* NR treatment of HSCs to lead to increased asymmetric HSC divisions, which resulted in a significantly enlarged pool of progenitor cells, without concurrent HSC exhaustion. Supplementation of NR to the diet of mice undergoing BMT accelerated hematopoietic recovery and improved survival by 80%. Our work demonstrated for the first time a positive effect of NAD⁺-boosting strategies on the most primitive HSCs, and established a novel link between HSC mitochondrial stress, mitophagy and stem cell fate decision.

Targeting the microenvironment has also been proposed as a means to indirectly regulate HSC and HPC (HSPC) function. The bone marrow adipocyte (BMA) has recently been recognized as a hematopoietic regulatory entity, although the mechanism by which it interacts with HSPCs *in vivo*, remains unknown. During the hematopoietic recovery period post-BMT, HSPCs increase their metabolism as a response to hematopoietic stress, which is modulated by the microenvironment. *In vitro* and *in vivo* studies have suggested BMA to maintain HSCs quiescent, which, while being of advantage to protect a scarce pool of HSCs, is detrimental to the increased expansion of HPCs in the recovery phase post-BMT. BM stromal cells (BMSC) are the cellular precursors of both adipocytes and osteoblasts, and they have been strongly implicated in supporting hematopoiesis by secreting cytokines such as SCF and Cxcl12. We observed that adipocytes accumulate in the marrow space of mice undergoing BMT, which was fuelled by a proliferation of Sca1⁺/CD24⁻ pre-adipocytes. In the late post-transplant period, hematopoiesis-supportive multipotent Sca1⁺/CD24⁺ stromal cells arise, coinciding with hematopoietic recovery. We developed a novel screening platform using Digital Holographic Microscopy (DHM), which was used to quantify *in vitro* adipocytic differentiation in non-perturbing manner, allowing for follow-up co-cultures with HSPCs. Using the OP9 BMSC-line, we modulated adipocyte differentiation prior to co-culture using a pharmacological approach and observed that high adipocytic content was associated to a decrease in HPC expansion. Screening through more than 4000 FDA-approved drugs and natural compounds identified calcipotriene, a synthetic analog of vitamin-D₃, to efficiently prevent adipocytic differentiation and maintain the hematopoietic supportive capacity of OP9 stroma.

Altogether, this work opens the door to alternative strategies accelerating hematopoietic reconstitution and unveils the potential of NR and Calcipotriene to improve recovery of patients undergoing BMT.

Keywords

Bone marrow transplantation, hematopoietic stem cell, stem cell fate, mitochondria, autophagy, metabolism, NAD⁺, Nicotinamide Riboside, Nicotinamide Mononucleotide, hematopoiesis, microenvironment, bone marrow, bone marrow adipocyte, adipogenesis, bone marrow stromal cell, OP9 cell, co-culture, holographic microscopy, screening, pharmacology, Calcipotriene, Vitamin-D.

Zusammenfassung

Weltweit werden jährlich mehr als 50.000 Knochenmarktransplantationen (BMT) durchgeführt, die prozessbedingte Sterblichkeitsrate liegt jedoch weiterhin nahe 25%. Die BMT ist nach wie vor ein riskantes Verfahren, das nur für lebensbedrohliche Krankheiten angezeigt ist. In absehbarer Zeit ist kein Ersatz dieser Technologie zu erwarten. Bescheidene Verbesserungen wie die Verwendung von G-CSF zur Beschleunigung der hämatopoetischen Erholung verringern die Sterblichkeit erheblich. Das Ziel dieser Arbeit besteht in der Suche nach neuen pharmakologischen Ansätzen zur Beschleunigung der hämatopoetischen Erholung in der Zeit nach der BMT und wird durch zwei Strategien angesprochen: (i) durch Stimulierung der Hämatopoese unter Verwendung von NAD⁺-Beschleunigern zur Förderung der Entfernung von beschädigten Mitochondrien in den primitivsten hämatopoetischen Stammzellen (HSC) und (ii) durch pharmakologischer Modulation der Differenzierung von Markadipozyten, die die Expansion von schnell proliferierenden Vorläuferzellen hemmen (HPC).

HSC befinden sich im Knochenmark (BM) und sind meistens im Ruhezustand. Sie teilen sich selten, um sowohl Vorläuferzellen zu erzeugen als auch ihre Selbsterneuerung zu bewirken. Ein stabiler HSC-Pool wird durch extrazelluläre Signale und Wechselwirkungen mit anderen Zelltypen des BM (Mikroumgebung) aufrechterhalten, was zu symmetrischen oder asymmetrischen selbsterneuernden Zellteilungen führt. HPCs wiederum vermehren sich ohne anhaltende Selbsterneuerung und differenzieren sich zu allen reifen Blutzelltypen. Das Entfernen von HSCs aus ihrer Mikroumgebung erhöht die oxidative Phosphorylierung, die in Verbindung mit einer Beeinträchtigung der mitochondrialen Stressreaktion, die Regenerationsfähigkeit von HSCs stark beeinträchtigen kann. Hier zeigen wir, dass der NAD⁺-beschleunigende-Wirkstoff Nicotinamid-Ribosid (NR) die Mitochondrienaktivität in HSCs durch erhöhte Mitophagie (den Wiederverwehrtungsmechanismus beschädigter Mitochondrien) reduziert. Wir beobachteten, dass die *In vitro*-NR-Behandlung von HSCs zu vermehrten asymmetrischen Teilungen der HSCs führte, was zu einem vergrößerten Vorrat von HPCs, ohne Erschöpfung der HSCs führte. Die Ergänzung von NR zur Ernährung von Mäusen, die einer BMT unterzogen waren, beschleunigte die hämatopoetische Erholung und verbesserte das Überleben um 80%. Unsere Arbeit zeigte zum ersten Mal eine positive Wirkung von NAD⁺-beschleunigenden Strategien auf HSCs und stellte einen neuen Zusammenhang zwischen mitochondrialem Stress, Mitophagie und der Entscheidung des Stammzellschicksals her.

Das Zielen auf die Mikroumgebung wurde auch als Mittel zur indirekten Regulierung der HSC- und HPC-Funktion (HSPC) vorgeschlagen. Der Markadipozyt (BMA) wurde kürzlich als hämatopoetische regulatorische Einheit erkannt, obwohl der Mechanismus, durch den er *in vivo* mit HSPCs interagiert, unbekannt bleibt. Während der hämatopoetischen Erholungsphase nach der BMT erhöhen HSPCs ihren Stoffwechsel als Reaktion auf hämatopoetischen Stress, der durch die Mikroumgebung moduliert wird. *In vitro*- und *In vivo*-Studien deuten darauf hin, dass BMA die HSCs im Ruhezustand aufrechterhalten, was zum Schutz eines knappen HSC-Pools von Vorteil ist, jedoch nachteilig für die zunehmende Expansion von HPCs in der Erholungsphase nach der BMT ist. BM-Stromazellen (BMSC) sind die zellulären Vorläufer sowohl von Adipozyten als auch von Osteoblasten. Sie sind stark an der Unterstützung der Hämatopoese beteiligt, indem sie Zytokine wie SCF und Cxcl12 ausgescheiden. Wir beobachteten, dass sich Adipozyten im Markraum von Mäusen, die sich einer BMT unterziehen, anhäufen. Diese BMA wurden ihrerseits durch eine Proliferation von Sca1⁺/CD24⁺ Präadipozyten angetrieben. In der späten Transplantationsphase entstehen hämatopoeseunterstützende multipotente Sca1⁺/CD24⁺ Stromazellen, die mit der hämatopoetischen Erholung einhergehen. Wir entwickelten eine neuartige Screening-Plattform mit Hilfe der Digitalen Holographischen Mikroskopie (DHM), mit der die Adipozytendifferenzierung *in vitro* auf nicht störende Weise quantifiziert werden konnte. Dies ermöglichte daher anschließende Co-Kulturen mit HSPCs. Mit der OP9 BMSC-Linie modulierten wir die Adipozyten-Differenzierung vor der Co-Kultur unter Verwendung eines pharmakologischen Ansatzes und beobachteten, dass ein hoher Adipozytengehalt mit einer Abnahme der HPC-Expansion zusammenhängt. Durch unser Screening von mehr als 4000 zugelassenen Arzneimitteln und Naturstoffen, wurde Calcipotrien, ein synthetisches Analogon von Vitamin-D₃, identifiziert, dass die Adipozytendifferenzierung effizient verhinderte und die hämatopoetische Unterstützungskapazität des OP9-Stromas aufrechterhielt.

Insgesamt öffnet diese Arbeit die Tür zu alternativen Strategien zur Beschleunigung der hämatopoetischen Erholung und zeigt das Potenzial von NR und Calcipotrien zur Verbesserung der Genesung von Patienten, die sich einer BMT unterziehen.

Stichworte

Knochenmarktransplantation, hämatopoetische Stammzelle, Stammzellschicksal, Mitochondrien, Autophagie, Metabolismus, NAD⁺, Nicotinamid-Ribosid, Nicotinamid-Mononukleotid, Hämatopoese, biologisches Milieu, Knochenmark, Adipozyten, Adipogenese, Knochenmarkstromazelle, OP9-Zelle, Co-Kultur, holographische Mikroskopie, Screening, Pharmakologie, Calcipotrien, Vitamin-D.

Contents

Acknowledgements.....	v
Abstract	vi
Keywords	vi
Zusammenfassung.....	vii
Stichworte.....	vii
List of Figures	xii
Chapter 1 Introduction	15
1.1 Bone marrow transplantation.....	15
1.1.1 HSC function and metabolism	15
1.1.2 HSC microenvironment.....	16
1.2 Bone marrow adipocytes (BMA)	17
1.2.1 On the origin of bone marrow adipocytes	17
1.2.2 Effect of BMA on hematopoiesis	18
1.2.3 Regulating bone marrow adipogenesis in a transplantation setting.....	19
1.3 Concluding remarks.....	19
1.4 Aims and objectives.....	21
1.5 Figures.....	22
Chapter 2 <i>In vivo</i> characterization of the red-to-yellow-to-red bone marrow transition.....	25
2.1 Introduction.....	25
2.2 Methods	26
2.2.1 <i>In vivo</i> transplantation assay.....	26
2.2.2 ‘Adipochaser’ transplant.....	26
2.2.3 Circulating blood cell (CBC) counting.....	26
2.2.4 Bone marrow extraction for flow cytometry.....	26
2.2.5 Antibodies.....	27
2.2.6 Histology.....	27
2.3 Results	27
2.3.1 The kinetics of BMAT expansion during bone marrow transplantation	27
2.3.2 Mesenchymal stromal cell proliferation in the post-transplant period.....	28

2.3.3	Searching for de-differentiation of BMA in the late post-transplant period	28
2.4	Discussion	29
2.5	Figures.....	32
Chapter 3	High-throughput, non-perturbing quantification of lipid droplets with Digital Holographic Microscopy....	39
3.1	Abstract	39
3.2	Introduction	39
3.3	Materials and Methods	40
3.3.1	Cell culture and adipocytic differentiation.....	40
3.3.2	Microscopy.....	40
3.3.3	Image processing.....	41
3.3.4	FACS.....	41
3.3.5	RT-PCR	41
3.3.6	Triglyceride (TG) content	42
3.3.7	Protein content	42
3.4	Results	42
3.4.1	DHM imaging is non-invasive and can be used to assess different features in lipid droplet accumulating cells	42
3.4.2	DHM can be used to assess adipocytic differentiation.....	43
3.4.3	DHM imaging is robust and high-throughput.....	43
3.5	Discussion	44
3.6	Acknowledgements	44
3.7	Figures.....	45
Chapter 4	Accelerating hematopoietic recovery post-transplantation.....	51
4.1	Introduction	51
4.2	Methods	52
4.2.1	<i>In vivo</i> transplantation assay.....	52
4.2.2	Circulating blood cell (CBC) counting.....	52
4.2.3	Bone marrow extraction	52
4.2.4	Antibodies.....	53
4.2.5	OP9 cell culture and cell line preparation	53
4.2.6	Compound plating.....	53
4.2.7	<i>In vitro</i> HSPC hemato-toxicity/proliferation assay.....	53
4.2.8	<i>In vitro</i> HSPC and OP9 cell co-culture	53
4.2.9	RNA-seq	54
4.2.10	CFU assay.....	54
4.2.11	Histology.....	54
4.3	Results	54
4.3.1	Screening for modulators of adipocyte differentiation.....	54

4.3.1.1. Primary screen	55
4.3.1.2. Hit confirmation: Potency and toxicity	55
4.3.1.3. Counter-screens and functional testing <i>in vitro</i>	55
4.3.1.4. RNA-seq of modulators of adipocyte differentiation.....	56
4.3.1.5. <i>In vitro</i> co-culture	57
4.3.2 <i>In vivo</i> modulation of adipocyte differentiation.....	57
4.3.2.1. Enhancing bone marrow adipogenesis	57
4.3.2.2. Inhibiting bone marrow adipogenesis.....	58
4.4 Conclusions and perspectives	59
4.5 Figures.....	61
Chapter 5 The NAD-booster nicotinamide riboside potently stimulates hematopoiesis through increased mitochondrial clearance.....	75
5.1 Abstract	77
5.2 Introduction.....	77
5.3 Experimental procedures.....	78
5.3.1 Study design.....	78
5.3.2 Mice.....	78
5.3.3 Food preparation.....	78
5.3.4 Antibodies.....	78
5.3.5 Flow cytometry	79
5.3.6 Analysis of mitochondrial activity.....	79
5.3.7 Analysis of autophagy flux	79
5.3.8 Murine HSC culture	79
5.3.9 CFUs assay	79
5.3.10 Murine bone marrow transplantation	79
5.3.11 CFSE	79
5.3.12 Seahorse Oxygen Respiration Rate (OCR) measurement	80
5.3.13 RNA preparation.....	80
5.3.14 RNA-seq	80
5.3.15 qRT-PCR	81
5.3.16 Western blotting	81
5.3.17 Hydrogel microwell array production and single cell cycle kinetics.....	81
5.3.18 LT-HSCs extraction, Imaging and Analysis for asymmetry analysis	81
5.3.19 Human hematopoietic cells.....	82
5.3.20 <i>In vitro</i> culture and transplantation of human CD34+ hematopoietic progenitor/stem cells.....	82
5.3.21 <i>In vivo</i> NR treatment of adult humanized NSG mice.....	82
5.3.22 Statistics.....	83
5.4 Results and Discussion.....	83

5.4.1	Mice supplemented with Nicotinamide Riboside expand the hematopoietic progenitor compartments	83
5.4.2	NR decreases mitochondrial membrane potential ($\Delta\Psi_m$) independently of cell cycle quiescence....	83
5.4.3	NR decreases $\Delta\Psi_m$ in human CD34+ cells and improves human blood reconstitution.	84
5.4.4	NR increases mitochondrial clearance and reduces mitochondrial metabolism.	84
5.4.5	NR induces mitochondrial stress <i>in vivo</i>	85
5.4.6	NR promotes asymmetric mitochondrial distribution in LT-HSCs upon cell division.....	85
5.4.7	Improved survival and enhanced blood cell production of post-transplanted mice treated with NR.	86
5.5	Conclusions and perspectives	86
5.6	Acknowledgements	87
5.7	Figures.....	88
Chapter 6	Conclusion	105
6.1	Kinetics of the bone marrow transplantation	105
6.2	Influence of BMA on hematopoiesis.....	106
6.3	HSC metabolism	106
6.4	Accelerating hematopoietic recovery post-transplant.....	107
6.5	Clinical perspectives	107
6.6	Pharmacological perspectives.....	108
Appendix	Standardized kinetics of murine hematopoietic recovery following chemo- and radio-ablative regimens	109
A.1	Introduction	109
A.2	Methods	110
A.2.1	Mice.....	110
A.2.2	Murine bone marrow transplantation and irradiation.....	110
A.2.3	5-fluorouracil treatment	110
A.2.4	Blood collection and analysis	110
A.3	Results	110
A.4	Discussion	111
A.5	Figures.....	112
References		115
Curriculum Vitae		127

List of Figures

Figure 1.1 Clinical outcome of the most common HSCTs for hematological diseases.	22
Figure 1.2 Regulation of HSC self-renewal and proliferation by the bone marrow microenvironment.	23
Figure 1.3 The knowns and unknowns of bone marrow adipose tissue (MAT).	24
Figure 2.1 Kinetics of the red-to-yellow-to-red marrow transition following lethal irradiation and bone marrow transplantation.	32
Figure 2.2 Kinetics of multipotent and pre-adipocytic stromal bone marrow cells in the red-to-yellow-to-red bone marrow transition.	33
Figure 2.3 Schematic representation of the modified ‘Adipochaser’ mouse model.	34
Figure 2.4 Searching for de-differentiation in the reattaching bone marrow adipose tissue (BMAT) during the late post-transplant period (the yellow-to-red marrow transition).	35
Figure 2.5 Schematic illustration of the kinetics of the red-to-yellow-to-red bone marrow transition following lethal irradiation and bone marrow transplantation.	36
Figure 3.1 Digital Holographic Microscopy (DHM) is non-invasive and can be used to assess different features in lipid droplet accumulating cells.	45
Figure 3.2 6-day timelapse of OP9 cells induced to differentiate towards adipocytes: Comparison of DHM and fluorescence microscopy.	46
Figure 3.3 Total TG and protein content of OP9 cells during the 6-day adipocytic differentiation.	47
Figure 3.4 OPD signal of FACS-sorted OP9 cells induced to differentiate towards adipocytes during a time period of 6 days.	48
Figure 3.5 DHM imaging can be used to identify inhibitors and enhancers of adipogenesis in a high-throughput manner.	49
Figure 4.1 High-throughput screening to identify novel modulators of adipocyte differentiation.	61
Figure 4.2 Hematotoxicity counterscreens.	62
Figure 4.3 RNA-seq of inhibitors of OP9 adipocytic differentiation.	63
Figure 4.4 Co-culture assay of compound-treated OP9 cells and HSPCs.	64
Figure 4.5 The effect of high fat diet (HFD) on hematopoietic regeneration post-transplant.	65
Figure 4.6 The effect of PPAR γ inhibition on hematopoietic regeneration post-transplant.	66
Figure 5.1 NR treatment expands ST hematopoietic progenitors <i>in vivo</i>	88
Figure 5.2 NR treatment decreases mitochondrial membrane potential ($\Delta\Psi$ m).	89
Figure 5.3 NR decreases $\Delta\Psi$ m in human CD34+ and improves human blood cell reconstitution.	90
Figure 5.4 NR induces the expression of autophagy/mitophagy-related genes and NAD salvage pathway.	91
Figure 5.5 NR induces mitophagy and downregulates mitochondrial energy pathways in HSCs.	92
Figure 5.6 NR induces asymmetric mitochondrial distribution in LT-HSCs.	93
Figure 5.7 NR improves survival and accelerates blood recovery after HSC transplant.	94
Figure S 2.1 Leakage issues encountered in the modified ‘Adipochaser’ mouse model.	37
Figure S 4.1 Summary of the screening for novel inhibitors of adipocyte differentiation.	67
Figure S 4.2 CFU assay of HSPCs co-cultured with compound-pre-treated OP9 cells.	68
Figure S 4.3 DHM imaging prior to co-culture, including DMSO controls.	69
Figure S 4.4 Summary of the <i>in vivo</i> data.	70

Figure S 4.5 The effect of HFD and Rosiglitazone on hematopoietic regeneration post-transplant: extended results.....	71
Figure S 4.6 The effect of PPAR γ inhibition on hematopoietic regeneration post-transplant: extended results.....	74
Figure S 5.1 Transcriptome analysis of NAD pathway genes and influence of NR on the hematopoietic system.	95
Figure S 5.2 NA/NAM-supplementation does not cause hematopoietic progenitor expansion.....	96
Figure S 5.3 NR exerts its effect through the NR/Nrk/NMN axis.	97
Figure S 5.4 NR <i>in vitro</i> affects mitochondrial mass and $\Delta\Psi_m$ in HSCs.....	98
Figure S 5.5 NR improves blood reconstitution and stem cell function of human CD34+ cells.	99
Figure S 5.6 NR induces autophagy, mitophagy, increased OCR and mitochondrial stress.....	100
Figure S 5.7 NR induces mitochondrial stress in K562 cells in a dose dependent manner and does not exhaust HSC function in secondary transplantation.....	102
Figure S 5.8 Graphical abstract.	103

Chapter 1 Introduction

1.1 Bone marrow transplantation

Hematopoietic stem cells (HSC) are the most successfully used stem cells in the clinic [1] and the bone marrow transplantation (BMT, or HSCT: hematopoietic stem cell transplantation) the best studied and described stem cell application to date. The HSCT is also the prime example of ‘personalized medicine’, as each patient is carefully monitored by a team of doctors and their regimen specifically designed to meet the physiological needs of each patient. BMT experts worldwide are connected to a large network of databases of potential donors, and with currently performing currently more than 40.000 HSCTs per year [2], [3]. While the use of HSCTs used to be restricted to blood cancers including lymphoma and leukemias, the ameliorated survival rate has expanded its application to more than 70 diseases including inherited and acquired immune deficiency disorders, inherited metabolic disorders, and congenital anemias [3]–[5].

There are two main types of HSCTs performed in the clinic: Autologous and Allogeneic. The autologous transplant involves harvesting the patient’s own stem cells, purifying or treating them *ex vivo* and subsequently transplanting them into the same patient. This allows to bypass the rejection of the donor’s stem cells and is therefore the ideal transplantation setting to minimize toxicity. However, not all patients have healthy stem cells that can be preserved *ex vivo* and therefore must undergo allogeneic transplantation, which is also the main indication for leukemia, requiring the immunosurveillance properties of a foreign immune system for long term remission. Allogeneic transplantation involves using human leukocyte antigen (HLA)-matched donor’s stem cells to replace the patient’s failing bone marrow. The number of HLA-matched donors for allogeneic transplantations remains however limited. In addition, the extreme rarity of HSCs and their limited *ex vivo* expansion capacity further exacerbates the outcomes of BMTs.

The mortality rate is still close to 50% within the first three years after transplantation. Major complications include bleeding, bone marrow failure, and Graft Versus Host Disease (GVHD) [6], [7]. Forty percent of these fatalities relate to the patient’s severe immune-compromised condition during the post-ablation period, before the graft has reconstituted the hematopoietic system [8]. The HSCT remains therefore a risky procedure and its indication restricted to life-threatening conditions (Fig 1.1).

A long-term analysis of European bone marrow transplantation centers [2] suggested that the investment into drug development to replace the HSCT is far greater than the investment into improving the transplant technology itself. The current standard of care to accelerate hematopoietic recovery is the parental administration of granulocyte colony stimulating factor (G-CSF), which directly stimulates hematopoietic stem cell (HSC) activation and accelerates exit of severe neutropenia by an average of 3-6 days [9], [10]. This modest improvement is sufficient to shorten infectious episodes significantly and decrease hospitalization costs. The transplantation-associated mortality rate remains nevertheless a very serious issue, which requires urgent lethality-reducing measures. More so when considering that HSC transplantation for hematopoietic malignancies represents the benchmark example of successful stem cell treatments. Both reducing the time of engraftment and decreasing the toxicity of the conditioning regimen are critical to increase the chance of survival in these patients and reduce the costs associated to the treatment [11]. This thesis proposes two strategies to address this problem: (i) by directly modulating HSC metabolism, and (ii) by regulating the differentiation of bone marrow adipocytes, the most abundant cell type in the adult bone marrow.

1.1.1 HSC function and metabolism

Adult stem cells are functionally defined as cells having the capacity to self-renew and give rise to all the mature cells of a given tissue [12]. Hematopoietic stem cells (HSC) reside on the top of the hierarchy of the hematopoietic system and therefore give rise to all blood cells. The regenerative potential of these cells is so great that in fact, it has been shown that upon successful engraftment, a single HSC can reconstitute the entire blood system of a mouse [13]. A recent study also reported the case of a 115-yr-old living woman, which had most of her circulating blood derived from only two HSCs [14]. One of the most common sources of HSCs used in the clinical setting is the umbilical cord blood (UCB). However, the limited number of UCB-derived HSCs has prevented a broader and safer applicability of HSC-based therapies [15]–[17]. This in turn has led to a variety of studies, which have been focusing on discovering novel systems capable of expanding HSCs *ex vivo* [6], [18]–[20]. The limited success of these studies is mainly due to the

loss self-renewal and therefore reduced regenerative potential of *in vitro* cultured HSCs. Since the ultimate function of HSCs is to expand their pool to replenish new blood cells, every division an HSC undergoes is coupled to a fate decision. The fate of dividing HSCs, or of adult stem cells in general, can be reduced to two generally accepted viable options: asymmetric self-renewal division, where one of the stem cells remains multipotent or symmetric commitment, where both cells lose their multipotency. Recent advances in inducible genetic labelling and visualization of stem cells undergoing divisions suggest that symmetric self-renewal may also play a role in maintaining homeostatic circulating blood levels [21], [22]. Though conceptually this is plausible, it is arguable whether the currently available methodology is able to identify the functionality by which stem cells are defined. The only functional long-term assay remains the *in vivo* transplantation, especially when looking at the fate of single stem cells [23]. For the sake of simplicity, we are assuming asymmetric self-renewal divisions as the major mechanism driving blood replenishment.

A variety of studies have suggested profound changes in the metabolic profile of HSCs undergoing commitment. Long-term HSCs (LT-HSCs), which are defined as the most primitive cells, given their long-term repopulating potential, are mostly quiescent and rely mainly on anaerobic glycolysis [24]–[26]. This is in strong contrast to short-term HSCs (ST-HSCs), multipotent progenitors (MPPs) or committed progenitors (CPs), which are obliged to produce higher levels of ATP via mitochondrial oxidative phosphorylation in order to sustain their rapid proliferation [25], [27]. This reduced mitochondrial respiration in LT-HSCs allows for a protection from cellular damage by reactive oxygen species (ROS) and appears therefore to play a critical role in maintaining long-term *in vivo* function [28]–[32]. The strong correlation between regenerative potency and low mitochondrial activity suggests a direct role of mitochondria in regulating HSC fate and poses the question of causality versus consequence. A recent study suggested the enforced lowering of mitochondrial activity using the mitochondrial uncoupler FCCP to induce self-renewal in LT-HSCs [33]. This hypothesis is supported by work demonstrating that the metabolic transducer and glucose sensor Lkb1 is crucial for HSC maintenance [32], [34]–[36]. In addition, the transcription factor hypoxia-inducible factor 1 α (HIF 1 α) promotes glycolysis, by preventing pyruvate from entering the tricarboxylic acid cycle via the induction of pyruvate dehydrogenase kinases (PDKs) expression [26], [37]. Interference with the metabolic checkpoints of HSC self-renewal HIF 1 α and PDK therefore induces premature HSC aging [25], [27], [31]. Whether the metabolic profile of HSCs is linked to a particular cell fate choice, rather than just an adaptation to an extreme microenvironment in the BM remains unknown. Finally, autophagy, the recycling mechanism of damaged intracellular compartments (such as mitochondria), has been shown to improve HSC maintenance [38]. This is particularly evident in hematopoietic stress conditions, of which, the previously described BMT, represents the best-described model [23]. Rapid proliferation of HSCs is needed to replenish the depleted progenitor cells and a dramatic increase in oxidative phosphorylation coupled with defective autophagic machinery, greatly compromises their regenerative function. In fact, both the FOXO3-mediated autophagy as well as the mitochondrial stress response have been shown to act as additional metabolic checkpoint regulating HSCs maintenance [39], [40].

The strong glycolytic profile of LT-HSCs has been often been associated to the highly hypoxic ‘niches’ [41], [42], whereas in self-renewing asymmetric stem cell divisions, the committed daughter cell is released from the niche. During this division, the mitochondria are asymmetrically distributed towards the committed daughter cell, while the self-renewing stem cell remains anchored to the niche with a lower number of active mitochondria [26].

1.1.2 HSC microenvironment

The development of the niche or ‘microenvironment’ concept [43]–[45] has opened up new opportunities to treat diseases related to stem cells and their abnormal behavior. This is especially evident in the field of hematopoiesis, where the adequate balance of quiescence, self-renewal and commitment towards progenitor cells is tightly controlled by a variety of cells within the bone marrow to ensure the organism’s lifelong blood replenishment [45]–[47]. The highly plastic bone marrow HSC niche has been associated with three anatomical regions (endosteal surfaces, sinusoidal walls and stroma) and four main cellular players (osteoblasts, adipocytes, endothelial cells and stromal cells) [47]. The anatomical structure of the bone marrow is very heterogeneous depending on skeletal location, age or physiological condition. Placing an HSC in a specific context may lead to an altered behavior, which is determined by an input of different soluble and immobilized factors as well as cell-to-cell contacts.

However, the inherent 3D structure of the HSC encapsulated into the difficult-to-visualize bone marrow has led to much controversy regarding the nature of the cellular components that directly associate with HSCs. In 2003, two main studies linked the HSC functionality geographically with osteoblasts and the endosteum [48], [49]. The osteogenic lineage was suggested as supportive towards hematopoiesis by increasing HSC numbers through the regulation of PTH, notch ligand and BMP [48]–[50] signaling. In addition, osteoblasts were shown to secrete Angiopoietin-1 (Ang1), a key player regulating HSC quiescence, by directly interacting with Tie-2 expressed on the HSCs surface [51]. It has however since then been demonstrated that although osteoblasts can produce trophic factors that favor HSC maintenance, it is mainly endothelial and LeptinR⁺ perivascular cells within the highly vascularized endosteum that are functionally required for HSC survival [52], [53]. In parallel, distinct perivascular Nestin⁺ cells with mesenchymal stem cell (MSC) properties have also been shown necessary and sufficient for HSC self-renewal *in vivo* [54]. In accordance to these

findings, many Mesenchymal stem and progenitor cells-like (MSPCs) cell lines have been implicated in supporting hematopoiesis, therefore challenging the current, but highly debated paradigm that osteoblasts and endothelial cells constitute a dual HSC niche [55]. A summary describing the different cell types and factors involved in regulating HSC self-renewal and proliferation within the bone marrow can be seen in Fig 1.2 [56].

MSPCs constitute a still ill-defined population capable of giving rise to osteoblasts, adipocytes and chondrocytes [57], [58], with recent studies giving strong evidence for the MSPC (Nestin⁺Sca1⁺ALCAM⁻) as true HSC niche [59]. Morphologically, they probably correspond to adventitial cells surrounding the sinusoidal capillaries, where they express high levels of CXCL12, V-CAM, Ang-1 and SCF, all key molecules for the homing and maintenance of HSCs. In this context, CXCL12-high adventitial reticular cells (CARs) have been histologically associated with HSCs within the bone marrow [60]. In order to conceal the seemingly disparate nature of endothelial and perivascular/mesenchymal cells and their role within the HSC niche, distinct homeostatic and regenerative HSC niches have since been proposed, probably corresponding to the formerly proposed notion of a quiescent and activated HSC niche [60], [61]. The bone marrow adipocyte (BMA), the other population that arises from MSPCs, has been shown to negatively regulate hematopoiesis [62]–[64], although the molecular mechanisms remain largely unknown. The approach presented in this thesis to modulate the hematopoietic microenvironment pertains precisely to the modulation of the stromal to adipocytic differentiation axis.

1.2 Bone marrow adipocytes (BMA)

Mammals developed two main distinct types of fat tissue that exert different functions: white adipose tissue (WAT), which has the capacity to store excess energy and brown adipose tissue (BAT), which is specialized in energy expenditure in the form of heat [65]. Brown adipocytes contain a large number of mitochondria and the defining feature of expressing the uncoupling protein-1 (UCP1) on their mitochondrial inner membrane, allowing it to depolarize and therefore converting energy into heat. Mature white adipocytes are composed of a single large lipid vacuole, which forces the nucleus to the cell periphery. Their primary functions are to mediate lipid and glucose transport, fatty acid synthesis and mobilization, and to regulate insulin sensitivity. Bone marrow adipose tissue has been considered to be either a mixture of brown and white adipocytes or even consisting of a different intermediate cell type, as it could be with the so-called 'beige' adipocyte (Fig 1.3). The role of adipocytes within the bone marrow has long been attributed to that of a passive "space-filler". Within the last decade however, they have been implicated in a variety of functions such as acting as organizer and support cells during bone fractures healing [66]. They have also been recognized as a distinct endocrine organ secreting hormones such as adiponectin and leptin therefore contributing to the organisms' local and systemic metabolism [67]. Most recently they have also been implicated in regulating hematopoiesis, though the extent and directionality of which remains highly debated. Bone marrow adipose tissue is now recognized as a distinct tissue with a distinct origin and function, acquiring increased attention from a variety of different research areas, such as metabolism, cancer, bone physiology and hematopoiesis [67], [68].

1.2.1 On the origin of bone marrow adipocytes

In the bone marrow space, adipose tissue occupies the largest volume besides the hematopoietic compartment. The 'yellow' and 'red' marrow have early been described as the fatty and the hematopoietic marrow, respectively. The Neumann's law from 1882 describes, the peripheral part of limb bones as containing more yellow marrow that would accumulate during ageing. It wasn't until 1976 that Tavasoli distinguished adipocytes within the red marrow from adipocytes within the yellow marrow via performic acid-Schiff staining (PFAS), indicative of differences in the lipid composition of these adipocytes [69]. Experiments administering phenylhydrazine to rabbits suggested adipocytes of the red marrow to undergo resorption in response hemolysis, in contrast to adipocytes of the yellow marrow, which were unaffected. He labelled them as 'labile' and 'stable' adipocytes [70]. In 2015, a thorough study investigating the composition and function of yellow and red marrow adipocytes in both rodents and humans, gave way to the concept of regulated (rMAT) and constitutive marrow adipose tissue (cMAT). It suggested rMAT, composed of more saturated lipids, isolated and interspersed between hematopoietic cells, to react to cold-exposure. cMAT, on the other hand, appears early after birth and is composed of more unsaturated lipids, and resembling more to traditional WAT [71]. To which extent these two different types of bone marrow adipose tissue derive from the same origin is unknown. The fact, that recent findings support a hematopoietic origin of a subpopulation of adipocytes [72], [73], is evidence to the complexity of the bone marrow adipocyte differentiation and function.

'Mesenchymal stem cells' (MSC) were initially defined as self-renewing stem cells necessary for bone and marrow homeostasis, with the ability to differentiate into all three mesenchymal lineages: osteogenic, chondrogenic and adipogenic. The field has however evolved in the last few years to suggest that, firstly, what we call 'MSCs' are organ specific. Secondly, that in the bone marrow two different progenitor populations may exist with *in vitro* 'MSC'-like behavior as defined by tri-lineage differentiation, but with differing *in vivo* reconstitution properties. The nomenclature has now come to the consensus referring to bone marrow-derived cells in close interaction with hematopoietic cells as bone marrow stromal cells (BMSC)[74].

Since the function of bone marrow adipocytes is tightly linked to their origin, lineage-tracing *in vivo* studies have greatly aided in this quest. In 2010, a group first described the existence of Nestin-expressing BMSCs using Nestin-GFP transgenic mice, which were closely associated to HSCs and depletion of which would significantly reduce HSC numbers [54]. Another group suggested, LepR-CRE expressing cells to be precursors to all adipocytes the main source of bone, and secreting high levels of SCF, essential for HSC maintenance [52]. In addition, it challenged the previous study by suggesting SCF deletion from osteoblasts, hematopoietic cells or Nestin-CRE expressing cells was not necessary for HSC maintenance. The isolation of stromal cells via PDGFR α and Sca1 expression (PaS cells) [75] also suggested another rich source of BMSCs with strong self-renewal and tri-lineage potency, secreting high levels of Ang-1 [76]. In parallel a newly developed CXCL12-GFP reporter strain aided in identifying functionally HSC-supportive BMSCs within the bone marrow leading to the definition of CXCL12-adventitial reticular (CAR) cells [77]. All the above described BMSCs are histologically identified as pericytes/adventitial reticular cells and their function is highly overlapping – all known to secrete high levels of SCF, an essential cytokine for HSC maintenance. For the sake of simplicity, we will call them CAR cells, as they were identified in the HSC niche.

The second BMSC-like population corresponds to the osteo-chondro-reticular or skeletal stem cell population (SSC), which has been isolated in stromal cells via CD105 expression, immediately adjacent to the growth plate and trabecular bone, via the Grem1-CreER system [76]. This population was reported to differentiate into osteoblasts and chondrocytes, but not adipocytes *in vivo*, while retaining limited capacity for *in vitro* adipogenic differentiation. Grem1-CreER expressing cells were suggested to be the main contributor to bone development and growth upon endochondral ossification before adulthood. Interestingly, Grem1-CreER also marked reticular marrow stromal cells, only a minority of which (4%) overlap with Nestin-GFP. In parallel, another study described a cell population with extremely similar characteristics, using CD105, Tie2, Thy and 6C3 marker expression. These cells were able to differentiate into bone, cartilage and reticular hematopoiesis-supportive bone marrow stroma, but not adipocytes [76].

The extent to which, the bone-supporting BMSC lineages functionally overlap with the hematopoietic supporting CAR cell lineages remains an open question. It would, for example, be interesting to understand how PDGFR α + cells overlap with Grem1-Cre, and to determine if the reticular marrow stromal cells generated by Grem1-Cre excised cells belong to the SCF-expressing (CAR/LepR+), to the Ang1-expressing (PDGFR α) reticular marrow stromal cells or to a distinct reticular stromal population. In addition, current data, has not yet found a perfect correlation between the above depicted mouse populations and the human marrow, for which a clear bone marrow organizing activity has been clonally characterized for CD146+ cells [78] pertaining to the CD271+ subpopulation [79]. Although the role is quite clear for CAR cells as HSC niche cells and of CD146+ human cells as bone marrow organizers, the comparative HSC niche capacity of all the aforementioned populations has not been investigated. It has indeed been suggested that cells forming bone and cells forming the hematopoietic microenvironment compete with each other for their common MSC precursor [80].

1.2.2 Effect of BMA on hematopoiesis

The amount of fatty marrow has long been inversely correlated to hematopoietic activity and has even, in fact, been used in the clinic as a diagnosis for hematopoietic failure [81]. It wasn't until 2009, when a pioneering study first described an active role of bone marrow adipocytes in preventing hematopoietic regeneration in mice [62]. The authors observed a decrease in number and function of ST-HSCs and multipotent progenitors in yellow marrow compartments, such as the distal part of the limb bones and posterior vertebrae (cMAT). However, the most primitive LT-HSCs remained conserved and quiescent in the yellow marrow. In addition, Genetic ablation of adipocytes in A-ZIP mice accelerated hematopoietic recovery after HSC transplantation. This study ignited the interest in bone marrow adipocytes as regulators of hematopoiesis and soon other studies emerged that challenged or confirmed this view. A recent study used a mouse model where SCF is conditionally deleted in adiponectin-CRE expressing cells [61]. They observed a decline in hematopoietic regeneration in these mice upon hematopoietic stress and a reduced number of HSCs in the highly adipocytic caudal vertebrae (cMAT), but not in the long bones (rMAT) at homeostasis. Another recent study observed severe extramedullary hematopoiesis in lipodystrophic PPAR γ KO mice and a dysregulation in the Cxcr4/Cxcl12 axis [82], which has previously also been suggested in PPAR γ hypomorphic mice [83]. These reports together with the identification of adiponectin and leptin as enhancers of HSC survival and proliferation *in vitro* [84], supported the notion that adipocytes are essential to HSC function. *In vitro* however, undifferentiated or pre-adipocytic populations have very different HSC niche functions as compared to mature adipocytes. A study performing 5-week co-cultures of human mature adipocytes with human CD34+ bone marrow HSPCs observed a maintained survival of LT-HSCs, while the undifferentiated stroma supported progenitor proliferation [85]. These observations seem consistent with other *in vitro* studies [86], [87].

The role of adipocytes in regulating hematopoiesis therefore remains highly debated and more complex than originally thought. The incongruencies can however, at least partially, be explained by segregating the effect of preadipocytes vs. terminally differentiated/lipid-accumulating adipocytes and by segregating the effect of adipocytes on LT-HSCs vs. ST-HSCs/MPPs. While

terminally differentiated adipocytes seem to induce or maintain HSC quiescence, the progeny of which (multipotent progenitors) seems to be prevented to perform their main function: proliferate and differentiate. *In vitro* co-culture experiments confirm this observation [85], [86]. We therefore argue that the definition of mature adipocyte is of central importance in this context. Adiponectin expression reflects the late steps of adipocyte commitment, however Adipo-Cre mediated excision has been observed to occur soon after commitment, before massive lipid vacuole formation occurs [88]. This suggests that the adiponectin-CRE-driven SCF excision, may have happened also in hematopoiesis-supportive pre-adipocytes. A most recent thorough adipocyte lineage-tracing study identified a multipotent, perivascular precursor cell based on Sca1 and CD24 expression [64]. *In vivo* these cells gave rise to PDGFR α ⁺ osteochondrogenic progenitor cells (OPCs), committed adipogenic progenitor cells (APCs), which were Sca1⁺ and CD24⁻. The latter population in turn gave rise to zfp423-GFP-expressing preadipocytes. Using these three stages of adipocyte differentiation, they submitted mice to hematopoietic stress via lethal irradiation and performed intra-tibial bone marrow transplants together with identified stromal and pre-adipocytic cell populations. They observed that even LT-HSCs were reduced in numbers when injected with cells of the later adipocytic lineage, while both LT-HSCs and cKit+Sca1⁺ multipotent progenitor numbers were supported by Sca1⁺/CD24⁺ multipotent MSCs. Taken together, the literature seems congruent with the hypothesis that pre-adipocytes are supportive of both LT-HSCs and ST/MPPs, while terminally differentiated adipocytes have a net inhibitory effect. Whether this prevention of hematopoietic proliferation by terminally differentiated adipocytes is dependent on an unidentified active inhibitor (Prostaglandins are a candidate [80]) or underlying a relative depletion of pre-adipocytic populations that are supportive to rapid ST/MPP expansion, remains unknown.

1.2.3 Regulating bone marrow adipogenesis in a transplantation setting

BMA tissue is always increased at the expense of hematopoietic tissue, a phenomenon known as the Neumann's law [89]. BMA tissue expansion can follow a variety of stimuli and physiological conditions, and is both highly dynamic and reversible. Most notably, and paradoxically, it expands both in obesity as well as in caloric restriction [90], [91]. BMA content is also increased at the expense of bone formation, as seen in osteoporotic patients or patients following anti-diabetic TZD treatments [68] and immunosuppressive glucocorticoid treatments [92]–[96]. One of the most plastic organ transitions known in the human adult is the red-to-yellow-to-red bone marrow transition. Following intensive chemo-therapeutic or radio-ablative regimens that precede the HSCT, bone marrow adipocytes rapidly populate the bone marrow space. Within the following two to three weeks, the bone marrow adipose tissue retreats, coinciding with hematopoietic expansion. The mechanisms underlying this highly dynamic and reversible transition, remain largely unknown and are further discussed in this dissertation. Clinical and experimental observations have revealed inhibition of bone marrow adipogenesis as a potential treatment for a variety of osteopenic disorders [97]. The previously described 2009 study also observed that pharmacologically preventing adipocyte differentiation via daily intraperitoneal injections of PPAR γ modulator BADGE in the early post-transplant period, would accelerate hematopoietic recovery. Targeting the stem cell niche has not yet not been clinically exploited, let alone thoroughly studied.

Traditionally, adipocytes are seen as terminally differentiated cells, which exert a specific function until the end of their life cycle. More recently though, independent *in vitro* ceiling culture studies have questioned this notion. This culture technique allows floating adipocytes to attach on the top of culture flasks and subsequently release their lipid content. *In vitro* differentiation and transcriptional profiling suggests they regain multipotent differentiation capacity [98], [99]. More recently, an *in vivo* lineage tracing study revealed de-differentiation of adipocytes in the lactating mammary glands of female mice, whereas the cells expressing the adiponectin-rtTA reporter were able to regain proliferation and multilineage differentiation potential [100]. If this mechanism of de-differentiation is proven to play part in adipocytes of the yellow-to-red bone marrow transition, this may be another target for pharmacological intervention.

1.3 Concluding remarks

All clinical approaches used so far have however been aimed to target the Hematopoietic Stem Cell (HSC) compartment and their success remains limited [6]. In the context of the bone marrow transplantation, pharmacological adipocyte inhibition seems to be the necessary next step, when considering niche-targeted approaches to accelerate hematopoietic recovery. As many of these patients have severe intestinal disruption in the immediate post-transplant period, are aged or cannot freely move, exercise or nutrition-based approaches are not sufficient [101].

We have with this dissertation therefore proposed to accelerate hematopoietic recovery by pharmacologically targeting the microenvironment of HSCs, more specifically the bone marrow adipose tissue. This dissertation investigates the kinetics of bone marrow adipogenesis during BMT and searches for novel regulators of adipocyte differentiation. Using novel imaging tools developed in the lab, we were able to accurately quantify adipocyte differentiation, both *in vitro* and *in vivo*. Together with the Biomolecular Screening Facility (BSF) at the EPFL we developed a high-throughput screening platform, which we have used to identify new

compounds affecting bone marrow adipogenesis. We have identified calcipotriene, a synthetic analog of vitamin-D₃, which we envision as an alternative strategy to improve hematopoietic recovery post-transplantation. The metabolism and function of HSCs is tightly regulated by a variety of extracellular signals and strong interactions with HSC niche cells. We have also identified a new pharmacologically compatible strategy to reduce mitochondrial metabolism through increased mitochondrial clearance. We showed herewith that treating HSCs *in vitro* with the vitamin B3-derivative Nicotinamide Riboside (NR) marked an increase in regeneration capacity and feeding transplanted mice with NR has led to an acceleration of the hematopoietic recovery and improvement of post-transplant survival.

1.4 Aims and objectives

Overarching Hypothesis: *Microenvironmental or metabolically driven HSC modulation can accelerate hematopoietic recovery after bone marrow transplantation*

Aim 1: *In vivo* characterization of the red-to-yellow-to-red bone marrow transition

Sub aim 1.1. Assessing adipocyte hyperplasia and hypertrophy in the red-to-yellow transition

Predicted result: both drive this transition, as seen in diet induced obesity in peripheral adipose tissues

Sub aim 1.2. Assessing pre-adipocytic and multipotent stromal populations in the expansion

Predicted result: the recruitment of pre-adipocytes underlies adipocyte hyperplasia in the red-to-yellow transition

Sub aim 1.3. To lineage-trace adipocytes in the yellow-to-red transition

Predicted result: adipocytes de-differentiate into pre-adipocytic stromal cells as seen in lactating murine mammary glands

Aim 2: Identifying novel inhibitors of bone marrow adipogenesis

Sub aim 2.1. Developing a high-throughput screening platform to assess novel modulators of adipocyte differentiation

Predicted result: Lipid droplet accumulation can be quantified by their light-refractive capacity using holographic microscopy

Sub aim 2.2. To identify novel inhibitors of adipocyte differentiation *in vitro*

Sub aim 2.3. To induce hematopoietic expansion by modulating adipocyte differentiation *in vitro*

Predicted result: Preventing adipocyte differentiation with the newly identified inhibitors, rescues the inhibition hematopoietic proliferation

Sub aim 2.4. To test candidates *in vivo* in a transplantation setting

Predicted result: Inducing adipogenesis *in vivo* delays hematopoietic recovery, while inhibition accelerates hematopoietic recovery

Aim 3: Enhancing hematopoietic stem cell function in the post-transplant period using NAD-boosters

Sub aim 3.1. To identify a clinically compatible compound capable of modulating HSC metabolism

Predicted result: Decreasing mitochondrial membrane potential in HSCs using NAD-boosters improves HSC blood reconstitution

Sub aim 3.2. To identify the mechanisms driving NAD-booster-driven improvements in HSC function

Predicted result: NAD-booster-induced decrease in mitochondrial membrane potential in HSCs is driven by mitophagy

Sub aim 3.3. To improve hematopoietic recovery and survival in mice undergoing bone marrow transplantation

Predicted result: NR-supplementation in the diet accelerates hematopoietic recovery post-aplasia

1.5 Figures

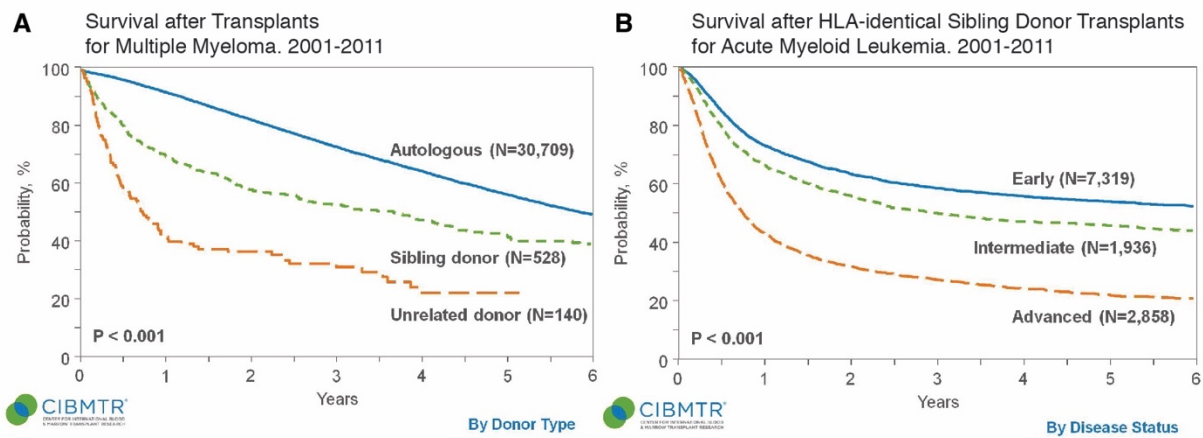


Figure 1.1 Clinical outcome of the most common HSCTs for hematological diseases. A. Multiple myeloma (MM) is the most common indication for autologous HSCT. Among 30,709 patients who received an autotransplant for MM, the 3-year probability of survival was 72%. Allogeneic transplantation for MM is reserved for patients with high risk disease. Among the 668 patients who received an allogeneic HCT for MM, the 3-year probabilities of survival were 52% and 31% for recipients of HLA-matched sibling and unrelated donor grafts, respectively. **B.** Acute Myeloid Leukemia (AML) is the most common indication for allogeneic HSCT. Their disease status at the time of transplant and the donor type are the major predictors of post-transplant survival. Among 12,113 patients receiving an HLA-matched sibling donor transplantation for AML, the 3-year probabilities of survival after HLA-matched sibling transplant in this cohort was 58%, 49%, and 26% for patients with early, intermediate, and advanced disease, respectively. Modified from Pasquini and Wang, 2013 [102]

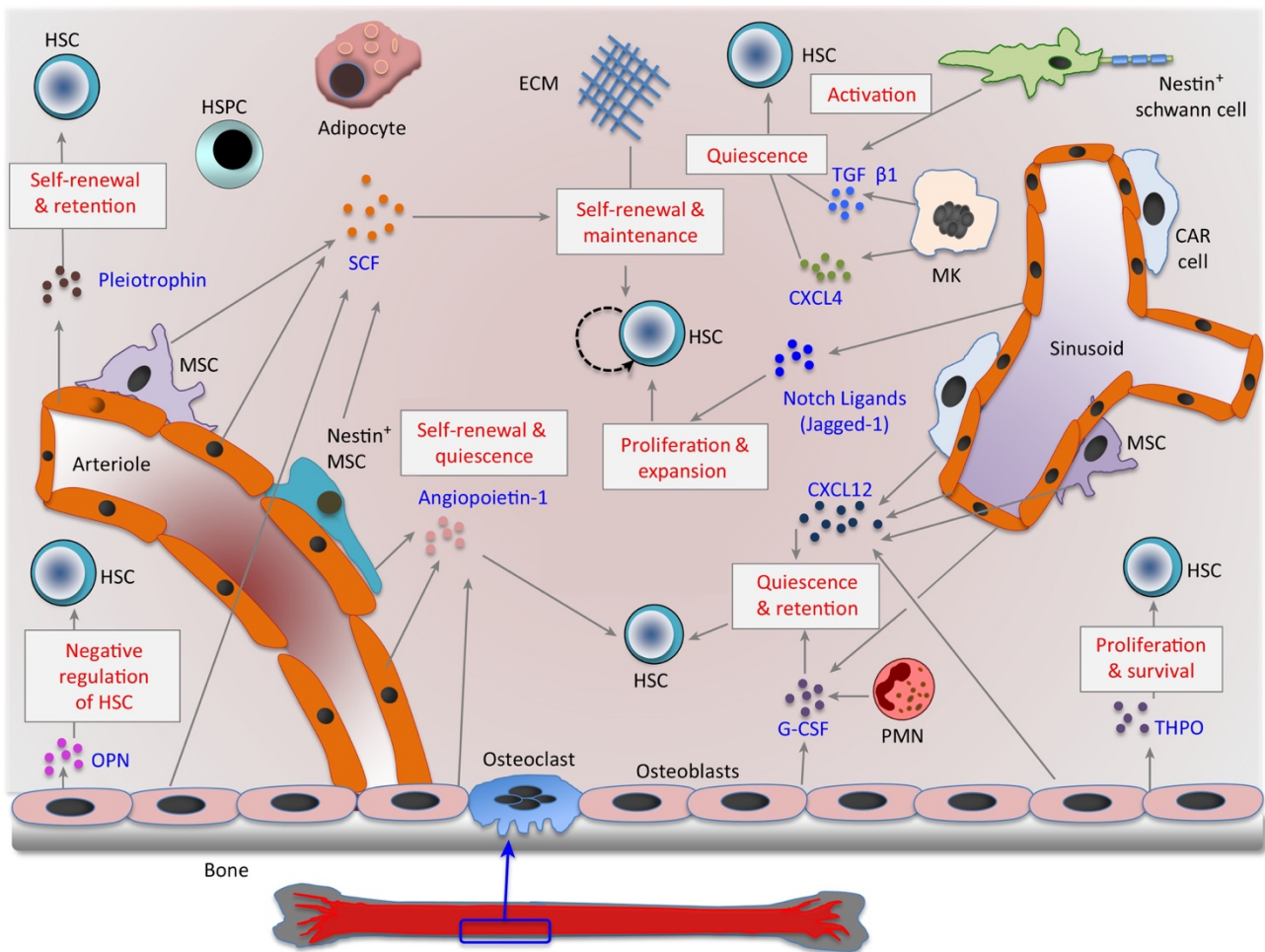
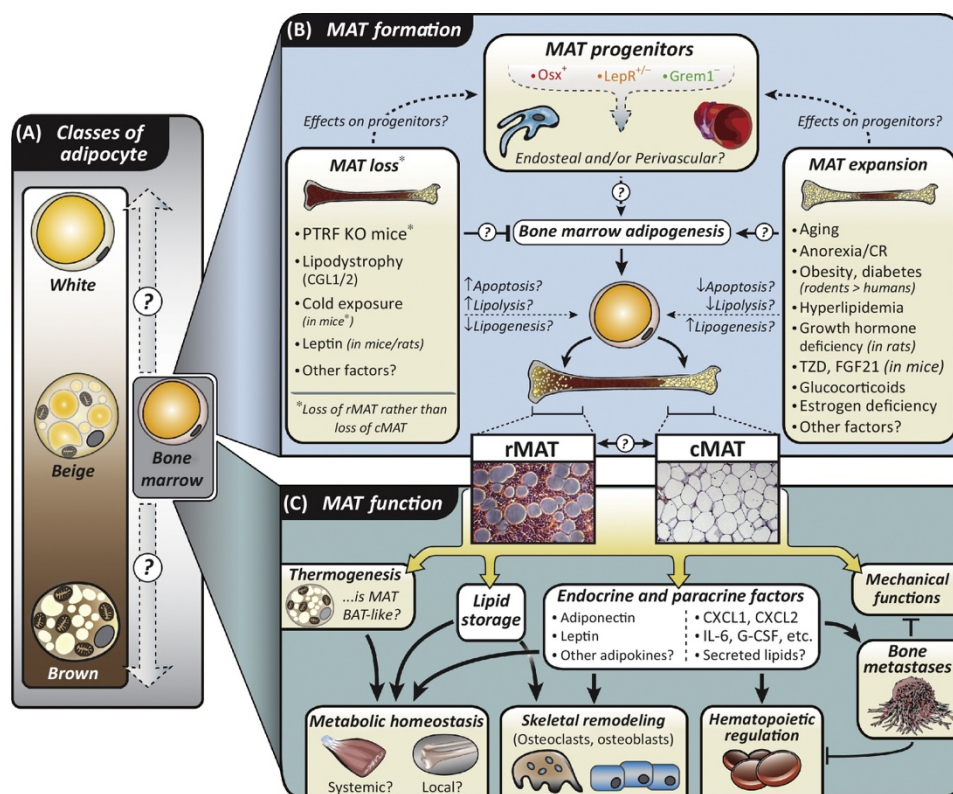


Figure 1.2 Regulation of HSC self-renewal and proliferation by the bone marrow microenvironment. The diagram shows the cellular composition and cytokines/growth factors that can impact on HSC self-renewal and function in the bone marrow (BM) niche. Recent research has identified the role of diverse BM niche cells and HSC progeny including osteoblasts, Nestin⁺ mesenchymal stem cells (MSCs), CXCL12-abundant reticular (CAR) cells, non-myelinating Schwann cells, BM endothelial cells and adipocytes, megakaryocytes, and neutrophils (PMN) in HSC self-renewal, differentiation, and function. Niche cells also produce/release several cytokines/growth factors, such as SCF, THPO, TGF-β1, CXCL-4, CXCL-12, G-CSF, OPN, Notch ligands, angiopoietin 1, and pleiotrophin, to regulate HSC self-renewal, maintenance, survival, retention, and function. The extracellular matrix (ECM) can also regulate HSC self-renewal and maintenance. Abbreviations: CXCL-4, CXC chemokine ligand 4; CXCL-12, CXC chemokine ligand 12; G-CSF, granulocyte-colony stimulating factor; HSPC, hematopoietic stem and progenitor cell; MK, megakaryocyte; OPN, osteopontin; PMN, polymorphonuclear cell; SCF, stem cell factor; THPO, thrombopoietin; TGF-β1, transforming growth factor β1. Taken from Kumar and Geiger, 2017 [56].



Trends in Endocrinology & Metabolism

Figure 1.3 The knowns and unknowns of bone marrow adipose tissue (MAT). **A.** Adipose tissue is typically classified as white, brown, or beige. Bone marrow adipocytes are morphologically similar to white adipocytes; however, it is unclear where they fall on this ‘white–beige–brown’ spectrum, if at all. **B.** Lineage-tracing studies demonstrate that bone marrow adipocyte progenitors express osterix (*Osx*), but not *Grem1*. Some marrow adipocytes are also derived from progenitors that express the leptin receptor (*LepR*). Based on these findings it is unclear if marrow adipocyte progenitors are endosteal and/or perivascular in origin, although they are clearly distinct to progenitors for white and brown adipocytes. Also unclear is how these progenitors are driven toward adipogenesis to generate bone marrow adipocytes, which can be classed as two distinct subtypes: regulated (rMAT) and constitutive (cMAT). Do these subtypes derive from distinct progenitors, and can rMAT and cMAT interconvert? In addition to physiological MAT formation, various conditions are associated with MAT loss or MAT expansion, predominantly in rMAT. However, the mechanisms linking these conditions to MAT loss or gain remain largely uncertain. **C.** The function of MAT is also yet to be firmly established. Some reports suggest that MAT has BAT-like properties, although this remains controversial. Instead, MAT may have more WAT-like properties such as lipid-storage and endocrine functions. It is now clear that MAT can release adipokines such as adiponectin and leptin, as well as paracrine factors such as cytokines and lipids. These secreted factors may allow MAT to exert both local and systemic effects on metabolic homeostasis, skeletal remodeling, hematopoiesis, and development of bone metastases. The diversity of these functions highlights the breadth of the potential impact of MAT on health and disease. Abbreviations: BAT, brown adipose tissue; CR, caloric restriction; KO, knockout; WAT, white adipose tissue. Taken from Scheller et al, 2016. [103]

Chapter 2 *In vivo* characterization of the red-to-yellow-to-red bone marrow transition

This chapter describes the cellular transitions following lethal irradiation and bone marrow transplantation in 8- to 12-week old female C57Bl/6J mice. Emphasis is put on the hematopoietic and adipocytic cellular components within the bone marrow. Subchapters 2.3.1 and 2.3.3 were planned and executed by Vasco Campos with the technical help of Dr. Shanti Rojas-Sutterlin, Josefine Tratwal and Aurelien Oggier. Subchapter 2.3.2 was planned and executed by Dr. Shanti Rojas-Sutterlin in the context of a MegaClust-driven identification of novel cellular players in the red-to-yellow-to-red transition. It was performed with the technical help of Josefine Tratwal. The development of the semi-automated image analysis tool for Hematoxylin- and Eosin-stained sections ('Mar-rowQuant') was performed by Josefine Tratwal and will be extensively described in the thesis dissertation of Josefine Tratwal. The chapter was written by Vasco Campos.

2.1 Introduction

Owing to the increased epidemic of diabetes and obesity in western societies, adipocyte turnover has received increased attention in the last few years [65]. In human adults, approximately 10% of fat cells are renewed each year and their numbers remain relatively stable after childhood [104]. This is in contrast to mice, where it was recently demonstrated that 0.6% of adipocytes are renewed each day [105]. While in obesity, both adipocyte size and number are increased; in weight loss, for example due to gastric bypass interventions, adipocytes seem to only decrease in size [104]. Although adipocytes have historically been defined as terminally differentiated cells, recent studies have suggested that they can, not only decrease in size and reduce their lipid content, but also reversibly transform into a fibroblast-like state (Reviewed in: Fu, Zhao and Hu, 2018 [106]). Using the 'Adipochaser' lineage-tracing mouse model, Scherer et al demonstrated that adipocytes reversibly undergo de-differentiation in the mammary glands during lactation [100]. Gene expression analysis suggested that these cells regain a pre-adipocytic phenotype, rather than just losing their lipid content. This may help explaining why adipose tissue can quickly expand to its preceding size, as seen in patients that stop exercising and/or regain a diet with high fat content.

In the bone marrow space, adipose tissue occupies the largest volume besides the hematopoietic compartment. The 'yellow' and 'red' marrow have early been described as the fatty and the hematopoietic marrow, respectively [89]. In fact, the Neumann's law from 1882 describes the distal parts of limb bones as accumulating more yellow marrow during ageing. It has been described to reach 50-70% of total marrow space by age 25 [101]. The amount of fatty marrow is indeed inversely correlated to the hematopoietic activity and is used in the clinic as a diagnosis for hematopoietic failure. BMA tissue expansion can follow a variety of stimuli and physiological conditions and is reversible. Most notably, and paradoxically, it expands both in obesity as well as in caloric restriction [90], [91]. BMA content is also increased at the expense of bone formation, as seen in osteoporotic patients or patients following anti-diabetic TZD treatments and immunosuppressive glucocorticoid treatments [92]–[96]. However, the most remarkable and rapid increase in BMA volume is observed following intensive chemo-therapeutic or radio-ablative regimens, as preceding a bone marrow transplantation [107]. Bone marrow adipocytes take up most of the marrow space within the first two to three weeks after irradiation. Variations in the volume of BMA, as seen in hematopoietic malignancies, are dependent of both adipocyte size and number [108]. In the context of bone marrow transplantation, it remains unknown whether it is adipocyte hyperplasia or hypertrophy that underlies this rapid increase in BMA volume.

Although the BMA is recognized as a hematopoietic regulatory entity, the mechanisms by which it expands, and retreats remain unknown. Most adipocytes occupy the distal part of the femur, region which has been coined 'cMAT' (constitutive MAT) or 'stable' marrow adipocytes, as they slowly, but stably accumulate over the lifetime of a mouse. Rare adipocytes are also seen in the hematopoietic marrow. These adipocytes have been termed 'rMAT' (regulated MAT) or 'labile' marrow adipocytes, given that adipocytes in this region can quickly expand and return to homeostatic levels.

In mice, bone marrow adipocytes increase in number following irradiation and bone marrow transplantation [61]. Whether bone marrow adipocytes also increase in size during the red-to-yellow marrow transition and whether a proliferation of pre-adipocytic stromal cells underlies BMA hyperplasia, has not yet been investigated and is our major focus in this chapter. Considering the fast expansion of adipocytes during the hematopoietic ablative regimen, *we hypothesize that, as in extramedullary adipocytes during obesity, bone marrow adipocytes would increase rapidly both in size and in number. In addition, we hypothesize that this rapid expansion is fueled by an increase of the pre-adipocytic stromal pool.*

We herewith developed a standardized assay to characterize the red-to-yellow-to-red transition during bone marrow transplantation and demonstrated that the recruitment of pre-adipocytes is underlying the red-to-yellow bone marrow transition *in vivo*. Using a modified version of the 'Adipochaser' lineage-tracing mouse model, we intended to assess de-differentiation of adipocytes in the yellow-to-red transition, but due to leakiness this hypothesis could not be tested.

2.2 Methods

2.2.1 *In vivo* transplantation assay

Mice were housed in 12h day-night light cycles and provided with sterile food and water. Experiments were carried out in accordance to the Swiss law and with approval of the cantonal authorities (Service Veterinaire de l'Etat de Vaud). 8- to 12-week old C57BL/6J mice (unless otherwise specified) underwent lethal x-ray irradiation (8.5 cGy, split in two doses 4 h apart using RS-2000, RAD SOURCE) followed the next day by the transplantation of 125.000 total bone marrow cells from MHC-compatible C57BL/6J Ly5.1 mice in volume of 200 μ l PBS 1mM EDTA via tail intravenous injection. Total bone marrow cells were extracted from femur, tibia and pelvis of MHC-compatible donors, by crushing using a mortar and pestle in ice-cold PBS, 1 mM EDTA. The samples were then filtered through a 70 μ m mesh, red blood cells lysed for 1 min at RT (420301, Biolegend), washed with ice-cold PBS, 1 mM EDTA and counted on a hemocytometer. 2 drops of blood were taken up to 2 times per week from the tail to monitor recovery of circulating blood cell (CBC) counts. Bones from three to five mice were extracted on different days post-transplantation and the adipocytic (yellow) versus hematopoietic (red) bone marrow content quantified from Hematoxylin and Eosin stained, full-length mid-longitudinal femoral sections. The stromal cell compartment was analyzed by flow cytometry from one femur and one tibia per mouse, and defined as the FSC/SSC singlet, DAPI⁺/CD45⁺/Ter119⁻/CD31⁻ compartment.

2.2.2 'Adipochaser' transplant

25-week old C57BL/6J 'Adipochaser' females underwent lethal irradiation and transplantation from MHC-compatible C57BL/6J Ly5.1 donors, as described above. The recipients were given Doxycycline (600 mg/kg) ad libitum in the diet (D09050204i, Research diets Inc.) between day 12 and day 19 post-transplant. One femur and one tibia were extracted per mouse on day 21 (peak of aplasia) and on day 40 post-transplant, to cover the beginning and the end of the yellow-to-red bone marrow transition. The controls used in this experiment include: (i) 'Adipochaser' mice, that are TRE-Cre^{-/-}, (ii) 'Adipochaser' mice not given Doxycycline and (iii) 'Adipochaser' mice not undergoing transplantation (steady-state control, or day 0 control). The stromal cell population was analyzed via flow cytometry and whole-mount bone sections visualized via confocal microscopy.

2.2.3 Circulating blood cell (CBC) counting

2 Drops of blood were taken from the tail-vein and collected in EDTA-coated tubes. Upon brief, low speed vortexing, the samples were analyzed and the blood cell counts recorded using the scil Vet ABC hematology analyzer (Scil, USA), to obtain total white blood cell (leukocyte) counts, monocyte counts, granulocyte counts (which are constituted by a great majority of neutrophils and a minority of eosinophils and basophils), red blood cell (erythrocyte) counts, platelet counts and hemoglobin content. For samples with platelets counts higher than $2 \times 10^6 / \text{mm}^3$, the samples were diluted and re-analyzed since the threshold of detection was reached.

2.2.4 Bone marrow extraction for flow cytometry

The bone marrow fraction was isolated from murine femur and tibia (unless otherwise stated), which were then flushed in PBS, 1 mM EDTA and 2 % FBS using a syringe (25 G). The samples were filtered through a 70 μ m mesh and centrifuged. The pellet was resuspended in 1 mL of the previous buffer and we refer to it as the 'BM (bone marrow) fraction'. Non-red blood cells were counted on a hemocytometer and 4 millions cells taken per sample for FACS analysis. The remaining part of the pellet was taken for further cell culture and FACS analysis and/or microscopy. For further enrichment of the stromal fractions, the flushed bones were cut into pieces and digested with 5mL Collagenase II (17101-015, Gibco) in MEMa media (Gibco) for 1 h at 36 °C. The sample was filtered through a 100 μ m mesh and centrifuged. The pellet is referred to as the 'BLC (bone lining cell) fraction'. The pellets of both the BM

fraction as well as the BLC fraction were resuspended in blocking buffer and subsequently in an antibody-mix containing following antibodies: Sca1-APC (1:100), CD45-AlexaFluor700 (1:150), Ter119-AlexaFluor700 (1:200), CD24-APCeFluor780 (1:1000), CD31-PeCy7 (1:100). After 30 min staining, the samples were washed and resuspended in PBS, 1 mM EDTA containing DAPI at 1 ng/mL, 2 % FBS and 20 μ L CountBright beads (C36950, Invitrogen). Flow cytometric analysis was performed on the LSRII (Becton Dickinson, USA) flow cytometer.

2.2.5 Antibodies

Sca1-APC (108112, Biolegend), CD45-AlexaFluor700 (103128, Biolegend), Ter119-AlexaFluor700 (116220, Biolegend), CD24-APCeFluor780 (47-0242-82, Invitrogen), CD31-PeCy7 (102418, Biolegend).

2.2.6 Histology

For the histological assessment of bone marrow adiposity and hematopoietic content, the extracted femurs and tibias were fixed in 10 % formalin for 24 h at 4 °C and washed 3 times for 15 min in PBS at RT. The bones were then decalcified overnight in a Tri-Na citrate and formic acid solution at RT, and then thoroughly washed under running tap water. The bones were placed in 70 % ethanol at 4 °C before paraffin inclusion. The bones were then cut longitudinally in 3-4 μ m sections and stained with Hematoxylin and Eosin. Semi-automated quantification of the red (hematopoietic) and yellow (adipocytic) bone marrow was performed using the MarrowQuant analysis tool developed in the lab.

2.3 Results

2.3.1 The kinetics of BMAT expansion during bone marrow transplantation

As a first approach to characterize the plasticity of both yellow and red compartments of the bone marrow throughout the skeleton, we established a standardized assay of the re-to-yellow-to red BM transition. This consisted of transplanting intravenously 125.000 total bone marrow mononucleated cells (MNCs) into lethally irradiated young female C56Bl6/J mice (Fig 2.1A). During the transplant period, three transplanted mice were sacrificed every five days and the femurs extracted and processed to obtain Hematoxylin and Eosin stained sections. The images of the histological sections were then used to quantify yellow versus red marrow using a semi-automated image analysis plugin for ImageJ, which has been developed in the lab. Within manually selected regions of interest, this tool automatically distinguishes adipocytes (seen as 'ghosts', when the membrane is intact), bone tissue (pink), nucleated hematopoietic cells (blue) and red blood cells (pink) based on color thresholds. We defined the hematopoietic and adipocytic marrow as Neumann had described it in 1882: as 'red' and 'yellow' bone marrow [89]. The area of both RBCs and bone tissue were subtracted from the quantification.

In the immediate post-transplant period, the bone marrow is highly hemorrhagic, as seen through high numbers of RBCs released from injured vessels. The nucleated hematopoietic compartment, which consists mostly of hematopoietic stem and progenitor cells is rapidly depleted in this period. At the same time, the hematopoietic marrow containing 'rMAT' is replaced by bone marrow adipocytes, reaching a maximum of expansion between day 15 and day 20 post-transplant (Fig 2.1B-C). Hematopoiesis is rapidly depleted, as circulating white blood cells and platelets are reduced by 10-fold on days 5 and 10 post-transplant (Fig 2.1F). Around day 25 post-transplant, hematopoiesis starts recovering, with circulating blood levels exiting the life-threatening neutropenic- (< 0.5 cells/ μ L) and thrombopoietic stage (< 200 cells/ μ L) (Fig 2.1F). Granulocytes and monocytes are the white blood cells with the shortest half-life and therefore represent early indicators of hematopoietic recovery. Red blood cells do not deplete as drastically as white blood cells, as their circulating number decrease to less than 3-fold. This may be explained by the long lifetime of RBCs (in mouse around 40 days [109]). A more detailed exploration of the recovery of different circulating mature hematopoietic cell types is described in the Annex of this thesis. The overall lethality observed in our laboratory in this setting accounts to 20%, whereby the most deaths occur between day 16 and day 28 post-transplant (Fig 2.1G).

Using the same in-house developed quantification tool, we were also able to address both adipocyte number and size distribution in the post-transplant period. As expected, from previous observations [61], both the size and number of adipocytes increased in the post-transplant period (Fig 2.1 D-E).

In our setting, adipocytes reached the peak of expansion (as defined by the percentage of area occupied) between 15- and 20-days post-transplant, whereas adipocyte numbers increased from around 5- to 10-fold. At first sight, we would interpret a peak in adipocyte number in the immediate post-transplant period (day 5 and day 10), however the number of adipocytes specially on the day 5 timepoint may be overestimated given that hemorrhagic marrow exhibits spaces between cells, that could be counted as

adipocyte ghosts. Current updates are being incorporated into the software to correct for this phenomenon, which will be described in length in J. Tratwal's thesis dissertation. Adipocyte hyperplasia is unequivocally seen in the later timepoints, which did not exhibit haemorrhage, as an increase in the average number of adipocytes per given unit of marrow area. Of note, given that not all bone sections had perfectly aligned midlongitudinal cuts, the total area of visualized marrow exhibited variations between images. We therefore normalized the adipocyte number to the area of interest, and for clarity indicated the increase in adipocyte number as fold-change relative to day 0 (Fig. 2.1E). We also found that the expansion of the yellow marrow additionally underlies an increase in the size of adipocytes. The mean size of adipocytes at homeostasis in young female mice is around $300\ \mu\text{m}^2$, increasing up to $500\ \mu\text{m}^2$ at the peak of aplasia. Note that the mean adipocyte size may be underestimated, given that 3-4 μm thin sections don't allow for the distinction between adipocytes that were only tangentially cut and spaces between cells, that are evident in hemorrhagic sections. The mean size of bone marrow adipocytes on day 35 post-transplant remained significantly higher than homeostatic mice. We therefore conclude that the expansion of the BMAT in the early post-transplant period is due to both hyperplasia and hypertrophy of adipocytes. We thus further hypothesized that bone marrow adipocytes hyperplasia would underlie a proliferation of mesenchymal stromal cells or pre-adipocytes.

2.3.2 Mesenchymal stromal cell proliferation in the post-transplant period

To address whether bone marrow adipocyte hyperplasia in the red-to-yellow transition is followed by an expansion of pre-adipocytic or multipotent stromal cells, we analyzed the bone marrow stroma via flow cytometry using the markers previously described in the study by Ambrosi et al [64]. We therefore transplanted 125,000 total bone marrow mononucleated cells (MNCs) into lethally irradiated young female C56Bl6/J mice, as previously described (Fig 2.2A). Five transplanted mice were sacrificed every seven days for the first three weeks post-transplant and in the very late post-transplant period (49 days). The bone marrow of three mice at homeostasis was also extracted on each of these days and, combined ($n=12$), plotted as 'day 0'. The bone marrow of femurs and tibias was flushed (called the 'BM' fraction) and the remaining bones digested with collagenase to extract bone lining cells ('BLC' fraction) (Fig 2.2B). The cells were immunophenotyped by flow cytometry for the MSC markers Sca1 [59] and CD24 [64]. The cell pellets were also stained for CD45, Ter119 and CD31 to analyze hematopoietic cells, RBCs and endothelial cells [17], respectively.

We observed hematopoietic cells ($\text{CD45}^+/\text{Ter119}^+$) to be most drastically decreased from 58×10^6 cells at homeostasis to 1×10^6 cells per one femur and one tibia on day 7 post-transplant, which is congruent with the histological data (Fig 2.2C). Endothelial cells (CD31^+) decreased from 20×10^3 to 6×10^3 cells and stromal cells ($\text{CD31}^-/\text{CD45}^-/\text{Ter119}^-$) from 3.2×10^5 to 1.6×10^5 cells per femur and tibia on day 7 post-transplant. Only endothelial cells fully recovered homeostatic numbers at 7 weeks post-transplant. Within the stromal cell compartment, we observed an opposing behavior. Both in BLC, as well as in the flushed BM fraction, we observed an increase in pre-adipocyte numbers in the immediate post-transplant period. Pre-adipocytes ($\text{Sca1}^+/\text{CD24}^-$) increased both in number as well as in percentage of stroma before the peak of aplasia, which was previously defined between day 15 and day 20 post-transplant. In the BLC fraction, pre-adipocytes increased from 0.3 % to 4.9 % of total stromal cells on day 7 post-transplant (Fig 2.2D). This behavior was followed by a delayed increase in multipotent stromal cells ($\text{Sca1}^+/\text{CD24}^+$), which remained unchanged in the first two weeks post-transplant. Their mean relative contribution to the stroma of the flushed BM fraction however increased from 0.5 % to 6.7 %, which was represented by an increase from 2×10^3 to 13×10^3 cells per femur and tibia three weeks post-transplant (Fig 2.2E). Of note, absolute numbers per bone are useful for comparison across timepoints, but are known to constitute an underestimation of cell numbers as compared to 3D histological quantification in whole mounts [110]. This is due to the fragile nature of the stromal components and the difficulty to incorporate them into single cell suspensions for flow cytometry studies.

Taken together these results confirm our hypothesis that post-transplant BMAT expands by both hypertrophy and hyperplasia, the latter being sustained by an increase of pre-adipocytes, followed by a delayed increase in multipotent cells in the early yellow-to-red bone marrow transition. We have herewith uncovered the kinetics of the adipocyte formation in the early post-transplant period (the red-to-yellow transition), while fate of mature adipocytes in the hematopoietic recovery phase (the yellow-to-red bone marrow transition) has yet to be elucidated.

2.3.3 Searching for de-differentiation of BMA in the late post-transplant period

Theoretically, there are three main mechanisms by which adipocytes retreat in the late post-transplant period: (i) by inhibition of adipocyte differentiation, leading to death of mature adipocytes over time, (ii) by activation of apoptosis in mature adipocytes or (iii) by induction of de-differentiation of mature adipocytes into pre-adipocytic stromal cells. Given that adipocytes retreat as rapidly as they appear in the early post-transplant period, we hypothesize that, as in the model of de-differentiation from the study by Scherer et al [100], differentiated adipocytes revert to their pre-adipocytic stromal stage, primed to undergo the same process, if necessary. We therefore used a modified version of the 'Adipochaser' mouse model, where we used TdTomato as reporter molecule, rather than lac-Z, to facilitate flow cytometric analysis of stromal cells.

Given the kinetics of adipocyte expansion in the early post-transplant period, we aimed at investigating whether the increase in pre-adipocytic and multipotent stromal cells could additionally be explained by de-differentiation of mature adipocytes, as seen in the lactating mammary glands of mice [100]. We therefore performed a 'pulse-chase' lineage tracing experiment using a modified version of the 'Adipochaser' mouse model [60]. These transgenic mice express the 'tet-on' transcription factor rtTA under the control of the adiponectin promoter (Fig 2.3). These mice were crossed with both a tet-responsive CRE mouse line (activated in the presence of doxycycline) as well as the Rosa26-fl-STOP-fl-TdTomato mouse line (which expresses TdTomato in the presence of CRE). This way, and upon doxycycline treatment, all cells that have once expressed adiponectin, i.e. terminally differentiated into adipocytes were expected to stably express TdTomato throughout the experimental timeline. We decided to use a Doxycycline inducible lineage-tracer, since Tamoxifen has been reported to induce transient adipocyte apoptosis, followed by de novo adipogenesis [111].

Using the same transplantation procedure as Section 2.2 and 2.3, we extracted the BM fraction from one femur and one tibia per mouse to trace the origin of stromal cells formed in the late post-transplant period (Fig 2.4A-B). We marked all adiponectin expressing cells by providing the mice with Doxycycline-containing diet (600mg/kg), as previously described [88], between day 13 and day 20 post-transplant, which corresponds to the timeframe where adipocytes have expanded the most. Half the cohort of mice were sacrificed on day 21 post-transplant, the other half of the cohort was sacrificed on day 40 post-transplant. Doxycycline washout has been reported to be successful after one day in the 'Adipochaser' model [100]. If adipocytes give rise to stromal cells during the retreat of BMAT (the yellow-to-red BM transition), we would expect a higher ratio of TdTomato⁺ / TdTomato⁻ cells in the stromal fraction of bone marrow on day 40 than on day 21 post-transplant. In the experiment we used three major control groups, which consisted of mice negative for the TRE-Cre allele, mice not receiving Doxycycline and mice not undergoing transplant (homeostatic mice). All groups were assigned to both extraction days (days 21 and 40) to control for leakiness in the system. Indeed, we observed a dramatic increase of TdTomato⁺ stromal cells from 15.9 % on day 21 to 70.7 % on day 40-post-transplant, indicating some terminally differentiated adipocytes gave rise to cells in the stromal fraction (Fig 2.4C-D). Although this is indicative of adipocyte de-differentiation in the yellow-to-red bone marrow transition, it does not exclude the possibility of the other two hypotheses: (i) inhibition of adipocyte differentiation, leading to death of mature adipocytes over time (ii) activation of apoptosis in mature adipocytes. Additionally, we found that a significant number of non-stromal cells also expressed TdTomato, as seen in the DAPI-fraction (Fig S2.1A-C). This led us to find other three problems, which hindered us from exploring this hypothesis.

Firstly, we found that mice that were not treated with Doxycycline, had a similar percentage of TdTomato⁺ cells as mice treated with Doxycycline (Fig S2.1D). This leakiness was TdTomato expression was found in CD31⁺ endothelial cells and CD45⁺ hematopoietic cells. In addition, we encountered an age-related increase in TdTomato expression in both mice undergoing transplantation, as well as mice in steady-state (Fig S2.1E). Given the small number of animals used in this experiment, we were not able to quantitatively assess de-differentiation. We therefore conclude that the TdTomato doxycycline-inducible 'Adipochaser' reporter mice are leaky and that leakiness is age-dependent. Therefore, the question remains open whether de-differentiation of adipocytes is underlying the yellow-to-red bone marrow transition.

2.4 Discussion

The mechanisms of bone marrow adipocyte expansion in stress conditions such as irradiation remain unknown, largely due to the visual inaccessibility of adipose tissue within bones and the fragility of extracted bone marrow adipocytes. Hematoxylin- and Eosin-stained bone marrow sections remain the diagnostic standard of clinical patients and the main means of distinguishing red and yellow bone marrow. However, this method is inherently biased, given the subjectivity of the observer. In our lab, we therefore developed a plugin for ImageJ, that allows for semi-automatic quantification of images from bone marrow sections stained with Hematoxylin and Eosin. This allows the user to distinguish bone, RBCs, and adipocytes and nucleated blood cells and consequently quantifies the distribution of both yellow and red bone marrow. Considering the heterogeneous localization of adipocytes (in cMAT and rMAT) in the bone marrow, the sections had to be longitudinal across the entire length of the bone. Although our software is capable of eliminating retraction artifacts, the quantification of adipocyte size and number remains limited to the intactness of adipocyte membranes, often perturbed in the bone marrow by the fixation, decalcification and cutting procedures. In the absence of intact membranes, the program approximates the missing membranes based on circularity measures and watershed-based fragmentation, which in highly hemorrhagic samples can lead to overestimation of adipocyte numbers due to the empty space left in between red blood cells.

To more accurately quantify adipocyte distribution in the bone marrow, we tested a method of whole mount confocal imaging of femurs, which does not require decalcification, while only requiring a mild fixation, in order to keep the adipocytes intact and base adipocyte quantification on lipid content. Considering the relative much lower speed of acquisition and subsequent analysis, this method cannot be used to quantify large amounts of samples, and it was reserved as a validation method. Therefore, for our purposes, Hematoxylin and Eosin stained longitudinal cuts were sufficient to describe the kinetics of the red-to-yellow-to-red bone

marrow transition, which we found to be reproducible in the femurs of young female C57Bl/6J mice. We herewith were able to conclude that in murine femurs adipocyte expansion reached the peak between days 15 and 20 post-transplant and that this was contributed by both adipocyte hypertrophy and hyperplasia, as observed in other cases of peripheral adipose tissue expansion [88], [104]. Interestingly, we have observed that, in contrast to rMAT, the irradiation-induced increase in cMAT volume, does not significantly retreat to pre-transplant levels. This finding is in congruence with other studies suggesting rMAT undergoes more active resorption than cMAT [70], [71]. Whether adipocytes of the rMAT areas undergo active de-differentiation in the late post-transplant period (yellow-to-red transition), is a question that could be investigated using the 'Adipochaser' lineage-tracer model, the results of which, are discussed below.

Via peripheral blood cell counts as well as flow cytometric analysis of the bone marrow of mice undergoing transplantation, we demonstrated that the rapid expansion of bone marrow adipocytes in the early post-transplant period is inversely correlated to the hematopoietic activity of the bone marrow. HSPCs are rapidly depleted, recovering out of thrombocytopenic and severe neutropenic risk on days ($200 \times 10^3/\text{ml}$) and ($0.5 \times 10^3/\text{ml}$), respectively. At 7 weeks post-transplant, hematopoietic activity was limited to around 60 % of basal activity, based on total CD45⁺ and Ter119⁺ cell counts. CD31⁺ endothelial and CD31⁺/CD45⁺/Ter119⁺ stromal cell numbers were also decreased during peak aplasia. However, within the stromal bone marrow fraction, we observed an increase of the previously described Sca1⁺/CD24⁺ pre-adipocytic population [64] in the early post-transplant period. We therefore conclude that the increase in adipocyte numbers seen in the red-to-yellow bone marrow transition is preceded by an increase in pre-adipocytes. This expansion is then followed by an increase in multipotent Sca1⁺/CD24⁺ stromal cells. Whether the initial increase of pre-adipocytes is due to differentiation of multipotent stromal cells into pre-adipocytes, followed by a proliferation of multipotent stromal cells at a later time-point remains open to investigation. Also, given that pre-adipocytes and cells from the osteogenic lineage compete for the same precursor cells, the irradiation-induced effect on the kinetics of osteogenic cells post-transplant could shed more light on this question. Since these preadipocytic and multipotent stromal populations were identified in the context of obesity, our data confirms their existence in the red-to-yellow-to-red transition, which is induced by hematopoietic demand.

Finally, using a modified version of the 'Adipochaser' lineage-tracer mouse, we intended to track the fate of bone marrow adipocytes retreating in the yellow-to-red transition. A controlled experiment would be able to explore whether adipocytes are actively undergoing apoptosis or de-differentiating into pre-adipocytes. Given that the average adipocyte life-time (0.6% of peripheral adipocytes are renewed per day [105]) is much longer than the post-transplant period itself, it has to be ruled out that adipocytes retreat solely through passive means, i.e. by reaching their maximum lifetime. However, due to the unexpected complexity of Cre excision in TdTomato reporter mice, we were not able to trace the fate of retreating adipocytes. Two main issues of leakiness were identified in our setting: (i) mice not receiving doxycycline, exhibited strong TdTomato expression (ii) TdTomato expression was detected in compartments, which in normal conditions should not express adiponectin (hematopoietic and endothelial). Considering we have the same AdnP-rTA transgene and the same TRE-Cre strain as the original articles describing the 'Adipochaser' model with a Rosa26_{LSL}-LacZ reporter, the problem should therefore concern the Rosa26_{LSL}-tdTomato transgene. One possible cause is the Ai9 Cre reporter allele, which has been observed as very sensitive to Cre, as only low levels of the molecule are enough for excision, particularly in the bone marrow [112]. This may explain differences observed between the 'Adipochaser'-mT/mG mouse model and our 'Adipochaser'-TdTomato mouse. Cre expression even in the absence of doxycycline administration, may happen in two different ways: either the rTA binds to the TRE promoter, or Cre is expressed in absence of rTA. We therefore sought for the controls used in the original 'Adipochaser' studies and we found that no 'non-doxycycline-induced' controls were used in the 'Adipochaser'-mT/mG mouse, only for the 'Adipochaser'-lacZ [88], [100], [113], [114]. Control mice without the adiponectin-rTA transgene, were also only shown in the 'Adipochaser'-lacZ mouse [88], [114].

The observed leakiness in the hematopoietic and endothelial compartments however suggests that Cre may be expressed, even in absence of rTA. We therefore also extracted the stromal vascular fraction from extramedullary fat tissue and observed the same leakiness in hematopoietic and endothelial compartments (data not shown). In addition, tdTomato expression was not found in the BM of young mice, which indicates either that adiponectin is not expressed in the BM of young mice, or that the TRE-Cre transgene is inaccessible due to unknown factors (e.g. chromatin state). Assuming no leakiness within the TRE-Cre transgene, our data may have broader implications. The age-dependent differences in adiponectin-driven TdTomato expression within the stromal compartment, may explain incongruencies from recently published data. While one study suggests that multipotent stem cells generate bone and adipocytes in the adult [115], another suggests that the skeletal stem cells isolated from then metaphyseal plate in very young mice and adult fetus don't generate any adipocytes *in vivo* [76].

In this chapter we described the kinetics of BMAT expansion in the early post-transplant period (the red-to-yellow transition) and observed that it retreats in the late post-transplant period (the yellow-to-red transition), while the hematopoietic compartment recovers. The two largest compartments occupying the same bone marrow space, obliges them to tightly regulate each other, which is displayed by the high degree of plasticity of both the BMAT as well as the HSPC compartment. A summary of the findings and open

questions is depicted in Fig 2.5. All in all, the mechanism of BMAT retreat in the late post-transplant period therefore remains open to whether it is due to an activation of adipocyte apoptosis or due to a de-differentiation of adipocytes, as in Scherer's mammary gland model [100].

In the next chapter, we explore a new method to identify novel pharmacological modulators of adipocyte differentiation. Considering the highly debated active role of adipocytes toward hematopoietic stem and progenitor cells, we performed *in vitro* co-cultures of mesenchymal stromal cells and HSPCs to elucidate the effects of adipocyte differentiation on the regenerative function of HSPCs. The aim is to identify new drugs that may improve and accelerate hematopoietic recovery in a non-cell autonomous manner during the post-transplantation period.

2.5 Figures

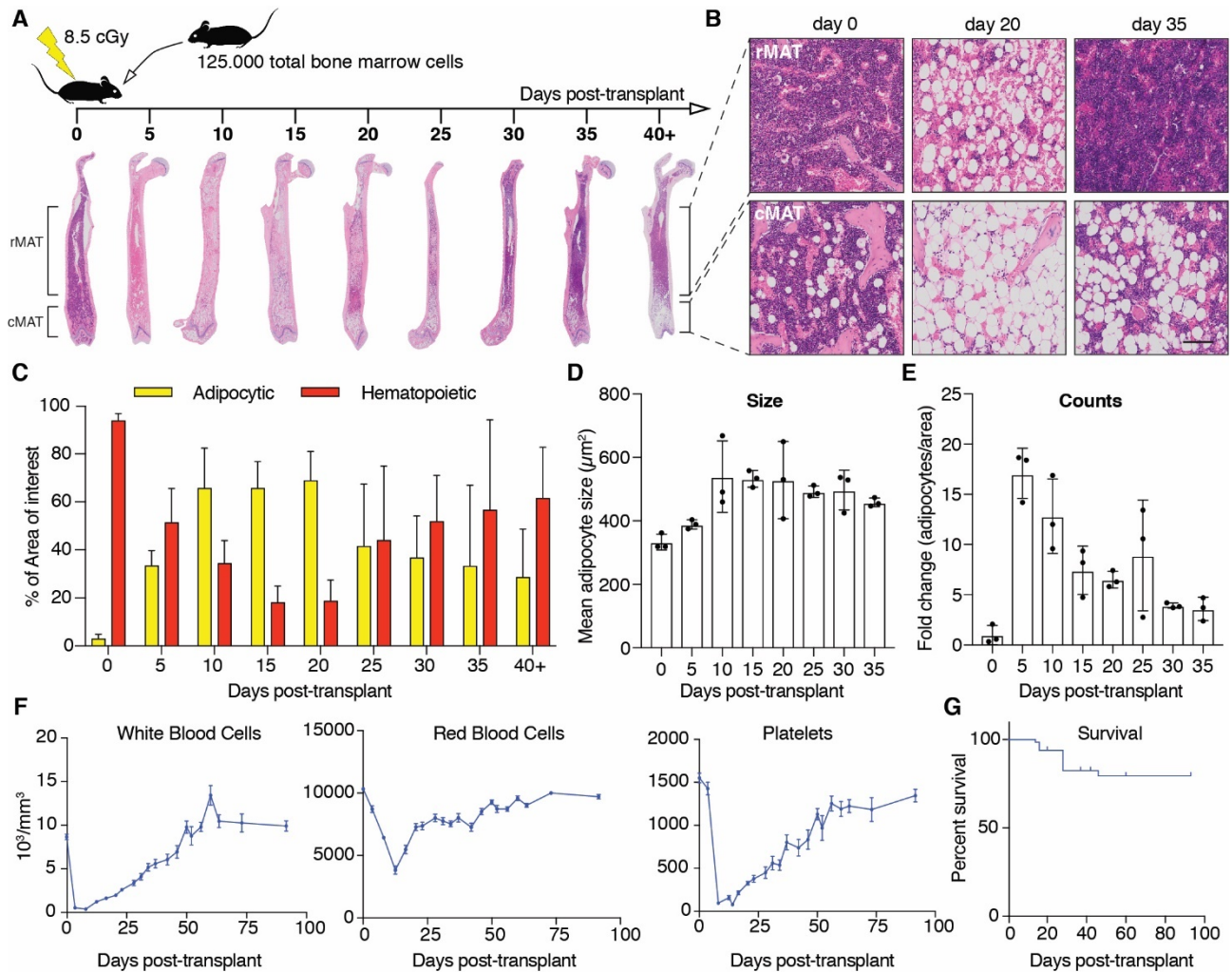


Figure 2.1 Kinetics of the red-to-yellow-to-red marrow transition following lethal irradiation and bone marrow transplantation. A. Schematic representation of the experimental setup. 8- to 12-week old female C57BL/6J mice underwent lethal x-ray irradiation (8.5 cGy) followed the next day by the transplantation of 125,000 total bone marrow cells from MHC-compatible C57BL/6J Ly5.1 mice via intravenous injection. Femurs were extracted every 5 days, processed for mid-sagittal cuts to cover the entire length of the bone and subsequently stained for hematoxylin and eosin (H&E). The cortical marrow contains regulated marrow adipose tissue (rMAT) or 'labile' adipocytes and the distal trabecular bone marrow contains constitutive marrow adipose tissue (cMAT) or 'stable adipocytes', which are less reactive to metabolic and hematopoietic demand. $n = 3$. **B.** Representative H&E images of rMAT and cMAT at homeostasis, day 20 and day 35 post-transplant. scale bar = 100 μm . **C.** Quantification of 'yellow' (adipocytic) and 'red' (hematopoietic) marrow areas using the ImageJ plugin 'MarrowQuant', a semi-automatic quantification tool developed in the lab by Josefine Tratwal and Chiheb Boussema. The entire area of the bone marrow was manually selected, whereas nucleated hematopoietic cells, red blood cells, adipocytes and bone could be distinguished by color thresholds. The area of adipocytes and hematopoietic nucleated cells was then automatically quantified. $n = 3$. Error bars are S.D. **D.** The mean size of adipocytes was quantified for each section using the same quantification tool. $n = 3$. Error bars are S.D. **E.** The adipocyte count was normalized to the manually selected area (AOI) and plotted as fold-change to steady-state (day 0). $n = 3$. Error bars are S.D. **F.** Circulating blood cell (CBC) counts, including white blood cells, red blood cells and platelets. These quantifications were compiled from seven independent experiments totalling 54 mice. **G.** Survival of 8- to 12-week old female C57BL/6J mice undergoing this transplantation procedure, compiled from seven independent experiments. $n = 54$.

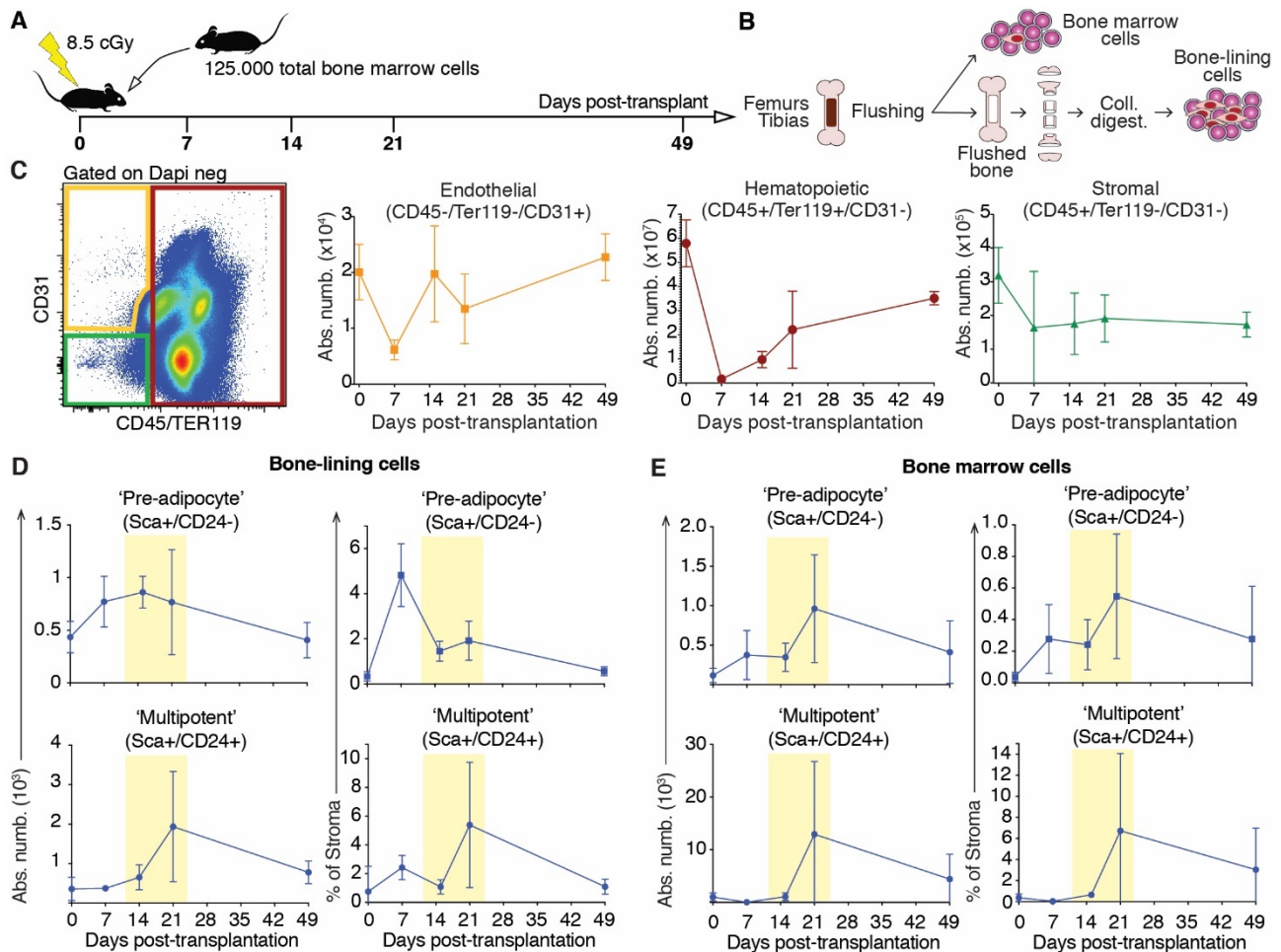


Figure 2.2 Kinetics of multipotent and pre-adipocytic stromal bone marrow cells in the red-to-yellow-to-red bone marrow transition. **A.** Schematic representation of the experimental setup. 8- to 12-week old female C57BL/6J mice underwent lethal x-ray irradiation (8.5cGy) followed the next day by the transplantation of 125,000 total bone marrow cells from MHC-compatible C57BL/6J Ly5.1 mouse via intravenous injection. One femur and one tibia were extracted per mouse on day 7, 14, 21 and 49 post-transplantation. *n* = 5. **B.** Schematic representation of the extraction of the flushed 'bone marrow' fraction and the collagenase-digested 'bone-lining cell' fraction. **C.** Flow cytometric gating strategy distinguishing endothelial (CD45⁻/Ter119⁻/CD31⁺), hematopoietic (CD45⁺/Ter119⁺/CD31⁻) and stromal (CD45⁻/Ter119⁻/CD31⁻) cells and subsequent quantifications of absolute numbers in the red-to-yellow-to-red bone marrow transition (from one femur and one tibia per mouse, *n* = 5). **D.** Kinetics of pre-adipocytic (Sca1⁺/CD24⁻) and multipotent (Sca1⁺/CD24⁺) stromal cells in the post-transplant period within the 'bone-lining' cell fraction, both in terms of absolute numbers (left) and as percentage of stromal cells (right). *n* = 5. **E.** Kinetics of pre-adipocytic (Sca1⁺/CD24⁻) and multipotent (Sca1⁺/CD24⁺) stromal cells in the post-transplant period within the flushed 'bone marrow' cell fraction, both in terms of absolute numbers (left) and as percentage of stromal cells (right). *n* = 5.

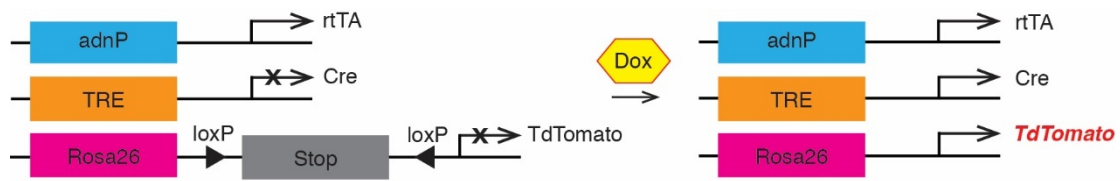


Figure 2.3 Schematic representation of the modified 'Adipochaser' mouse model. A. These mice contain three transgenes: (i) a adiponectin-driven 'tet-on' transcription factor (rtTA), (ii) a tetracycline-responsive element (TRE) expressing the Cre-recombinase and (iii) a TdTomato reporter within the Rosa26 locus, which is preceded by a Stop codon, preventing the expression of TdTomato. In the response to Doxycycline exposure (600mg/kg for one week in the diet), the Cre-recombinase excises the loxP-flanked Stop codon in the Rosa26 locus, therefore enabling the permanent expression of the TdTomato reporter molecule throughout the entire timeline of the experiment.

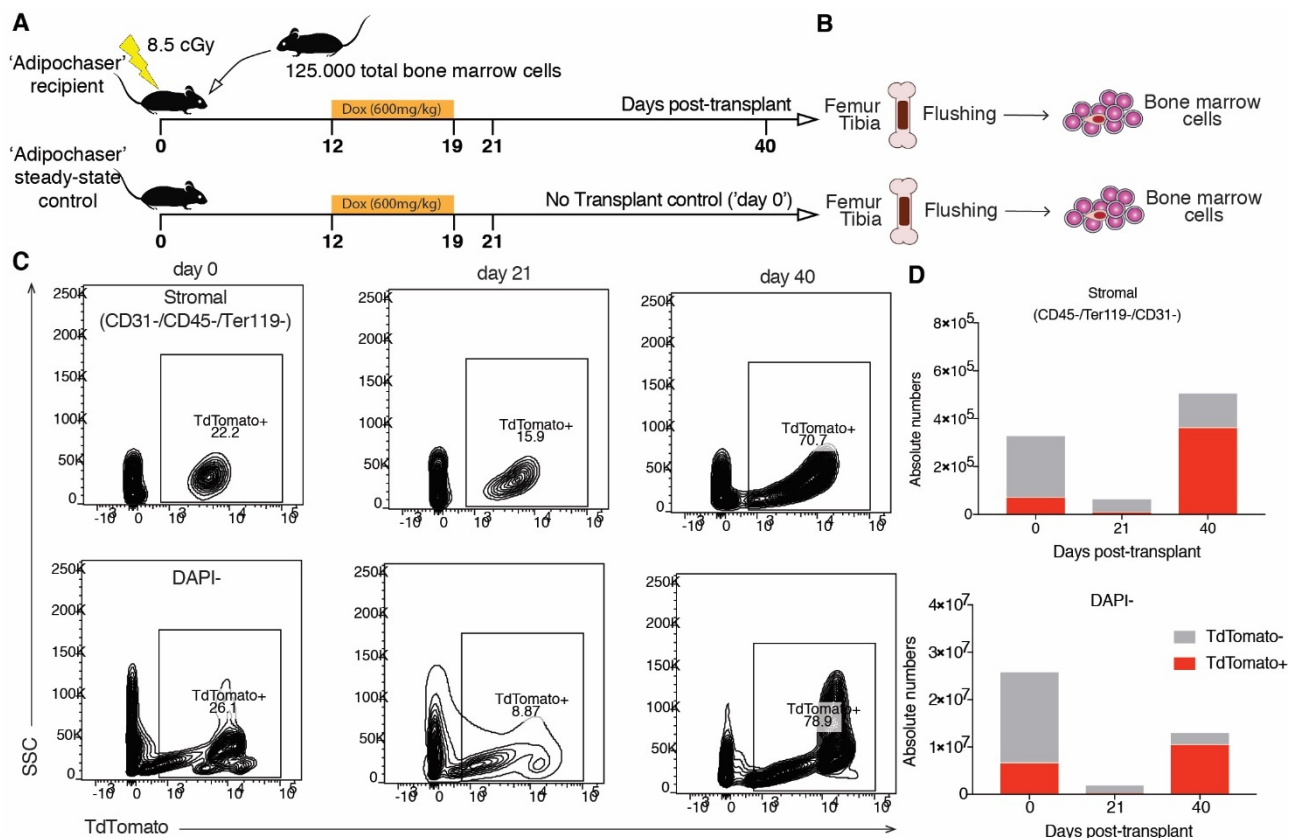


Figure 2.4 Searching for de-differentiation in the reatreating bone marrow adipose tissue (BMAT) during the late post-transplant period (the yellow-to-red marrow transition). **A.** Schematic representation of the transplantation procedure. 4-month-old 'Adipochaser' mice underwent lethal x-ray irradiation (8.5cGy) followed the next day by the transplantation of 125.000 total bone marrow cells from MHC-compatible C57BL/6J Ly5.1 mice via intravenous injection. 'Adipochaser' mice were given Doxycycline via diet (600mg/kg) between day 12 and day 19. One femur and one tibia was extracted per mouse on day 21 (peak of aplasia) and on day 40 post-transplant, to cover the beginning and the end of the yellow-to-red bone marrow transition. The controls used in this experiment include: (i) 'Adipochaser' mice, that are TRE-Cre^{-/-}, (ii) 'Adipochaser' mice not given Doxycycline and (iii) 'Adipochaser' mice not undergoing transplantation (steady-state control, or day 0 control). n = 1. **B.** Schematic representation of the flushed 'bone marrow' fraction. One femur and one tibia was flushed per mouse and stained for subsequent flow cytometric analysis. **C.** TdTomato expression in the stromal (CD45-/Ter119-/CD31-) cell fraction (top) and whole bone marrow (DAPI-) cells (bottom) on days 21 and 40 post-transplant as well as at homeostasis. **D.** Absolute number quantification of TdTomato+ stromal cells and DAPI- whole bone marrow cells on days 21 and 40 post-transplant as well as at homeostasis.

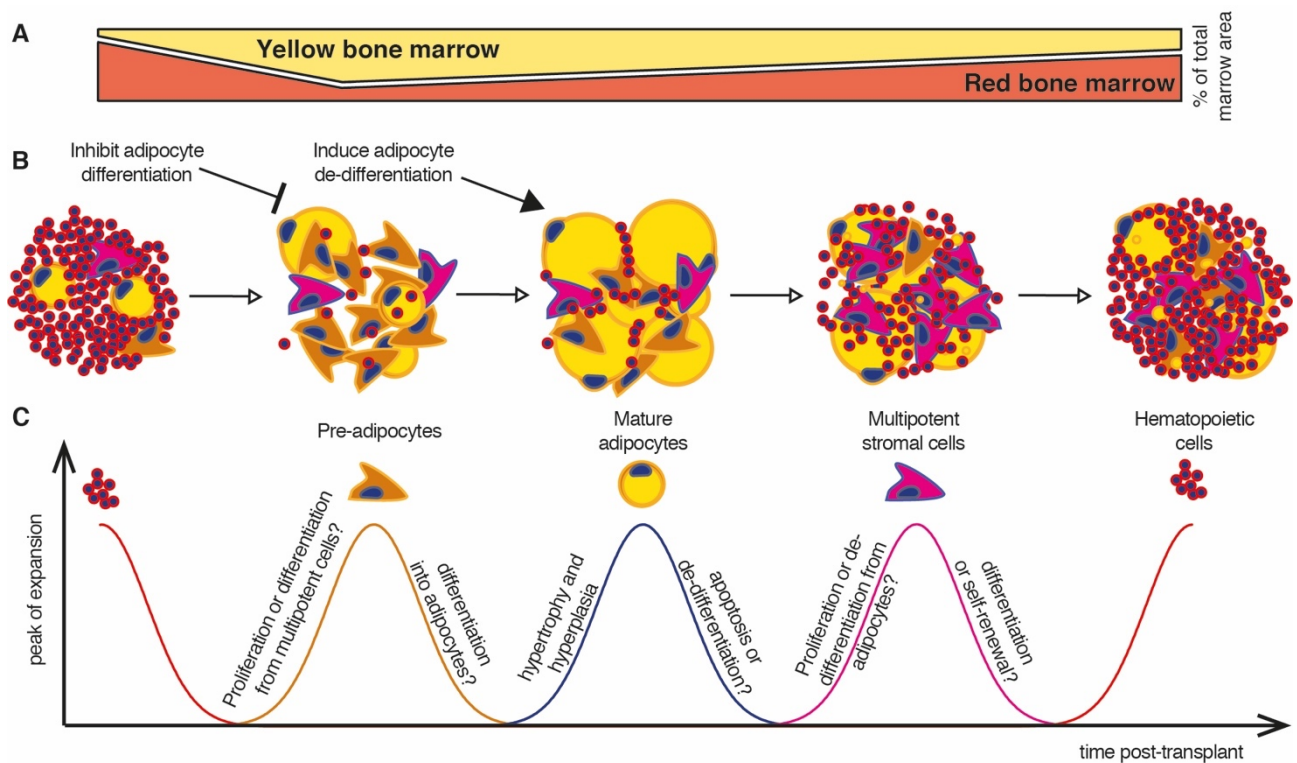


Figure 2.5 Schematic illustration of the kinetics of the red-to-yellow-to-red bone marrow transition following lethal irradiation and bone marrow transplantation. **A.** Schematic illustration of the areas occupied by red and yellow bone marrow along the post-transplant period. **B.** Schematic illustration depicting the analysed cell fractions during the different stages of the post-transplant period. **C.** Visualisation of the different waves of expansion of the analysed bone marrow cell populations during the post-transplant period. Hematopoietic cells are rapidly depleted within the first days following the irradiation and transplantation, due to the cytotoxicity of irradiation on cycling cells. This is followed by either a proliferation of pre-adipocytes or a differentiation of pre-existing multipotent cells into pre-adipocytes. We hypothesize that at this point, inhibition of adipocyte differentiation leads to an accumulation of hematopoietic-supportive multipotent cells and pre-adipocytes, therefore accelerating hematopoietic recovery post-transplant. The peak of the pre-adipocytic cell expansion is the earliest in the post-transplant period and we suggest that the fate of these cells is to ultimately differentiate into mature adipocytes. The bone marrow adipocyte expansion is characterized by both adipocyte hypertrophy as well as hyperplasia. After the peak of aplasia, the adipose tissue retreats, either by activation of apoptosis or by de-differentiation of adipocytes, which may be another target to accelerate the expansion of hematopoietic supportive multipotent and pre-adipocytic cells. Multipotent stromal cells expand in the late post-transplant period (yellow-to-red marrow transition) and this may be either due to proliferation or from de-differentiated (pre-)adipocytes. Nevertheless, the timing of multipotent stromal cell expansion coincides with hematopoietic recovery. At recovered homeostasis, the number of multipotent stromal cells can be regulated by a balance between self-renewal and differentiation.

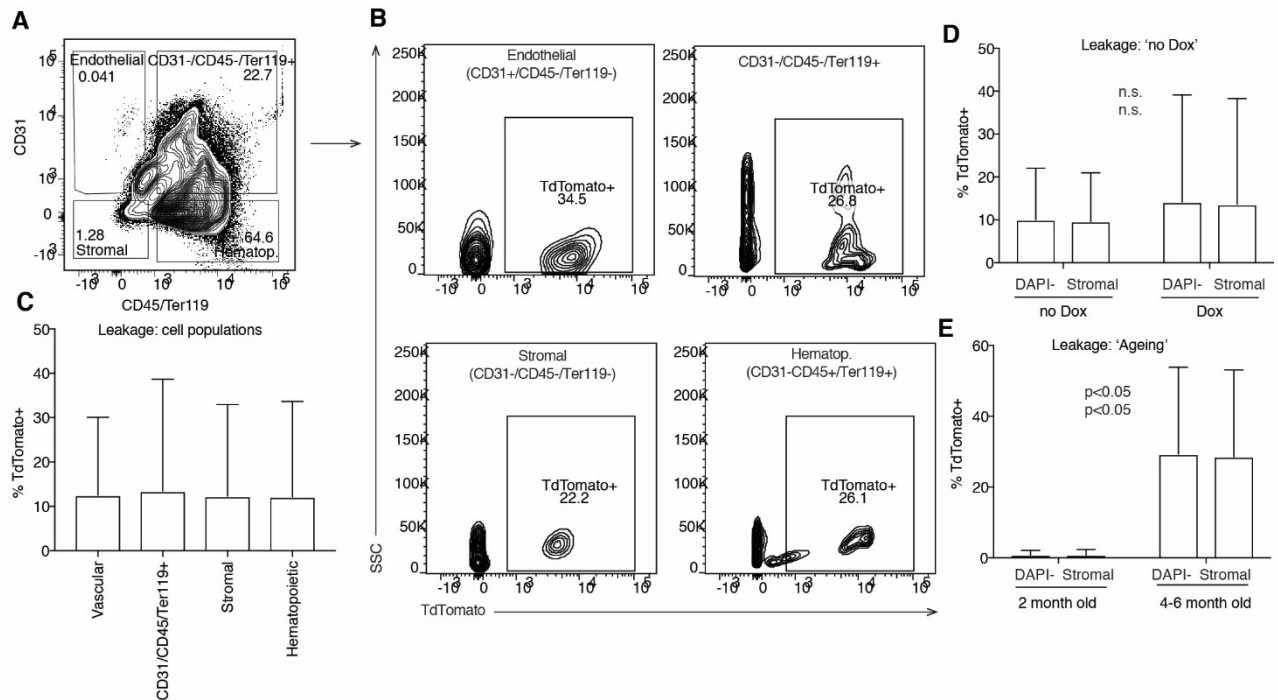


Figure S 2.1 Leakage issues encountered in the modified 'Adipochaser' mouse model. **A.** Flow cytometric gating strategy distinguishing endothelial (CD45-/Ter119-/CD31+), hematopoietic (CD45+/Ter119+/CD31-) and stromal (CD45-/Ter119-/CD31-) cells within the flushed 'bone marrow' cell fraction. **B.** TdTomato leakage in different cell types: endothelial, hematopoietic, stromal and triple-positive (CD45+/Ter119+/CD31+) cells. **C.** Quantification of TdTomato leakage, which includes: transplanted and non-transplanted young (2-month-old) and old 'Adipochaser' mice (4-6 month old), both male and female as well mice given Doxycycline and mice not given doxycycline. **D.** Quantification of TdTomato leakage in 'Adipochaser' mice not given Doxycycline. **E.** Quantification of TdTomato expression in young (2-month-old) and old (4-6 month old) 'Adipochaser' mice.

Chapter 3 High-throughput, non-perturbing quantification of lipid droplets with Digital Holographic Microscopy

Authors: Vasco Campos¹, Benjamin Rappaz², Fabien Kuttler², Gerardo Turcatti², Olaia Naveiras^{1,3}

Affiliations:

¹Laboratory of Regenerative Hematopoiesis (GR-NAVEIRAS), École Polytechnique Fédérale de Lausanne (EPFL), Lausanne, Switzerland

²Biomolecular Screening Facility (BSF), École Polytechnique Fédérale de Lausanne (EPFL), Lausanne, Switzerland

³Hematology Service, Department of Oncology, Centre Hospitalier Universitaire Vaudois (CHUV); Lausanne, Switzerland.

This work belongs to a manuscript prepared for the *Journal of Lipid Research*. Vasco Campos planned and executed the experiments, as well as wrote the manuscript. The goal of it was to develop a screening platform that would allow us to find novel inhibitors of adipocyte differentiation.

3.1 Abstract

In vitro differentiating adipocytes are sensitive to liquid manipulations and have the tendency to float. Assessing adipocyte differentiation using current microscopy techniques involves cell staining and washing, while using flow cytometry involves cell retrieval in suspension. These methods induce biases, are difficult to reproduce and involve tedious optimizations. In this study we present Digital Holographic Microscopy (DHM) as a label-free, non-perturbing means to quantify lipid droplets in differentiating adipocytes in a robust medium- to high-throughput manner. Taking advantage of the high refractive index of lipid droplets, DHM can assess the production of intracellular lipid droplets by differences in phase shift in a quantitative manner. Adipocytic differentiation, combined with other morphological features including cell confluence and cell death was tracked over six days in live OP9 mesenchymal stromal cells. We compared DHM with other currently available methods of lipid droplet quantification and demonstrated its robustness with modulators of adipocytic differentiation in a dose-responsive manner. Taken together, this study suggests DHM as a novel marker-free non-perturbing method to study lipid droplet accumulation and may be envisioned for drug screens and mechanistic studies on adipocytic differentiation.

Keywords: Adipogenesis, Lipid droplet, Holographic Microscopy, High-Throughput, Adipocyte

3.2 Introduction

Considering the prevalence of obesity and its rising burdens on the health and costs of western societies [116], [117], understanding the mechanisms underlying adipocyte physiopathology has become increasingly important. Central to the nature of adipocytes is the differentiation and subsequent lipid droplet accumulation in mesenchymal stromal cells (MSC) and pre-adipocytes [118]–[120]. Novel methods that are robust enough to detect early stages of differentiation would accelerate our understanding of metabolic diseases and other disorders involving lipid accumulation

Various methods have been used to quantify adipogenesis *in vitro* [121]–[127]. However, they all rely on liquid handling steps including fixation, diverse staining, imaging and image analysis procedures, which all require lengthy process optimizations and are therefore difficult to reproduce quantitatively [128]. Other methods rely on RNA quantification or biochemical assays, but these fail

to capture the morphological changes and single cell properties that define adipogenesis. One of the main challenges when assessing adipocytic differentiation is the extreme fragility of mature adipocytes. Not only are adipocytes sensitive to temperature fluctuations or oxygenation, but they also have a natural tendency to detach and float, which increases variation and quantification biases [129]. In order to avoid procedural biases, it has become standard to detect and assess adipocyte differentiation at early stages by using rapidly differentiating clonal lines [121]. This approach limits our understanding of the mechanisms of adipocyte differentiation to the existing lines and may fail replication in alternative lines. In addition, improving adipocyte differentiation detection methods would be compatible with measurements at earlier timepoints. Here we report a new method that enables detection of lipid droplets in differentiating adipocytes, without the need of washing, staining or other liquid manipulations. Digital Holographic Microscopy (DHM) allows for the reconstruction of images based on the ability of tissue to refract light [130], [131]. While the sample is illuminated with a laser emitting a specific wave, a reference beam passes in parallel to the sample and the combination of both waves creates a hologram encoding phase shift information [132]. Quantitative phase images are then numerically reconstructed from the hologram, which contains morphological and intracellular information related to the refractive index of the monitored cells. Lipids droplets have a higher refractive index, producing a very strong contrast and are thus easily quantified. The ability to numerically ‘refocus’ the image post-acquisition allows for rapid and non-invasive sampling [133]. In this study we used the bone marrow-derived MSC line OP9 [134], as it is both described as a model of rapid adipocytic differentiation and it was derived non-clonally, allowing us to assess the heterogeneity of cells undergoing adipocytic differentiation [135], [136]. We compared the ability of DHM to capture adipocytic differentiation with other existing quantification methods, including flow cytometry [137] and fluorescence imaging. We performed a timelapse analysis of OP9 adipocytic differentiation and tested the capacity of DHM to capture modulations of adipocytic differentiation using different enhancers and inhibitors added in a dose-responsive manner. Additionally, we showed how the optical phase shift could be used to quantify other morphological changes, including cell confluence and cell death. Taken together, these results point to DHM as being a rapid, robust, marker-free and non-perturbing method, suitable for medium- to high-throughput screenings of adipocytic differentiation.

3.3 Materials and Methods

3.3.1 Cell culture and adipocytic differentiation

OP9 cells (provided by T. Nakano, Kyoto University, Japan) were maintained in Minimum Essential Media alpha (MEMa) with GlutaMax™ (Gibco, 32561), 10 % FBS (Gibco, 10101) and Penicillin/Streptomycin (Gibco, 15140) at 37 °C, 5 % CO₂. The cells were split when subconfluent every 3 to 4 days. For every experiment the cells were plated at confluence, i.e. 20.000 cells per cm² (unless otherwise specified). Microscopy experiments were performed in 384-well plates, for which we plated 2000 cells per well in a volume of 30 µl using an automatic liquid dispenser. Tested compounds were plated before the cells using the ECHO500 acoustic dispenser (Labcyte, USA). Adipocytic differentiation was performed during 6 days using a differentiation cocktail containing Dexamethasone (Sigma, D4902, 10 µM), Insulin (Sigma, I0516, 5 µg/ml) and Isobutyl-methylxanthine (IBMX, I5879, 0.5 mM). The differentiation cocktail was added at double concentration in 30 µl of medium immediately after the cells were plated, making a final volume of 60 µl per well. For toxicity assessment, cells were incubated with Gambogic acid, Colchicine, Taxol and Staurosporine in concentrations ranging from 1 nM to 30 µM.

3.3.2 Microscopy

DHM technology and image reconstruction are described in detail elsewhere [130], [133], [138]. DHM is a label-free interferometric microscopy technique, which provides a quantitative measurement of the optical path difference (OPD, related to the optical density of the cell). It is a two-step process where a hologram consisting of a 2D interference pattern is first recorded on a digital camera (Fig. 3.1A), and the quantitative phase images are then numerically reconstructed using a specific algorithm (Fig. 3.1B). The phase contrast in DHM images is quantitatively related to the optical path difference (OPD, Fig. 3.1C), expressed in terms of physical properties as:

$$OPD(x,y) = d(x,y) \cdot [n_c(x,y) - n_m]$$

Equation 3:1 – Score definition in the primary screen

Whereas $d(x,y)$ is the cell thickness, $n_c(x,y)$ is the mean z-integrated intracellular refractive index at the (x,y) position and n_m is the refractive index of the surrounding culture medium. Simply, Equation 3:1 means that the OPD signal is proportional to both the cell thickness (providing information about cell morphology) and the intracellular refractive index (providing information about the intracellular content of the cells, mostly protein and lipid content).

DHM systems generally use a low intensity laser as light source for specimen illumination. Here, the 684 nm laser source delivers roughly 200 $\mu\text{W}/\text{cm}^2$ at the specimen plane, approximately six orders of magnitude less than intensities typically associated with confocal fluorescence microscopy. With that amount of light, the exposure time is only 400 μs . An extensive quality control of DHM can be found in (Rappaz, Cytometry A, 2008) [139].

Digital holographic imaging was performed in black wall 384-well imaging plates (Corning, 353962) using Transmission DHM® T1000 (Lyncée Tec, Switzerland). Plates were pre-coated with Poly-ornithine (Sigma, P3655, 100 mg/L) to prevent cell detachment. The cells were imaged live and without prior liquid manipulation using both a 10x/0.3 NA and 20x/0.4 NA microscope objectives. By taking four images per well we covered almost one fifth of the well surface (using the 10x objective). The best-focus phase images were reconstructed automatically in MATLAB (MathWorks, USA) from the acquired holograms and the average quantitative phase signal or optical path difference (OPD) [131] was automatically measured using a fixed threshold value.

Fluorescence Images were taken with the InCell Analyzer 2200 (GE Healthcare, USA) Imaging system. The neutral lipid droplets were stained with either LipidTox Deep Red (LifeTechnologies, 34477) at 1:500 or Nile Red (Sigma, N3013) at 10 μM . The nuclei were stained with Hoechst 33342 (1 $\mu\text{g}/\text{ml}$, ThermoFisher). For LipidTox imaging, the dyes were directly added to the wells, while for Nile Red imaging the dyes were added with new media. The wells were washed once with media after 30 min, as recommended by the manufacturer. For toxicity assessment, dead cells were stained using Ethidium-Homodimer (Invitrogen, E1169) and all cells were stained with Hoechst (33342, ThermoFisher), by directly adding the dyes into each well and imaging without any washing steps after 30 min incubation. As was done with DHM, four pictures were taken per well. Digital Phase Contrast images were additionally taken with the InCell Analyzer 2200.

3.3.3 Image processing

For Digital holographic imaging, the cells were first automatically segmented using a fixed threshold at a value slightly higher than the background to remove the contribution of noisy pixels. The average optical path difference (OPD) is then measured within the segmented cells. Subsequently, the value of the four images taken per well was averaged and used as the quantified value for adipocytic differentiation. To count cell numbers or to quantify dead cells with DHM images, a segmentation tool for CellProfiler software [140] was used (Ridler Calvard's algorithm). Cells were categorized to either 'undifferentiated', 'adipocytic', 'dead' or 'errors' within the machine learning-based CellProfiler Classifier. The cells were subsequently counted automatically, using either the Random Forest or k-Neighbors classification algorithms, with cells at the borders of the images excluded from the analysis.

Fluorescence images were processed using the CellProfiler image analysis software. Uneven illumination gradients were corrected using the CorrectIllumination modules through a Gaussian blur. For LipidTox Deep Red signal quantification, the intensity was measured in a radius of 20 μm around each Hoechst stained nucleus. For Nile Red signal quantification, a mask of the cytoplasm was first created using the faint membrane staining of Nile Red. The Nile Red fluorescence intensity of the lipid droplets was then measured within this mask and the median of all cells calculated for each image. For both Nile Red and LipidTox stains, the median fluorescence intensity was quantified within the masks, and the four pictures taken per well were then averaged. For Ethidium-Homodimer (Et-HD) signal quantification, an automatic threshold was used to segment the cells and a fixed threshold was used to set the separation between positive and negative cells. The ratios of Et-HD positive cells within all four images were calculated and averaged for each well.

3.3.4 FACS

OP9 cells were plated in pre-coated 6-well plates at a density of 20.000 cells per cm^2 and induced to adipocytic differentiation for 6 days. Previous to flow cytometric sorting, cells were stained with LipidTox Deep Red and Propidium Iodide (81845, Sigma-Aldrich) for 30 min, washed with PBS and subsequently detached by incubating for 5 min in 0.05 % trypsin-EDTA (Gibco, 25300) at 37 °C. The OP9 cells were then gently resuspended in PBS and sorted using the FACS Aria Fusion (BD Biosciences) Cell Sorter. They were collected into Eppendorf tubes, filtered using a 150 μm mesh and subsequently plated into black wall 384-well plates at a density of around 4000 cells per well. The settings for the side scatters (SSC) and the forward scatters (FSC) were based on the signal of non-induced OP9 cells as previously described [125].

3.3.5 RT-PCR

OP9 cells were plated in pre-coated 24-well plates at a density of 20.000 cells per cm^2 and induced towards adipocytic differentiation for 6 days as described above. RNA was extracted using ZR RNA Microprep (R1060, Zymo) following the manufacturers instructions. A DNase I digestion step was included. cDNA was synthesized using the SuperScript VILO cDNA synthesis kit (11754-050, Life

technologies) following the manufacturers instructions. Quantitative real time PCR was performed on a QuantStudio 6 (Life technologies) using the following primer pairs:

pparg: Fw 5'-ACCACTCGCATTCTTTGAC Rv 5'-TGGGTCAGCTCTTGTGAATG

c/ebpa: Fw 5'-GTTAGCCATGTGGTAGGAGACA' Rv 5'-CCCAGCCGTTAGTGAAGAGT

glut4: Fw 5'-GGCTTCTTCATCTTCACCTTC Rv 5'-TGGGTTTCACCTCCTGCTCT

adipoq: Fw 5'-TGTTCTCTTAATCCTGCCCA Rv 5'-CCAACCTGCACAAGTCCCTT

actb: Fw 5'-CTAAGGCCAACCGTAAAAAGAT Rv 5'-CACAGCCTGGATGGCTACGT

hprt1: Fw 5'-GCAGTACAGCCCCAAATGG Rv 5'-AACAAAGTCTGGCCTGTATCAA

The geometric mean of both housekeeping genes (*actb*, *hprt1*) was used as reference to calculate the Fold-expression of each gene relative to the samples of non-induced OP9 cells one day after plating.

3.3.6 Triglyceride (TG) content

OP9 cells were plated in pre-coated 24-well plates at a density of 20.000 cells per cm² and induced to adipocytic differentiation for 6 days. The cells were washed once with PBS and homogenized in 300 µl 10% Triton X (M143-1L, VWR). Triglycerides were solubilized by heating to 80°C in a water bath, cooling down to room temperature and repeating, before storing at -80°C. After thawing, 25 µl of each sample were taken for the biochemical assay using Triglyceride Quantification Colorimetric/Fluorometric Kit (K622-100, BioVision) following the manufacturers instructions in a 96-well black-walled plate. After 1-hour reaction the plate was read on an Infinite F5000 (Tecan, Switzerland) Spectrophotometer using the Ex/Em = 535/590 nm filter set for the Fluorometric assay. The background signal was subtracted from all samples and the Triglyceride concentration estimated using the linear standard curve, which was not forced to intercept the y-axis at y=0.

3.3.7 Protein content

The protein content was quantified in parallel using the same samples that were solubilized in 10 % Triton X for the TG content measurements. 25 µl of each sample were taken and measured using the Pierce BSA Protein Assay Kit (23227, Thermo Scientific) following the manufacturers instructions. After 30 min reaction the Absorbance was read on the Spectrophotometer using the 560 nm filter. The protein concentration was estimated using the linear standard curve, which was not forced to intercept the y-axis at y=0.

3.4 Results

3.4.1 DHM imaging is non-invasive and can be used to assess different features in lipid droplet accumulating cells

In this study, we show how the ability of DHM to detect morphology and refractive index in a non-perturbing manner makes this technique ideal to quantify lipid droplets in differentiating adipocytes.

We used the murine bone marrow-derived OP9 stromal cells [134]. OP9 cells have been characterized as a useful model to study adipocytic differentiation thanks to their rapid rate of lipid droplet accumulation [135], even at high confluence or over long culture periods. When observing the signal intensity histogram of the cross-section of differentiating OP9 cells, both the cytoplasmic signal and the highly refractive lipid droplets are clearly distinguishable from the background noise (Fig. 3.1E). This signal can also be used to assess different features of the cells including cell size, morphology and confluence. Using a machine learning-based CellProfiler Classifier, we were able to categorize cells and assign them to either 'undifferentiated', 'adipocytic' or 'dead' phenotypes. Undifferentiated cells were defined as large and with low OPD signal, adipocytic as large with high OPD signal and dead cells as small and round with a high OPD signal. We plated OP9 cells at different concentrations, imaged them after 24 hours and counted individual cells (result of the CellProfiler segmentation in Fig. 3.1F). As expected, a higher proportion of cells were detected in wells, which were initially seeded at a higher concentration (Fig. 3.1G). The exponentiality of the curve may represent the proliferation kinetics of cells; a higher initial cell number will predict a greater increase in cell numbers after 24 hours. To assess the capacity of our workflow to detect dead cells, we first incubated OP9 cells with different known toxic compounds and acquired DHM images. The cells were then

stained with Ethidium-Homodimer (Et-HD) and Hoechst 33342 (for dead cells and total cells respectively) and imaged using the InCell Analyzer 2000 (GE Healthcare). We plotted each well and compared the fraction of Et-HD positive cells from the fluorescence images with the fraction of dead rounded cells detected in DHM images. This correlation is linear with $R^2=0.85$, $p<0.0001$ (Fig. 3.1H). The variability is increased with a higher proportion of dead cells, which may be due to dead cells detaching from the bottom, characterized by a shift towards the right of the correlation curve.

3.4.2 DHM can be used to assess adipocytic differentiation.

To assess the capacity of DHM imaging to recapitulate the quantification of lipid droplets, we compared it to classic imaging of stained neutral lipids. Specifically, we compared the OPD signal with the fluorescence signal of both LipidTox Deep Red and Nile Red along a 6-day adipocytic differentiation period (Fig. 3.2). Due to the preadipocytic nature of OP9 cells, around 5% of the cells spontaneously differentiate towards adipocytes when left confluent over 6 days (data not shown). The DHM images detect changes in differentiation after 2 days in culture ($Z'=-2.2$, 0.06, 0.23, 0.53, 0.65 and 0.6 for day 1-6 respectively; Fig. 3.2A and 3.2C), while it takes at least 5 days to see any detectably stained lipid droplets by fluorescence images (Fig. 3.2B and 3.2D-E). Unfortunately, on the day 4 datapoint the Nile Red staining did not yield sufficient cytoplasmic membrane staining, which in turn, reveals a low overall intensity of lipid droplet quantification and thus reveals an outlier datapoint (Fig. 3.2E). This common artifact highlights the advantages of an alternative non-perturbing method to quantify lipid droplet accumulation. DHM reduces the number of variables introduced into each experiment, thus increasing the robustness and reproducibility of lipid droplet quantification. The DHM-derived OPD signal correlates non-linearly with both the LipidTox Deep Red and Nile Red Fluorescence signal with $R^2=0.6$ and $R^2=0.54$ respectively, $p<0.0001$ (data not shown).

In parallel, we quantified biochemically both the Triglyceride (TG) and the protein content over the course of the 6-day adipocytic differentiation (Fig. 3.3A-B). As expected, the protein content stays relatively constant, while the TG-content increased almost 30-fold, reaching the plateau on day 4 to 5 post-induction. For comparison, the TG-content of OP9 cells increased almost 5-fold over 6 days without induction of differentiation. We also analyzed the transcriptional profile using a set of known markers of adipocyte differentiation and function. We quantified two transcription factors (*pparg* and *c/ebpa*) and two functional adipocyte markers (*adipoq* and *glut4*). Owing to the pre-adipocytic nature of OP9 cells, all gene transcripts were upregulated after 6 days, even without induction of differentiation (Fig. 3.3C). Induction of adipocytic differentiation significantly increased the transcription of all analyzed genes (*pparg* increased 2.5-fold; *c/ebpa* increased ~10-fold; *glut4* increased ~20-fold and *adipoq* increased ~30-fold). All gene transcripts measured plateaued at 5 days of differentiation.

Further, we stained OP9 cells with LipidTox Deep Red and sorted them based on their granularity as previously shown [125], [137] (Fig. 3.4A). Note that the dynamic range and resolution of cells exhibiting different levels of adipocytic differentiation was higher in the SSC in linearity than along the fluorescence axis in exponentiality. The cells were plated and underwent DHM imaging 24 hours later (Fig. 3.4C). As expected, cells with a higher initial SSC signal also had a higher OPD signal. Of note, cells sorted from the A3 gate (representing the most mature adipocytes), exhibited less adherent behavior, explaining why the cell density is lower on their corresponding images. These mature, A3 cells, also appeared rounder, although their OPD signal was not significantly different (Fig. 3.4B).

3.4.3 DHM imaging is robust and high-throughput

Finally, we assessed the capacity of DHM imaging to identify modulators of adipocytic differentiation in a high-throughput manner. We cultured OP9 cells with known enhancers (Rosiglitazone, Pioglitazone, Indomethacin) of adipocytic differentiation (Fig. 3.4A, right half) as well as with known PPAR γ inhibitors (T0070907, GW9662, BADGE, Fig. 3.4A, left half) in a dose-responsive manner in a 384-well plate. Inhibitors of adipocytic differentiation were plated in combination with the adipogenesis induction cocktail DMI to test the strength of their inhibitory capacities. The compounds were tested in 14 different concentrations ranging from 100 μ M (Fig. 3.4A, Top) to 4.6 nM (Fig. 3.4A, Bottom). As visualized from the images, PPAR γ -inhibitors increasingly prevent adipocyte differentiation at higher concentrations while adipogenesis enhancers trigger adipocytic differentiation more efficiently at higher concentrations. As shown in the high magnification inserts, PPAR γ -inhibitors are toxic at high concentrations (>10 μ M), making the cells appear round with a high phase shift signal (Fig. 3.4A). T0070907 presented the most potent effect of the three tested inhibitors, and can revert the OPD signal back to control levels before reaching toxic concentrations. Specifically, T0070907 exhibited an $IC_{50}=1.49$ μ M, GW9662 $IC_{50}=4.49$ μ M and BADGE $IC_{50}>100$ μ M (Fig. 3.4B). Within the enhancers of adipocyte differentiation, Rosiglitazone exhibited the most potent effect with an $IC_{50}=19.5$ nM, while Pioglitazone and Indomethacin had IC_{50} values of 1.23 μ M and 2.77 μ M, respectively (Fig. 3.4C).

3.5 Discussion

OP9 cells are bone marrow-derived MSCs/pre-adipocytes that can efficiently differentiate into adipocytes [134], [135], [141]. Their differentiation process can be studied from day 2, is characterized by the early expression of PPAR γ , C/EBP α , C/EBP β and SREBP1 [135] transcription factors. PPAR γ is a master regulator of adipocytic differentiation. It translocates to the nucleus upon activation and drives adipocytic commitment, while preventing the cells from differentiating along the osteogenic lineage by directly inhibiting *runx2* transcription [142]. In addition, OP9 cells are non-clonal, allowing us to evaluate heterogeneity within differentiating cells.

Label-free and non-invasive imaging of *in vitro* differentiating adipocytes is crucial to limit the adverse effects caused by staining, washing and other liquid manipulations used in fluorescence microscopy. In this study, we have shown that the quantitative phase images generated by holographic microscopy are able to provide a variety of information on cell morphology including cell confluence, cell death and lipid droplets in a non-perturbing manner, thus reflecting true physiologically relevant measurements. Using the freely available machine learning plugin for CellProfiler we were able to categorize OP9 cells into ‘adipocytic’, ‘undifferentiated’ or ‘dead’ phenotypes. The information given on cell confluence and categorization can also be envisioned to study hypertrophy vs. hyperplasia behavior in differentiating adipocytes. To quantify adipocytic differentiation in bulk, simply the optical path difference (OPD) within the cytoplasmic areas provided an accurate quantification of lipid droplets. We correlated the OPD measurement to fluorescence microscopy: Ethidium-Homodimer/Hoechst 33342 co-staining for cell death and LipidTox Deep Red/Hoechst 33342 co-staining for lipid droplets. Variations caused by liquid manipulations, illumination irregularities, dependence on dye concentrations, staining times and bleaching are key issues in fluorescence microscopy and therefore strongly compromise quantification accuracy and robustness. DHM proved to be more sensitive than fluorescence microscopy, allowing detection of differences in adipocyte differentiation up to three days earlier. Another key feature of DHM is that multiple independent timepoints can be measured; the same cells were imaged in a timelapse without any of the compromises of fluorescence microscopy. In our study, we took four pictures per well on a 384-well plate, which took roughly 10 min. The ability to digitally re-focus on the cells post-imaging speeds up the process of data collection and adds to the simplicity of the imaging procedure towards a higher throughput. We also compared DHM imaging with flow cytometry, another validated strategy of adipogenesis quantification. In this case, DHM quantification also correlates with the flow cytometric measurement. However, within late-stage differentiating adipocytes, the increase in OPD signal does not seem to increase significantly, which may be due to floating cells not being measured at late differentiation stages with DHM. Quantification of lipid droplets using flow cytometry is also limited by variabilities in cell collection, cell floating and the fragility of terminally differentiated adipocytes. We further tested the robustness of DHM to assess lipid droplet accumulation in differentiating adipocytes by incubating OP9 cells with PPAR γ agonists and antagonists in a dose-responsive manner. We were able to calculate the IC₅₀ for each of the tested compounds and showed that, with high doses of PPAR γ agonists, adipocytic differentiation can be pushed further than with our standard differentiation cocktail. Taken together, our study shows that this novel, non-perturbing imaging method can be used to assess a variety of morphological features without the need of developing lengthy and tedious staining protocols. The DHM, besides reducing costs in consumables, is therefore a powerful tool envisioned for future drug screenings and mechanistic studies on adipocyte differentiation.

3.6 Acknowledgements

This work has been funded by the Swiss National Science Foundation (SNSF), the “Fondation Pierre Mercier pour la Science” and the “Fondation Dr Henri Dubois-Ferrière Dinu Lipatti” (DFDL). We thank the Fundacion Josep Carreras and the European Hematology Association (EHA), who financed the preliminary work, which led to this study. We also acknowledge the BSF-ACCESS screening platform at the EPFL and the support of SNSF/NCCR Chemical Biology. Finally, we thank the FACS facility at EPFL for performing the sort, Aurelien Oggier for his help in performing the biochemical assays and the qPCR experiments and Julien Bortoli Chapalay for plating compounds.

3.7 Figures

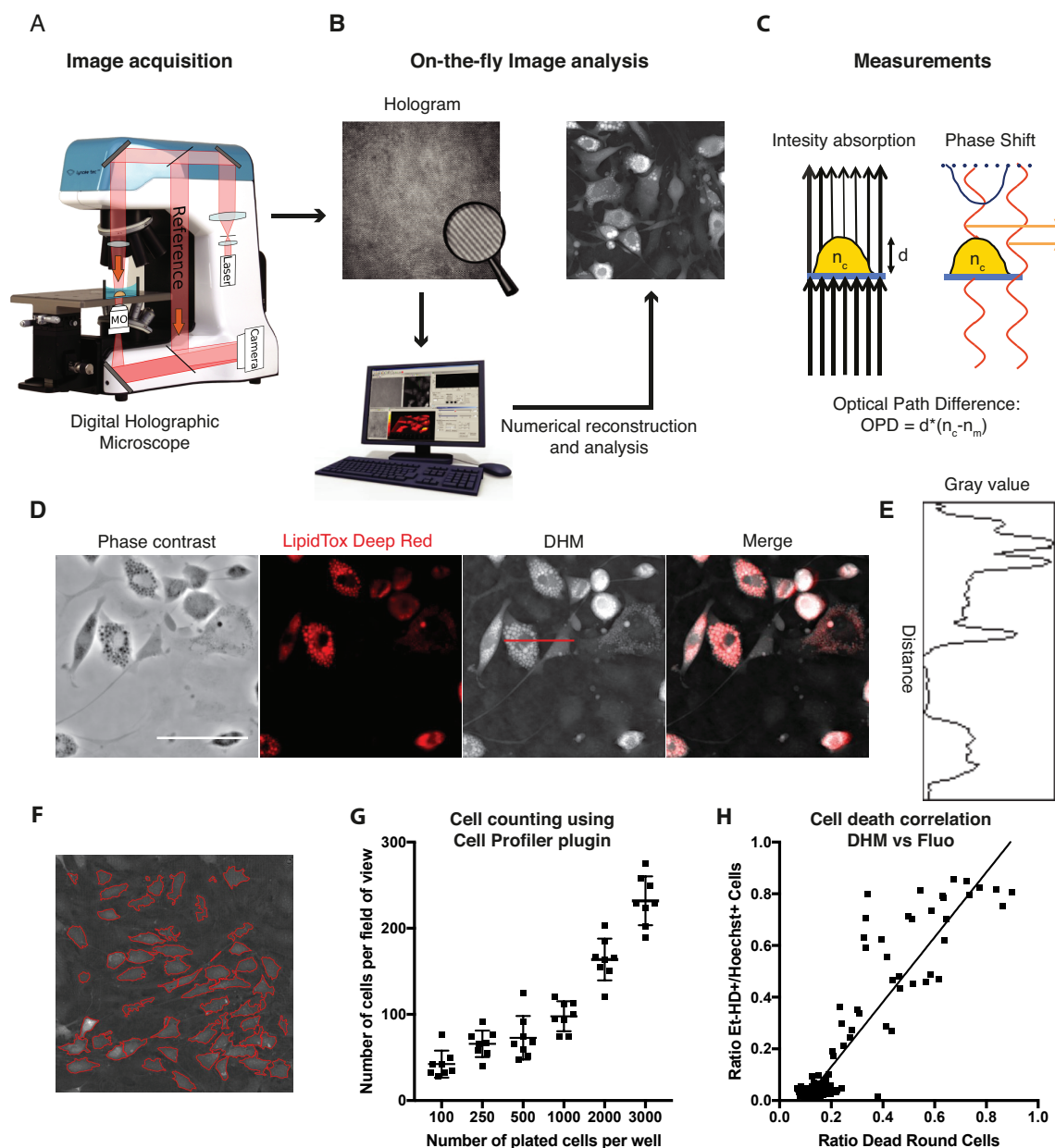


Figure 3.1 Digital Holographic Microscopy (DHM) is non-invasive and can be used to assess different features in lipid droplet accumulating cells. **A:** Schematic representation of DHM image acquisition. An infrared laser beam passes through the sample, while a reference beam passes in parallel without crossing the sample. **B:** Image reconstruction and analysis. The superimposition of both waves creates a hologram containing the phase shift information, which can then be mathematically reconstructed into a single-plane image. **C:** Information contained within the hologram. In addition to the phase shift information, DHM records the intensity absorption **D:** Superimposition of fluorescence lipid staining with DHM image. On the left, a Digital Phase Contrast image (non-quantitative) and LipidTox Deep Red fluorescence images. On the right the superimposition of LipidTox Deep Red signal with DHM signal. **E:** Signal intensity histogram of the cross-section seen as a vertical red line passing through a lipid droplet-accumulating cell on the DHM image in Fig. 1D. **F:** CellProfiler Software image analysis detects single cells, represented by their red outlines. Cells touching the borders are excluded. **G:** Cell counting using the aforementioned CellProfiler plugin. Increasing numbers of cells were seeded into a 384-well plate and counted from DHM images acquired 24 hrs after plating. **H:** Correlation of detection of OP9 dead cells exposed to various toxic compounds from DHM images as compared to fluorescence images from Ethidium-Homodimer and Hoechst 33342 stains. Dead cells were defined in the CellProfiler plugin as small rounded with a high phase shift signal. Error bars are S.D. Scale bar = 100 μ m.

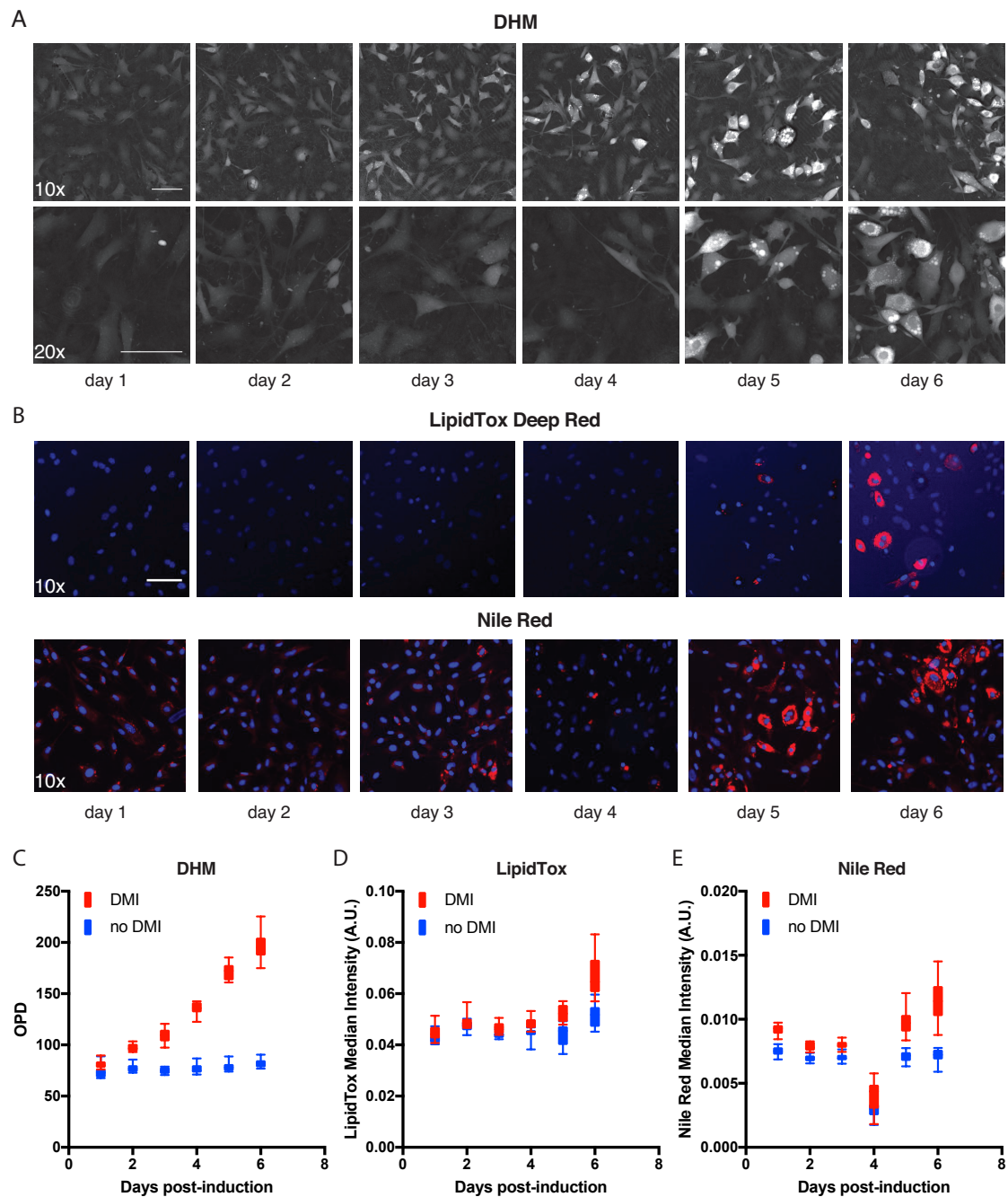


Figure 3.2 6-day timelapse of OP9 cells induced to differentiate towards adipocytes: Comparison of DHM and fluorescence microscopy. A: DHM images from day 1 to day 6 post-plating and induction. Top 10x, bottom 20x. **B:** Fluorescence images taken from day 1 to day 6 post-plating and induction. Blue is Hoechst 33342 and Red is either LipidTox Deep Red (top) or Nile Red (bottom). **C:** Optical Path Difference (OPD) values of OP9 cells induced to differentiate (red) versus non-induced OP9 cells (blue). **D-E:** LipidTox Deep Red and Nile Red median signal intensities in both induced and non-induced OP9 cells. Note the error during the Nile Red staining procedure on day 4 post-induction of adipocytic differentiation. $R^2=0.6$ for OPD vs. LipidTox Deep Red and $R^2=0.54$ for OPD vs. Nile Red. Error bars are S.D. Scale bar = 100 μm .

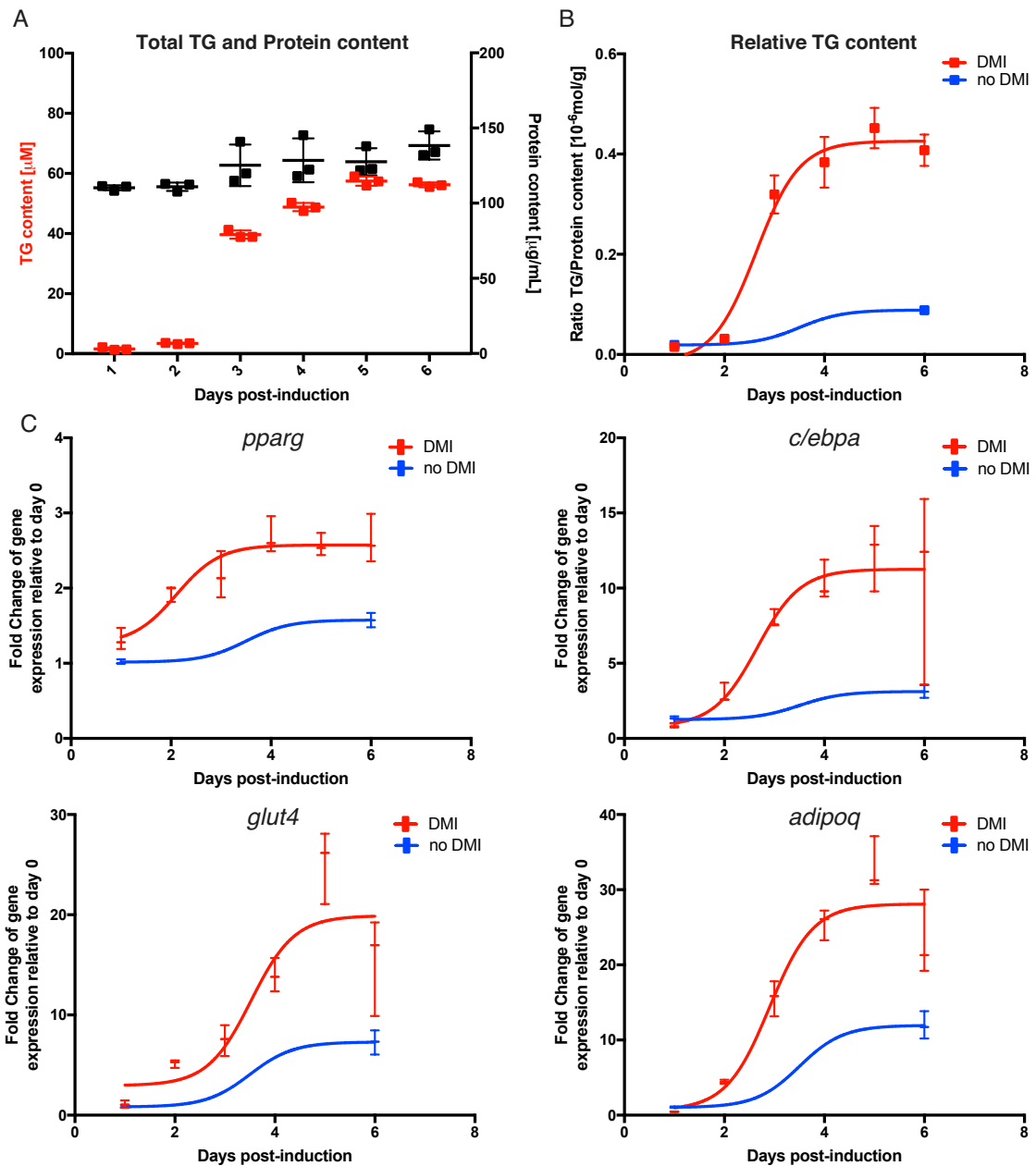


Figure 3.3 Total TG and protein content of OP9 cells during the 6-day adipocytic differentiation. A: Quantification is based on the standard curve from the manufacturer's control. B: Relative TG content over protein content during the 6-day differentiation. C: The transcriptional profile of relevant genes involved in the adipocytic differentiation of OP9 cells. Values are normalized to non-induced OP9 cells 1 day post-plating and the geometric mean of two housekeeping genes: *hprt1* and *actb*. Error bars are S.D.

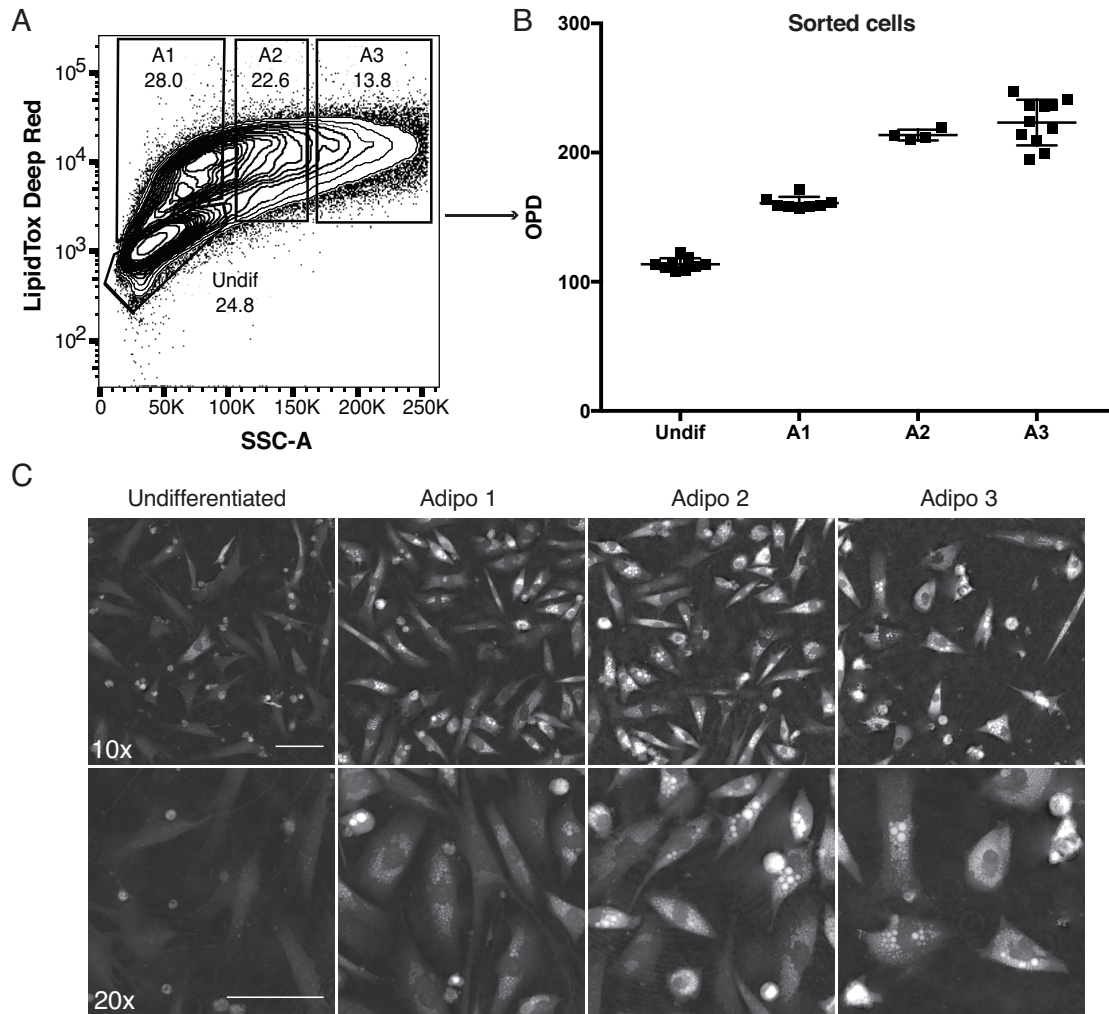


Figure 3.4 OPD signal of FACS-sorted OP9 cells induced to differentiate towards adipocytes during a time period of 6 days. **A:** Flow cytometric gates were chosen along the Side-Scatter signal (representing different stages of lipid accumulation), sorted separately and subsequently plated into a 384-well plate. **B:** Average OPD signal of sorted OP9 cells 24 hrs after plating. Images without cells were removed from analysis. **C:** Representative DHM images of sorted OP9 cells. Top 10x, bottom 20x. Error bars are S.D. Scale bar = 100 μ m.

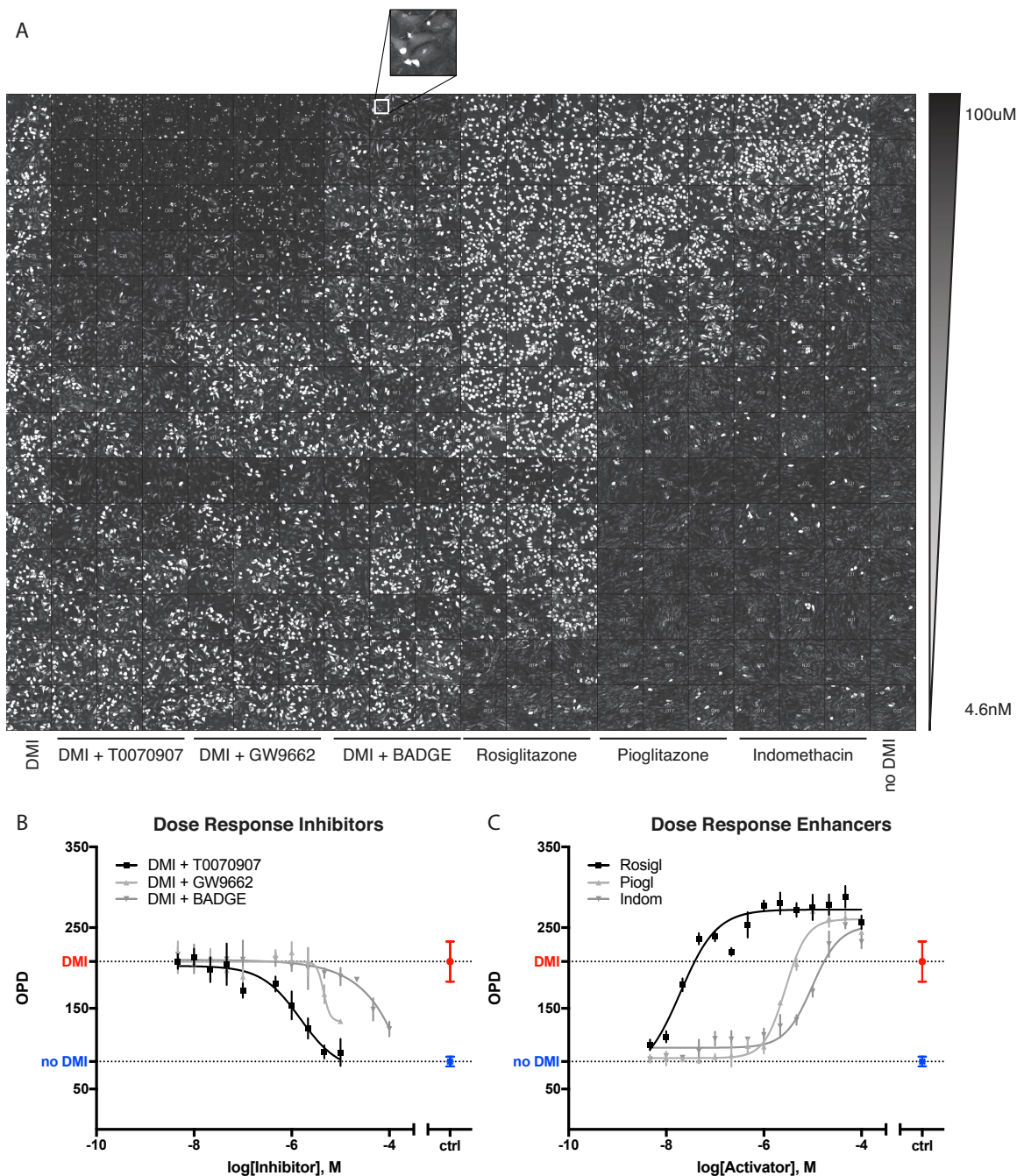


Figure 3.5 DHM imaging can be used to identify inhibitors and enhancers of adipogenesis in a high-throughput manner. **A:** Snapshot of a 384-well plate presenting a montage of DHM images of OP9 cells incubated with different PPAR γ antagonists and agonists at different concentrations (one image per well). On the left half of the plate, OP9 cells were induced to differentiate to adipocytes while incubated with different PPAR γ inhibitors (T0070907, GW9662 and BADGE). On the right half of the plate, OP9 cells were not induced with the standard differentiation cocktail, but incubated with different PPAR γ agonists (Rosiglitazone, Pioglitazone and Indomethacin). The small inlet on the top shows dead cells **B:** Dose-response curves of different tested PPAR γ inhibitors. **C:** Dose-response curves of the different tested PPAR γ agonists. Dashed lines represent baseline OPD values for induced (DMI) or non-induced (no DMI) OP9 cells. Error bars are S.D.

Chapter 4 Accelerating hematopoietic recovery post-transplantation

Vasco Campos planned and executed the experiments as well as wrote this chapter. The *in vivo* work was performed with the technical help of Dr. Shanti Rojas-Sutterlin, Josefine Tratwal and Aurelien Oggier. The experiment in Fig. 4.5B was performed by Dr. Nicola Vannini. RNA sequencing was performed in collaboration with the laboratory of Bart Deplancke, with the help of Pernillie Rainer (data analysis) and Dr. Daniel Alpern (brb-seq).

4.1 Introduction

Hematopoietic Stem Cells (HSCs) reside in the bone marrow, which tightly regulates the balance of quiescence, self-renewal and commitment towards progenitor cells by an input of different soluble and immobilized factors as well as cell-to-cell contacts [46]. This highly plastic niche has been associated with four main cellular players (osteoblasts, stromal cells, endothelial cells and adipocytes) [47]. Bone marrow stromal cells (BMSCs), which constitute the progenitors of both osteoblasts and adipocytes [6], have been shown to express high levels of Cxcl12, V-CAM, Ang-1 and SCF, all key cytokines for the homing and maintenance of HSCs. In accordance to these findings, many BMSC-like cell lines have been implicated in supporting hematopoiesis both *in vitro* and *in vivo*, which have come to complete the paradigm of osteoblasts and endothelial cells to constitute the dual HSC niche [54], [134]. BMA tissue expansion can follow a variety of stimuli and physiological conditions is both highly dynamic and reversible. Most notably, and paradoxically, it expands both in obesity as well as in caloric restriction [90], [91]. BMA content is also increased at the expense of bone formation, as seen in osteoporotic patients or patients following anti-diabetic TZD treatments and immunosuppressive glucocorticoid treatments [92]–[96]. The study by Naveiras et al observed that in mice, bone marrow adipocytes had negative effects on hematopoietic regeneration [62]. The authors suggested that HPSCs from highly adipocytic bone marrow compartments, such as the distal part of the limb bones and posterior vertebrae had a decreased hematopoietic regenerative capacity. In addition, they showed that preventing adipocyte differentiation using Bisphenol A diglycidyl ether (BADGE) in the early post-transplant period, which is when adipocytes take up most of the marrow space, accelerated hematopoietic recovery. The authors finally proposed to indirectly target HSC proliferation through manipulation of their niche as a complementary strategy to improve post-transplant survival. This study revived the interest in the long forgotten but nonetheless most abundant cell type of the human adult bone marrow and was reproduced by others with some limitations. The study by Zhu et al [143] demonstrated that BADGE also accelerated hematopoietic recovery in mice where hematopoietic aplasia was chemotherapy-induced (Arabinosylcytosine; Ara-C). The authors demonstrated an increase in CD45⁺ hematopoietic stem and progenitor cells (HSPC) as well as higher CFU activity in BADGE-treated mice, however the levels of Cxcl12 were paradoxically decreased. In addition, in an aplastic anaemia model (T-cell-mediated bone marrow failure), another study demonstrated an attenuation of hematopoietic failure in mice treated with the PPAR γ -inhibitors BADGE and GW9662 [144]. However, they suggested this to be mediated by a decreased activation and subsequent infiltration of T-cells into the bone marrow. *In vitro* however, undifferentiated or pre-adipocytic populations may have different HSC niche functions as compared to mature adipocytes. Transcriptional profiling of *in vitro*-differentiating C3H10T1/2-derived lines suggested cells of the adipocyte lineage to support hematopoiesis through higher expression of Ang-1, SCF and Cxcl12, while terminally differentiated adipocytes decreased the expression of these key cytokines [87]. Long-term co-cultures of mature adipocytes with bone marrow HSPCs maintained survival of LT-HSCs, while progenitor proliferation was supported by the undifferentiated stroma in mice and human cells [85], [86].

The role of bone marrow adipocytes in regulating hematopoiesis, therefore, remains largely unknown and more complex than originally thought. However, we argue that the definition of mature adipocyte is of central importance, given that these incongruencies may be explained by segregating the effects of preadipocytes and terminally differentiated/lipid-accumulating adipocytes and by segregating the effect of adipocytes on LT-HSCs vs. ST-HSCs/MPPs. With this chapter we intend to examine the functionality of bone marrow adipocytes using a pharmacological approach linked to a phenotypic approach to define adipocyte maturation. The PPAR γ -inhibitor BADGE is a known toxic for humans, which motivated us to find novel inhibitors of adipocyte differentiation that would be clinically compatible. In this context, we hypothesize that *preventing the hematopoietic-supportive*

BMSC to differentiate towards the less hematopoietic-supportive adipocytic lineage increases the proliferation of HSPC upon co-culture. In vivo, we hypothesize that inducing adipocytic differentiation delays hematopoietic proliferation, while preventing adipocytic differentiation accelerates hematopoietic proliferation post-transplantation.

We therefore treated the bone marrow-derived BMSC line OP9 using a wide range of chemical compounds and demonstrated that low adipocytic differentiation is associated with stronger support of HSPC proliferation in co-culture. Treatment of BMSCs using calcipotriol, a synthetic analog of vitamin D₃, prevented adipocyte differentiation and increased lin⁻/cKit⁺/Sca1⁺ (LKS) progenitor cell expansion in pre-treated stroma, via increased expression of hematopoietic supportive cytokines. In addition, using the PPAR γ -inhibitor GW9662 as control, we developed an *in vivo* standardized assay that allows to test the non-cell-autonomous, calcipotriol-induced acceleration of hematopoietic recovery post-transplantation.

4.2 Methods

4.2.1 *In vivo* transplantation assay

Mice were housed in 12h day-night light cycles and provided with sterile food and water. Experiments were carried out in accordance to the Swiss law and with approval of the cantonal authorities (Service Veterinaire de l'Etat de Vaud). 8- to 12-week old C57BL/6J mice (unless otherwise specified) underwent lethal x-ray irradiation (8.5 cGy, split in two doses 4 h apart using RS-2000, RAD SOURCE) followed the next day by the transplantation of 125.000 total bone marrow cells from MHC-compatible C57BL/6J Ly5.1 mice in volume of 200 μ l PBS 1mM EDTA via tail intravenous injection. Total bone marrow cells were extracted from femur, tibia and pelvis of MHC-compatible donors, by crushing using a mortar and pestle in ice-cold PBS, 1 mM EDTA. The samples were then filtered through a 70 μ m mesh, red blood cells lysed for 1 min at RT (420301, Biolegend), washed with ice-cold PBS, 1 mM EDTA and counted on a hemocytometer. FVB mice were also given 125.000 total bone marrow cells, except that from DBA MHC-compatible donors. The x-ray irradiation dose was optimized to the minimal lethal dose of 800 cGy, split in two doses 4 h apart. The mice were given antibiotics Baytril (30 mg Enrofloxacin, Bayer) and AmoxyMepha (5 mg Amoxicillin, Mepha Pharma AG) as well as paracetamol (500 mg, Dafalgan) in 250 ml sterile water for the first two weeks after the transplantation (changed once per week). C56Bl6/J mice received high fat diet (D12492i, Research Diet, 60 % fat) starting at 4 weeks pre-transplantation until the end of the experiment unless specified. The corresponding control mice were given control diet (D12450Ji, Research Diet, 10 % fat) with matching sucrose levels during the same period. For mice given Rosiglitazone (20 mg/kg diet, AG-CR1-3571-G001, AdipoGen), the compound was dissolved in water and mixed with 2916 powdered diet (Charles River). The control mice were given 2916 powdered diet (Charles River) for these experiments. The treatment would also start 4 weeks pre-transplant until the end of the experiment. Both, the HFD as well as the Rosiglitazone diet were given ad libitum. For the *in vivo* administration of PPAR γ inhibitors, the mice were injected into the peritoneum (IP) for the first two weeks after the transplantation, starting on the day of irradiation (day -1). BADGE (1675-54-3, Sigma) was solubilized at 60 mg/ml, while GW9662 (M6191, Sigma) at 2 mg/ml, both in DMSO and stored at -20 °C. The aliquots were thawed and resuspended with PBS and finally administered at 30 mg/kg mouse weight for BADGE and 1 mg/kg mouse weight for GW9662, all in 10 % DMSO. Two drops of blood were taken up to 2 times per week to monitor recovery of circulating blood cell (CBC) counts. Three weeks (day 17 or day 21) post-transplant the bone marrow was extracted. Frequency and absolute counts of different populations of hematopoietic stem and progenitor cells was assessed using flow cytometry. CFUs were performed from total bone marrow cells to functionally assess the bone marrow of inhibitor-treated mice and a femur was extracted to assess the adipocytic content via histology.

4.2.2 Circulating blood cell (CBC) counting

2 Drops of blood were taken from the tail-vein and collected in EDTA-coated tubes. Upon brief, low speed vortexing, the samples were analysed, and the blood cell counts recorded using the scil Vet ABC hematology analyser (Scil, USA).

4.2.3 Bone marrow extraction

The bone marrow fraction of post-transplant mice was isolated from murine femur, tibia and pelvis as previously described Chapter 2. For the CFU assays, the pellets of were resuspended in 1mL ice-cold PBS, 1 mM EDTA and 10 μ l of the resuspension added to an antibody mix containing antibodies against CD45-APCeFluor 780 at a final concentration of 1:200, Ter119-Alexa Fluor 700 at 1:200 and 10 μ l CountBright beads (C36950, Invitrogen). After 30 min staining on ice and no washing step, the volume was raised with PBS EDTA containing DAPI at 1 ng/mL and 2 % FBS. The samples were then run on the LSRII (Becton Dickinson, USA) flow cytometer and hematopoietic cells were counted based on FSC/SSC singlets and DAPI/CD45⁺ to determine the volume of unstained cells for subsequent plating into methylcellulose.

For HSPC sorting prior to co-culture with OP9 stroma, the crushed and filtered bone marrow pellet was resuspended in 5 mL RBC lysis buffer (420301, Biolegend) for 1 min at RT. The buffer was washed with PBS 1mM EDTA and the pellet stained on ice for 15 min with 50 µl biotinylated 'lineage' antibodies (558451, BD), per 6 bones (or 1 mouse) in PBS, 1 mM EDTA. The sample was washed and stained on ice for 10 min with 50 µL magnetic beads of the same kit in PBS, 1 mM EDTA. The samples were washed and filtered prior to lineage depletion using the AutoMACS Pro (Miltenyi Biotec, USA). After depletion the negative fraction was resuspended in an antibody mix containing antibodies against Streptavidin-TxRed (1:200), cKit-PECy7 (1:200), Sca1-APC (1:100) and PI (1:1000). Cell sorting was performed on a FACSAria II or a FACSAria Fusion (Becton Dickinson, USA) cell sorter.

4.2.4 Antibodies

The 'lineage' antibody cocktail from BD contains a mixture of biotinylated antibodies against CD3, CD11b, CD45R/B220, Ly-6G, Ly-6C and TER-119 (51-9000794, BD Biosciences). Additional antibodies used were: Streptavidin-TxRed (S872, Invitrogen), cKit-PECy7 (105814, Biolegend), Sca1-APC (108112, Biolegend), CD45-APCeFluor 780 (47-0451-82, Invitrogen), CD45-APC/Cy7 (103116, Biolegend) Ter119-Alexa Fluor 700 (116220, Biolegend).

4.2.5 OP9 cell culture and cell line preparation

As discussed in the previous Chapter 3.

4.2.6 Compound plating

As discussed in the previous Chapter 3.

4.2.7 *In vitro* HSPC hemato-toxicity/proliferation assay

2000 KLS cells were extracted from 8-12-week-old female C57Bl/6J mice and cultured in low adherence round bottom 96-well plates (ThermoScientific) in serum-free Stemline II Hematopoietic Stem Cell Expansion medium (S0192, Sigma) containing 1 % Pen/Strep (Gibco), 100 ng/mL SCF (RnD) 2 ng/mL Flt3-L (RnD) and 20 ng/mL IL-3 (RnD). After a two-day culture, the cells were stained on ice with a mix containing anti-CD45-APCCy7 antibody (1:200), AnnexinV-488 (1:250), PI and 2 µl CountBright beads directly added into the media. After 30 min staining and without any further manipulation (to ensure less variability between samples), the plates were analysed using the High Throughput Sampler (HTS) module of a LSR II (Becton Dickinson, USA) flow cytometer. For accurate cell counting, the HTS module was programmed to mix the wells thoroughly before sample uptake.

4.2.8 *In vitro* HSPC and OP9 cell co-culture

OP9 cells were plated at 20.000 cells per cm² in 96-well plates (6.666 cells per well) and treated with the compounds at three concentrations: from the EC₅₀ of inhibition of OP9 adipocyte differentiation (for Rosiglitazone: EC₅₀ of induction), half Log higher and one Log higher. After 5 days and without any further manipulation, the cells were imaged with the DHM after washing the media to replace it with pre-warmed IMDM 10 % FCS and 1% Pen/Strep. The washing was done using the Caliper Sciclone ALH 3000 (Caliper Life Sciences, USA) and consisted of 4 cycles of removing 140 µl media and adding 140 µl fresh IMDM media, to dilute the previous media and the compounds by > 100-fold. The wells were left with 100 µl IMDM 10 % FCS and 1 % Pen/Strep. The OPD value of each well was recorded to correlate the extent of adipogenesis with hematopoietic proliferation post-co-culture. KLS cells were extracted from B6 ACTb-EGFP mice and plated at a ratio of 1:10 initial OP9 cells (666 KLS cells per well) in volume of 100 µl IMDM, totalling 200 µl volume per well. We added a high number of KLS cells to confound effects of the heterogeneity of this cell population and therefore avoid the stochastic, clone effects secondary to differences in the HSC content across wells which, even if small, would be exponentially exaggerated after the 7-day co-culture. After 7 days co-culture, the 96-well plates were removed from the incubator and laid on ice. To count non-adherent cells, the cells were stained with CD45-PacBlue at final concentration of 1:200, PI at 1:1000 and 5 µl CountBright beads (C36950, Invitrogen) directly added to the media. Without any further manipulation, the plates were analysed using the High Throughput Sampler (HTS) module of a LSR II (Becton Dickinson, USA) flow cytometer. The settings were programmed to mix the wells thoroughly before sample uptake. To count adherent cells, separate plates were taken from the incubator, the media manually removed, and wells washed once with 200 µl PBS. 40 µl of Trypsin EDTA (0.5 %, 25300-054, Gibco) was added to each well and incubated for 5 min at 37 °C. 160 µL of ice-cold PBS containing FCS (to neutralize the trypsin), CD45-APCCy7 (1:200), PI (1:1000) and CountBright beads were added to the plates. The plates were stained on ice and directly analysed via flow cytometry with the same settings as for the non-adherent cells.

4.2.9 RNA-seq

OP9 cells were plated at 20.000 cells per cm² in 96-well plates (6.666 cells per well) and treated with the compounds at a concentration 1 Log higher than their respective EC₅₀ inhibition of OP9 adipocyte differentiation. After a 5-day incubation, the wells were washed once with PBS and the total RNA was extracted using the ZR-96 Quick-RNA extraction kit (R1050, Zymo Research) following the manufacturer's instructions. The extraction included a DNA-digestion step and was finally reconstituted in 25 µl ddH₂O. 20 ng of RNA was used to prepare the library following BRB-seq protocol previously described in Alpern et al [145]. Only genes expressed in at least three samples with a cpm (counts per million) greater than 1 were kept for the rest of the analysis. The data was normalized using DESeq2 [146]. The differential expression analyses were performed using DESeq pipeline with a cut-off of 2-Fold increase and FDR > 0.05. The adipogenic, osteogenic and hematopoietic-supportive cytokine genes were calculated as the sum of the expression of marker genes (Adipogenic genes: Adipoq, Fabp4, Lpl, Cidea, Plin4, Plin1, Lipe, Pparg, Slc2a4; Osteogenic genes: Runx2, Sp7, Alpl, Bglap, Col1a1, Ogn; Hematopoietic cytokine genes: Mif, Lif, Ccl3, Csf3, Ccl4, Ccl2, Il23a, Cxcl12, Timp1, Il6, Cxcl10, Cxcl2, Pf4, Spp1, Il1b, Socs5, Tgfb2, Fgf2, Inhba, Hgf, Angpt2, Angpt1, Dkk1, Kitl (Scf), Igf1, Gas6, Tgfb1 [85]).

4.2.10 CFU assay

The CFU assay was performed according to the manufacturer's instructions of the STEMvision automated CFU counter (STEMCELL Technologies, USA). For the analysis of the regenerative function of murine HSPCs, the equivalent of 10.000 DAPI/CD45⁺ cells (from homeostatic mice or 30.000 DAPI/CD45⁺ cells from aplastic mice), previously counted on the flow cytometer as described above were added to the methylcellulose (Methocult GF M3434, STEMCELL Technologies) and plated at 1.1 mL per well in a SmartDish 6-well plate (STEMCELL Technologies, USA) in duplicates. For the analysis of the regenerative function of total bone marrow cells treated with the screening compounds, the methylcellulose aliquots were prepared with the compounds on the previous day and kept at 4 °C. The concentrations of the compounds were adapted to the volume of methylcellulose, as well as the corresponding DMSO controls. 10.000 MNCs from the bone marrow of crushed, filtered and RBC-lysed pellets were then plated into methylcellulose (STEMCELL Technologies, USA). Finally, and after 8 days of culture, the wells were imaged using the STEMvision automated CFU counter (STEMCELL Technologies, USA). Total colony numbers were automatically counted, and 4 different colony sizes distinguished.

4.2.11 Histology

For the histological assessment of bone marrow adiposity and hematopoietic content, the extracted femurs and tibias were fixed in 10 % formalin for 24 h at 4 °C and washed 3 times for 15 min in PBS at RT. The bones were then decalcified overnight in a Tri-Na citrate and formic acid solution at RT, and then thoroughly washed under running tap water. The bones were placed in 70 % ethanol at 4 °C before paraffin inclusion. The bones were then cut longitudinally in 3-4 µm sections and stained with Hematoxylin and Eosin. Semi-automated quantification of the red (hematopoietic) and yellow (adipocytic) bone marrow was performed using the MarrowQuant analysis tool developed in the lab.

4.3 Results

4.3.1 Screening for modulators of adipocyte differentiation

The primary screen was performed on OP9 cells, a murine non-clonal BMSC line, derived from the calvaria of newborn M-CSF deficient mice [134]. They were originally described as a feeder layer to efficiently differentiate embryonic stem cells (ESC) into HSCs. OP9 cells have been hypothesized as more supportive to hematopoiesis, as they originate from the calvaria, a craniofacial bone structure which derives from membranous ossification with great contribution from neural crests. Actually, it has been proposed that cells deriving from this region overlap with the embryological precursors of BMSCs [147]. Due to the lack of M-CSF production in OP9 cells, ESCs were prevented from differentiating towards the myeloid lineage and thus OP9 cells enhanced the support of more undifferentiated progenitors. We found that co-culture with HSPCs did not require the use of any external growth factors, as OP9s cells have been shown to secrete high amounts of key molecules Cxcl12 [148] and Stem cell factor (SCF) [149]. The multipotency of OP9 cells has been demonstrated as they efficiently differentiate into the three main mesenchymal lineages [141]. Given their propensity to spontaneously differentiate into adipocytes, however, they have also been characterized as a robust model for adipogenesis [121].

In the setting of this screening, OP9 cells were exposed to an adipocytic differentiation cocktail containing Dexamethasone, IBMX and Insulin (DMI) in presence of 10 % FCS and antibiotics (Penicillin/Streptomycin) (Fig 4.1A). Owing to the fragile and floating nature of *in vitro* differentiating adipocytes, the cells were imaged using our label-free DHM approach after 6 days of incubation, without any further manipulation. The Prestwick Chemical Library of FDA-approved drugs, a library containing natural products and library of

chemicals generated from swiss academic laboratories (totalling together more than 4000 compounds) were screened with the aim of facilitating translation to the clinic (Fig S4.1).

4.3.1.1. Primary screen

The compounds of all libraries were stored in 100% DMSO stock solution at 10 mM and tested in duplicates at 10 μ M in combination with the standard adipocytic differentiation cocktail (DMI) containing Dexamethasone (Sigma, D4902, 10 μ M), Insulin (Sigma, I0516, 5 μ g/ml) and Isobutyl-methylxanthine (IBMX, I5879, 0.5 mM). The libraries have previously been selected based on their 'drug-likeness' profile and propensity to affect a variety of different biological processes. In drug discovery, the 'drug-likeness' is defined by variety of factors, such as its bioavailability, potency and feasibility of synthesis [150]. Each 384-well screening plate contained three columns of cells incubated in three different control conditions: DMI, no DMI and DMI containing 10 μ M of the standard PPAR γ inhibitor T0070907. The latter one was used as positive control for inhibition of adipocytic differentiation. After 6 days of incubation and no further manipulation the cells were imaged using Digital Holographic Microscopy (Fig 4.1B). The resulting hologram was reverse-Fourier-transformed into a single-plane image using Matlab, where the average OPD of each well was measured. This method of quantification was validated in the previous chapter.

Compounds were considered hits if the OPD value of both duplicates lay below three times the standard deviation of the mean of the wells containing DMI (Fig 4.1C). As the duplicates were plated in separate plates, only compounds passing this threshold independently on both plates, were considered hits. This first round of screening resulted in 332 hits and 120 alternative hits (enhancers of adipocytic differentiation) from initially more than 4000 compounds. Alternative hits were defined as compounds that resulted in increasing the OPD value above three times the standard deviation of the mean of the DMI control condition (independently). Both the adipocytic differentiation inhibitors as well as the enhancers were selected for a second round of screening of which 180 inhibitors and 87 activators were reaffirmed as hits and alternative hits, respectively. The compounds were ranked by a Score, which for compound x is defined as:

$$Score_x = \left| \frac{OPD_{DMI+T007} - OPD_x}{OPD_{DMI+T007} - OPD_{DMI}} \right|$$

With $Score_x > 1$, compound x inhibits DMI-induced adipocyte differentiation more efficiently than the control inhibitor T0070907.

4.3.1.2. Hit confirmation: Potency and toxicity

In order to quantify the potency of the inhibition of *in vitro* adipocyte differentiation, the 180 inhibitors were subsequently tested for a dose-response in eight different concentrations with a half-log dilution, starting from 10 μ M. The curves were fitted to a plateau at 0 % response for baseline differentiation, while 100 % was considered the positive control with the PPAR γ inhibitor T0070907 (Fig 4.1D). All compounds exhibiting an EC₅₀ at concentrations above 1 μ M were filtered out rendering a total of 85 compounds from the initial 180 (Fig 4.1E).

A Cell Profiler machine learning plugin was developed to count individual cells from the images closest to their EC₅₀ concentration (description in the previous chapter). All inhibitors that reduced the number of cells to less than three times the standard deviation of the mean of the DMI (baseline) control were filtered out (Fig 4.1F). The same plugin was additionally able to assign each cell to be either live or dead, with the latter ones clearly distinguished as small and rounded shapes. Each compound comprising a dead cell percentage higher than three times the standard deviation of the mean of the DMI control was finally filtered out (Fig 4.1G). This rendered a total of 49 inhibitor hits from the initial 85 compounds, that exhibited strong potency (EC₅₀ < 1 μ M), didn't compromise on cell confluence (more than 353 cells per field of view) and were non-toxic (Cell death < 15 % of total cells per field of view) (Fig S4.1A). From those 49 hits, 7 additional compounds were removed, given that their maximum effect (Top asymptote in the EC₅₀ curve) only reached a Score < 0.7. However, other 8 compounds were manually added to the hemato-toxicity assay, since they showed strong inhibition of adipocyte differentiation (most compounds had a maximum effect Score > 1) albeit at lower potency (1 μ M < EC₅₀ < 10 μ M). This rendered a total of 50 compounds chosen for the following counter-screens (Fig S4.1B). Interestingly, we found that within the compounds that passed these filters, eight were flavonoids. OP9 cells treated with this family of compounds displayed a fibrillar phenotype (Fig 4.1B, 'Alt Phenotype', which we will discuss in the RNA-seq section of this chapter.

4.3.1.3. Counter-screens and functional testing *in vitro*

Taking into consideration the ultimate goal of this project, which is to accelerate HSPC proliferation post-transplantation, we developed a short *in vitro* assay to remove compounds that may be toxic to the hematopoietic compartment and/or impede hematopoietic proliferation. This assay involved a 2-day *in vitro* culture of (lin/cKit⁺/Sca1⁺) LKS cells extracted from 8- to 12-week old

C57Bl/6J mice in Stemline II (Sigma) with low dose SCF (100ng/ml, R&D) and Flt-3L (2ng/ml, R&D), which constitute basal conditions known to maintain a certain degree of self-renewal divisions [33], [151] (Fig 4.2A). The 50 remaining compounds were tested on the proliferation and viability of LKS cells in this setting. To impose stringency on the assay, the hits were tested at a concentration 1 Log higher than the EC₅₀ concentration at which they inhibit OP9 adipocyte differentiation. The compounds were tested in duplicates in 96-well round bottom plates and cultured with LKS cells. After 48 h we stained the cells and counted total cell numbers via flow cytometry, using counting beads. 15 compounds passed the *in vitro* assay, which was defined as the total DAPI/Annexin V/CD45⁺ cell count being above three times the standard deviation of the control sample (3091 cells) (Fig 4.2B).

At this point, we sought to acquire the currently commercially available compounds within the remaining 15, instead of relying on the stock of the Biomolecular Screening Facility, which left us with 8 compounds. We manually included Deferoxamine mesylate into this selection, because of the high dosage that it is currently used at in patients suffering from disorders of hematopoiesis [152]. Of note, administration of deferoxamine in these patients for the purpose of iron chelation has been associated with a yet-unexplained improvement in hematopoietic function. Antimycin A was also manually added to this selection, given that inhibitors of the mitochondrial respiratory chain, such as oligomycin, are known to induce glycolysis and therefore may modulate HSPC function [33], [153], [154]. For the following assay, we chose two representatives of the flavonoids and included the three enhancers of adipogenesis described in the previous chapter (Rosiglitazone, Pioglitazone and Indomethacin). This left us with a selection of 10 inhibitors and three enhancers of adipogenesis. The compounds were tested on the hematopoietic progenitor activity upon culture of 10.000 total bone marrow cells in methylcellulose for 8 days (CFU assay) to determine if they induced any deleterious, cell autonomous effect at the level of HSPC proliferation or differentiation (Fig 4.2C). Three doses were tested in duplicates: EC₅₀ of inhibition of OP9 adipocyte differentiation (for enhancers: the EC₅₀ of activation), half Log higher and one Log higher. The regenerative capacity of the treated cells was assessed by counting the total number of colonies using the STEMvision automated CFU counter (STEMCELL Technologies). Three of the tested compounds did not pass the stringency test, which was defined as laying within three times the standard deviation of our control samples (DMSO 0-0.3%) (Fig 4.2D). Deferoxamine was amongst the three compounds which did not pass the stringency test, although it is used in the clinic at high concentrations (Fig 4.2E). However the EC₅₀ at which Deferoxamine inhibits OP9 adipocytic differentiation is almost 1 Log higher than the plasma concentration quoted for its clinical use [155]. For Tiapride hydrochloride, the deleterious effect of the highest concentration tested could not be distinguished from the toxic effect of high concentration of DMSO used in this condition (2.2 %).

4.3.1.4. RNA-seq of modulators of adipocyte differentiation

In collaboration with the laboratory of Bart Deplancke, we then performed RNAseq on OP9 cells treated with the remaining 10 inhibitors and three enhancers of adipogenesis to examine the expression of hematopoietic supportive cytokines. In addition, we tested various flavonoids, which although passing the counter-screen thresholds, always provided OP9 cells a distinct fibrillar morphology and no lipid droplet accumulation. Principle component analysis along the first two dimensions of the transcriptional data suggests 4 groups, three of which are differentiated along the first principle component (PC1) (Fig 4.3A). Note that some inhibitors were segregated into two groups, which we will call 'strong inhibitors' and 'weak inhibitors'. OP9 cells treated with the flavonoid compounds were distinguished along the second principle component (PC2). Visualization of the OPD values as measured by DHM of the four groups, suggests that the extent of adipocytic differentiation is distinguished in the first principle component, while flavonoid-treated OP9 cells are not distinguishable from DMI-treated cells via OPD (Fig 4.3B). Indeed, adipocytic differentiation as measured by DHM correlates with the expression of adipocyte-specific genes ('adipocytic score') with R²=0.82 (Fig 4.3C). Taken together, these results highlight DHM as a reliable tool to measure adipocyte differentiation. We then also correlated the expression of adipocyte-specific genes with the expression of hematopoietic-supportive cytokines ('hematopoietic score') (Fig 4.3CD). Interestingly, the correlation was not significant, which may be explained by an optimum balance between adipocyte differentiation and expression of hematopoiesis-supportive cytokines. Indeed, compounds inducing either a very high or a very low adipocytic score had a decreased hematopoietic score. The two compounds which exhibited a high hematopoietic score, while maintaining a low adipocytic score were Calcipotriene and Antimycin A. More in depth analysis of the expression of Calcipotriene- and Antimycin A-treated OP9 cells, suggests that both osteogenic and adipocytic genes are reduced in comparison to only DMI-treated cells, while hematopoiesis-supportive cytokine expression is maintained (Fig 4.3E). Rosiglitazone, which was the compound showing highest potency in enhancing adipocyte differentiation in our primary screen, also displayed the strongest expression of adipocyte-specific genes and a highly variable reduction in the expression of hematopoiesis-supportive cytokines. The transcriptional profile of flavonoid-treated OP9 cells, which displayed a fibrillar morphology, consistently showed increased expression of *osteopontin* (*spp1*) and *sca1* (Fig 4.3F). However, the expression of *cxl12* was decreased and when inferring the cell type based on the top 200 differentially expressed genes (vs DMI control) using the EnrichR Geneset enrichment tool (Mount Sinai Medical School, NY, USA), flavonoid-treated OP9 cells more closely resembled the C2C12 myotubule forming cell line (data not shown). These results may

suggest the myogenic differentiation potential of bone marrow-derived stromal cells, which are currently used in regenerative therapies for muscle repair [156], [157] and whose myogenic potential is still highly debated.

4.3.1.5. *In vitro* co-culture

Finally, and as a last step before the *in vivo* administration, we tested the hematopoietic supportive functionality of OP9 cells pre-treated with the compound hits. The compounds were added in triplicates and in a dose-response: from the EC₅₀ of inhibition of OP9 adipocyte differentiation (for Rosiglitazone: EC₅₀ of induction), half Log higher and one Log higher. We induced adipocytic differentiation of OP9 cells with DMI for 5 days, while incubating the cells with the inhibitor hits. To highlight the differential effects of Rosiglitazone- and DMI-induced adipocyte differentiation, the enhancers of adipocyte differentiation were not incubated with DMI (Fig 4.4A). After 5 days of incubation, the OP9 stroma was washed carefully, and imaged via DHM before starting co-culture (Fig S4.3A). Co-culture consisted of adding LKS cells (at a ratio of 1:10 to initial OP9 cells) and co-culturing LKS and the previously differentiated OP9 cells for seven days. After co-culture, the output of hematopoietic proliferation was quantified as total number of PI-/CD45⁺ cells via flow cytometry using standardized counting beads. We quantified cells adherent to the stromal layer independently from non-adherent cells. It is commonly known from cobblestone area forming cell assays, that more primitive and quiescent HSPCs maintain attached to the stromal layer, while differentiating cells are released from the stroma [158]. We observed adherent cells to be generally higher in numbers after seven days co-culture. Linearly correlating the hematopoietic scores from the RNA-seq data with HSPC proliferation exhibited post-co-culture, exhibited a regression in both adherent cells ($R^2=0.52$) and in non-adherent cells ($R^2=0.53$) (Fig 4.4D and I). We found that untreated OP9 cells allowed for the most rapid expansion of HSPCs and that this effect was hampered after adipocytic differentiation of OP9 cells, both when DMI- or Rosiglitazone-induced (Fig 4.4E and J). The standard PPAR γ inhibitor, T0070907, partially rescued the DMI-induced 'loss-of-function'. It has however to be taken into consideration that the presence of the DMI cocktail itself, reduced the cell confluence of OP9 cells (Fig 4.1F), which may explain the only partial rescue. Although high OPD was predictive of low hematopoietic proliferation, consistent with the RNA-seq data (Fig 4.4C-D and H-I), inhibition of adipocytic differentiation was not *per se* an indicator of increased expression of hematopoiesis-supportive cytokines, as inhibitor treated OP9 cells exhibit large variability in the ability to support HSPC proliferation. We therefore fitted the data in a bell-shaped curve (Fig 4.4B and G). Note that at the lowest concentration of Rosiglitazone tested (20 nM), adipocyte differentiation was not efficient (Fig S4.3A). We also tested a flavonoid in this setting, and although increasing concentrations of this compound were associated to increased HSPC proliferation, these cells had significantly lower functionality than controls in supporting hematopoiesis, which is consistent with their low expression of *cxcl12* (Fig 4.4 E and J). Consistent with the RNAseq data, deferroxamine-treated OP9 cells completely lost the ability to support HSPC proliferation. Taken together these results suggest adipocyte differentiation as detrimental to the support of HSPC proliferation. Inhibition of adipocyte differentiation on the other hand exhibited mixed results, with some inhibitors being detrimental to the support of HSPC proliferation while others partially rescued the DMI-induced 'loss-of-function'. Note that, as in the transcriptional expression of hematopoietic cytokines, there was an optimum in adipocyte differentiation: both very high and very low OPD values were associated to a decreased support of HSPC proliferation. To exclude effects of hematopoietic exhaustion after expansion, we cultured the progeny of the HSPCs post-co-culture into methylcellulose and assessed the colony-forming capacity (Fig S4.2A). We multiplied the fold-expansion of HSPCs with the colony-forming capacity per cell and observed a similar behaviour as with the HSPC proliferation. Indeed, we observed a bell-shaped curve, where both very low OPD and very high OPD was associated with lower colony-forming capacity (Fig S4.2B). Note the ability of DMSO itself to inhibit OP9 adipocytic differentiation and how this inhibition results in an optimum of hematopoietic expansion at 0.55% DMSO (S4.3B-D). Within the inhibitors of adipocyte differentiation, only Tiapride hydrochloride and Calcipotriene were found to rescue the DMI-induced loss of hematopoietic support (Fig S4.2D). Given that Calcipotriene exhibited the best results in all performed screening assays, it will be the candidate tested *in vivo* for its capacity to accelerate hematopoietic recovery post-transplantation.

4.3.2 *In vivo* modulation of adipocyte differentiation

We set out in parallel to compare different modulations of adipocyte differentiation in this setting in order to design the optimal *in vivo* assay to test our hypothesis stating that inhibiting adipocyte differentiation *in vivo* accelerates hematopoietic recovery post-irradiation and bone marrow transplantation. A summary is represented in Fig. (Fig S4.4).

4.3.2.1. Enhancing bone marrow adipogenesis

Adipocytes accumulate within the marrow space upon a variety of physiological needs and as a consequence to different stresses. One major source of increased bone marrow adiposity in western societies is high fat diet-induced obesity. We therefore set to test the effect of a 4-week pre-transplant high fat diet (HFD) on the hematopoietic recovery post-bone marrow transplantation in C57Bl6 mice (Fig 4.5A and C). At homeostasis, there was no evident difference in the hematopoietic colony forming capacity of young females treated with HFD or normal diet (ND) as seen in an 8-day methylcellulose colony forming unit assay (CFU) (data not shown). In the

post-transplant period though, the replacement of HFD to ND significantly improved the regenerative capacity of bone marrow stem and progenitor cells extracted 3 weeks post-transplant (Fig 4.5D), despite an increase in CD45⁺ cells in the bone marrow of HFD-treated mice (Fig 4.5E). This may however be explained by an infiltration of myeloid cells in the bone marrow adipose tissue, as seen in obesity-induced inflammatory conditions [159]. To assess the regenerative capacity of the more primitive hematopoietic stem cell compartment, we transplanted the bone marrow from mice fed with HFD for 4 weeks into lethally irradiated mice (Fig 4.5B). Recipient and donor mice are distinguished by an allelic variation on the CD45 hematopoietic cell marker (CD45.1/CD45.2 allelic system), allowing to assess the amount of blood cells derived from the donor bone marrow, using e.g. flow cytometry. We observed a decrease in total chimerism at 4 weeks and 8 weeks post-transplantation in mice which had received bone marrow from HFD treated mice, with no significant difference at 16 weeks post-transplant. The decrease in chimerism is mainly attributed to the myeloid compartment. The regenerative capacity of ST-HSCs and progenitors is seen at 4 weeks post-transplantation, while the most primitive LT-HSC projects its regenerative capacity at 16 weeks post-transplantation or later [33]. These results indicate a compromise in regenerative capacity of ST-HSCs and progenitors from HFD treated mice, while maintaining LT-HSC function. These observations are in accordance with other findings that bone marrow adipocytes maintain LT-HSC quiescence and function while compromising short term progenitor expansion [62], [85], [86]. Another major factor of increased bone marrow adiposity is ageing. This set us out to test the hematopoietic regeneration capacity in one-year-old male mice. Most strikingly, we found that the post-transplant survival was significantly reduced in HFD-fed aged mice, especially in the early post-transplant period (between day 7 and day 12) (Fig 4.5F). Taken together, these observations indicate that ageing and diet are predictors of survival in the early post-transplant period, as reflected by the detrimental effects of HFD seen in young mice, which are further exacerbated in aged mice.

The major limitation of these experiments is that the inflammatory response to HFD may override the detrimental effect of homeostatic adipocytes on hematopoietic regeneration. We therefore tested another well characterized inducer of bone marrow adipocyte accumulation: Thiazolidinediones (TZD). TZDs, such as Rosiglitazone, are PPAR γ agonists that are used as treatment in diabetes mellitus type 2 patients [160]. Rosiglitazone is also implicated in adipose tissue browning and in increasing circulating adiponectin levels [161]. In the clinic, Rosiglitazone has been associated to a variety of strong side-effects, most specifically increased osteoporotic bone fractures upon long-term treatment, reason for which its clinical use has dramatically decreased in recent years [162]. We tested Rosiglitazone at a very low dose (20 mg/kg diet), in order to reduce confounding effects of increased adiponectin levels or adipose tissue browning. Although we observed a slight decrease of the colony forming capacity of Rosiglitazone-fed mice at homeostasis (data not shown), we were not able to see differences at 3-weeks post-transplant. This could be either due to the low concentration used and/or due the high variability of hematopoietic recovery post-transplant. Another interesting observation is that both in HFD and in Rosiglitazone treatment, the circulating RBC levels do not decrease as much as in control mice on day 7 post-transplantation (Fig S 4.5 A3 and C3). This may be either due to a delayed response or to an increase of RBC production in the post-transplantation marrow of HFD or Rosiglitazone treated mice. Taken together, these observations suggest that, independently of the cause, factors increasing bone marrow adiposity are detrimental to the hematopoietic recovery post-transplant.

4.3.2.2. Inhibiting bone marrow adipogenesis

As a first step towards inhibiting adipocyte accumulation in the post-transplant marrow, we set out to reproduce the findings by Naveiras et al. (Nature, 2009). We transplanted the bone marrow of DBA mice into lethally irradiated MHC-compatible FVB mice and treated them with BADGE (30 mg/kg and 60 mg/kg) or the corresponding volume of vehicle (DMSO) via intraperitoneal injections for the first two weeks post-transplantation (Fig S4.6A). In this case, DBA mice harbour the CD45.2, while the recipient FVB mice contain the CD45.1 allelic variant with the same MHC haplotype, ensuring immune compatibility. At three weeks post-transplantation we assessed the colony-forming capacity of the bone marrow via CFU assays. Surprisingly, no increase in the colony forming capacity of BADGE treated mice was observed. In fact, it was even significantly decreased. During the experiments we have observed solubility issues with BADGE, reason for which we decided to repeat the experiments with GW9662. We therefore tested the three PPAR γ inhibitors in parallel (GW9662 at 1 mg/kg, T0070907 at 1 mg/kg and BADGE at 30 mg/kg) via *in vivo* IP injections (Fig S4.6D). Due to the high mortality of the FVB cohort (possibly due to strong sensitivity to radiation and manipulation), we decided to perform the experiment in C57Bl6J mice. We observed that only the bone marrow of GW9662-treated mice consistently and significantly increased colony-forming capacity at three weeks post-transplant (Fig 4.6B-C). The bone marrow of BADGE-treated mice also increased the total number of colony-forming units, but not significantly, due to its high variability. Consistently with the previous experiment, we observed a higher colony forming capacity in the bone marrow of GW9662-treated mice, which was accompanied by an almost significant increase in CD45⁺ bone marrow cell counts. We also observed slight improvements of post-transplant survival in mice treated with GW9662. For the future testing of the inhibitor hits, higher numbers of mice per group will be needed due to the strong variabilities observed in hematopoietic recovery post-transplantation. Using GW9662 as a control, this assay will be used to test the effect of Calcipotriene on recovering hematopoiesis post-transplant.

4.4 Conclusions and perspectives

In the search for new modulators of bone marrow adipocyte differentiation we have developed a non-invasive high-throughput screening platform, which was described in the previous chapter. In brief, Digital holographic microscopy (DHM) is able to reconstruct images based on the ability of tissue to refract light and since lipid vesicles have a high refractive index compared to the cytoplasm, they can reliably be quantified by assessing the optical path difference (OPD). We therefore treated the bone marrow-derived OP9 stromal cells using a wide range of chemical compounds, which lead us to a selection of compounds that either induced or prevented adipocyte differentiation. Given our hypothesis stating that *preventing the hematopoietic-supportive BMSC to differentiate towards the less hematopoietic-supportive adipocytic lineage would increase the proliferation of HSPC upon co-culture*, we focused on finding compounds that inhibited adipocytic differentiation *in vitro*. Using a standard adipocyte differentiation cocktail (Dexamethasone, IBMX, Insulin), we screened a library of FDA approved drugs, a library containing natural products and a library of chemicals from swiss academic labs for their ability in a 6-day *in vitro* culture assay. Using DHM, more than 4000 compounds were tested, and 180 compounds rendered as primary hits. The hits were then further tested in a dose-response and filtered based on high potency ($EC_{50} < 1 \mu M$) and low toxicity, while maintaining cell confluence. Given that these compounds are envisaged to accelerate hematopoiesis in a non-cell autonomous manner, the remaining 49 hits were separately tested for their toxicity and their permissiveness to hematopoietic proliferation and regeneration using short *in vitro* cultures and colony-forming unit (CFU) assays. In close collaboration with the laboratory of Bart Deplancke, we performed RNA-seq on OP9 cells treated with the 10 remaining hits (that were commercially available) and examined the expression of hematopoietic supportive cytokines.

These experiments, apart from further strengthening the capacity of DHM to assess adipocyte differentiation, also suggested Calcipotriene and Antimycin A as two compounds that suppress the expression of adipocyte-specific genes, while maintaining the expression of hematopoiesis-supportive cytokines. To model the modulation of the *in vivo* yellow-to-red bone marrow transition, the remaining hits were tested in a co-culture setting *in vitro*. We have herewith observed that our hypothesis is supported to the extent that inhibiting *in vitro* OP9 adipocytic differentiation is associated with a higher support of HSPC proliferation. Rosiglitazone, which exhibited the strongest enhancement of OP9 adipocytic differentiation of the screened compounds, also markedly decreased the capacity of OP9 cells to support hematopoiesis. This is in congruence with a previous study, that observed a decreased support of HSPC myeloid differentiation co-cultured with Rosiglitazone-treated C3H10T1/2 stromal cells [163]. Nevertheless, some compounds that prevented OP9 cell lipid droplet accumulation also diminished the hematopoietic supportive capacity of the OP9 stroma, most notably with the example of Deferoxamine, which is used at high doses in the clinical setting, paradoxically, for hematopoietic diseases [155]. Interestingly, DMSO- also prevented OP9 cells from accumulating lipid droplets, while increasing hematopoietic support at higher concentrations. Although the mechanism is still unknown and open to further investigation, we observed an optimum of hematopoietic support within the axis of OP9 *in vitro* adipocytic differentiation, both in the DMSO dose-response, as well as within all the compound-treated OP9 cells. This is consistent with another study suggesting pre-adipocytes to support hematopoiesis through higher expression of Ang-1, SCF and Cxcl12, which decreases in terminally differentiated adipocytes [87]. Interestingly, we found that OP9 cells treated with a variety of flavonoids displayed a myoblast-like phenotype, while transcriptional profiling suggested high levels of osteopontin expression, a protein involved in bone mineralization [164]. Flavonoid-treated OP9 cells had a strongly decreased capacity to support hematopoietic proliferation, although increasing concentrations paradoxically improved hematopoietic support. Flavonoids are a family of natural products, which in bone marrow stromal cell culture have been associated with osteoblast differentiation, at the expense of adipogenesis [165]. OP9 cells treated with Calcipotriene, a synthetic vitamin-D₃-derivative, showed the strongest capacity to support hematopoietic proliferation, while inhibiting adipocytic differentiation efficiently. *In vitro*, vitamin-D₃ is an inducer of osteogenic differentiation in stromal cells [166]. *In vivo*, vitamin-D₃ is strongly linked to calcium and bone metabolism [167] whereas it is strongly suggested for the prevention of bone fractures, especially in osteoporotic patients [168]. In our setting, higher doses of calcipotriene decreased the hematopoietic-supportive capacity of the OP9 stroma, suggesting that there may also be an optimum in hematopoietic support possibly prior to osteogenic lineage commitment. Taken together, Calcipotriene, will be the candidate tested in the developed *in vivo* model of the yellow-to-red-bone marrow transition.

The *in vivo* model of the yellow-to-red marrow transition consisted of lethally irradiating and transplanting mice and subsequently analysing the peripheral blood production and colony-forming capacity of the bone marrow during the early recovery period. Similar to compound-treated OP9 cells, we tested mice in various settings expected to modulate bone marrow adiposity in an effort to uncover the net effect of bone marrow adipocytes on the hematopoietic recovery. Strikingly, we observed a compromise in the post-transplant survival of aged male mice fed with a high fat diet. This difference may be accentuated given that aged mice already have an increased marrow adiposity [64]. In young female mice, we also observed a delayed capacity of the bone marrow of HFD-diet fed mice to form colonies. Although there are reports of sex-specific differences in relation to bone marrow adiposity, given the importance of sexual hormones on bone formation [169], we observed a deficiency in hematopoietic recovery in both sexes, when

HFD-fed. Interestingly, the HFD-induced decrease in colony-forming capacity was often linked to an increase in CD45⁺ hematopoietic cells in the marrow, as well as higher white blood cell (WBC) and red blood cell (RBC) count in the post-transplant period. In Rosiglitazone-treated mice, we also observed an increase in RBC post-transplant, however it cannot be concluded whether it is due to a delayed hematopoietic reaction or due to an increase of blood production secondary to accelerated hematopoietic recovery. The low dose of Rosiglitazone used (20 mg/kg diet) [161] did not result in a delayed hematopoietic recovery as seen at higher doses [163]. The transplantation of the bone marrow of HFD-fed donor mice, demonstrated that the function of ST-HSCs and progenitors was decreased, supporting our hypothesis that bone marrow adipocytes are detrimental to HSPC proliferation.

Irradiation itself induces a rapid expansion of the yellow marrow. Therefore, we attempted to inhibit adipocyte differentiation *in vivo* with the standard PPAR γ inhibitors via intraperitoneal injections (IP) for the first two weeks after irradiation and bone marrow transplantation. We found that GW9662 treatment, but not BADGE, improved the regenerative capacity of HSPCs from the bone marrow of mice in the post-transplant period as seen by increased colony-forming capacity of the bone marrow at three weeks post-transplant. We were therefore not able to reproduce previously described results by Naveiras et al and Liu et al [62], [143]. *In vitro*, we observed the PPAR γ inhibitor controls to be toxic and to compromise on the OP9 cell confluence. BADGE, besides having a very low solubility in water and a low potency inhibiting OP9 adipocyte differentiation *in vitro*, did not show signs of inhibiting adipocyte differentiation *in vivo*. However, our observation that DMSO itself was able to prevent adipocyte differentiation *in vitro* (and was coupled to an improvement in hematopoietic support), may therefore suggest a masking of the *in vivo* effect of the PPAR γ inhibitors by DMSO, which was used at high doses (10 – 20 μ l per mouse every day). Indeed this inhibitory role of DMSO has previously been demonstrated in the adipocytic differentiation of 3T3-L1 cells *in vitro* [170], [171] and interestingly, significant doses of DMSO are administered as cell protectant for cryopreservation to patients receiving HSPC transplantation.

Taken all the *in vivo* data together, we observed detrimental effects on the post-transplant recovery in aged mice and mice fed with HFD, as well as aberrant hematopoietic effects in Rosiglitazone-fed mice, while *in vivo* inhibition of adipocyte differentiation using PPAR γ inhibitors, slightly improved hematopoietic regeneration (Fig S4.4). Although these observations support our hypothesis that bone marrow adipocytes are detrimental to hematopoietic recovery post-transplantation, the effects can hardly be distinguished from systemic changes in the metabolic state of these mice (which may include increases in circulating IGFs produced by the liver [172], [173]). This is especially evident given that we did not observe differences in BMA content between different treatments in post-aplastic mice., which in turn, did not translate into an accelerated peripheral blood production in PPAR γ inhibitor-treated mice. We therefore highlight the importance of the *in vitro* co-culture assays, where only the direct interactions between BMSC/adipocytes and HSC/HSPCs are considered. Using these *in vitro* assays, we have been able to demonstrate that cells of the adipocytic lineage (pre-adipocytes) support hematopoietic proliferation, while terminally differentiated adipocytes, suppress it. An *in vivo* dose-response of GW9662, would be ideal to test if inhibition of BMA can be reached at higher doses. In addition, the development of an assay in which the *in vivo* treatment, would selectively target the niche, without cell-autonomous effects on HSPCs, would reduce confounding effects and accelerate the search for modulators of adipocyte differentiation, to improve post-transplant blood production. For example, Vitamin-D Receptor KO donor mice could be used as donors to assess the effects of calcipotriene on the hematopoietic recovery of mice undergoing bone marrow transplantation [174]. In addition, other mouse strains such as the C3H/HeJ, have reportedly significantly increased adipose tissue in the marrow as compared to C57Bl/6J and may therefore be more suitable to observe differences in BMA modulation [175], [176]. However, given the complications associated with improving post-transplant hematopoietic recovery via indirectly targeting the HSPC microenvironment, we set out to directly target the primitive hematopoietic compartment, the LT-HSC, using a clinically-compatible pharmacological strategy as described in the next chapter.

4.5 Figures

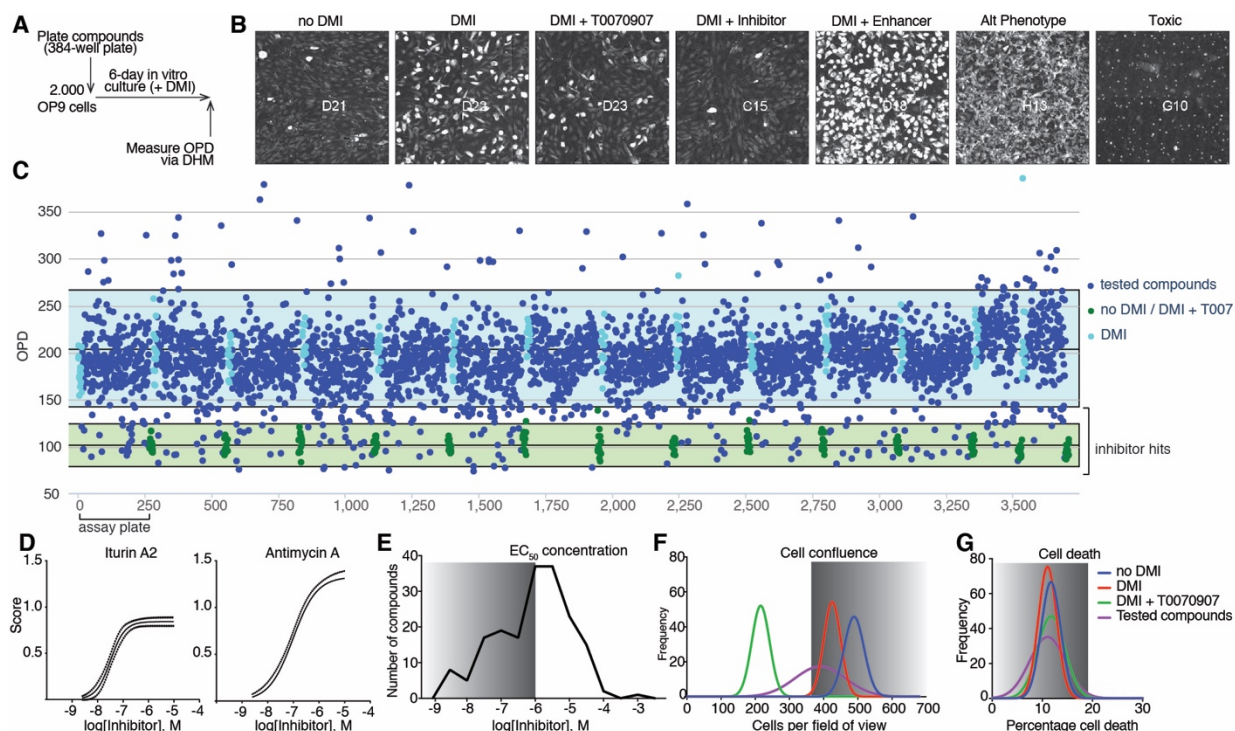


Figure 4.1 High-throughput screening to identify novel modulators of adipocyte differentiation. **A.** Schematic representation of the assay. Compounds were plated in duplicates (on different plates) as described in the previous chapter. 2,000 OP9 cells were plated in each well of a poly-ornithin-coated 384-well plate, and induced to differentiate to adipocytes using a standard cocktail containing 10 μM Dexamethasone, 0.5 mM IBMX, and 5 μg/ml Insulin (DMI). After 6 days of *in vitro* culture and without any further manipulation, the cells were imaged using Digital Holographic Microscopy (DHM). **B.** Representative DHM images of OP9 cells in control wells (4 images per well) and in wells plated with compounds exhibiting enhancement, inhibition of differentiation, or alternative phenotypes. **C.** Representation of the OPD values for all compounds tested, including the controls. Compounds were considered inhibitor hits, when both duplicates exhibited OPD values below three times the standard deviation of DMI independently. **D.** Representative dose-responses for two inhibitors of adipocyte differentiation: Iturin A2 and Antimycin A. **E.** Histogram of the EC₅₀ concentration at which each compound exhibited inhibition of adipocyte differentiation. Only compounds with potent inhibition (EC₅₀ < 1 μM) were selected for further counter-screens (grey area). **F.** Frequency distribution of compounds exhibiting differences in OP9 cell confluence, assessed as described in the previous chapter. Only compounds exhibiting OP9 cell numbers within three times the standard deviation of the control wells (DMI) were selected for further counter-screens (grey area). **G.** Frequency distribution of compounds exhibiting differences in OP9 cell death, assessed as described in the previous chapter. Only compounds exhibiting OP9 cell death within three times the standard deviation of the control wells (DMI) were selected for further counter-screens (grey area).

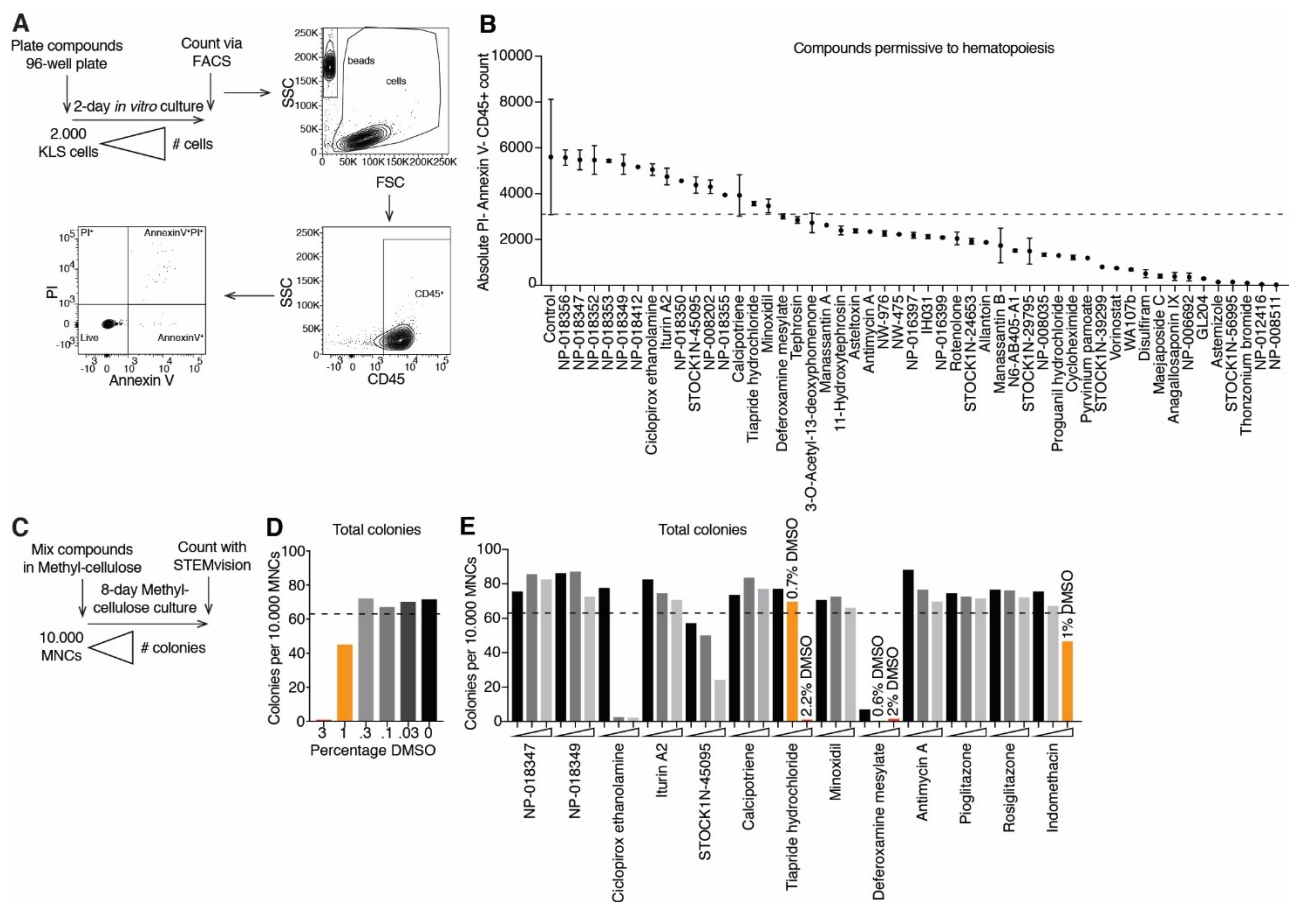


Figure 4.2 Hematotoxicity counterscreens. **A.** Schematic representation of the flow cytometric assay. Compounds were plated at 1 log higher than the EC_{50} at which they inhibit OP9 adipocytic differentiation, in duplicates and in 96-well low adherence round-bottom plates. 2000 KLS cells were cultured in each well in serum-free Stemline II HSC Expansion medium containing 100 ng/mL SCF, 2 ng/mL Flt3-L and 20 ng/mL IL-3. After a two-day culture, the cells were stained with anti-CD45-APCCy7 antibody, AnnexinV-488, PI and CountBright beads directly added into the media, and live CD45⁺ cells counted using the High Throughput Sampler (HTS) module of a LSRII flow cytometer. **B.** Absolute count of CD45⁺ cells cultured with the inhibitors of OP9 adipocytic differentiation. Only compounds exhibiting cell numbers within three times the standard deviation of the control, would be selected for further counterscreens (above dashed line). **C.** Schematic representation of the colony forming unit (CFU) assay. Methylcellulose aliquots were prepared with the compounds on the previous day and kept at 4 °C. The concentrations used ranged from the EC_{50} , at which they inhibit OP9 adipocytic differentiation, to half-log higher and 1 log higher. 10,000 MNCs from the bone marrow of crushed, filtered and RBC-lysed pellets were then plated into methylcellulose. After 8 days of culture, the wells were imaged using the STEMvision automated CFU counter (STEMCELL Technologies, USA). **D-E.** Total colony numbers were automatically counted. Dashed line represents three times the standard deviation of the DMSO controls (0 – 0.3%). Yellow and red bars represent cases in which the toxic effect of the compound cannot be distinguished from the DMSO concentration used.

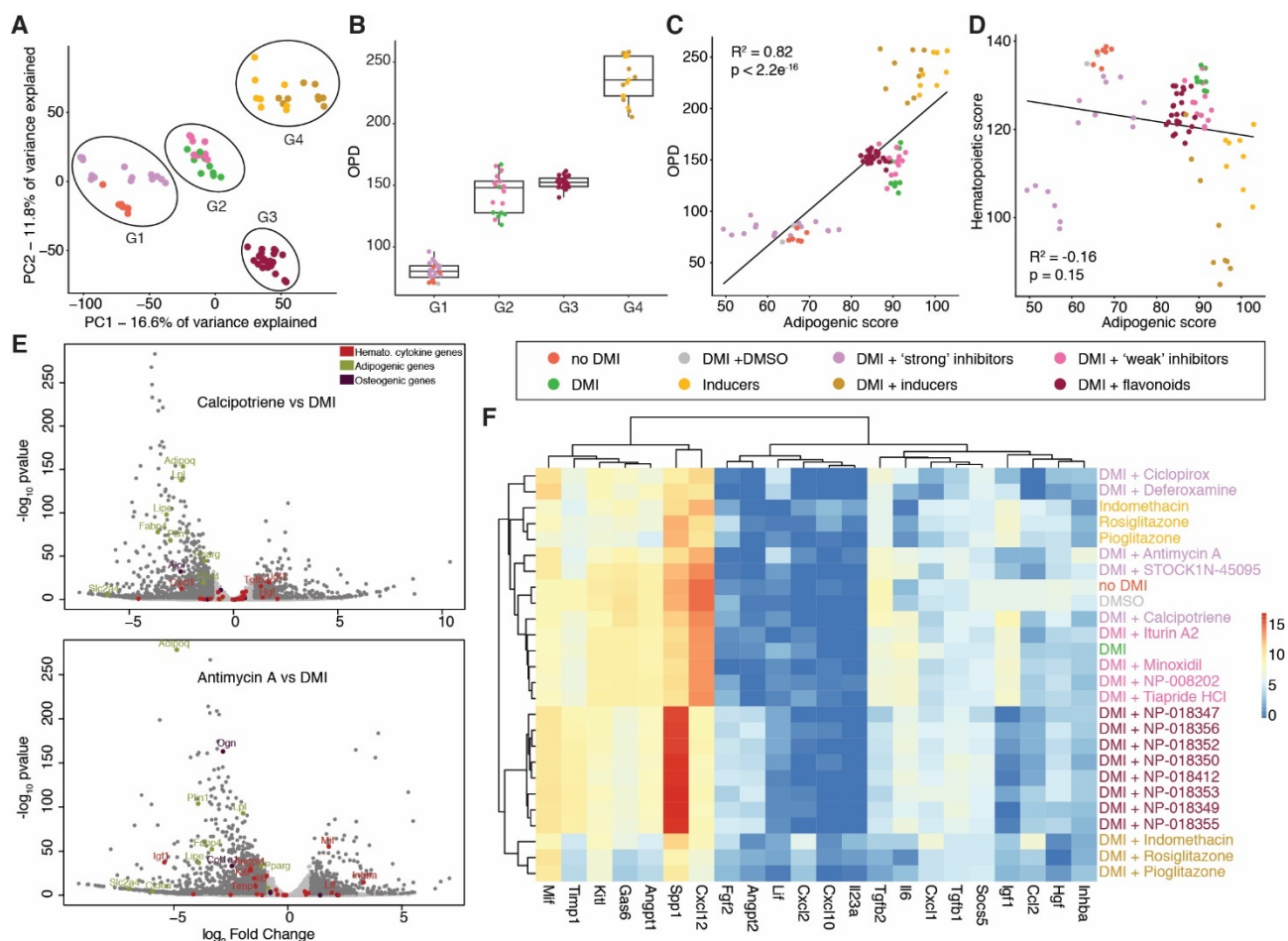


Figure 4.3 RNA-seq of inhibitors of OP9 adipocytic differentiation. **A.** Principal component analysis (PCA) of OP9 cells treated for 5 days with the compounds at a concentration 1 log higher than the EC_{50} at which they inhibit OP9 adipocytic differentiation. For the enhancers of adipocyte differentiation, the OP9 cells were treated at 1 log higher than the EC_{50} at which the compounds induce adipocyte differentiation. **B.** OPD values, as previously measured by DHM, of the four groups established in the PCA. **C.** Correlation with linear regression between OPD and 'Adipogenic' score (the expression of adipocyte-specific markers) for OP9 cells treated with the tested compounds. **D.** Correlation with linear regression of 'Hematopoietic' score (the expression of hematopoiesis-supportive cytokines) and 'Adipogenic' score for OP9 cells treated with the tested compounds. **E.** Representative volcano-plots for OP9 cells treated with two representative compounds (Calcipotriene and Antimycin A) compared to the control condition (DMI), including a representation of key genes involved in osteogenesis, adipogenesis or hematopoiesis-supportive cytokines. Genes that have a positive fold-change, were increased in compounds-treated OP9 cells versus DMI-only treated OP9 cells. **F.** Heat-map of the expression of hematopoiesis-supportive cytokines for each of the compounds tested.

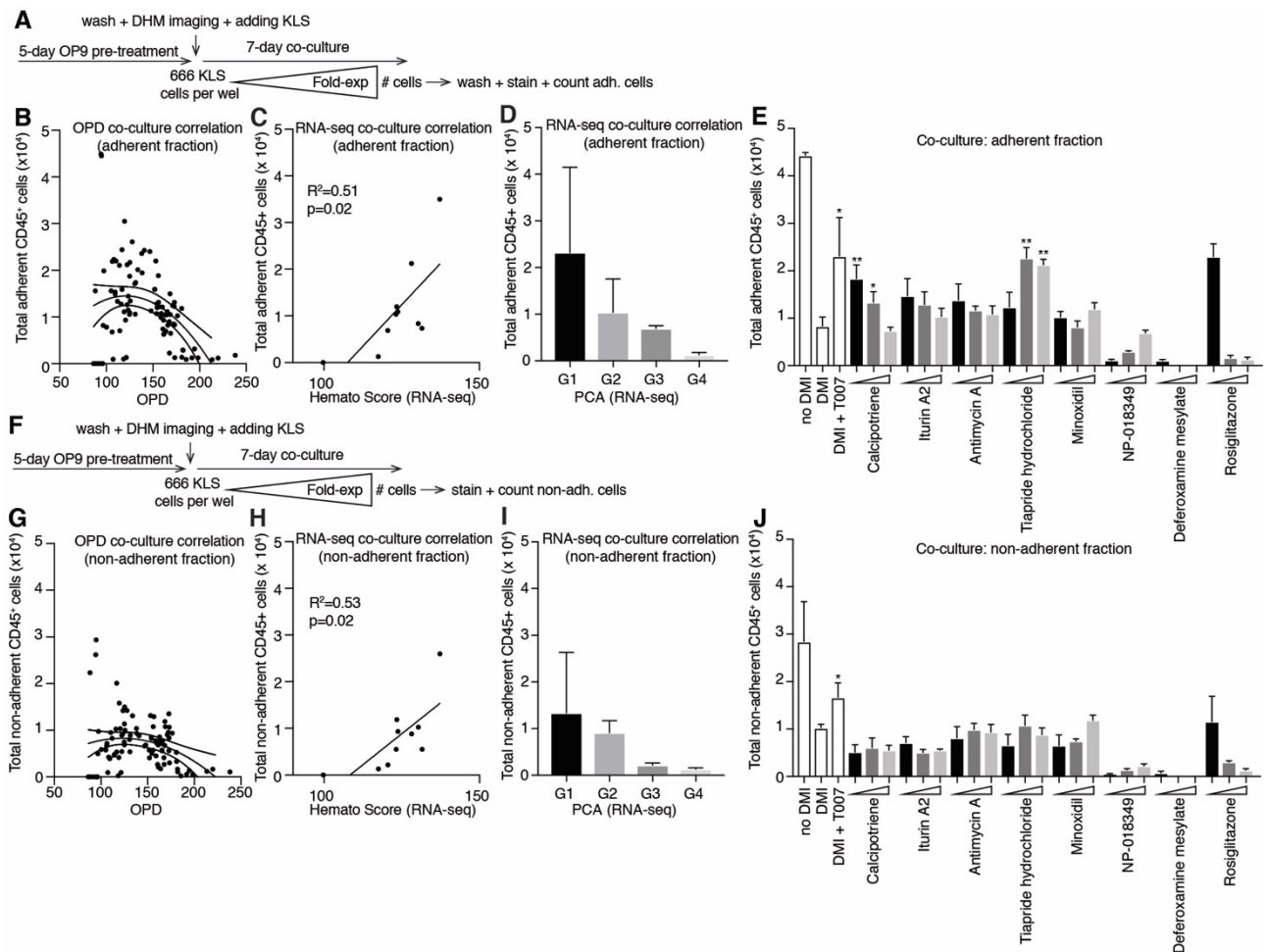


Figure 4.4 Co-culture assay of compound-treated OP9 cells and HSPCs. **A.** Schematic representation of the co-culture assay, assessing adherent CD45⁺ cells. OP9 cells were plated at 20,000 cells per cm² in 96-well plates (6,666 cells per well) and treated in triplicates with the compounds at three concentrations: from the EC₅₀ of inhibition of OP9 adipocyte differentiation (for Rosiglitazone: EC₅₀ of induction), half Log higher and one Log higher. Inhibitors were treated with DMI, Rosiglitazone not. After 5 days and without any further manipulation, the cells were imaged with the DHM and then washed with IMDM medium, ensuring complete removal of the previous media and the compounds. The OPD value of each well was recorded to correlate the extent of adipogenesis with hematopoietic proliferation post-co-culture. KLS (lin⁺/cKit⁺/Sca1⁺) cells were extracted from B6 ACTb-EGFP mice and plated at a ratio of 1:10 initial OP9 cells (666 KLS cells per well). After 7 days co-culture, the media manually removed, the wells washed once, and trypsinized before staining the cells with CD45-PacBlue, PI, and CountBright beads. CD45⁺ cells were then counted using the High Throughput Sampler (HTS) module of a LSRII flow cytometer. **B.** Second order polynomial correlation between the OPD values of compound-treated OP9 cells and adherent CD45⁺ cell counts post-co-culture. **C.** Linear correlation between 'Hematopoietic' score as measured previously by RNA-seq and adherent CD45⁺ cell count post-co-culture. Only concentrations one Log higher than the EC₅₀ concentration at which OP9 adipocytic differentiation is inhibited, are included. **D.** Non-adherent CD45⁺ cell count post-co-culture sorted by the four groups observed in the PCA of the RNA-seq data. Only concentrations one Log higher than the EC₅₀ concentration at which OP9 adipocytic differentiation is inhibited, are included. **E.** Total adherent CD45⁺ cell count after co-culture for each individual compound tested. **F.** Schematic representation of the co-culture assay, assessing non-adherent CD45⁺ cells. Co-culture was performed, as described for adherent CD45⁺ cell counts. At the end of the co-culture however, the wells were not washed and directly stained and counted using the High Throughput Sampler (HTS) module of a LSRII flow cytometer. **G.** Second order polynomial correlation between the OPD values of compound-treated OP9 cells and non-adherent CD45⁺ cell counts post-co-culture. **H.** Linear correlation between 'Hematopoietic' score as measured previously by RNA-seq and non-adherent CD45⁺ cell count post-co-culture. Only concentrations one Log higher than the EC₅₀ concentration at which OP9 adipocytic differentiation is inhibited, are included. **I.** Non-adherent CD45⁺ cell count post-co-culture sorted by the four groups observed in the PCA of the RNA-seq data. Only concentrations one Log higher than the EC₅₀ concentration at which OP9 adipocytic differentiation is inhibited, are included. **J.** Total non-adherent CD45⁺ cell count after co-culture for each individual compound tested. Error Bars are S.D.

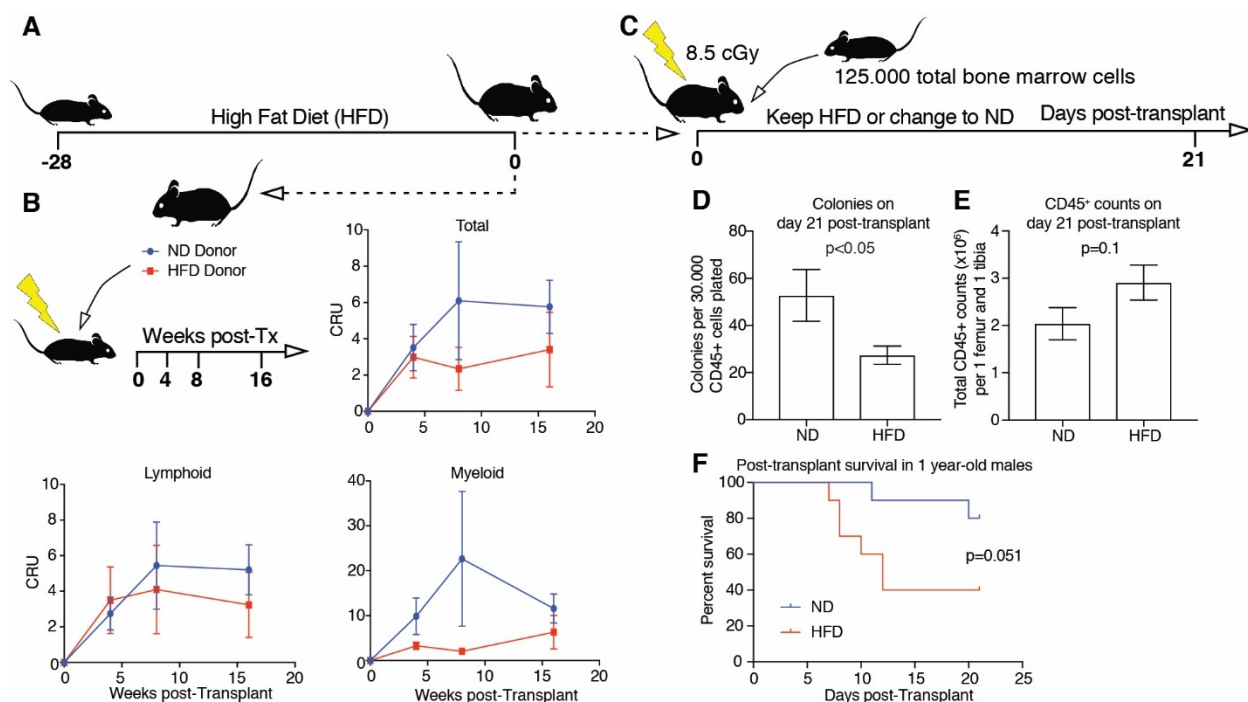


Figure 4.5 The effect of high fat diet (HFD) on hematopoietic regeneration post-transplant. **A.** 8- to 12-week old female C57Bl/6J mice were fed with HFD (D12492i, Research Diet, 60 % fat) or normal diet (ND, D12450Ji, Research Diet, 10 % fat) for 4 weeks. **B.** 200,000 total bone marrow cells from HFD- or ND-fed donor mice were transplanted into lethally irradiated non-MHC-mismatched mice. Using the CD45.1/2 system, the competitive repopulating units (CRU) were assessed for both lymphoid and myeloid lineages on weeks 4, 8, and 16 post-transplantation. CRU are calculated using poisson statistics and represent the quantity of HSCs in the donor bone marrow [177], [178]. **C.** Mice that were fed with HFD for 4 weeks, were transplanted with 125,000 total bone marrow cells from MHC-compatible donors. Half the mice changed to ND, while the other half remained on HFD during the transplant period. On day 21 post-transplant, the bones of transplanted mice were extracted. **D.** Colony-forming capacity of the bone marrow of mice on day 21 post-transplant. **E.** CD45⁺ cells from the bone marrow of mice on day 21 post-transplant were previously counted on a LSRII flow cytometer. **F.** Post-transplant survival of 1 year old C57Bl/6J males kept on HFD or ND for 4 week pre-transplant as well as three weeks post-transplant.

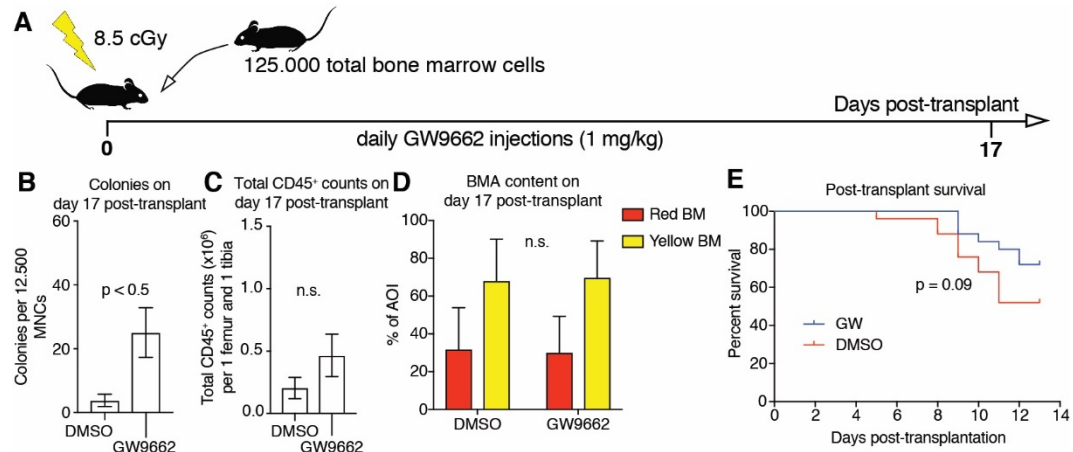


Figure 4.6 The effect of PPAR γ inhibition on hematopoietic regeneration post-transplant. **A.** 8- to 12-week old female C57Bl/6J mice were transplanted with 125,000 total bone marrow cells from MHC-compatible donors. The mice were treated with daily intraperitoneal injections of GW9662 (1 mg/kg) or corresponding volume of vehicle (DMSO) from day -1 to day 17 post-transplant. On day 17 post-transplant the bones of the transplanted mice were extracted. **B.** Colony-forming capacity of the bone marrow of mice on day 17 post-transplant. **C.** Total CD45⁺ cell counts from the bone marrow of mice on day 17 post-transplant counted on a LSRII flow cytometer. **D.** Quantification of 'yellow' and 'red' bone marrow, using the in-house developed image analysis plugin for ImageJ, as previously described in Fig 2.1. **E.** Post-transplant survival of 1-year old C57Bl/6J males kept on HFD or ND for 4 weeks pre-transplant as well as three weeks post-transplant.

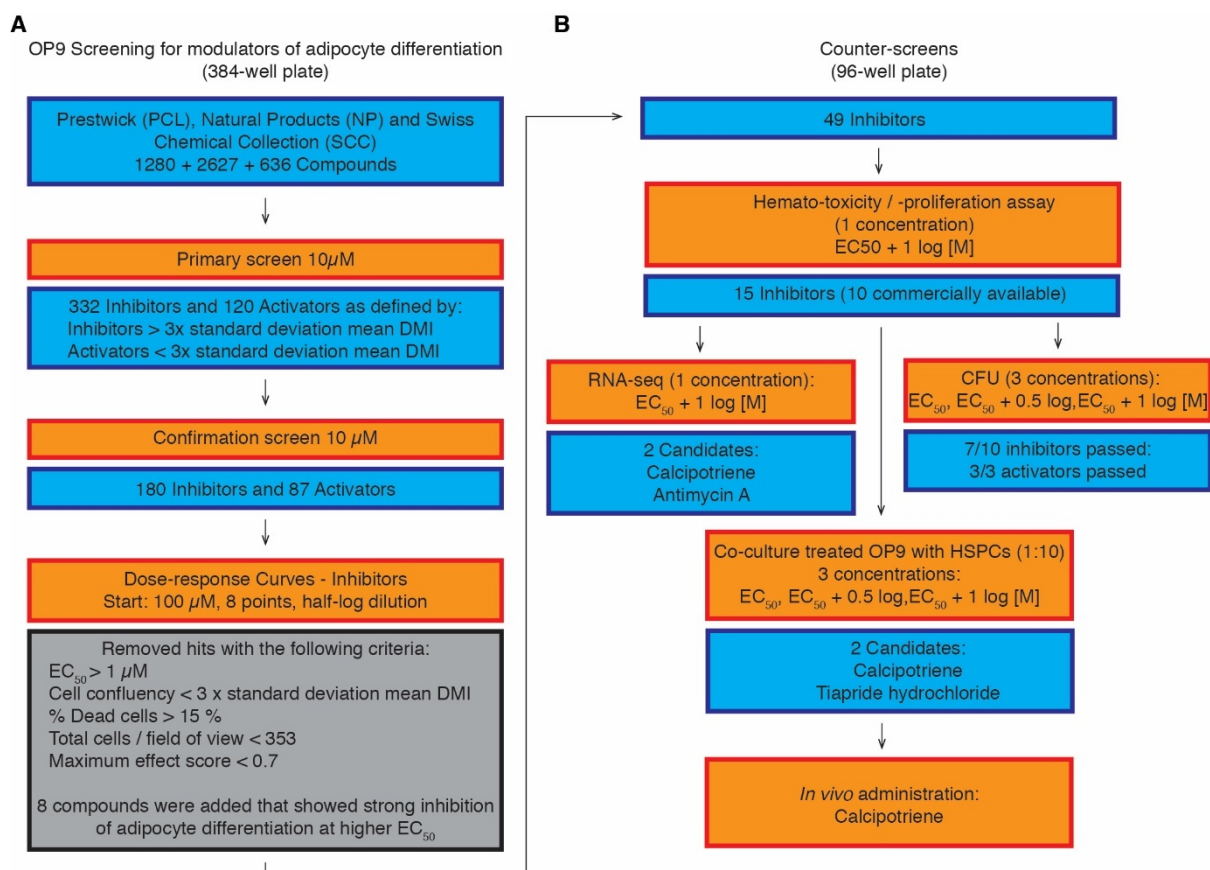


Figure S 4.1 Summary of the screening for novel inhibitors of adipocyte differentiation. **A.** Screening for inhibitors of OP9 adipocyte differentiation, performed in 384-well plates. Orange boxes represent the different assays, whereas blue boxes represent the compounds tested or the corresponding hits to each assay. The grey box represents the criteria for the choice of inhibitors in the OP9 screening. **B.** Counter-screens are performed in 96-well plates and were designed (i) to ensure no deleterious effect of the compounds on HSPCs and (ii) to test the capacity of compound-treated OP9 cells to support hematopoiesis. Therefore, the counter-screens involve either culturing HSPCs with the previously identified modulators of adipocyte differentiation ('hemato-toxicity' and CFU assays) or HSPCs in co-culture with compound-pre-treated OP9 cells. The RNA-seq assay was performed to identify compounds inhibiting adipocyte-specific gene expression as well as maintaining expression of hematopoiesis-supportive cytokines in OP9 cells. The screening led us to calcipotriene, a synthetic vitamin-D₃ analog, which inhibited OP9 adipocyte differentiation efficiently while maintaining hematopoiesis-supportive capacity. It is the chosen candidate to test the acceleration of hematopoietic recovery post-transplantation *in vivo*.

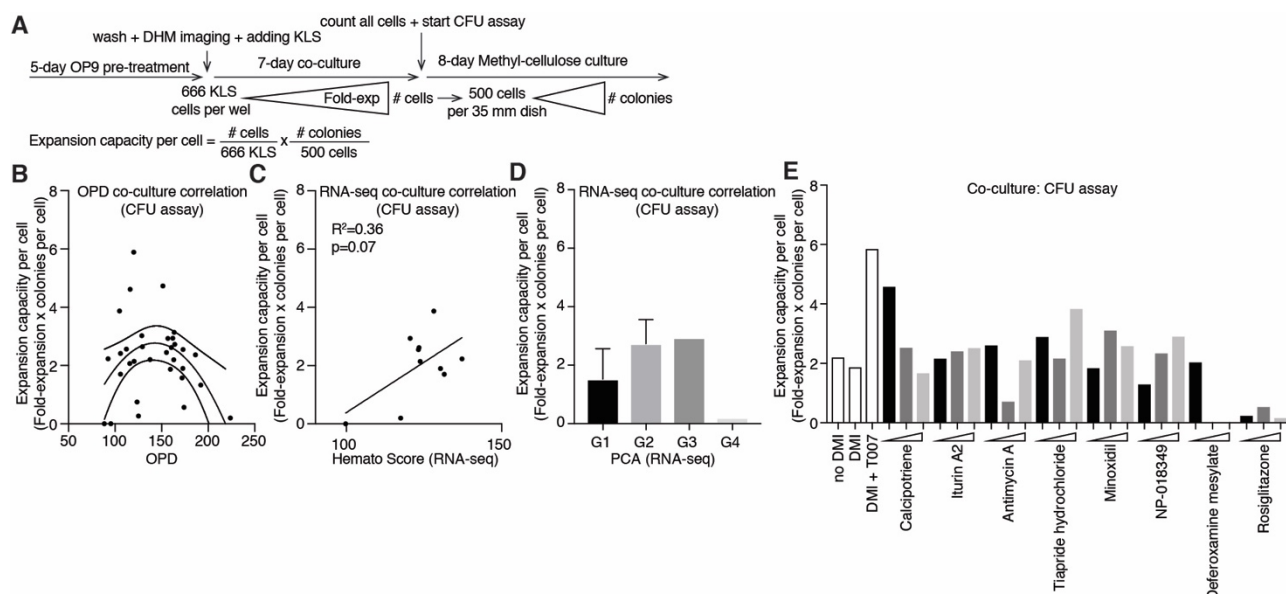


Figure S 4.2 CFU assay of HSPCs co-cultured with compound-pre-treated OP9 cells. **A.** Schematic representation of the co-culture assay, with the aim of assessing colony-forming capacity of HSPCs after co-culture. Co-culture was performed, as described for adherent and non-adherent CD45⁺ cell counts. At the end of the co-culture however, both adherent and non-adherent cells from triplicate wells were pooled, a portion of which, stained with CD45-PacBlue, PI, and CountBright beads. CD45⁺ cells were counted using the High Throughput Sampler (HTS) module of a LSRII flow cytometer and 500 CD45⁺ cells plated into methylcellulose. After 8 days of culture in methylcellulose, the colonies were counted using the STEMvision automated CFU counter (STEMCELL Technologies, USA). The expansion capacity per KLS cell was calculated by multiplying the fold-expansion of CD45⁺ cells during co-culture with the number of colonies per CD45⁺ plated in methylcellulose. **B.** Second order polynomial correlation between the OPD values of compound-treated OP9 cells and the expansion capacity per initial LKS cell. **C.** Linear correlation between ‘Hematopoietic’ score as measured previously by RNA-seq and the expansion capacity per initial LKS cell. Only concentrations one Log higher than the EC₅₀ concentration at which OP9 adipocytic differentiation is inhibited, are included. **D.** Expansion capacity per initial LKS cell sorted by the four groups observed in the PCA of the RNA-seq data. Only concentrations one Log higher than the EC₅₀ concentration at which OP9 adipocytic differentiation is inhibited, are included. **E.** The expansion capacity per initial LKS cell for each individual compound tested.

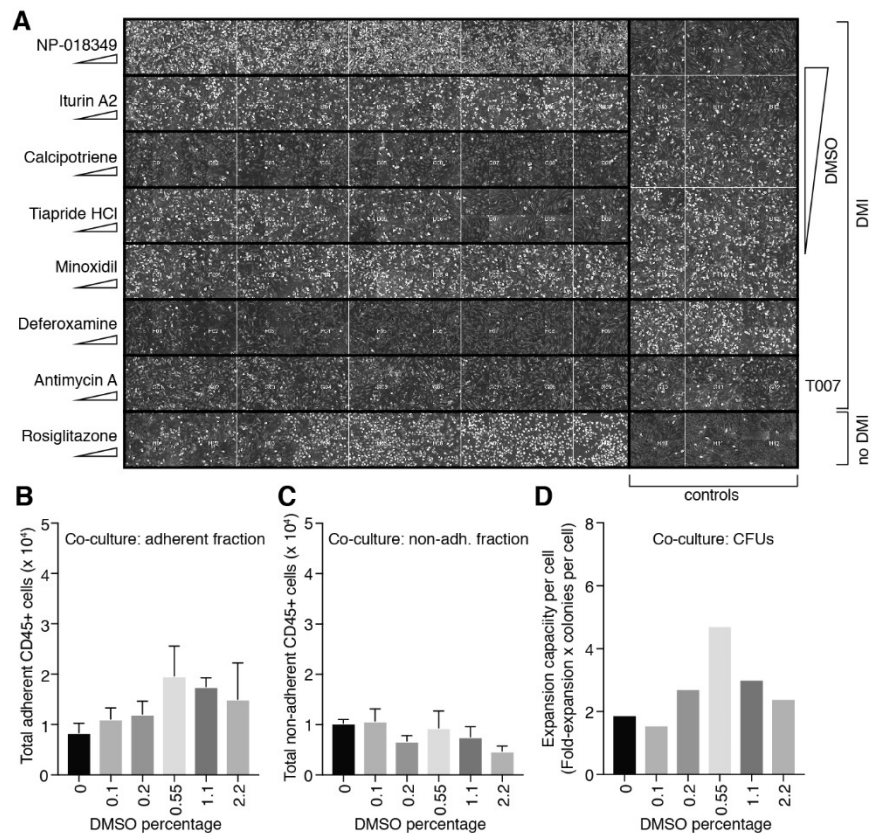


Figure S 4.3 DHM imaging prior to co-culture, including DMSO controls. **A.** Representative DHM snapshot of a 96-well plate, containing OP9 cells pre-treated with the selected compounds. For all three co-culture assays (adherent fraction, non-adherent fraction and CFU-capacity), the snapshots were identical. Compounds were plated in triplicates and in three doses: from the EC₅₀ of inhibition of OP9 adipocyte differentiation (for Rosiglitazone: EC₅₀ of induction), half Log higher and one Log higher. **B.** Total adherent CD45⁺ cell count after co-culture for each concentration of DMSO tested (the assay way previously described in Fig. 4.4). **C.** Total non-adherent CD45⁺ cell count after co-culture for each concentration of DMSO tested (the assay way previously described in Fig. 4.4). **D.** The expansion capacity per initial LKS cell for each concentration of DMSO tested (the assay way previously described in Fig. S 4.2).

GW9662	BADGE	Rosi	HFD	
				Survival
				CFU
				CD45 ⁺
				WBC
				RBC
				Plt
				BMA

Significant increase

Trend increase

No change or N/A

Trend decrease

Significant decrease

Figure S 4.4 Summary of the *in vivo* data. All results are concerning the effects of the *in vivo* modulation of adipocyte differentiation on day 21 post-transplant.

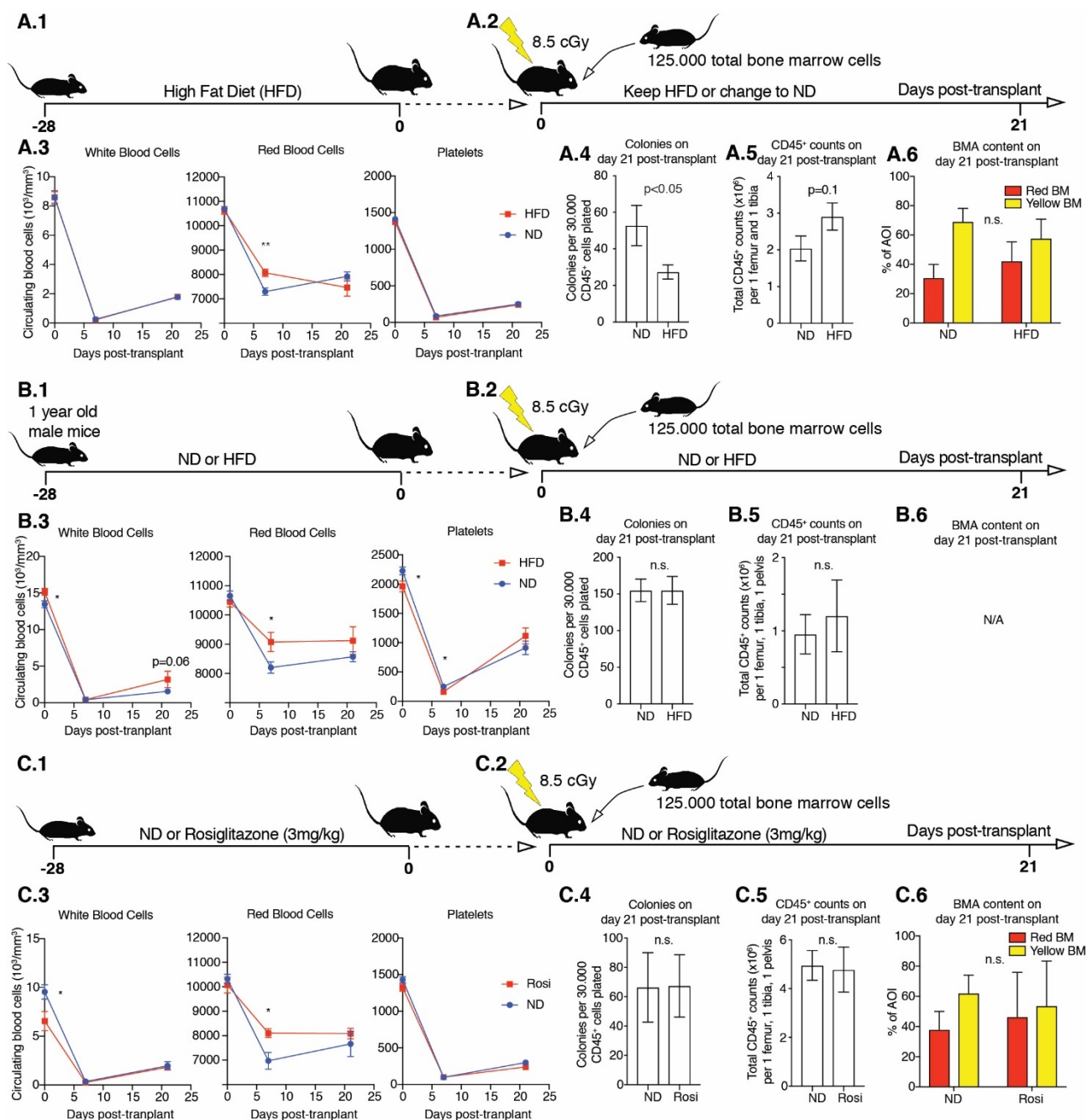


Figure S 4.5 The effect of HFD and Rosiglitazone on hematopoietic regeneration post-transplant: extended results. **A.1.** 8- to 12-week old female C57Bl/6J mice were fed with HFD (D12492i, Research Diet, 60 % fat) or normal diet (ND, D12450Ji, Research Diet, 10 % fat) for 4 weeks. **A.2.** Mice that were fed with HFD for 4 weeks, were transplanted with 125,000 total bone marrow cells from MHC-compatible donors. Half the mice changed to ND, while the other half remained on HFD during the transplant period. On day 21 post-transplant, the bones of transplanted mice were extracted. **A.3** Circulating white blood cells, red blood cells and platelets in the post-transplant period. **A.4.** Colony-forming capacity of the bone marrow of mice on day 21 post-transplant. **A.5.** CD45⁺ cells from the bone marrow of mice on day 21 post-transplant were previously counted on a LSRII flow cytometer. **A.6.** Quantification of 'yellow' and 'red' bone marrow, using the in-house developed image analysis plugin for ImageJ, as previously described in Fig 2.1. **B.1.** 1-year old C57Bl/6J mice were kept on either HFD or ND for the entirety of the experiment. **B.2** After 4 weeks of treatment the mice were lethally irradiated and transplanted with 125,000 total bone marrow cells from MHC-compatible donors. On day 21 post-transplant, the bones of transplanted mice were extracted. **B.3** Circulating white blood cells, red blood cells and platelets in the post-transplant period. **B.4.** Colony-forming capacity of the bone marrow of mice on day 21 post-transplant. **B.5.** CD45⁺ cells from the bone marrow of mice on day 21 post-transplant were previously counted on a LSRII flow cytometer. **C.1.** 8- to 12-week old female C57Bl/6J mice were fed with chow diet containing 20 mg/kg diet for the entirety of the experiment. **C.2.** After 4 weeks of treatment the mice were lethally irradiated and transplanted with 125,000 total bone marrow cells from MHC-compatible donors. On day 21 post-transplant,

the bones of transplanted mice were extracted. **C.3.** Circulating white blood cells, red blood cells and platelets in the post-transplant period. **C.4.** Colony-forming capacity of the bone marrow of mice on day 21 post-transplant. **C.5.** CD45⁺ cells from the bone marrow of mice on day 21 post-transplant were previously counted on a LSRII flow cytometer. **C.6.** Quantification of 'yellow' and 'red' bone marrow, using the in-house developed image analysis plugin for ImageJ, as previously described in Fig 2.1.

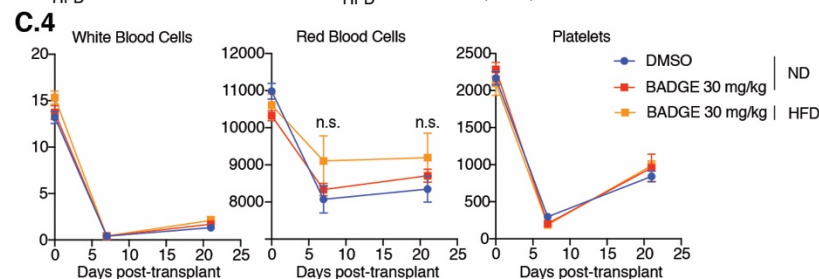
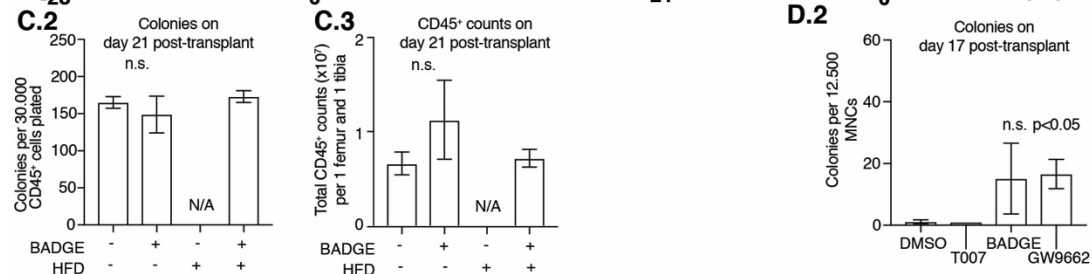
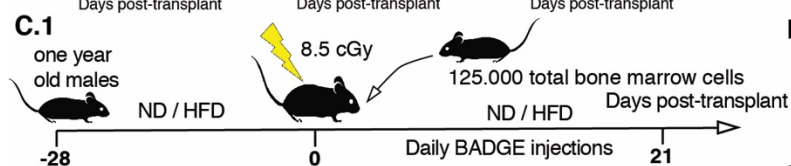
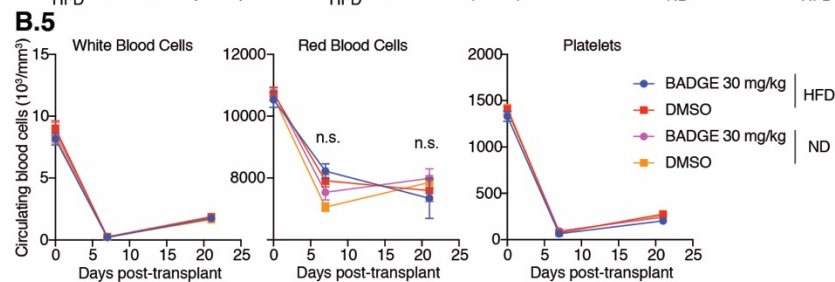
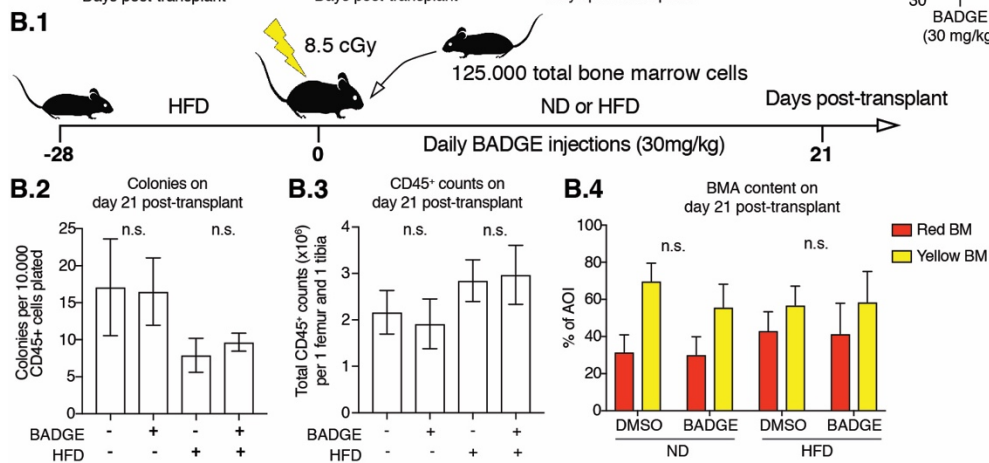
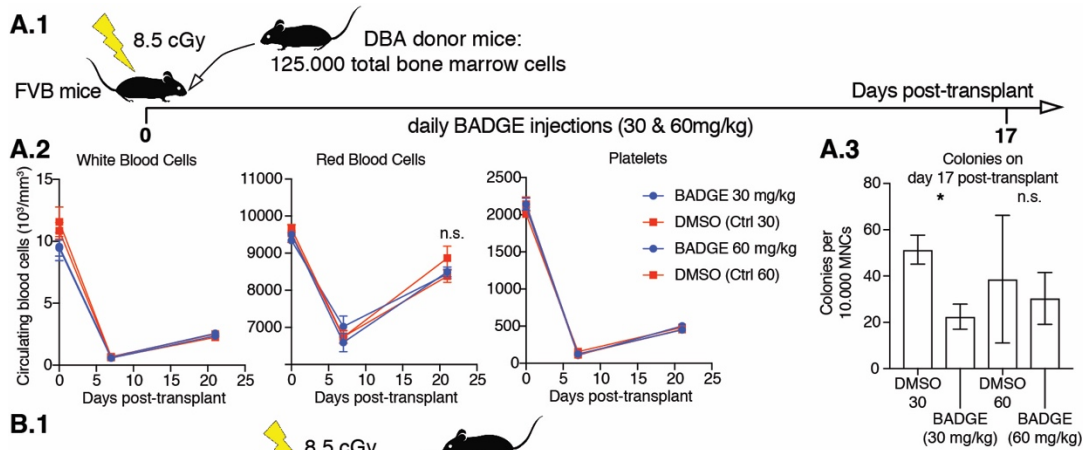


Figure S 4.6 The effect of PPAR γ inhibition on hematopoietic regeneration post-transplant: extended results. **A.1.** 8- to 12-week old female FVB mice were transplanted with 125.000 total bone marrow cells from MHC-compatible DBA donors. The mice were treated with daily intraperitoneal injections of BADGE (30 and 60 mg/kg) or corresponding volume of vehicle (DMSO) from day -1 to day 17 post-transplant. On day 17 post-transplant the bones of the transplanted mice were extracted. **A.2.** Circulating white blood cells, red blood cells and platelets in the post-transplant period. **A.3.** Colony-forming capacity of the bone marrow of mice on day 17 post-transplant. **B.1.** 8- to 12-week old female C57Bl/6J mice were fed with HFD (D12492i, Research Diet, 60 % fat) or normal diet (ND, D12450Ji, Research Diet, 10 % fat) for 4 weeks. Mice that were fed with HFD for 4 weeks, were transplanted with 125.000 total bone marrow cells from MHC-compatible donors. Half the mice changed to ND, while the other half remained on HFD during the transplant period. The two groups were further split into four, given that the mice were treated with daily intraperitoneal injections of BADGE (30 mg/kg) or corresponding volume of vehicle (DMSO) from day -1 to day 21 post-transplant. On day 21 post-transplant, the bones of transplanted mice were extracted. **B.2.** Colony-forming capacity of the bone marrow of mice on day 21 post-transplant. **B.3.** CD45⁺ cells from the bone marrow of mice on day 21 post-transplant were previously counted on a LSRII flow cytometer. **B.4.** Quantification of 'yellow' and 'red' bone marrow, using the in-house developed image analysis plugin for ImageJ, as previously described in Fig 2.1. **C.1.** 1-year old C57Bl/6J males kept on HFD or ND for the entirety of the experiment. After 4 weeks of treatment the mice were lethally irradiated and transplanted with 125.000 total bone marrow cells from MHC-compatible donors. The two groups were further split into four, given that the mice were treated with daily intraperitoneal injections of BADGE (30 mg/kg) or corresponding volume of vehicle (DMSO) from day -1 to day 21 post-transplant. On day 21 post-transplant, the bones of transplanted mice were extracted. **C.2.** Colony-forming capacity of the bone marrow of mice on day 21 post-transplant. **C.3.** CD45⁺ cells from the bone marrow of mice on day 21 post-transplant were previously counted on a LSRII flow cytometer. **C.4.** Circulating white blood cells, red blood cells and platelets in the post-transplant period. **D.1.** 8- to 12-week old female C57Bl/6J mice were transplanted with 125.000 total bone marrow cells from MHC-compatible donors. The mice were treated with daily intraperitoneal injections of GW9662 (1 mg/kg), T0070907 (1 mg/kg), BADGE (30 mg/kg) or corresponding volume of vehicle (DMSO) from day -1 to day 17 post-transplant. On day 17 post-transplant the bones of the transplanted mice were extracted. **D.2.** Colony-forming capacity of the bone marrow of mice on day 17 post-transplant.

Chapter 5 The NAD-booster nicotinamide riboside potently stimulates hematopoiesis through increased mitochondrial clearance

This work belongs to a manuscript prepared for *Cell Stem Cell*. It was published on March 7th 2019.

Authors:

N. Vannini^{1,2*}, V. Campos^{1*}, M. Girotra^{2,3}, V. Trachsel³, S. Rojas-Sutterlin¹, J. Tratwal¹, S. Ragusa², E. Stefanidis^{2,4}, D. Ryu^{5†}, P.Y. Rainer⁶, G. Nikitin³, S. Giger³, Y.L. Terytty⁵, A. Semilietof^{2,4}, A. Oggier¹, Y. Yersin¹, L. Tauzin⁷, E. Pirinen^{5†}, W.C. Cheng², J. Ratajczak⁸, C. Canto^{8,9}, M. Ehrbar¹⁰, F. Sizzano⁸, T.V. Petrova^{2,11}, D. Vanhecke², L. Zhang^{2†}, P. Romero², A. Nahimana¹², S. Cherix¹³, M.A. Duchosal¹², P.C. Ho², B. Deplancke⁶, G. Coukos^{2,11}, J. Auwerx⁵, M. P. Lutolf^{3,14} and O. Naveiras^{1,11,12}

*These authors contributed equally to this work

Affiliations:

¹ Laboratory of Regenerative Hematopoiesis, Swiss Institute for Experimental Cancer Research (ISREC) & Institute of Bioengineering (IBI), School of Life Sciences, Ecole Polytechnique Fédérale de Lausanne (EPFL); Lausanne, Switzerland.

² Department of Oncology UNIL CHUV, Ludwig Institute for Cancer Research Lausanne, University of Lausanne, Epalinges 1066, Switzerland.

³ Laboratory of Stem Cell Bioengineering, Institute of Bioengineering, Ecole Polytechnique Fédérale de Lausanne (EPFL); Lausanne, Switzerland.

⁴ Department of Molecular Biology and Genetics, Democritus University of Thrace, Alexandroupolis, Greece

⁵ Laboratory of Integrative and Systems Physiology, Institute of Bioengineering, Ecole Polytechnique Fédérale de Lausanne (EPFL); Lausanne, Switzerland.

⁶ Laboratory of System Biology and Genetics, Institute of Bioengineering, Ecole Polytechnique Fédérale de Lausanne (EPFL); Lausanne, Switzerland.

⁷ Flow Cytometry Platform, School of Life Sciences, Ecole Polytechnique Fédérale de Lausanne (EPFL), Lausanne, Switzerland.

⁸ Nestlé Research, EPFL Innovation Park, 1015 Lausanne, Switzerland

⁹ School of Life Sciences, Ecole Polytechnique Fédérale de Lausanne (EPFL); Lausanne, Switzerland.

¹⁰ Department of Obstetrics, University Hospital Zürich, University of Zürich, Zürich, Switzerland.

¹¹ Swiss Institute for Experimental Cancer Research (ISREC), School of Life Sciences. Swiss Federal Institute of Technology Lausanne (EPFL), Lausanne, Switzerland.

¹² Service and Central Laboratory of Hematology, Departments of Oncology and of Laboratories, Centre Hospitalier Universitaire Vaudois (CHUV), Lausanne, Switzerland.

¹³ Service d'orthopédie et de traumatologie, Centre Hospitalier Universitaire Vaudois (CHUV), Lausanne, Switzerland

¹⁴ Institute of Chemical Sciences and Engineering, School of Basic Sciences, Ecole Polytechnique Fédérale de Lausanne (EPFL); Lausanne, Switzerland.

Author Contributions: N.V., V.C., O.N., M.P.L and J.A. conceived ideas, designed experiments, analyzed results and wrote the manuscript. N.V, O.N., V.C., D.R., M.G., S.R., W.C.C, P.C.H and T.V.P. performed and interpreted the murine autophagy and mitochondrial clearance experiments, while M.G., S.G., V.C., Y.L.T., A.N. and M.A.D performed and interpreted human autophagy and mitochondrial clearance experiments. J.R and C.C. provided Nr1h1^{-/-};Nr1h2^{-/-} double knock-out mice. M.E. recruited patients and provided cord blood units. V.T., G.N. and M.P.L. performed and interpreted mito-GFP and asymmetry experiments. O.N., V.C, N.V., S.R.S., J.T., A.O. and Y.Y., performed and interpreted FACS, CFU progenitor and murine *in vivo* transplantation studies. M.G., E.S., A.S., D.V. and G.C. performed, designed and/or analyzed experiments in humanized mice. L.T., F.S. and A.P. contributed to FACS data acquisition and analysis of murine BM and cord blood. P.Y.R. and B.D. analyzed RNAseq data. L. Z. and P.R. performed OCR experiments. S.C. contributed to the design of the human ethical protocol, ensured patient recruitment and provided all adult BM samples. E. P. and J.A. conceived ideas, provided key reagents and comprehensively contributed to experimental design. N.V., M.P.L. and O.N. co-initiated the project. All authors edited and reviewed the final manuscript.

Competing Interest: Some elements of this work have been submitted as application P1828EP00 to the European Patent Office. The authors have no other competing financial interest.

5.1 Abstract

It has been recently shown that increased oxidative phosphorylation, as reflected by increased mitochondrial activity, together with impairment of the mitochondrial stress response can severely compromise hematopoietic stem cell (HSC) regeneration. Here we show that the NAD⁺-boosting agent Nicotinamide Riboside (NR) reduces mitochondrial activity within HSCs through increased mitochondrial clearance, leading to increased asymmetric HSC divisions. NR dietary supplementation results in a significantly enlarged pool of progenitors, without concurrent HSC exhaustion, improves survival by 80%, and accelerates blood recovery after murine lethal irradiation and limiting-HSC transplantation. In immune-deficient mice, NR increased the production of human leucocytes from hCD34⁺ progenitors. Our work demonstrates for the first time a positive effect of NAD⁺ boosting strategies on the most primitive blood stem cells, establishes a novel link between HSC mitochondrial stress, mitophagy and stem cell fate decision, and unveils the potential of NR to improve recovery of patients suffering from hematological failure including post-chemo/radiotherapy.

Keywords: hematopoietic stem cell, HSC, long-term hematopoietic stem cell, mitochondria, mitochondrial clearance, mitochondrial recycling, autophagy, mitophagy, mitonuclear protein imbalance, unfolded protein response mitochondria, UPR^{mt}, asymmetric stem cell division, hematopoietic stem cell transplantation, bone marrow transplantation, bone marrow failure, bone marrow aplasia, human CD34⁺ progenitors, immune thrombocytopenia, aplastic anemia, chemotherapy, radiotherapy

5.2 Introduction

A remarkably small pool of hematopoietic stem cells (HSCs) is responsible for the production of a staggering 10¹¹ mature blood cells per day [179], [180]. HSCs are predominantly quiescent during homeostasis [181], entering the cell cycle in response to the physiological demands of the blood-producing system. Consistent with their quiescent state, most HSCs exhibit a relatively low mitochondrial potential and low NAD⁺/NADH content, reflecting their glycolysis-driven metabolic profile when residing in their homeostatic hypoxic niche [25], [27], [42]. Stress-induced hematopoiesis occurs after extensive injury of intermediate progenitors and their terminally differentiated progeny: platelets, red blood cells and/or leucocytes, which induces rapid proliferation of HSCs to replenish the depleted progenitor populations. HSC transplantation, a procedure where HSCs from an immune-compatible donor are transferred intravenously to a host that has received a lethal dose of radiation or chemotherapy, constitutes the best-characterized model of stress-induced hematopoiesis [23]. One single long-term (LT) HSC can actually reconstitute the whole hematopoietic system of a mouse in these conditions [13]. In humans, HSC transplantation has become the first and most extensively exploited stem cell therapy to date, and the only curative regime for most types of leukemia and aggressive lymphomas [182]. However, the slow nature of hematopoietic recovery still translates into up to 25% toxicity-associated mortality, in large part due to the severe infections that accompany the period of bone marrow (BM) and immune aplasia [182][8].

The proliferative stress imposed on HSCs to reconstitute the full hematopoietic system in the 3-6 weeks following HSC transplantation entails activation of oxidative phosphorylation within mitochondria [24], interferes with pyruvate dehydrogenase kinase (PDK) and hypoxia-inducible factor (HIF α)-driven metabolic checkpoints of HSC self-renewal [25], [27] and thus induces premature HSC aging [31]. In turn, activation of the mitochondrial stress response, and more specifically of the mitochondrial unfolded protein response (UPR^{mt}), has been shown to enhance mitochondrial health and to prolong lifespan from *C. elegans* to mice [183]. In conditions where mitochondrial activity is boosted, a two-step stress signaling pathway is initiated, involving an early UPR^{mt} induction and a delayed ROS-mediated Foxo/DAF-16 activation that can promote lifespan extension in *C. elegans* [184]. Indeed, FOXO3-mediated autophagy initiation together with activation of the mitochondrial stress response has been shown to act as a metabolic checkpoint that regulates HSCs maintenance [39], [40].

We set out to test whether a clinically-compatible pharmacological strategy to induce the mitochondrial stress response would improve HSC mitochondrial homeostasis and improve hematological reconstitution after HSC transplantation. We chose a NAD⁺-boosting strategy because it has been characterized as a means of activating the SIRT1 axis via the induction of the mitochondrial stress response in the context of aging, liver and muscle regeneration [184]–[188]. Interestingly, the NAD⁺ precursor Nicotinamide (NAM) has been shown to increase the homing of hematopoietic progenitors and to enhance platelet formation *in vitro* [189][190][191], but efforts to use NAM supplementation to enhance hematopoiesis *in vivo* have failed [192]. Here we reveal the ability of a different NAD⁺ boosting agent, nicotinamide riboside (NR), to reduce mitochondrial potential in HSCs and enhance hematopoiesis *in vivo* via activation of autophagy, increased mitochondrial clearance and increased proliferative asymmetry in LT-HSCs.

5.3 Experimental procedures

5.3.1 Study design

HSC function is strongly regulated by their metabolic state. In this study we aimed to test the modulation of intracellular NAD as a possible strategy to influence HSC fate. In the first part of the study we analyzed the effect of NR on the hematopoietic stem and progenitor compartments. The phenotypic analysis was performed by FACS while functional analysis consisted of CFU colony assay and BM transplantation.

In the second part we evaluated the effect of NR on mitochondrial metabolism. As readout we chose TMRM staining for FACS, a rhodamine based that is absorbed by the mitochondria based on a functional membrane potential, as well as mitochondrial dye MitoTracker Deep Red and JC1 for confocal microscopy. Unfortunately, other type of analysis (i.e., proteomics or use of Seahorse metabolic analysers) was not technically possible due to the limited number of cells (LT-HSCs \approx 1000/mouse and ST-HSCs \approx 2500/mouse).

In the third part we evaluated the activation of autophagy/mitophagy and mitochondrial stress response as candidate pathways for the reduction in mitochondrial activity. The analysis was performed by RNA sequencing (*in vitro* NR-treated HSCs) and quantitative RT-PCR (*in vivo* NR-treated HSCs) in order to assess changes in gene expression for the components of these pathways. As above, RNA transcription analysis is one of the few methods that allows the analysis of molecular mechanism in such rare populations. Mitonuclear imbalance was validated at the protein level by Western blotting of FACS-sorted LT-HSCs.

In the fourth part we assessed asymmetrical HSC division via confocal microscopy analysis of paired-daughter cells, to evaluate asymmetrical distribution of active mitochondria immediately after cell division.

In the last section we translated our findings to a clinically relevant scenario. Due to the effect of NR on the hematopoietic progenitor compartments, we investigated the capacity of NR to boost blood cell production in post-transplant mice and to improve the survival of mice transplanted with a limited number of BM cells.

5.3.2 Mice

C57Bl/6J and C57Bl/6J Ly5.1 were purchased from Charles River Laboratories International and maintained at the Center for Studying Living System (CAV) at the EPFL in microisolator cages. Mito-QC in C57Bl/6J background were provided by P.C. Ho, bred at the Ludwig Institute for Cancer Research Lausanne and their BM analyzed at EPFL. *Nrk1*^{-/-}; *Nrk2*^{-/-} mice, also in C57Bl/6 background, were provided by C. Cantó, then bred and analyzed at EPFL. Mice were provided continuously with sterile food, water and bedding. All *in vivo* procedures were carried out in accordance with the Swiss law after approval from the local authorities (Service Vétérinaire de l'Etat de Vaud). All experiments were designed according to the ARRIVE guidelines.

5.3.3 Food preparation

NR diet was prepared by mixing NR triflate (custom synthesized by Novalix, beta form isomer purity > 95%) dissolved in water with 2916 powder diet (Charles River) and air dried into pellets in sterile conditions. The NR dosage in the mix was calculated by taking into account the average mouse food intake per day (5g food/ mouse/ day) for a calculated intake of 12mg NR triflate /mouse/day (=7.57mg/mouse/day of NR+). NA and NAM were provided at the same dose, that is, 480mg/kg of food chow [187]. The food was provided ad libitum during the entire period of the experiment. Niagen was purchased from Live Cell Research; NR dose was calculated based on the manufacturer's report of NR chloride content, and capsules were then opened and their full powder content (containing cellulose and silicon dioxide as excipients) was mixed with "2916" powder diet as for custom-synthesized NR triflate.

5.3.4 Antibodies

The following antibodies were used in this study: rat mAbs against cKit (2B8), Sca1 (D7), CD150 (TC-15-12F12.2), CD34 (RAM34), CD48 (HM48-1), CD45.2 (104), CD45.1 (A20), Gr1 (RB6-8C5), F4/80 (BM8), CD19 (6D5), CD3 (17A2), CD16/CD32 (2.4G2). The antibodies were purchased from Biolegend, eBiosciences and BD. A mixture of biotinylated mAbs against CD3, CD11b, CD45R/B220, Ly-6G, Ly-6C and TER-119 was used as lineage marker ("lineage cocktail") and it was purchased from BD. Human specific antibodies were: hCD56 (NCAM16.2), hCD16 (3G8), hCD45 (HI30), hCD19 (HIB19), hCD4 (RPA-T4), hCD3 (SK7), hCD14 (M5E2), hCD8b (SIDI8BEE), hCD34 (8G12), hCD38 (HB-7) and were either from eBioscience or BD. DAPI or propidium iodine (PI) staining was used for live/dead cell discrimination.

5.3.5 Flow cytometry

Flow cytometry analysis of stem and progenitor hematopoietic compartments was performed on freshly isolated bone marrow (BM). BM was extracted from crushed femora and tibia. Cells suspension was filtered through 70µm cell strainer and erythroid cells were eliminated by incubation with red blood cells lysis buffer (eBiosciences). Isolation and stains were performed in ice-cold PBS 1mM EDTA. Lineage positive cells were then removed with a magnetic lineage depletion kit (Milteny Biotechnology). Cells suspension were then stained with specific antibodies for stem/progenitor compartments and analyzed or sorted respectively on BD LSR2 and BD FACS Aria 2.

5.3.6 Analysis of mitochondrial activity

Freshly isolated BM cells were incubated at 37°C for 1 hour with 200nM TMRM (Invitrogen) and subsequently stained with specific antibodies for different hematopoietic compartments. Cells were then analyzed or sorted by flow cytometry. For confocal imaging, LT-HSC and ST-HSC were sorted into StemLine II supplemented with SCF+Flt3L +/- NR as for HSC culture, and let adhere on a poly-lysine coated slide for 6 hours. JC-1 was then added in the cell media according to the manufacturer instructions (Cayman Chemical) and live cell images were acquired on a Leica SP5.

5.3.7 Analysis of autophagy flux

Sorted LT and ST cells were cultured in complete growth medium in presence or absence of $\pm 500\mu\text{M}$ NR for 24hours and treated with 5nM Bafilomycin or PBS for additional 12 hours. The cells were treated with Mitotracker Deep Red (Thermo Scientific), fixed with PFA 4%, stained for Lc3b (Cell Signaling) and mounted using Prolong mounting medium with DAPI (Thermo Scientific). For Lc3b, we used donkey anti-rabbit 555 secondary antibody (Alexa). The fluorescent pictures were taken using Zeiss 880LSM Airyscan. 3D whole cell reconstructions were analyzed using Imaris software (Bitplane) to calculate Lc3b punctae number and mitochondria surface, utilizing dot and surface analyses functions.

5.3.8 Murine HSC culture

HSCs were sorted and cultured for 2 or 5 days. Cultures were maintained in Stemline II (Sigma) supplemented with 100ng/ml SCF (R&D) and 2ng/ml Flt3 (R&D), +/- 500µM NR or increasing concentrations up to 2mM for the dose-response curves. NR and NMN were replenished every 24 (2-day cultures) or 48h (5-day cultures) into the culture media. At the end of the culture period cells were stained with TMRM or JC1 and analyzed by flow cytometry or confocal microscopy

5.3.9 CFUs assay

12500 total bone marrow cells were isolated from the legs and hips of C57Bl/6J mice and cultured in MethoCult (StemCell technology) containing recombinant SCF, EPO, IL-3 and IL-6. Number and morphology of the colonies were analyzed with phase contrast microscope after 7 days of culture.

5.3.10 Murine bone marrow transplantation

C57Bl/6 Ly5.2 mice were lethally irradiated with a total 850 rad dose in a X-ray radiator (RS-2000, RAD SOURCE) 24h before transplant. The dose was split in two doses of 425 rads separated by a 4-hour interval. Mice were injected with donor cells derived from C57Bl/6 Ly5.1 mice and competitor cells derived from C57Bl/6 Ly5.1/5.2 mice, via tail-vein injection. For the 7-day NR treatment, donors received 150×10^3 total BM donor cells together with 150×10^3 total BM competitor cells. For at least two weeks after lethal irradiation mice were treated with paracetamol and antibiotics in the form of either Bactrim for the limiting-dose transplantation studies (Sulfa and TMP 60mg/Kg/day: 250ml of water with 2.5ml of Bactrim (200mg Sulfa /40mg TMP)) or Baytril/Co-amoxiciline (300 ul of Baytril 10% solution plus 2.5 ml of Amoxymepha to 250 ml of drinking water) for all other transplants. Peripheral blood was collected at 1, 2 and 4 months to determine the percentage of chimerism by FACS analysis. For the limiting transplant experiment, mice received 75×10^3 total BM donor cells and the health status of the animals was monitored twice daily. For the blood recovery curves mice were transplanted with 150×10^3 total BM donor cells. Blood was collected twice per week (blood volume 50 microliters) and analyzed by standard veterinarian blood cell counter (ABCtm).

5.3.11 CFSE

Freshly sorted LT-HSCs were incubated for 20 min at 37°C with 1:400 CFSE stock solution (Cayman chemicals; CFSE cell division assay kit). The cells were pelleted and re-suspended in 1ml of Stemline II (Sigma) containing 10% FBS for 20 min at 37°C. Thereafter, the

cells were washed twice with 1ml of Stemline II (Sigma) and put in culture as described above. KLSCD150- cells were sorted with LT- and ST-HSCs and, given their higher frequency and higher proliferative state, used as controls for determining the peaks of CFSE intensity corresponding to 0 and 1 divisions.

5.3.12 Seahorse Oxygen Respiration Rate (OCR) measurement

OT-1 splenocytes were stimulated *in vitro* with SIINFEKL peptide and IL-2 for in the presence of NR or Ctrl treatment. Cells were plated at equivalent cell number, and ECAR and OCR measurements were assayed upon stimulation in the Seahorse XF24 bioanalyzer (Seahorse Bioscience). Cells were washed and resuspended in serum-free unbuffered KHB medium containing 25mM Glucose, 2mM Glutamine, 1mM pyruvate, 150μM Oleate and 1.5mM Carnitine. The cells were then were plated onto Seahorse cell plates (4 × 10⁵ cells per well) coated with Cell-Tak (BD Bioscience) to allow their attachment. Perturbation profiling of substrate was achieved by addition of oligomycin (1 μg/ml), FCCP (1.5 μM), Etomoxir (200μM), rotenone (100nM) and Antimycin A (1μM; all from Sigma-Aldrich). Experiments with the Seahorse apparatus were done with the following assay conditions: 2-3 min mixture; 2 minutes wait; and 3-4 min measurement.

5.3.13 RNA preparation

LT-HSC and ST-HSCs were FACS sorted (>10⁴ cells per sample), cultured for two days in presence or absence of NR as indicated above, then resuspended in RNA lysis buffer (Zymo Research) and total RNAs extracted using the Quick-RNA Microprep Kit (R1050, Zymo Research) following the manufacturer's instructions. The extraction included a DNA-digestion step and was finally reconstituted in 12.5 μl ddH₂O. In parallel, and as a quality control, some cells were stained with TMRM and analyzed by flow cytometry to verify a significant decrease in ΔΨ_m upon NR-treatment.

Total RNA content was quantified using the Qubit 3 Fluorometer (Invitrogen), and RNA quality control was performed by profile analysis on a TapeStation 4200 system (Agilent) following the manufacturer's protocol. The cDNAs were prepared from 2.5 ng RNA per sample with the "SMART-seq v4 Ultra Low Input RNA Kit for Sequencing" (Clontech), and subsequently processed into sequencing libraries with the Nextera XT kit (Illumina FC-131-1096), in both cases following manufacturer's instructions. The resulting libraries were quantified using a Qubit 3 Fluorometer and their profile monitored on a TapeStation 4200 system.

5.3.14 RNA-seq

Sequencing was performed on a NextSeq 500 system (Illumina) using a High Output cartridge with up to 4*10⁸ Single-End 75 nt reads, following manufacturer's instructions.

The fastq files were evaluated using FastQC v0.11.2 and aligned to the Ensembl-91 gene annotation of GRCh81 using STAR v2.5.0b. The number of tags belonging to each gene was then counted using HTSeq v0.6.1 with the following parameters "htseq-count -s no -m union -f bam". A good quality of mapping was reached since a sufficient proportion of reads (from 60% to 80%) were uniquely mapped to exonic regions. Raw counts for each gene were expressed in counts per million (cpm) for filtering. Only genes expressed in at least three samples with a cpm greater than 0.5 were kept for the rest of the analysis, resulting in a filtered data set of 14034 genes expressed across 12 samples. After this step the 6 replicates (3 control and 3 NR treated, corresponding to three separate FACS isolation and culture batches) for LT or ST-HSCs were processed separately. As a first step the raw counts were normalized using VOOM from Limma v3.34.9 and corrected for batch effect using ComBat. NR-treatment became significantly correlated with the first principal component (PC) of the PC analysis. At this stage, the batches were not significant anymore, meaning that the batch correction was successful. The differentially expression analysis between NR treated cells versus control was performed using Limma pipeline with a cutoff of 2-Fold increase and FDR > 0.05. Finally, we used Gene Set Enrichment Analysis (GSEA software from Broad Institute v3.0) to determine whether some specific gene sets revealed significant difference upon NR treatment. We tested five gene sets defined in the Gene Ontology Consortium: Autophagy (GO:0006914), Oxidative Phosphorylation (GO:0006119), Fatty acid oxidation (GO:0019395), Tricarboxylic Acid Cycle (GO:0006099) and Mitophagy (GO:000423) as well as two manually defined genes sets, since they were not defined by any GO term: NAD salvage and *de novo* synthesis pathway (*Nmnat1*, *Nmnat2*, *Nmnat3*, *Nampt*, *Nmrk1*, *Nmrk2*, *Naprt*, *Nadsyn1*, *Tdo2*, *Afmid*, *Kmo*, *Kynu*, *Haa0*, *Qprt* and *Ido1*) from [193] and mitochondrial unfolded protein response (*Hsp60*, *mt-Hsp70*, *Hsp10*, *ClpP*, *Lonp1*, *Jnk2*, *c-Jun*, *Chop*, *Cebp-beta*, *Yme1l1*, *Afg3l2*, *Spg7*, *Sirt1* and *Ubl5*; from [194].

The differences between the means of the conditions were used to calculate the fold changes and the enrichment score was estimated using the weighted statistical approach and evaluated for significance by doing 20000 genes set based permutations.

5.3.15 qRT-PCR

1,000-50,000 LT-HSCs and ST-HSCs were sorted directly in lysis buffer from ZR RNA MicroPrep (Zymo Research) and RNA extraction was performed accordingly to the manufacturer instructions. RNA was eluted and re-suspended in 6µl of H₂O. 2µl of RNA was retro-transcribed to cDNA with Vilo Script system (Invitrogen). Subsequently cDNA was diluted 5 times in water. For QPCR 1.5µl of cDNA, 5µl of *Power Syber Green* mastermix (Applied Biosystem) and 200nM of primers were used to a final volume of 10µl for each reaction. The reactions were performed on the 7900HT system (Applied Biosystem).

Murine primer sequences are as follows:

Sirt1-F AGTTCCAGCCGTCTCTGTGT

Sirt1-R CTCACGAACAGCTTCACAA

Hsp60-F GCTGTAGCTGTTACAATGGGG;

Hsp60-R TGACTTTGCAACAGTGACCC;

Hspa9-F AATGAGAGCGCTCCTTGCTG;

Hspa9-R CTGTTCCCCAGTGCCAGAAC;

LonP1-F ATGACCGTCCCGGATGTGT;

LonP1-R CCTCCACGATCTTGATAAAGCG;

Atg5-F AAGTCT GTCCTTCCGAGTC;

Atg5-R TGAAGAAAGTTATCTGGGTAGCTCA;

Arbp-F AGATTCGGGATATGCTGTTGG;

Arbp-R AAAGCCTGGAAGAAGGAGGTC.

Gene expression was normalized to *Arbp* as housekeeping control. Amplification of the template at more than 40 cycles (Ct>40) was considered as indeterminate expression of the gene of interest.

5.3.16 Western blotting

For murine mitonuclear imbalance assessment, 30,000 LT- or 30,000 ST-HSCs were FACS sorted from Lineage depleted bone marrow from 32 mice after 7-day NR or control diet treatment. Cells were directly sorted in urea lysis buffer [20 mM HEPES pH 8, 9 M Urea, 1 mM sodium orthovanadate, 2.5 mM sodium pyrophosphate, 1 mM β-glycerophosphate, and 1X protease inhibitor cocktail (Roche)]. Proteins were separated by SDS-PAGE and transferred to a PVDF membrane (0.45 µm). Blocking and antibody incubations were performed in 3% BSA in Tris-buffered saline with Tween 20 (TBS-T). The following primary antibodies were used against MTCO1 (Abcam, ab14705) and ATP5A (abcam, ab14748).

For mitonuclear imbalance assessment in human cells, K562 cells were cultured with RPMI 10% FCS 1% Penicillin/Streptomycin in 96 well plates. K562 cells were then treated with NR in a dose-response for 2 days, with a replenishment dose after 24h. Total cell lysates were prepared using a lysis buffer [20 mM Tris-HCl (pH7.5), 150 mM NaCl, 1 mM EDTA, 1 mM EGTA, 1% Triton X-100, 2.5 mM Sodium pyrophosphate, 1 mM β-Glycerophosphate, and 1X protease inhibitor cocktail (Thermo, Cat. 78430)], proteins were then normalized by a DC protein assay (BIO-RAD, Cat. 500-0116). Western blotting was performed with antibodies against MTCO1 (Abcam, ab14705), SDHA (Abcam, ab14715), ATP5A (abcam, ab14748), HSP60 (Santa Cruz, sc-1052).

5.3.17 Hydrogel microwell array production and single cell cycle kinetics

Hydrogel microwell arrays were directly casted within individual wells of a 96-well plate as described [195]. Briefly, stoichiometrically balanced aqueous solutions of multi-arm poly(ethylene glycol) (PEG), end-functionalized with thiol and vinylsulfone groups were mixed and molded against a PDMS microstamp. Upon completion of crosslinking, the stamp was removed and the hydrogel microwell array was hydrated overnight at 4 °C and then sterilized with ultraviolet light. To follow the behavior of HSCs at single cell level, cells were sorted directly into 96-well plates coated with microwell arrays. Microwells containing a single cell at the time of plating were tracked by time-lapse microscopy. Cells were cultured in basal medium (Stemline II containing 2ng/ml Flt3 and 100ng/ml SCF) supplemented with or without 500µM NR. Proliferation kinetics were assessed using a Zeiss Axio Observer microscope equipped with an incubator chamber, temperature and CO₂ control. Images were automatically acquired every three hours over five days using the imaging analysis software of MetaMorph (Visitron, Germany).

5.3.18 LT-HSCs extraction, Imaging and Analysis for asymmetry analysis

Hematopoietic stem cells were isolated from crushed bone marrow of 24 weeks female R26-Mito-EFEG mice. Red blood cells were removed by incubation with a lysis buffer (BioLegend). Lineage positive cells were eliminated using a magnetic lineage depletion kit (Miltenya Biotech). Cells in suspension were stained with SAV-PO (Life Technologies), Kit-PE-CY7 (2B8, BioLegend), Sca1-PE (D7,

BioLegend), CD150-BV784 (TC15-12F12.2, BioLegend), CD48-PB (HM48-1, BioLegend), CD34-eF660 (RAM34, eBioscience) and FACs-sorted. LT-HSC compartment was defined as Lin⁻ C-kit⁺ Sca1⁺ CD150⁺ CD48⁻ CD34⁻ EGFP⁺.

Freshly isolated LT-HSCs were directly seeded onto a platform containing rectangular cavities (grooves) enabling single cell tracking during culture. The platform was immersed in serum free medium (Sigma-Aldrich, St. Louis, USA) supplemented with 100ng/ml stem cell factor (SCF) and 2ng/ml Flt-3 ligand (R&D Systems, Minneapolis, USA). To track precisely each cell, brightfield images were acquired every 30mn. After 35 hours of culture, TMRM was added to a final concentration of 20nM. Mitochondrial mass and potential were acquired by performing z-stacking on live cells on a Visitron CSU-W1 microscope. Paired-daughter cells asymmetry was quantified as the difference of their respective potential normalized by their mitochondrial mass (intensity thresholded TMRM signal divided by thresholded EGFP signal).

5.3.19 Human hematopoietic cells

Cord blood and fetal liver came from consent donors. Collection and experimental procedures were carried out in accordance with the Swiss law after approval from the local authorities: Swiss Ethics Commissions on research involving humans (Vaud canton protocol number (VD2797). to G.C. and Zurich canton protocol number Stv22/2006 to M.E.). Human CD34⁺ hematopoietic primary cells were purified cord blood bag provided by the “Etablissement de Transfusion Sanguine Bourgogne Franche-Comté” (Besançon) or from fetal liver (ethical protocol: 336/1).

5.3.20 *In vitro* culture and transplantation of human CD34⁺ hematopoietic progenitor/stem cells

Human CD34⁺ cells isolated from fetal liver/cord blood by human CD34 positive selection (StemCell Technologies #18056) were cultured either directly after isolation or after cryopreservation in StemSpan media (StemCell Technologies, #09600) supplemented with SCF (100ng/ml), FLT3L (100ng/ml), TPO (50ng/ml), LDLP (10ug/ml) and different concentrations of NR. Each well of a 96-round-well plate contained 90,000 CD34⁺ progenitors in 200 µl of media. The culture media was supplemented with fresh NR every 24 hours. After the indicated culture period the cells were stained, washed and analyzed by flow cytometry.

NSG mice were purchased from Jackson Laboratory, bred and maintained under pathogen-free conditions in-house. Animal experimentation followed protocols approved by the Service Vétérinaire de l'Etat de Vaud. For transplantation, one day old NSG pups were irradiated with 1Gy and few hours later injected intrahepatically with *in vitro* expanded HSCs. Each pup was injected with a cell mass containing 50,000 CD34⁺ cells post *in vitro* culture. Mice were bled, via tail vein, every 4 weeks, starting from 8 weeks until 36 weeks to estimate human reconstitution levels (% human CD45⁺ cells) in the peripheral blood. Antibody combinations were used to further estimate human B cells, T cells, Monocytes, Neutrophils and NK cells. At the endpoint (36 weeks), BM and spleen were isolated to determine the level of human reconstitution at these two sites.

For secondary transplantation, adult (8-10 weeks) NSG mice were irradiated with 2Gy and one day later injected intravenously with bone marrow cells isolated from primary recipients. Bone marrow from each primary recipient was injected in 3 secondary recipients (8 million cells per mouse). Mice were bled, via tail vein, every 4 weeks, starting from 8 weeks until 24 weeks to estimate human reconstitution levels (% human CD45⁺ cells) in peripheral blood. Antibody combinations were used to further estimate human B cells, T cells, Monocytes, Neutrophils and NK cells. At the endpoint (24 weeks), bone marrow and spleen were isolated to determine the level of human reconstitution at these two sites.

5.3.21 *In vivo* NR treatment of adult humanized NSG mice

Cryopreserved mobilized CD34⁺ cells from healthy donors (purified CD34⁺ from mobilized blood, Cellsystems Biotechnologie GmbH, Troisdorf, DE or STEMCELL Technologies, SARL) were thawed and used immediately for transplantation.

NSG mice were purchased from The Jackson Laboratory and bred, treated, and maintained under pathogen-free conditions in-house. Animal experimentation followed protocols approved by the Service Vétérinaire de l'Etat de Vaud. Nine to ten-week-old NSG mice were irradiated with 1.8Gy and 6 hours later injected intravenously with 10⁶ human CD34⁺ HSC (purified CD34⁺ from mobilized blood, Cellsystems Biotechnologie GmbH, Troisdorf, DE or STEMCELL Technologies, SARL). The level of human reconstitution (% human CD45⁺ cells) was analyzed 12 weeks later by FACS staining of tail vein blood samples. Mice were regrouped based on level of reconstitution into two comparable cohorts of 5 mice each. The following day and for a total of 7 days, cohorts received 2916 powder chow diet supplemented or not with NR, as for C57BL/6 mice. After 7 days tail vein blood was collected in EDTA tubes and mice sacrificed for BM analysis. BM cells were collected as described for C57BL/6 mice, and both blood and BM cells stained and analyzed for a panel of human lineage specific antibodies as described above.

5.3.22 Statistics

Data were statistically analyzed by Student's t test, one- and two-way ANOVA as specified in each figure legend. The modified Z Score was used to test for outliers.

5.4 Results and Discussion

5.4.1 Mice supplemented with Nicotinamide Riboside expand the hematopoietic progenitor compartments

Nicotinamide Riboside (NR) was recently identified as a *bona-fide* NAD⁺ vitamin B₃ precursor in vertebrates, naturally present in milk and indirectly quantifiable in plasma [193], [196]. NR uses a dedicated transporter and enters the NAD⁺ salvage pathway via the NR kinase (Nr1/2)-mediated phosphorylation of NR into nicotinamide mononucleotide, NMN [193][197]. Transcripts associated with the enzymatic machinery necessary to directly incorporate NR onto the NAD salvage pathway, most notably *Nmnat3* and *Nrk1*, are expressed in both long-term (LT) and short-term (ST-) HSCs in homeostatic conditions (Figure S 5.1A; [198]). We provided dietary NR supplementation to mice for seven days (Figure 5.1A) and found increased BM cellularity (Figure S 5.1B) accompanied by expansion of all short-term hematopoietic progenitors (ST-HSCs, MPPs, CMPs and MEPs, see Figure 5.1B). Short-term reconstitution 4 weeks after competitive BM transplantation (Figure 5.1C) and *in vitro* colony forming unit (CFU) assays (Figure 5.1D) confirmed a functional increase of short-term hematopoietic progenitors upon NR treatment. Importantly, NR did not significantly affect the most primitive, self-renewing compartment of LT-HSCs, whose overall number and function did not change as measured phenotypically by surface marker and functionally by competitive repopulation 16 weeks after BM transplantation (Figure 5.1B and Figure S 5.1C). Analysis of terminally differentiated blood cells in NR-treated mice showed a significant increase in circulating platelets, monocytes and granulocytes, although still within the physiological range for C57BL/6 mice (Figure 5.1E, Figure S 5.1D). Niagen, a food supplement containing GMP-grade NR chloride for human use, induced the same effect on baseline blood counts, although more moderately than our custom-synthesized NR triflate (2.4g of NR per Kg of food) (Figure 5.1E and Figure S 5.1D). Interestingly, mice receiving food supplemented with NAD precursors with independent entry points within the NAD⁺ salvage pathway, such as nicotinic acid (NA) and nicotinamide (NAM), did not display any significant differences in their hematopoietic compartments after the same seven-day treatment, indicating that the effect on the hematopoietic system is specific to NR and not to other NAD precursors (Figure S 5.2A-H). Conversely, mice supplemented with NMN, which constitutes the first intracellular intermediate of NR metabolism upon NRK-mediated phosphorylation of NR, exhibited a significant expansion of the hematopoietic progenitor compartments (Figure S 5.3A-C). Hematopoietic progenitor pools were not affected by NR supplementation in *Nrk1*^{-/-}/*Nrk2*^{-/-} double knockout mice (Figure S 5.3D-F; [199]) indicating a specific role of the NR-Nrk1/2-NMN axis on NAD-driven hematopoietic progenitor expansion.

We conclude from this data that NR and NMN dietary supplementation expands the ST-HSC and committed hematopoietic progenitors within the murine BM, without significantly affecting the size of the LT-HSC pool.

5.4.2 NR decreases mitochondrial membrane potential ($\Delta\Psi_m$) independently of cell cycle quiescence

Because NR has been shown to enhance mitochondrial fitness [187], we tested its capacity to modify mitochondrial homeostasis. We expected NR to increase mitochondrial activity and biogenesis in HSCs, as it does in mammalian hepatocytes and skeletal muscle through the activation of Sirt1 and its downstream target, PGC1 α [197]. We isolated HSCs from one-week NR-treated mice and stained them with the mitochondrial membrane potential ($\Delta\Psi_m$) sensitive dye tetramethylrhodamine methyl ester (TMRM). Unexpectedly, we found a striking decrease in $\Delta\Psi_m$ both in LT- and ST-HSCs after *in vivo* treatment (Figure 5.2A). Of note, the expression of *Sirt1* remained unchanged (Figure 5.2B). To test whether the unexpected NR-mediated decrease in $\Delta\Psi_m$ was cell-autonomous, we exposed dividing HSCs to NR *in vitro* for 2 days and again detected a decrease in $\Delta\Psi_m$ as compared to controls, which persisted when separately analyzing LT- and ST-HSCs (Figure 5.2C and S 5.4A,B). The NR-mediated decrease in $\Delta\Psi_m$ was dose-dependent and also occurred in HSCs exposed to NMN, the first intracellular intermediate of NR metabolism (Figure S 5.4B). We thus concluded that the NR-mediated decrease in $\Delta\Psi_m$ is cell-autonomous in HSCs. Blocking the ABC transporters expressed in HSCs, *Brcp1* and *Mdr 1a/b*, by verapamil treatment only mildly affected NR-induced $\Delta\Psi_m$ decrease (Figure S 5.4C), thus indicating that ABC-transporter-mediated dye efflux on HSCs does not explain the NR-induced reduction on TMRM stains [200], [201]. In order to investigate if the mitochondrial phenotype was associated to cell cycle arrest, we exposed both LT-HSCs and ST-HSCs to NR *in vitro* and used a cell-labelling strategy based on carboxy-fluoresceinsuccinimidyl ester (CFSE) to measure $\Delta\Psi_m$ in cells that had divided one time [33]. NR-exposure slowed entry into first division for both LT-HSCs and ST-HSCs, but the majority of cells divided after 2 days of culture (Figure 5.2D). Within the cells that underwent first division, the proportion of LT-HSCs and ST-HSCs that exhibited a

low $\Delta\Psi_m$ (termed here TMRM^{low}) was significantly increased by exposure to NR (Figure 5.2E), whereas non-dividing LT-HSCs did not present changes in $\Delta\Psi_m$, indicating that the NR-mediated decrease in $\Delta\Psi_m$ preferentially occurs in dividing HSCs. Of note, we have previously demonstrated that the TMRM^{low} HSC subset contains, after first division in the same conditions, the functional self-renewing HSC subset [33]. We thus conclude that NAD⁺ boosting via NR reduces $\Delta\Psi_m$ in LT and ST-HSCs in a cell-autonomous manner, independently of cell-cycle quiescence, and preferentially in dividing cells.

5.4.3 NR decreases $\Delta\Psi_m$ in human CD34+ cells and improves human blood reconstitution.

As NR was found capable of strongly modulating mitochondrial biology, a key player of HSCs function [33], [154], [202] decided to evaluate the effect of NR on human CD34+ hematopoietic progenitor cells. Since a decrease in $\Delta\Psi_m$ is associated with improved HSC function both in mouse and in human [33], [42], [203], we first tested the effect of NR on murine HSCs in primary and secondary CFUs and demonstrated the ability of NR to improve CFU re-plating efficiency (Figure S 5.4D) without affecting cell viability (Figure S 5.4E). We then tested NR treatment on cultured human CD34+ cells. NR decreased $\Delta\Psi_m$ of fetal liver, cord blood and adult BM derived human CD34+ (Figure 5.3A and Figure S 5.4F). Fetal liver derived human CD34+ cells cultured in the presence or absence of NR and transplanted into irradiated NSG recipient mice engrafted significantly better than controls, and they were capable of sustaining long-term blood production in both primary and secondary recipient NSG mice (Figure 5.3B). Importantly, analysis of peripheral blood and spleen demonstrated that both the lymphoid and myeloid lineages reconstituted significantly better in mice transplanted with NR-treated CD34+ cells (Figure S 5.5), confirming the superior functionality of NR-treated CD34+ cells and excluding possible lineage biases introduced by NR treatment. BM analysis of primary and secondary recipient NSG mice congruently revealed a higher proportion of human hematopoietic progenitor cells (CD34+ and CD34+CD38-) in the NR treated group than in the control marrow (Figure S 5.5).

Taken together, our data demonstrates that human CD34+ hematopoietic progenitors also exhibit a very significant reduction on $\Delta\Psi_m$ upon NR exposure, which improves hematopoietic stem cell function.

5.4.4 NR increases mitochondrial clearance and reduces mitochondrial metabolism.

We then set to investigate the molecular mechanisms underlying the striking mitochondrial phenotype induced by NR treatment in HSCs. RNAseq analysis of *in vitro* cultured LT and ST-HSCs revealed induction of autophagy genes in both cell populations upon NR supplementation (Figure 5.4A). Increased expression of autophagy-related genes was associated with up-regulation of NAD salvage pathway and *de novo* synthesis genes (Figure 5.4B) and key mitophagy players, including *Pink1* and *Ulk1* (Figure 5.4C), [204]. To study whether increased autophagy/mitophagy underlies the NR-mediated decrease in $\Delta\Psi_m$, we treated LT- and ST-HSCs with bafilomycin A1, which inhibits autophagy and mitophagy by blocking the fusion of autophagosomes and lysosomes. We then quantified the size of Lc3b+ punctae by immunofluorescence to estimate autophagic flux [39], [205]. Bafilomycin successfully blocked the autophagic flux of control LT-HSCs, as shown by the accumulation of significantly bigger Lc3b+ punctae in comparison to the control cells (Figure S 5.6A). When LT-HSCs were exposed to NR, bafilomycin A1 treatment resulted in restored mitochondrial activity as measured by Mitotracker Deep Red signal in confocal microscopy (Figure 5.5A) and TMRM staining by FACS (Figure S 5.6B), and a tendency to increased autophagy flux (Figure 5.5A, and Figure S 5.6A top panel). Note that the accumulation of bigger LC3b+ punctae is more pronounced in LT-HSCs than ST-HSCs upon bafilomycin A1 treatment (Figure S 5.6A bottom panel), indicating a higher basal autophagic flux in the more primitive LT-HSCs as compared to ST-HSCs, consistent with previous data comparing HSCs to more committed bipotent granulocyte-monocyte GMP progenitors [39]. Transplantation of HSCs cultured *in vitro* with Bafilomycin A1 for 48 hours into lethally irradiated mice hampered the NR-mediated HSC gain of function, reestablishing a similar engraftment capacity to untreated cells (Figure S 5.6B). We thus concluded that NR exposure mediates increased mitochondrial clearance in HSCs, an effect which is more pronounced in LT-HSCs.

The NR-mediated increase in HSC mitochondrial clearance was also associated with a significant reduction of all RNA transcripts related to the major mitochondrial energy pathways, including the tricarboxylic acid (TCA) cycle and Oxidative phosphorylation (OxPh) (Figure 5.5B), while fatty acid oxidation was slightly affected, and glycolysis remained unchanged (Figure 5.5C). This observation supports the hypothesis that NR-mediated $\Delta\Psi_m$ reduction in HSCs is a cooperative process involving mitophagy and potentially some changes in metabolic checkpoints, and possibly that these two processes orchestrate together the clearance of damaged mitochondria to maintain mitochondrial quality control [154], [206]. The NR-mediated increase in HSC mitochondrial clearance was also associated with a significant reduction of all RNA transcripts related to the major mitochondrial energy pathways, including the tricarboxylic acid (TCA) cycle and Oxidative phosphorylation (OxPh) (Figure 5.5B), while fatty acid oxidation was slightly affected, and glycolysis remained unchanged (Figure 5.5C). This observation supports the hypothesis that $\Delta\Psi_m$ reduction in HSCs is a cooperative process involving mitophagy and metabolic checkpoints, and potentially that these two processes orchestrate together the clearance of damaged mitochondria [206]. Remarkably, in spite of reduced $\Delta\Psi_m$ and reduced transcription of the major

mitochondrial gene pathways, one of the genes most significantly induced by NR-treatment is the HSC metabolic checkpoint regulator pyruvate dehydrogenase kinase 4 (*PDH4*) (Figure 5.5D), which catalyzes the inhibitory phosphorylation of pyruvate dehydrogenase (PDH), responsible for the formation of Acetyl-CoA from pyruvate [207]. PDK4 has been demonstrated a key metabolic checkpoint for hematopoietic stem cell function and quiescence. Indeed, upregulation of PDK4 reduces the intake of metabolites in the mitochondria, induces mitochondrial clearance via PINK1 stabilization, and thus imposes a more glycolytic cellular metabolism [25], [39], [206]. In order to directly measure changes in the metabolic response of hematopoietic cells in presence of NR, and given the impossibility of sorting a sufficient number of LT-HSCs to perform reproducible seahorse assays, we resorted to analysis of splenocytes as a surrogate assay [32]. Splenocytes exposed to NR displayed a significant reduction in $\Delta\Psi_m$, while exhibiting an increase in respiratory capacity (Figure S 5.6C), indicating that the NR-mediated decrease in $\Delta\Psi_m$ is associated to improved metabolic fitness at the cellular level, as previously described in other tissue systems [208], [209].

To determine if NR could actually induce specific mitophagy *in vivo*, we supplemented the diet of mitophagy reporter mice (mito-QC) with NR [210], [211]. Mito-QC mice express ubiquitously a tandem mCherry-GFP fusion protein fused with mitochondrial outer membrane targeting sequence of FIS1. In steady state mitochondria fluoresce in both red and green. Upon mitophagy induction, however, mitochondria are delivered to lysosomes where the mCherry signal remains stable, while the GFP signal is quickly quenched by the acidic microenvironment. The GFP-mCherry+ population thus represents a snapshot of cells undergoing active mitophagy [212], [213]. Mice whose diet was supplemented with NR presented a higher proportion of LT-HSCs undergoing mitophagy, while no major effect was detected in ST-HSCs (Figure 5.5E). Downstream hematopoietic progenitors, MPPs (KLS CD150-) and CPs (Lin- cKit+), exhibited lower mitophagy as compared to the most primitive hematopoietic compartments and were unaffected by NR supplementation (Figure S 5.6D). Importantly, the use of a “dye free” system to analyze mitophagy confirmed previous studies where mitophagy has been proposed as an important mechanism for HSCs maintenance [33], [154], [202], [214]

5.4.5 NR induces mitochondrial stress *in vivo*.

We then tested if our NAD⁺ boosting strategy could induce mitochondrial stress in HSCs, for the mitochondrial stress response has been proposed in other tissues as a regulator of energy homeostasis and increased mitochondrial clearance [215]. Similarly, to the NR-induced increase in mitochondrial clearance, mRNA levels of mitochondrial-stress-associated chaperones, *Hsp60* and *Hspa9*, as well as of the mitochondrial protease *LonP1* were increased in LT-HSCs from mice whose diet was supplemented with NR, while the effect was more moderate in ST-HSCs (Figure S 5.6E). By Western blotting, we could further observe a mitonuclear protein imbalance specifically in LT-HSCs, but not ST-HSCs- isolated from these mice (Figure S 5.6F). The nuclear-DNA-encoded subunit of Oxphos complex V ATP5a was expressed at equivalent levels in LT- and ST-HSCs regardless of NR treatment. However, the mitochondrial-DNA-encoded MTCO1 protein, a component of Complex IV, was induced by NR-treatment in LT- but not ST-HSCs, indicating a stoichiometric mitonuclear protein imbalance which could be the trigger for the NR-mediated mitochondrial stress response, as previously suggested [184], [194], [216]. We further tested activation of the mitochondrial stress response at the protein level in human hematopoietic stem cell-like leukemic cell line K562. Increasing concentrations of NR up to 2mM did not affect cell survival over 48h of treatment (Figure S7A). However, NR treatment induced mitonuclear imbalance (MTCO1/SDHA ratio) and mitochondrial stress-associated protein HSP60 in a dose dependent manner (Figure S 5.7B). Of note, there was no increase in K562 leukemic colonies upon NR treatment (data not shown).

We conclude that NR treatment causes a mitonuclear protein imbalance in HSCs and induces the mitochondrial stress response in a cell-autonomous manner, preferentially in the most primitive LT-HSC compartment. The fact that NR-supplementation induces mitochondrial clearance in HSCs, as opposed to the increased mitochondrial activity observed in other mammalian tissues upon NR exposure [184], [217], is surprising, but points to cell-specificity and directionality of the mitochondrial stress response.

5.4.6 NR promotes asymmetric mitochondrial distribution in LT-HSCs upon cell division

Since both NR-induced mitochondrial clearance and NR-induced activation of the mitochondrial stress response occurred preferentially in the most primitive, dividing LT-HSCs, we postulated that the expansion of short-term progenitors observed in NR-treated mice may be a consequence of altered HSC fate decisions. As the size of the LT-HSC pool remained unchanged upon NR-treatment (Figure 5.1, Figure S 5.1C) we did not expect an increase in HSC self-renewing divisions but hypothesized that NR might increase ST-HSCs and their progeny by increasing asymmetric divisions in HSCs. This hypothesis is consistent with the current view that asymmetric cell division regulates stem cell fate and self-renewal [218], [219], and that mitochondrial metabolism plays an important role in the modulation of asymmetric cell division in HSCs [220]. Of note, in support of this hypothesis, purified ST-HSCs from mice fed with a NR-supplemented diet showed no increase in cell cycle entry (Figure S 5.6G). Single-cell tracking of NR-treated HSCs showed a significant increase in time-asynchronous divisions (Figure 5.6A), which has been proposed as an epiphenomenon associated to increasing asymmetric stem cell divisions [221]. We applied state-of-the-art single cell analysis to evaluate NR-induced asymmetry of cell divisions in HSCs. LT-HSCs were purified from mito-EGFP mice, which express EGFP tagged by the importing signal

of the mitochondrial cytochrome *c* oxidase subunit VIII [212], [213], thus ubiquitously and exclusively expressing EGFP in the mitochondria [222]. By combining the use of mito-EGFP mice and mitochondrial DNA quantification, we could evidence that the more primitive hematopoietic compartments have lower mitochondrial content than the populations of MPP and CP committed progenitors (Figure S 5.7C) [33], [42]. Mito-EGFP LT-HSCs were then sorted by FACS and cultured into a microwell system designed to track both cell division by time lapse microscopy and mitochondrial distribution by confocal imaging (Figure 5.6B-D). Both mitochondrial mass (EGFP) and $\Delta\Psi_m$ (TMRM) were measured and analyzed in daughter cells (paired-daughter cells, PDCs) at the end of the culture. The TMRM/EGFP ratio was used as readout for normalized mitochondrial activity (Figure 5.6B, D). LT-HSCs exposed to NR showed significantly higher asymmetric distribution of active mitochondria in daughter cells as compared to the control group (Figure 5.6E). Specifically, log10 asymmetric distribution of active mitochondria in daughter cells happened in 20% of LT-HSCs exposed to NR, as opposed to 7.5% of the cells in control LT-HSCs. These results, combined with our previous study demonstrating that only TMRM^{low} but not TMRM^{high} LT-HSCs retain long-term engrafting capacity after first division *in vitro* [33], support the role of NR in increasing LT-HSC asymmetric divisions and highlight the role of mitochondria as determinants of stem cell fate decision. Recent data from us and others actually demonstrated that maintenance of a low mitochondrial potential through autophagy is necessary to maintain HSC self-renewal [33], a process mediated by PPAR-dependent increase in fatty acid oxidation through enhanced Parkin recruitment in mitochondria [154].

These results open important questions in regard to recent publications highlighting higher mitochondrial content in HSCs as compared to more committed progenitor populations and arguing on the role of mitophagy in the maintenance of a functional HSCs pool [201], [223]. Our data and that of others (Figure S 5.7C; [33], [202], [214]) indicate that increased mitochondrial recycling and lower mitochondrial content in the most primitive HSCs associate to enhanced stem cell function, and encourage future studies to better understand the link between mitochondrial dynamics and HSC function and fate.

5.4.7 Improved survival and enhanced blood cell production of post-transplanted mice treated with NR

Finally, as survival after transplantation depends on the formation of sufficient ST-HSCs to maintain rapid stress hematopoiesis [224], we tested whether NR supplementation would be sufficient to accelerate blood recovery following HSC transplantation. Indeed, limiting-dose-HSC transplantation proved lethal for all control mice, while 80% of mice receiving the NR-supplemented diet survived (Figure 5.7A-B). We further transplanted mice with an excess dose of CD45.1 BM cells, such that survival would not be compromised upon repeated bleeding to monitor blood counts. Platelet and neutrophil recovery were significantly faster in NR-treated mice as compared to controls (Figure 5.7C-D). Time of exit of severe neutropenia is a critical factor for patient outcome, typically determining hospital discharge. Mice treated with NR supplementation exited agranulocytosis (neutrophils > 0.5 G/l), on average, one week before controls (Figure 5.7D). Recovery from severe thrombocytopenia as defined by platelet count > 200 G/l, which is the functional cutoff for severe bleeding in mice [225], occurred on average 10 days earlier in NR-treated mice (Figure 5.7C). Increased survival and faster blood recovery were not due to a NR-mediated radio-protective effect, as there was no difference in residual CD45.2 cells from recipient mice (Figure S 5.7D). Importantly, there was no HSC exhaustion after extended NR treatment, as secondary transplants from the marrow of these mice showed equivalent CD45.1 long-term engraftment at 16 weeks (Figure S 5.7E). Lethally irradiated mice transplanted with total bone marrow from mitoQC mice and supplemented with NR in the diet during the entire post-transplant period (similar to Figure 5.7A) presented higher mitophagic rate in their stem and multipotent progenitor compartments during the blood recovery period (Figure 5.7F). NR supplementation in stress hematopoiesis is thus coupled to induction of mitophagy in the most primitive hematopoietic compartments.

Moreover, humanized mice fed with NR-supplemented diet for one week presented enhanced human hematopoiesis as reflected by a significant increase in lymphocyte (Figure 5.7E) and possibly monocyte production (Figure S 5.7F). Human neutrophil recovery is unfortunately not measurable in standard humanized NSG mice [226]. We thus conclude that NR supplementation accelerates both murine and human hematopoiesis, significantly increasing survival in mice upon limiting-HSC transplantation.

5.5 Conclusions and perspectives

Collectively, our work links the NAD salvage pathway to mitochondrial clearance in wildtype HSCs, via induction of mitochondrial stress response and increase in asymmetric divisions. The mitochondrial effects of NAD replenishment *in vivo* were observed at the level of the most primitive HSCs, both during homeostatic and stress hematopoiesis, which demonstrates the cell-type specific directionality of the mitochondrial stress response. Moreover, our results reveal NR and NMN as potential boosters of hematopoiesis which could prove useful either *in vitro* for HSC expansion protocols, such as in the context of expansion for adoptive cell transfer or for increased immune cell metabolic fitness in immune-therapy; or *in vivo* to reduce mortality in the setting of BM aplasia and in particular in elderly patients after radio/chemotherapy, possibly in the context myelodysplastic syndromes where an age-dependent

mitochondrial defect has been suggested [227]. Given the efficient enhancement of megakaryopoiesis, NR supplementation could also prove beneficial for the treatment of refractory autoimmune idiopathic thrombocytopenic purpura (ITP) or other auto-immune BM failure syndromes. Of note, the wide-ranging protective effects of NR on mitochondrial activity in non-hematopoietic tissues would be of additional value for HSC-ablative chemotherapy regimens, which often carry significant secondary cardio/neurotoxicity due to mitochondrial impairment [193], [197].

5.6 Acknowledgements

We thank Elena Katsyuba (EPFL), Laurent Mouchiroud (EPFL), Nina Dumauthioz (UNIL) and George Q. Daley (Harvard Medical School) for critical reading of the manuscript, the members of the Center for the Study of Living Systems (EPFL) and Francis Derouet (UNIL) for animal care, Evan Williams for help with normalization of RNA expression data, Evangelos Panopoulos and Magdalena Plotczyk for technical support, and Bastian Mangeat at the Genetics Expression Core Facility (EPFL) for RNA sequencing support. Andrea Negro helped with statistical analysis. Flow cytometry analysis / cell sorting was performed both at the EPFL Flow Cytometry Core Facility with the help of Sintia Winkler, Telma Lopes and Miguel Garcia, and at the Nestlé Institute of Health Sciences (NIHS) Flow Cytometry facility with the help of Filippo de Franceschi and Gabriele Dammone. A special thanks to the EPFL Kebab truck crew for the numerous late meals.

O.N. was supported by the Machaon Foundation, the Dr Henri Dubois-Ferrière Dinu Lipatti Leukemia Foundation, the Pierre Mercier Foundation, and Swiss National Science Foundation (SNF) Professorship grants PP00P3_144857 and PP00P3_176990. The work performed in the laboratory of M.P.L. was supported by a Swiss National Science Foundation Sinergia grant (CRSII3_147684) and an ERC grant (StG_311422). The work in the JA laboratory was supported by the EPFL and grants from Krebsforschung Schweiz /SwissCancerLeague (KFS-3082-02-2013), Systems X (SySX.ch 2013/153) and SNSF (31003A-140780). The work performed in the laboratory of P.C.H. was supported in part by the Swiss Cancer Foundation (KFS-3949-08-2016) and Swiss National Foundation Project grant (31003A_163204).

5.7 Figures

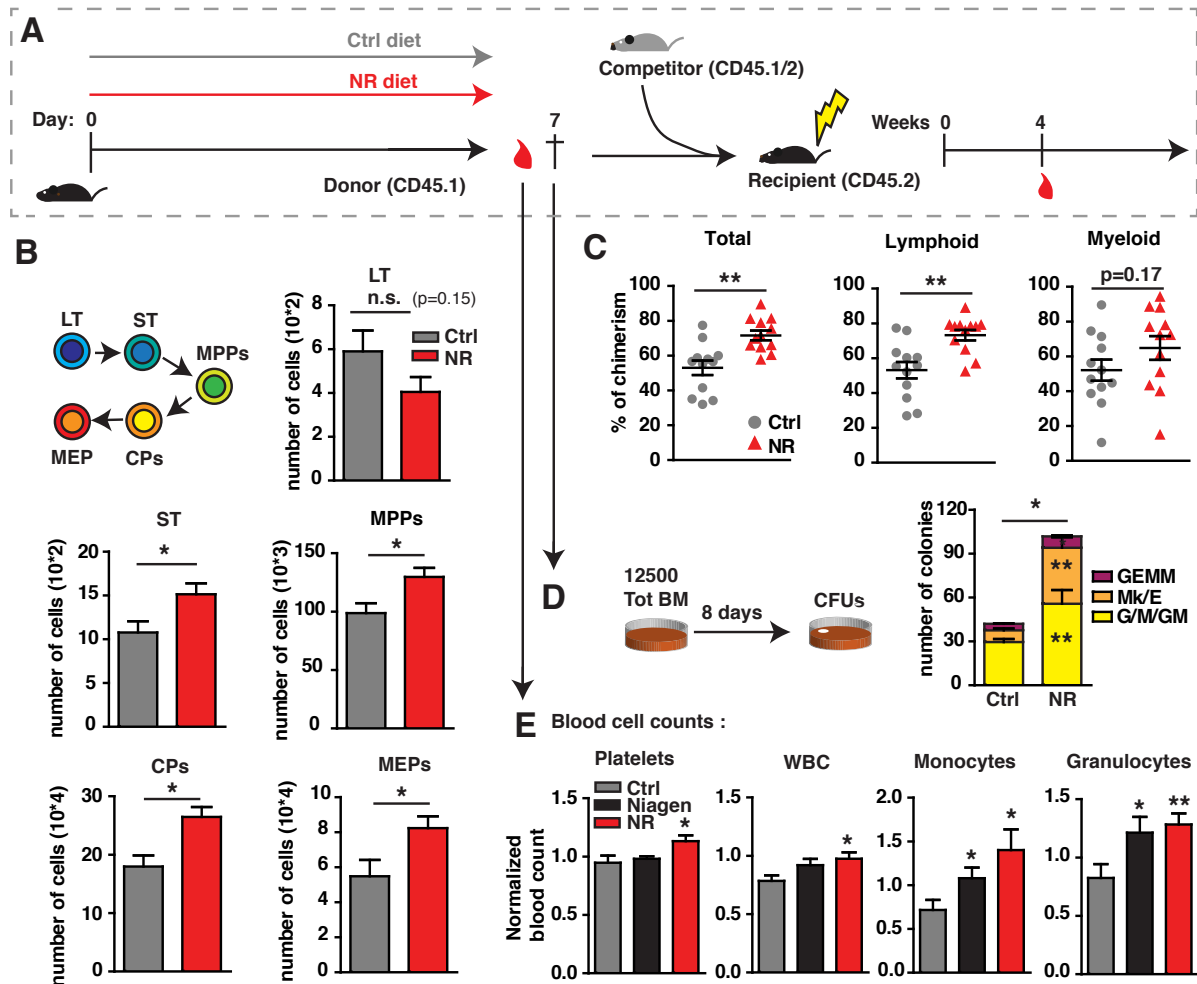


Figure 5.1 NR treatment expands ST hematopoietic progenitors *in vivo*. **A**, Mice were fed for 7 days with control or NR diet (12mg NR /mouse/day). Blood was sampled, and mice were sacrificed for BM analysis (FACS and CFUs) and secondary transplants. **B**, Phenotypic analysis of the different BM hematopoietic stem/progenitor compartments from control (ctrl) or NR fed mice by flow cytometry, $n=5$; LT-HSCs are *Lineage-cKit+Sca1+(KLS+)CD48-CD150+CD34-*, short-term(ST)-HSCs are *KLS+CD48-CD150+CD34+*, multipotent progenitors (MPPs) are *KLS+CD48+*, committed progenitors (CPs) include common myeloid progenitors (CMPs: *Lineage-cKit+Sca1-(KLS-) FcR^{low}CD34+*), granulocyte-macrophage progenitors (GMPs: *KLS-FcR^{low}CD34+*) and megakaryocyte-erythroid progenitors (MEPs: *KLS-FcR-CD34-*). **C**, BM derived from NR- or control-fed mice was transplanted into lethally irradiated mice and peripheral blood chimerism was measured 4 weeks after transplantation, $n=12$. **D**, 12,500 BM cells from ctrl- or NR-fed mice were plated in Methocult for colony forming unit (CFU) analysis 8 days after plating, $n=5$; GEMM, granulocyte-erythroid-monocyte-megakaryocyte mixed CFU; GM, granulocyte-monocyte CFU; M, monocyte CFU; G, granulocyte CFU; Mk, megakaryocyte CFU; E, erythroid and erythroid blast forming CFUs **E**, Blood cell counts of mice fed with ctrl, Niagen or NR diet as in (a.), $n=5$. Student's *t* test * $p<0.05$, ** $p<0.01$, *** $p<0.001$.

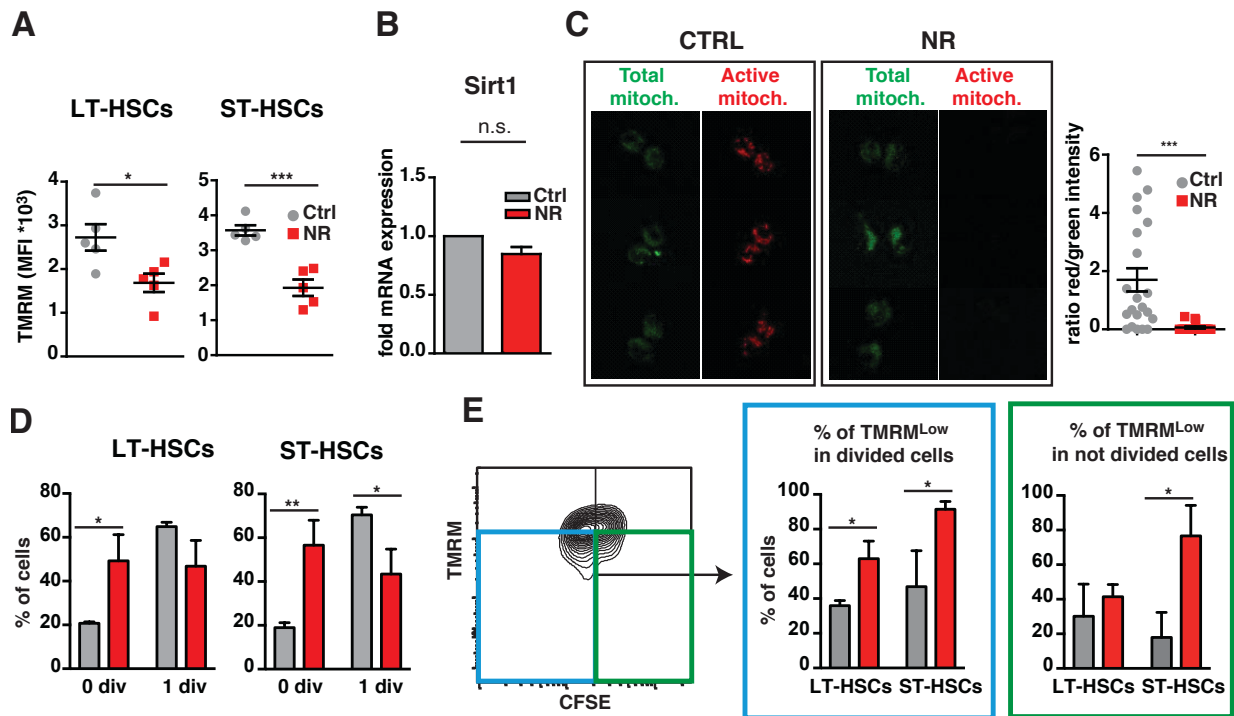


Figure 5.2 NR treatment decreases mitochondrial membrane potential ($\Delta\Psi_m$). **A**, LT and ST-HSC mitochondrial potential measured by TMRM staining, from BM of control- or NR-diet fed mice, $n=5$. **B**, Gene expression analysis of Sirt1 in LT-HSCs derived from control- or NR-diet fed mice, $n=5$. **C**, HSCs were cultured *in vitro* for 2 days in presence or absence of NR and then stained with JC-1 dye, which reports mitochondrial depolarization by a decrease in the red (total mitochondria) to green (active mitochondria) fluorescence intensity ratio. Confocal imaging of JC1 stained mitochondria from HSCs cultured in presence or absence of NR, $n=20$. **D**, Proportion of dividing and not dividing LT and ST-HSCs as measured by CFSE staining $n=3$. **E**, Mitochondrial potential of dividing and not dividing LT and ST-HSCs as measured by TMRM staining in combination with CFSE staining, $n=3$. Student's *t* test * $p<0.05$, ** $p<0.01$, *** $p<0.001$.

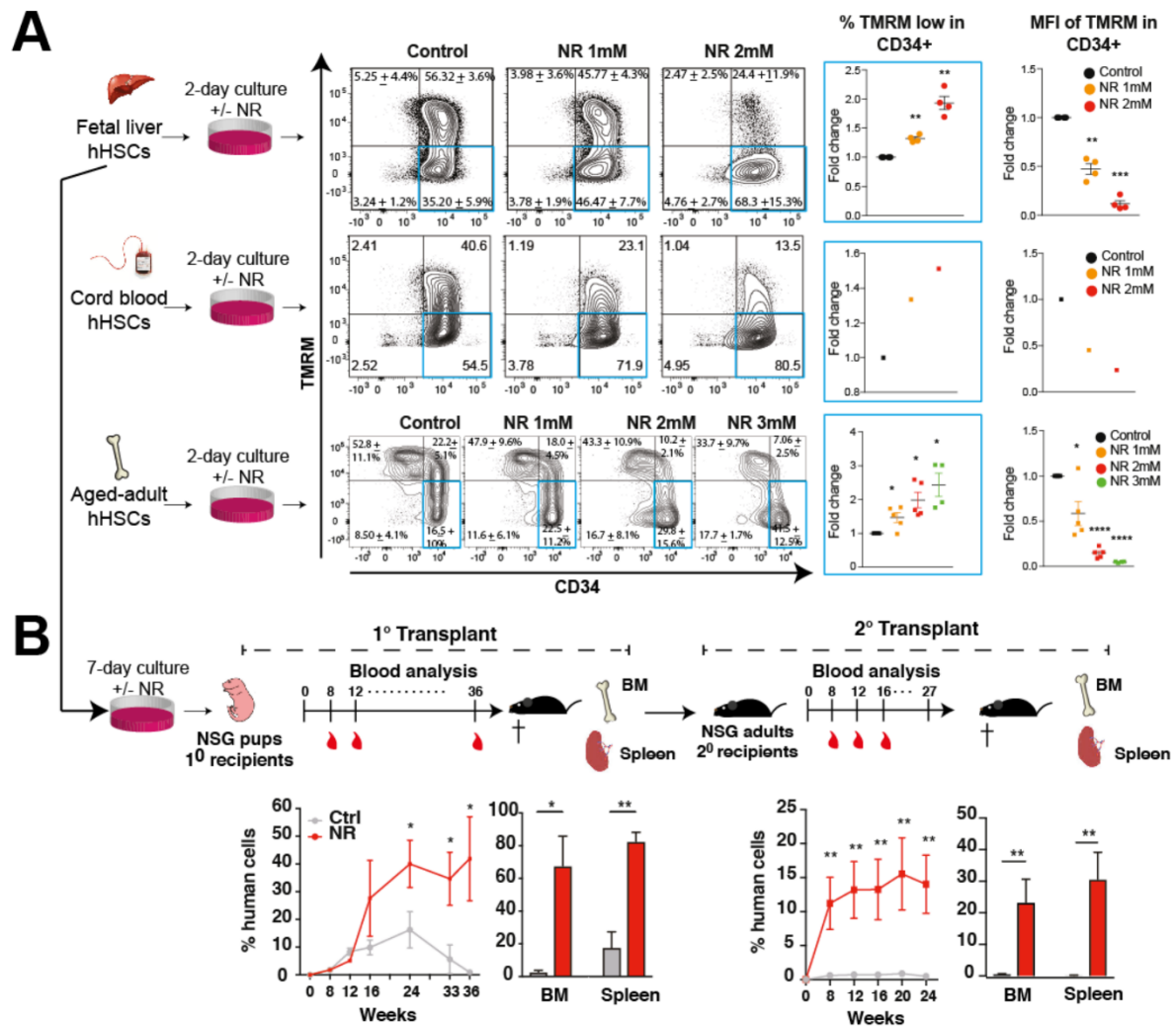


Figure 5.3 NR decreases $\Delta\Psi_m$ in human CD34⁺ and improves human blood cell reconstitution. **A, Human CD34⁺ cells from fetal liver, cord blood and adult femoral bone marrow were cultured in the presence or absence of NR for 2 days and the TMRM^{low} population (blue outline) and TMRM MFI were quantified by FACS after TMRM staining. Fold changes in MFI are calculated by normalization over control group values. Each data point represents a different donor (fetal liver $n=4$, cord blood $n=4$ with Fig. S4F, adult bone marrow $n=5$). **B**, Human CD34⁺ cells from fetal liver were cultured for 7 days *in vitro* in the presence or absence of 1mM NR and were transplanted in primary ($n=6$) and secondary ($n=12$) recipient NSG mice. Blood reconstitution was analyzed over time while bone marrow (BM) and spleen analysis were performed at the experimental endpoints. Student's *t* test * $p<0.05$, ** $p<0.01$, *** $p<0.001$**

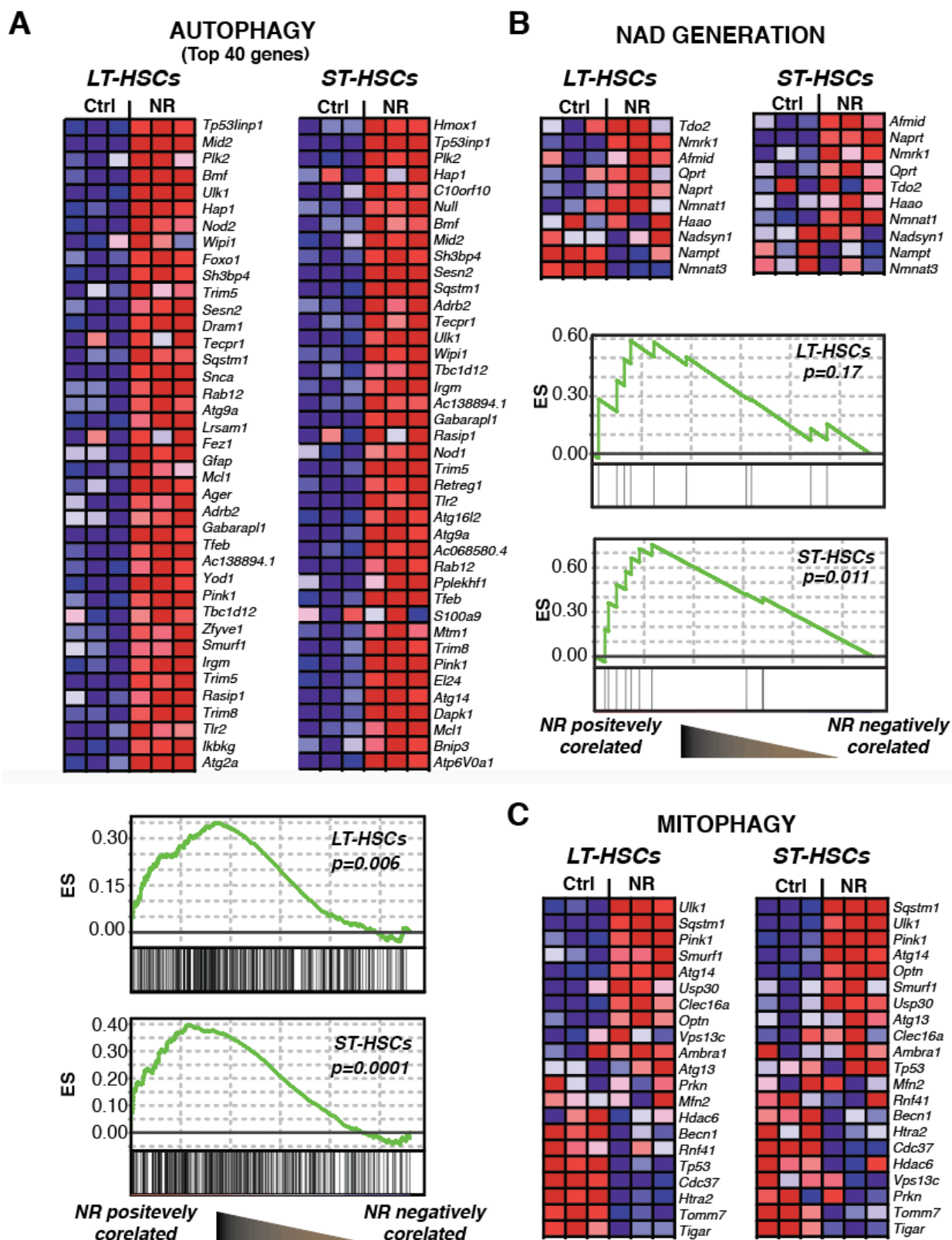


Figure 5.4 NR induces the expression of autophagy/mitophagy-related genes and NAD salvage pathway. **A**, Heatmap of the top 40 up-regulated autophagy-related genes in NR treated LT and ST-HSCs (top panel) and gene enrichment (GE) analysis quantified via enrichment score (ES, bottom panel) (in blue: low expression genes, in red: high expression genes). **B**, Heatmap of NAD salvage pathway gene expression and GE analysis. **C**, Heat-map of mitophagy-related genes produced with GSEA software analysis

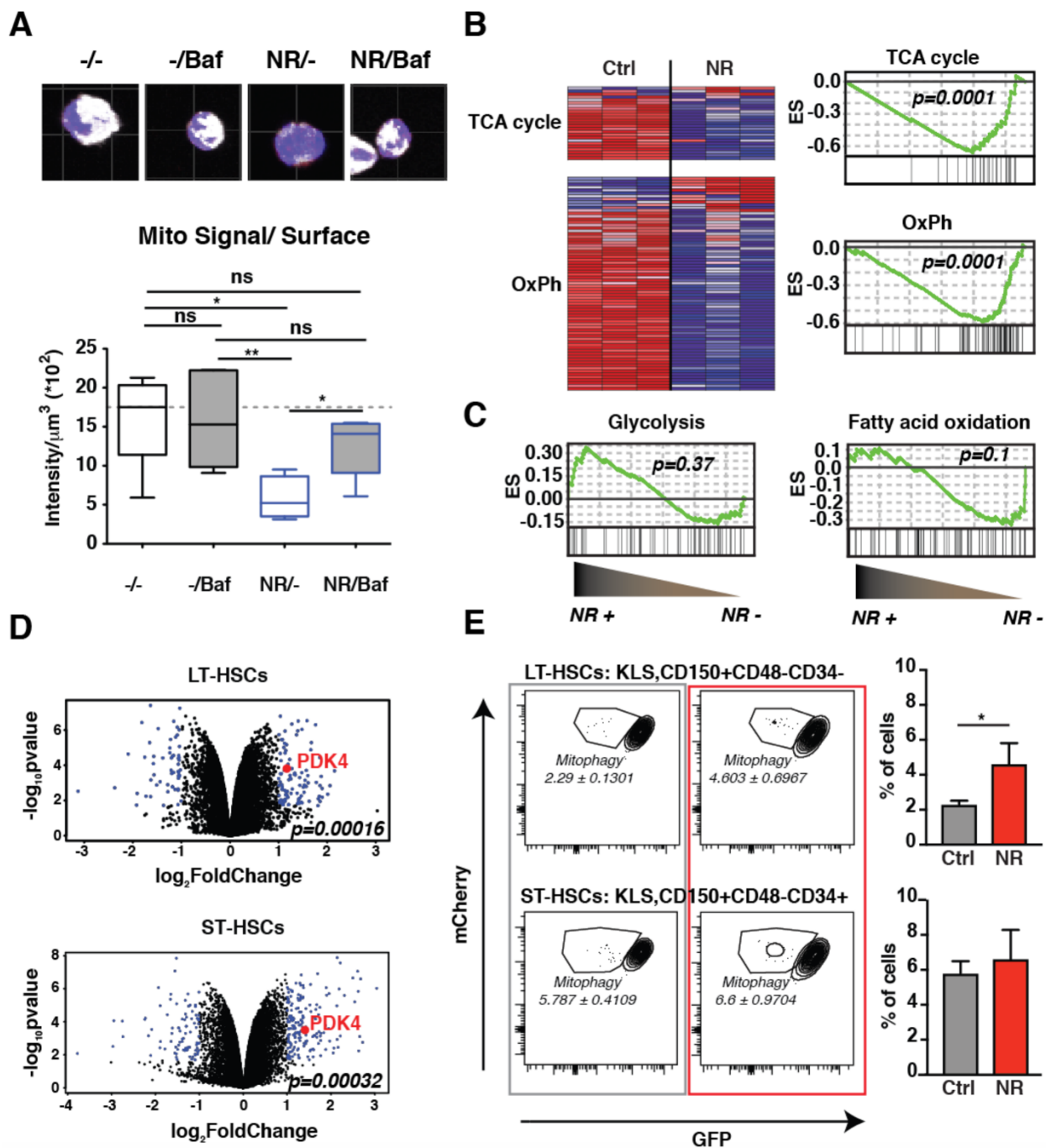


Figure 5.5 NR induces mitophagy and downregulates mitochondrial energy pathways in HSCs. **A**, Confocal imaging analysis of active mitochondria in sorted LT-HSCs treated with NR +/- autophagy inhibitor bafilomycin A1 for 2 days, as quantified by Mitotracker Deep Red staining, a mitochondrial potential sensitive dye $n=5$. Note that the decrease in mitochondrial mass of active mitochondria upon NR treatment is corrected in the presence of bafilomycin, thus indicating increased mitochondrial clearance in NR-treated LT-HSCs. **B**, **C**, RNAseq analysis of key energy pathways. Heat map representation (in blue: low expression genes, in red: high expression genes) and gene enrichment analysis are presented. **D**, Volcano plot of gene transcripts most induced by NR treatment in LT- and ST-HSCs. PDK4 metabolic checkpoint expression is highlighted. **E**, Mito-QC mice were supplemented with Ctrl or NR diet for 1 week. Proportion of cells undergoing mitophagy were quantified by flow cytometry measuring mCherry and GFP signal in both LT and ST-HSCs (see text for details) $n=3$. Student's t test $*p<0.05$, $**p<0.01$, $***p<0.001$.

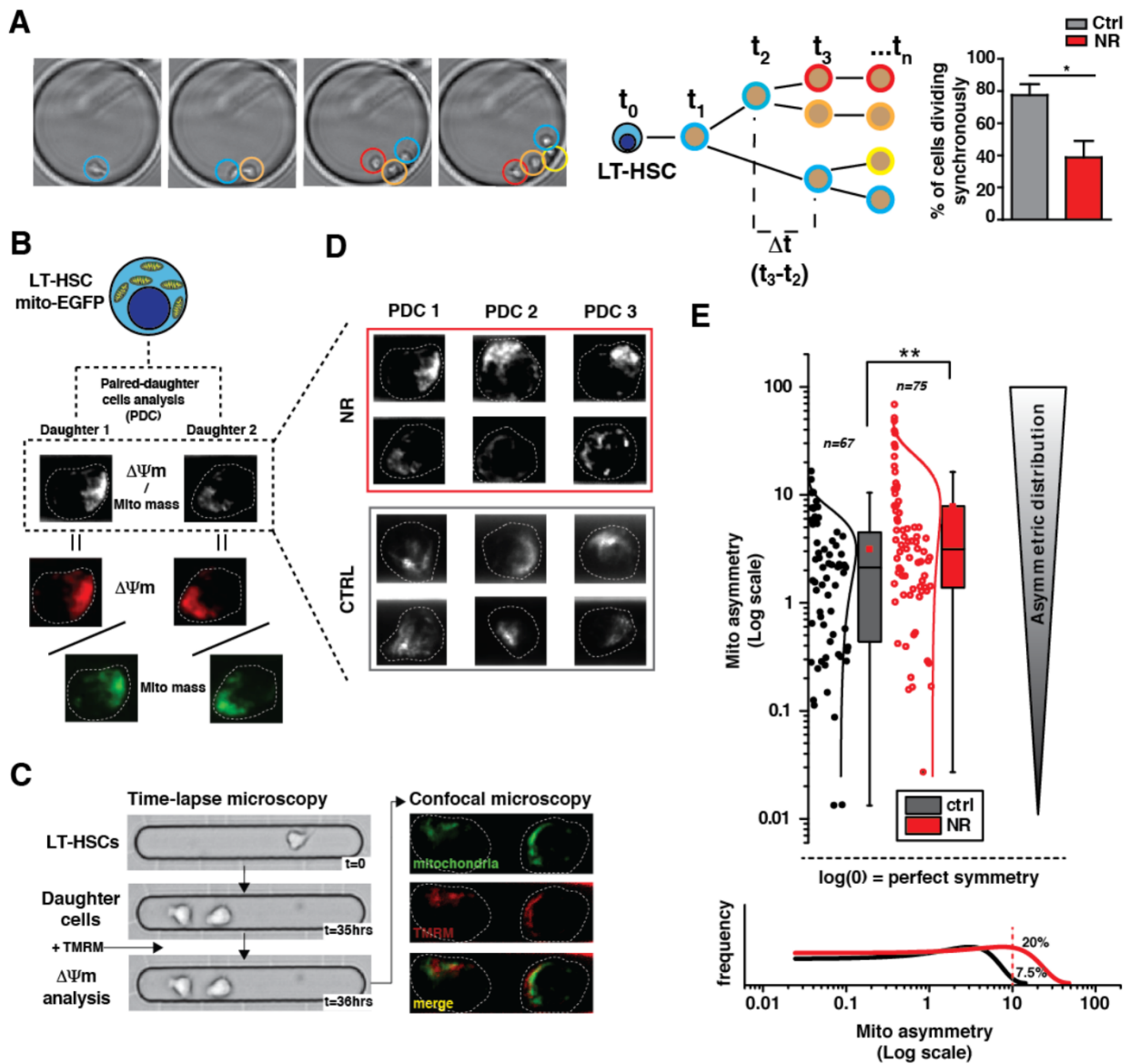


Figure 5.6 NR induces asymmetric mitochondrial distribution in LT-HSCs. **A**, Synchrony of cell division analysis in LT-HSCs upon first division was performed by following cell cycle kinetics in the micro-well array system. Cell division was considered asynchronous, thus suggestive of asymmetric HSC divisions, when 2 daughter cells were dividing in a time gap (Δt) > 6 h, $n=3$. **B**, LT-HSC paired-daughter cell (PDC) analysis of $\Delta\Psi m$ (TMRM) and mitochondrial mass (EGFP). Ratio between $\Delta\Psi m$ and mitochondrial mass was used to normalize all values for mitochondrial activity. **C-E**, Cell division kinetic was followed by time-lapse microscopy in a microwell system and **C,D**, PDC analysis was performed after TMRM quantification of mitochondrial activity as measured by confocal microscopy. Note that EGFP signal and thus mitochondrial mass does not change upon NR treatment, so all changes in TMRM signal normalized to EGFP reflect changes in $\Delta\Psi m$ and in mitochondrial mass. **E**, PDC analysis on mitochondrial distribution was evaluated in cells treated +/- NR as in C,D and the frequency of cells with highly asymmetric mitochondrial distribution ($> \log 10$) was quantified; $n=67$ and $n=75$. Student's t test * $p < 0.05$, ** $p < 0.01$, *** $p < 0.001$.

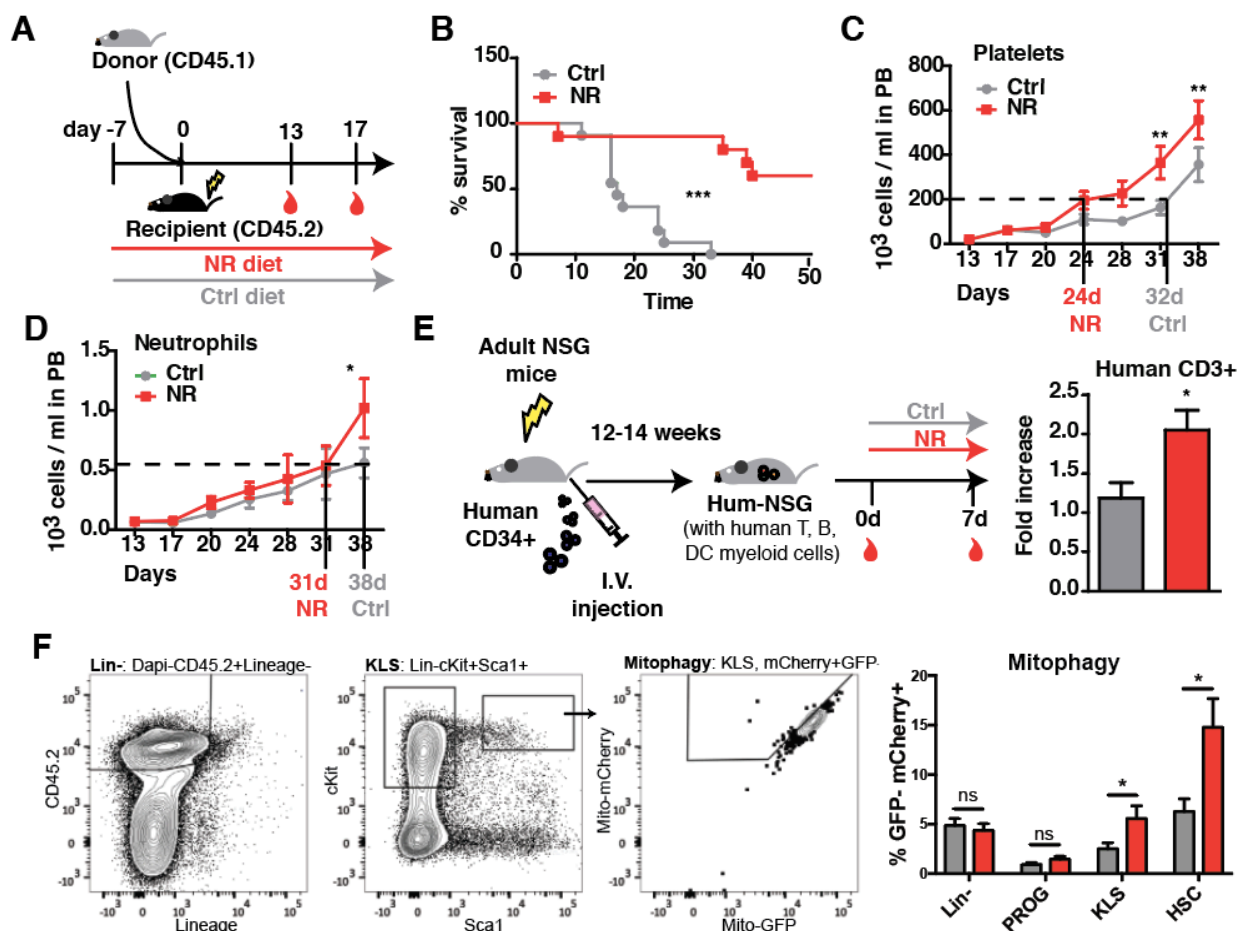


Figure 5.7 NR improves survival and accelerates blood recovery after HSC transplant. **A**, Mice were fed with ctrl or NR-supplemented diet (12mg NR triflate /mouse/day) from 1 week prior to transplantation until the end of all experiments. **B**, Survival of mice transplanted with a limited number of cells (70×10^5 total BM cells) was assessed over a period of 40 days, $n=10$. Mantel-Cox *** $p<0.001$. **C**, **D**, Recovery of blood cell counts was assessed over a period of 40 days after transplant of 150×10^5 total BM cells, $n=10$. 2 way ANOVA, Bonferroni post test * $p<0.05$, ** $p<0.01$, *** $p<0.001$. **E**, NSG humanized mice were produced by intrahepatic injection of human CD34+ cells in adult NSG mice. Human CD3+ T lymphocyte levels were assessed in humanized mice after 7 day treatment with control (ctrl) or NR diet (12mg NR /mouse/day). For each mouse the change in % CD3+ cells within the HuCD45+ population following 7d treatment was calculated as fold increase relative to d0, $n=5$. **F**, Wildtype recipient mice were lethally irradiated and transplanted with BM derived from mitoQC mice. Transplanted mice received diet supplemented with NR during throughout the post-transplant recovery period. Mitophagy rate was measured by FACS at 35 days post-transplant in the different hematopoietic progenitor and stem cell compartments. Student's t test * $p<0.05$, ** $p<0.01$, *** $p<0.001$.

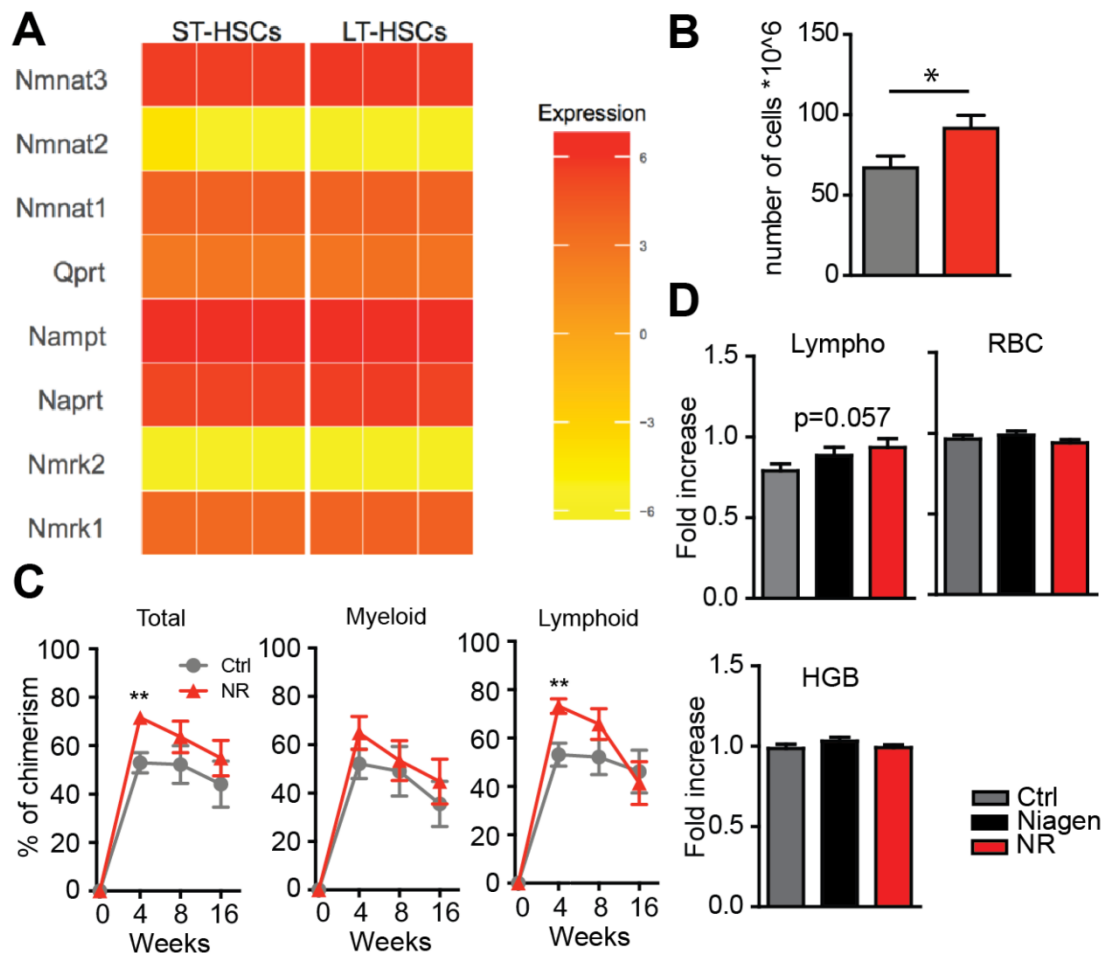


Figure S 5.1 Transcriptome analysis of NAD pathway genes and influence of NR on the hematopoietic system. A, Normalized expression for key genes of the NAD salvage pathway in LT-HSCs and ST-HSCs freshly sorted from the bone marrow of 10-week-old C57BL6 females. $n=3$. **B**, BM cellularity of mice fed for 1 week with ctrl or NR diet (legs and hips), $n=5$. **C**, Blood chimerism of mice transplanted with BM derived from ctrl or NR fed mice was assessed at 4, 8 and 16 weeks, $n=10$. Readings at 16 weeks show no significant difference, indicating that the LT-HSC pool is neither expanded nor exhausted after NR treatment, $n=10$. **D**, Analysis of peripheral blood for Lymphocytes, Red blood cells (RBC) and hemoglobin (HGB) in mice fed with ctrl, Niagen or NR diet, $n=5$. Student's *t* test * $P<0.05$, ** $P<0.01$, *** $P<0.001$.

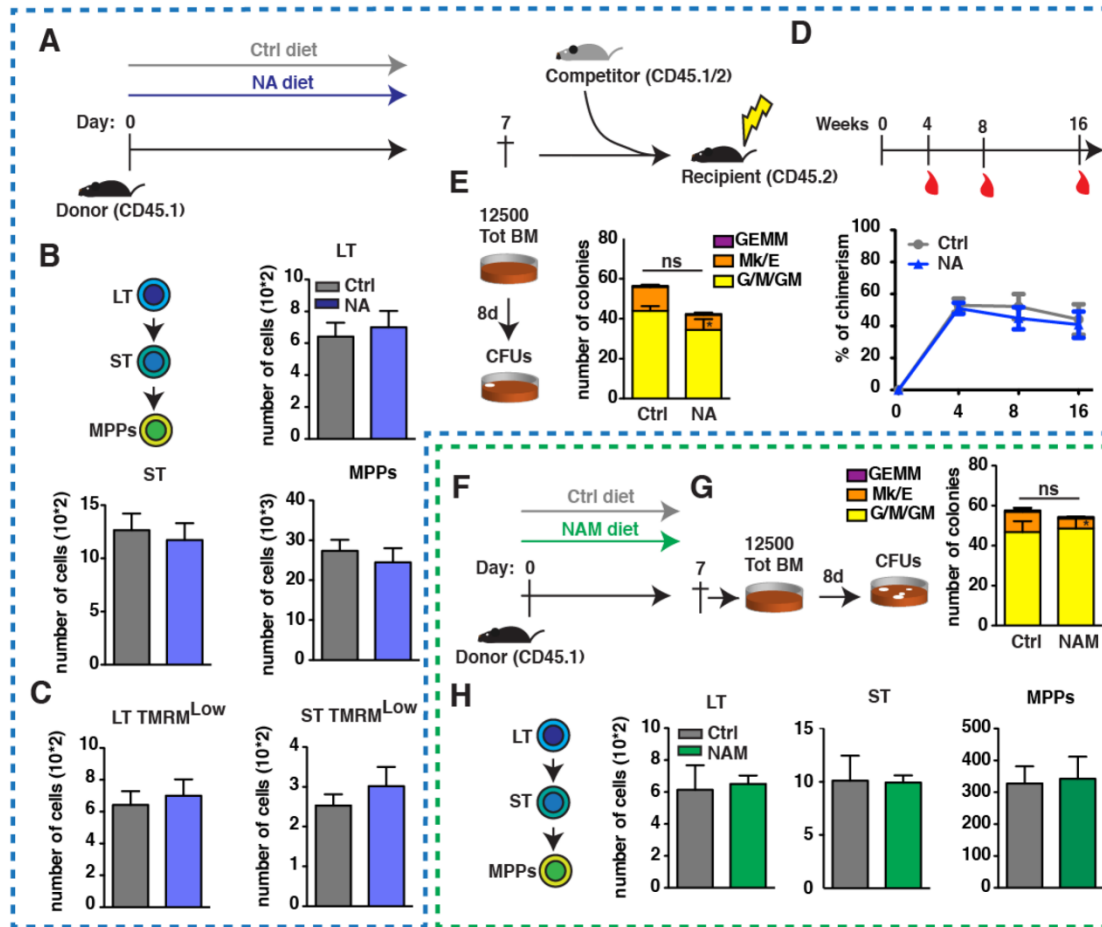


Figure S 5.2 NA/NAM-supplementation does not cause hematopoietic progenitor expansion. **A**, Mice were fed 1 week with control or NA diet, mice were sacrificed for BM analysis and primary transplant. **B**, Phenotypic analysis of the different BM hematopoietic stem/progenitor compartments from ctrl or NA fed mice by flow cytometry, $n=5$. **C**, LT and ST-HSC mitochondrial potential measured by TMRM staining from BM of ctrl or NR diet fed mice, $n=5$. **D**, Blood chimerism of mice transplanted with BM derived from ctrl or NA fed mice was assessed at 4, 8 and 16 weeks, $n=10$. **E**, 12,500 BM cells from ctrl- or NA-fed mice were plated in Methocult for colony forming CFUs analysis 8 days after plating, $n=5$. **F**, Mice were fed 1 week with control or NAM diet, mice were sacrificed for BM analysis and secondary transplants. **G**, 12,500 BM cells from ctrl- or NAM-fed mice were plated in Methocult for colony forming CFUs analysis 8 days after plating, $n=5$. **H**, Phenotypic analysis of the different BM hematopoietic stem/progenitor compartments from ctrl or NAM fed mice by flow cytometry, $n=5$. Student's t test * $P<0.05$, ** $P<0.01$, *** $P<0.001$.

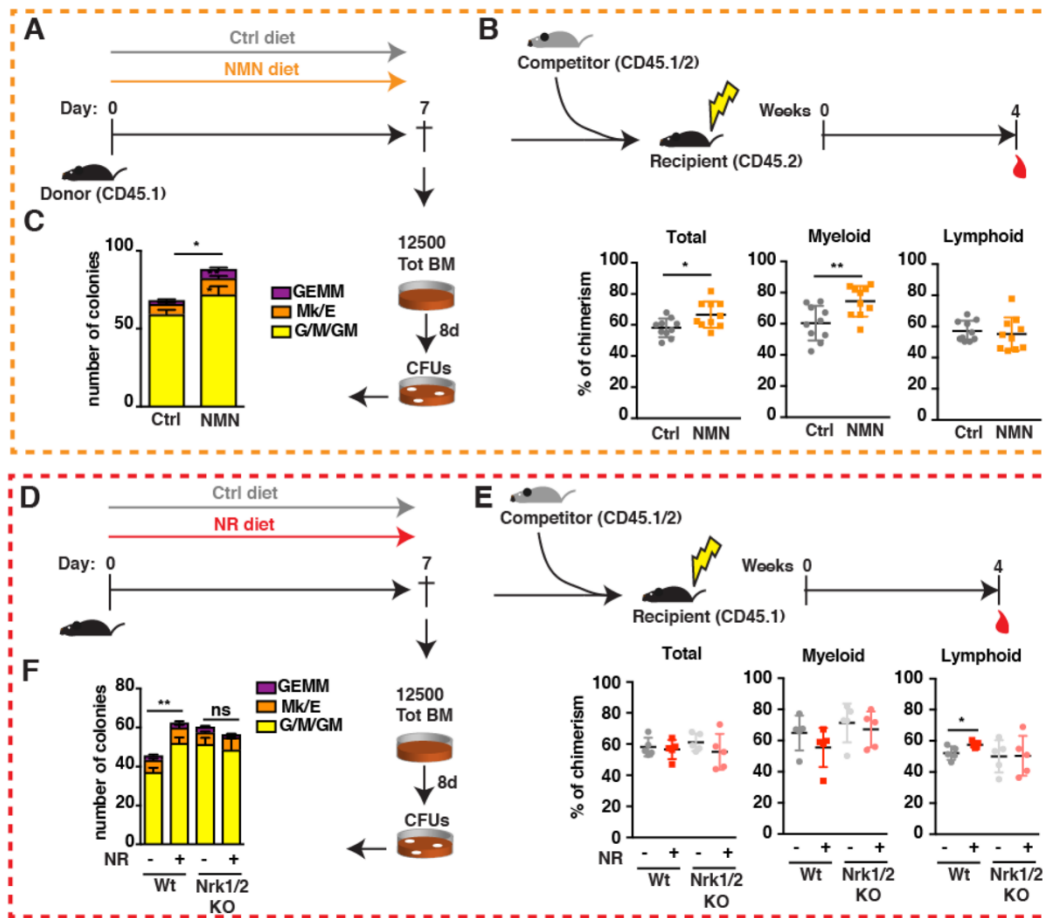


Figure S 5.3 NR exerts its effect through the NR/Nrk/NMN axis. **A**, Mice were fed 1 week with control or NMN diet, mice were sacrificed for BM analysis and secondary transplants. **B**, Blood chimerism of mice transplanted with BM derived from ctrl or NMN fed mice was assessed at 4 weeks, $n=10$. **C**, 12,500 BM cells from ctrl- or NMN-fed mice were plated in Methocult for colony forming CFUs analysis 8 days after plating, $n=5$. **D**, Nr1/2-/-; Nr2/2-/- double KO mice were fed 1 week with control or NR diet, mice were sacrificed for BM analysis and secondary transplants. **E**, Blood chimerism of mice transplanted with BM derived from wt or Nr1/2 KO mice fed with ctrl or NR diet was assessed at 4 weeks, $n=10$. **F**, 12,500 BM cells from wt or Nr1/2 KO mice fed with ctrl or NR diet were plated in Methocult for colony forming CFUs analysis 8 days after plating, $n=5$. Student's t test * $P<0.05$, ** $P<0.01$, *** $P<0.001$.

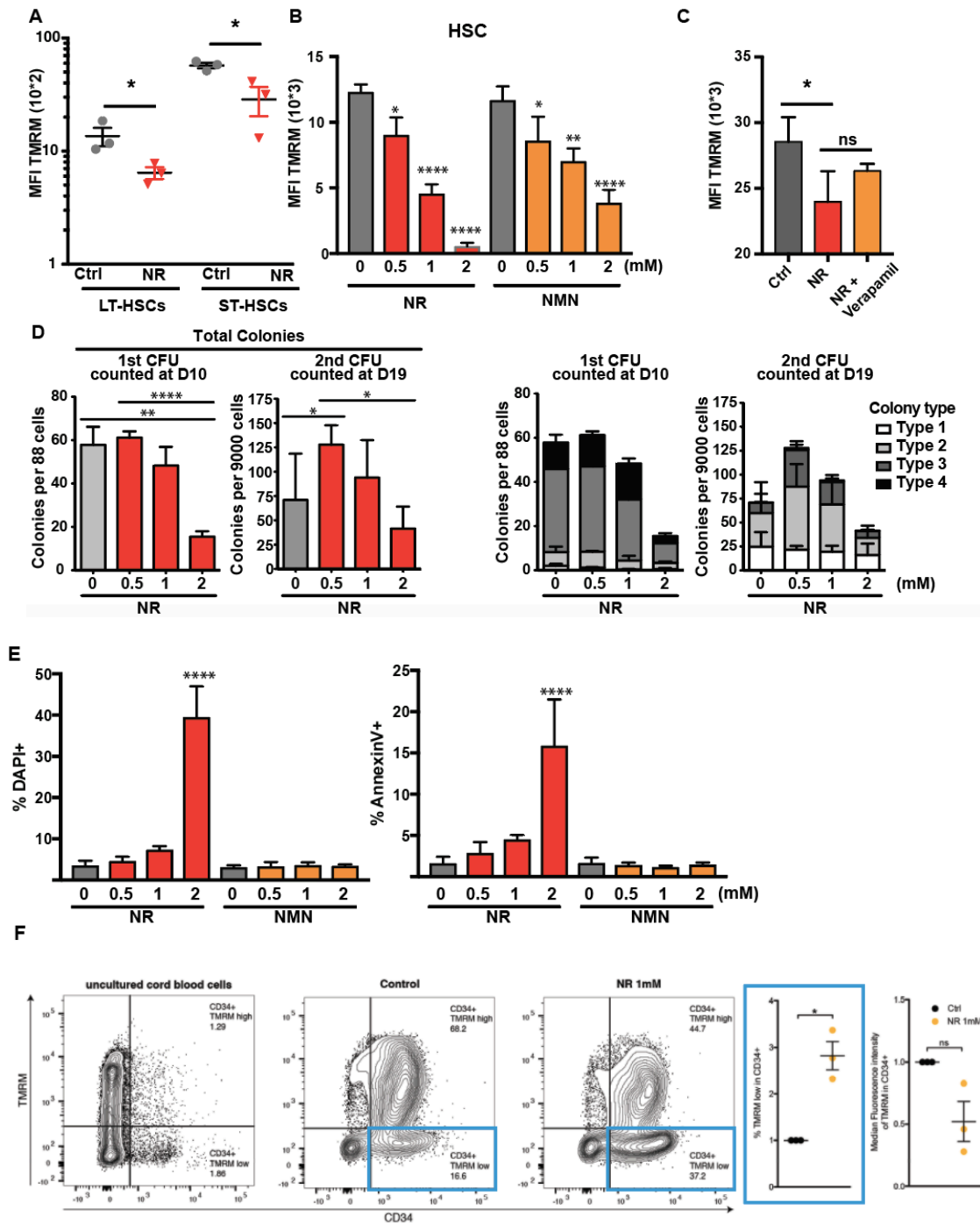


Figure S 5.4 NR *in vitro* affects mitochondrial mass and $\Delta\Psi_m$ in HSCs. **A**, LT- and ST-HSCs were FACS sorted and treated *in vitro* for 48 hours with 0.5 mM NR (**A**), or increasing concentrations of NR or NMN (**B**), then stained with TMRM and analyzed by FACS. **C**, HSCs were cultured for 48h with NR. The calcium dependent ABC pump inhibitor verapamil was added at 50 μ M 1 h before TMRM staining and subsequent flow cytometric analysis. There was no significant difference on the NR-mediated decrease in TMRM signal in presence or absence of verapamil. **D**, HSCs cultured with NR for 48h, were plated in M3434 methylcellulose and their long-term colony-forming capacity was analyzed in secondary CFU assays. CFUs were scored using the StemVision software (StemCell Technologies). Colony type depends on the colony size and cell density, with Type 1 being the smallest and less dense colony. Note that there is no differences in the primary CFU and that the highest NR concentration of 2mM was toxic to murine HSCs, but not to human CD34+ progenitors (Figure 3A). **E**, HSCs cultured with NR or NMN at different concentrations, stained with DAPI and Annexin V, and analyzed by FACS. **F**, Cord blood derived human CD34+ cells were cultured for 2 days in the presence or absence of NR as in Fig. 3A. Shown is the experimental replicate for cord blood in a different laboratory with completely independent donors (upper panel & lower panel). Both the fold change in the TMRM^{low} population (labeled in blue) and the TMRM MFI of total CD34+ were quantified. $n=3$. Student's *t* test * $P<0.05$, ** $P<0.01$, *** $P<0.001$

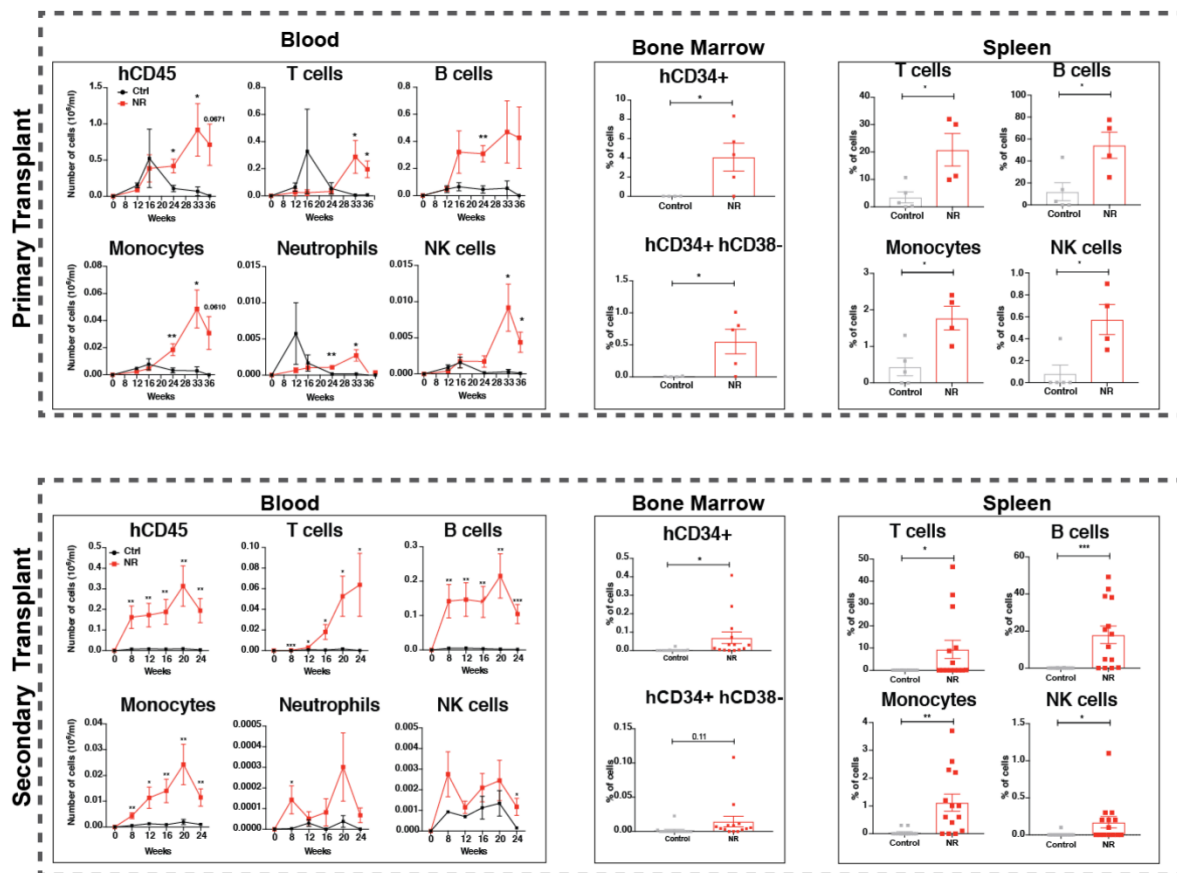


Figure S 5.5 NR improves blood reconstitution and stem cell function of human CD34+ cells. Fetal derived human CD34+ cells were cultured for 5 days in the presence or absence of NR and transplanted in irradiated NSG mice. Reconstitution of different blood lineages (Blood panels) was followed over time in primary (1^0 Transplant) and secondary (2^0 Transplant) recipient mice. At the endpoint hematopoietic progenitors (CD34+ and CD34+CD38-) and blood lineages were quantified in the bone marrow and spleen of recipients' mice respectively. $n=6$ & $n=12$. Student's t test * $P<0.05$, ** $P<0.01$, *** $P<0.001$.

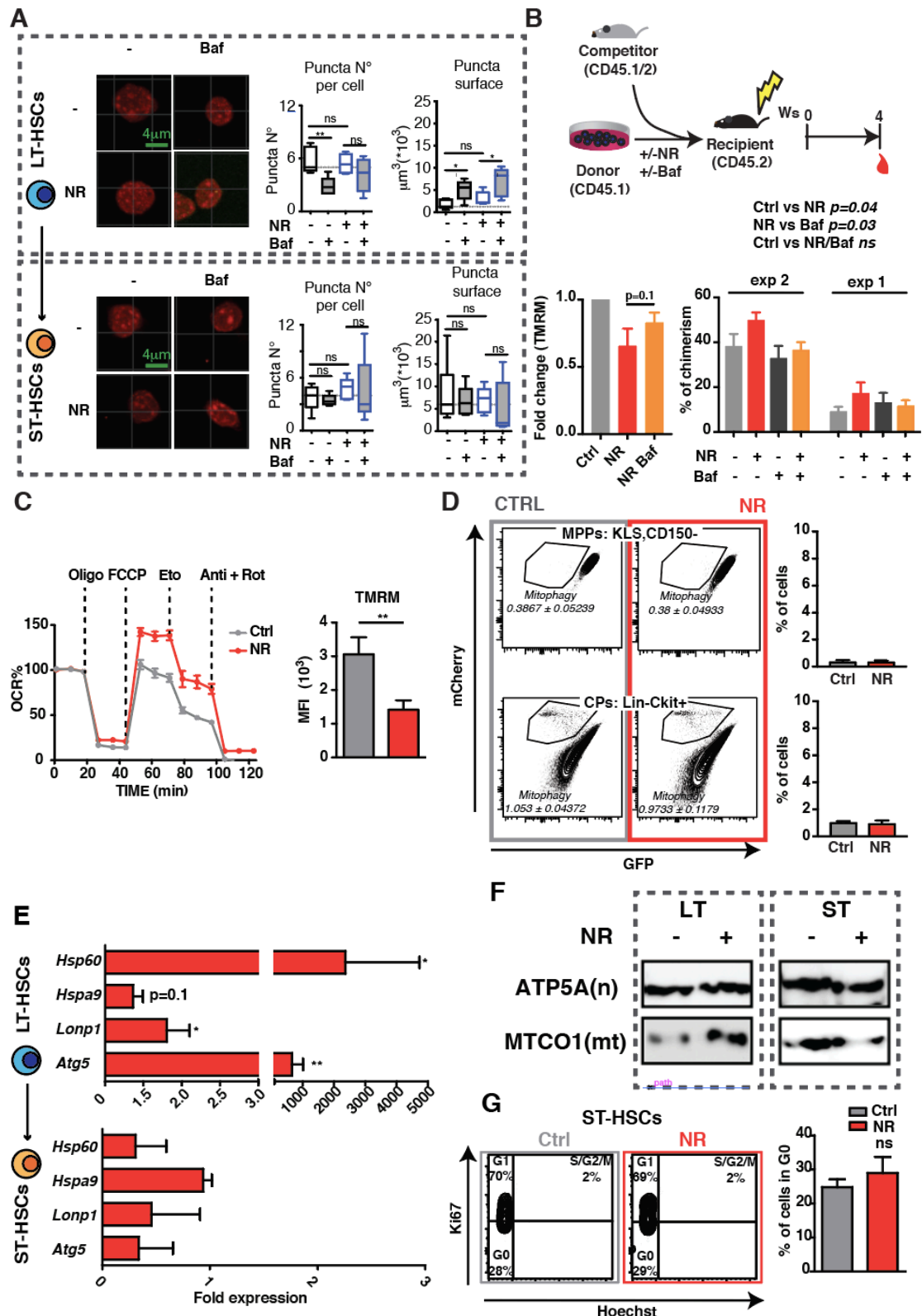


Figure S 5.6 NR induces autophagy, mitophagy, increased OCR and mitochondrial stress. **A**, Confocal analysis of HSCs exposed to NR, autophagy blocker Bafilomycin, or both. Cells were stained with Lc3B antibody and number and size of autophagosomes was measured. (Upper panels LT-HSCs; Lower panel ST-HSCs). **B**, LT-HSCs (CD45.1) were cultured for 2 days in the presence of absence of NR and Bafilomycin (Baf). 200µm of HSCs was then analyzed by flow cytometry with TMRM staining in presence or absence of bafilomycin (lower left, n=4). LT-HSCs were cultured for a total of two days and transplanted into lethally irradiated mice (CD45.2) together with total bone marrow competitor cells (CD45.1/2). Engraftment capability was measured by blood analysis in 2

independent experiments (lower right). Statistics are for the combined experiments, which are shown separately because the baseline engraftment was very different for both cohorts. **C**, Splenocyte-derived cells were cultured with NR over 3 days. Oxygen consumption rate (OCR) of splenocyte-derived cells was measured at basal level and in response to oligomycin (Oligo), FCCP, etomoxir (Eto) and antimycin (Anti) in combination with rotenone (Rot) (left panel); and $\Delta\Delta m$ was measured by TMRM staining and analyzed by FACS (right panel). **D**, Mito-QC mice were fed for 1 week with control or NR diet. Percentage of cells undergoing mitophagy was quantified. Downstream hematopoietic progenitors, MPPs (KLS CD150-) and CPs (Lin- cKit+) showed lower mitophagy rates as compared to the most primitive hematopoietic compartments and most importantly, their mitophagy rates were not affected by NR supplementation. **E**, Backgating analysis of Mito-QC cells. In the Mitophagy analysis of LT and ST-HSCs the mCherry^{high} population (left panels) was excluded, as it represented P^{interm} cells which backgated away from the core HSC population both in the FSC and KLS gates. **F**, Gene expression analysis of ST or LT-HSCs isolated from the BM of NR or control diet fed C57BL6 mice, $n=4$. **G**, Mitonuclear protein imbalance in HSCs FACS sorted from mice fed control vs. NR diet for 7 day. Western blotting protein analysis of mitochondrial proteins encoded by nuclear subunit (ATP5a) and mitochondrial subunit (MTCO1) of the oxidative phosphorylation complex (see text for interpretation, data derived from the pooled bone marrow of 32 mice). **G**, Cell cycle analysis of ST-HSCs derived from NR or control diet fed mice, $n=5$. Student's *t* test * $P<0.05$, ** $P<0.01$, *** $P<0.001$.

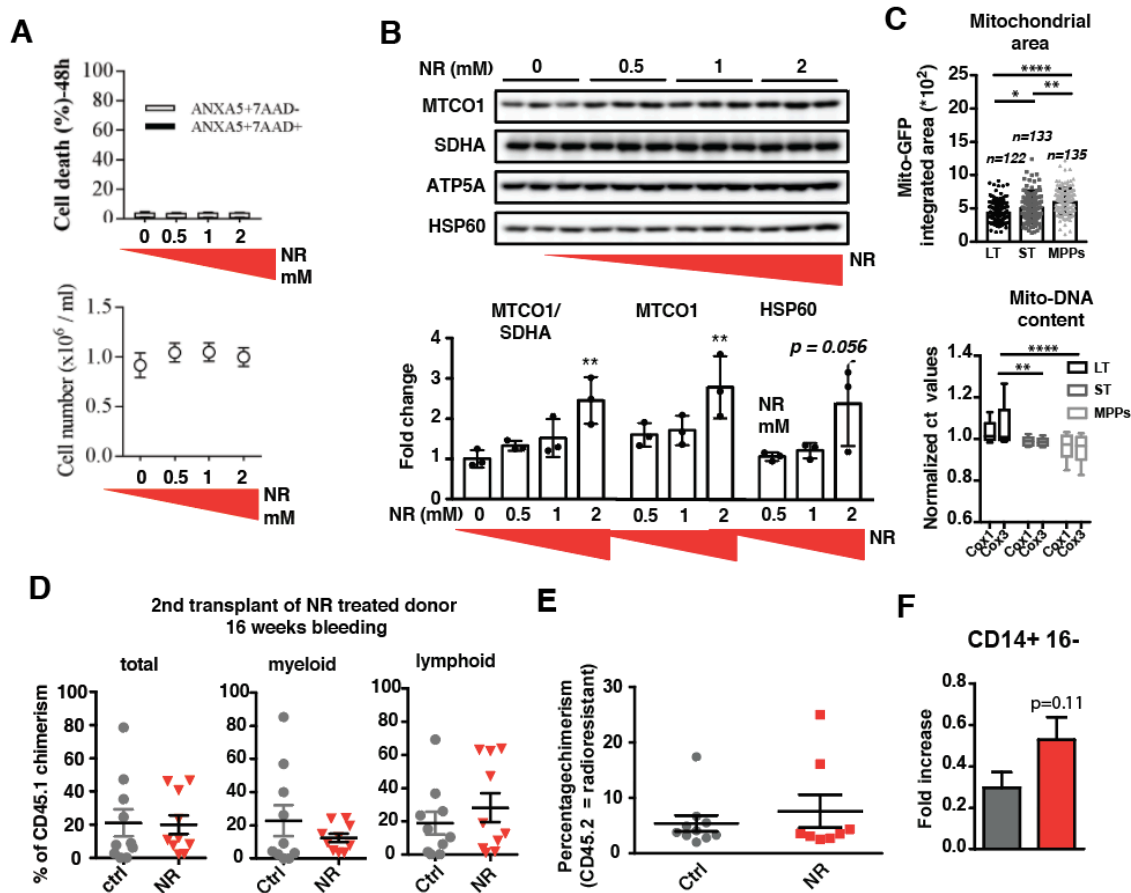


Figure S 5.7 NR induces mitochondrial stress in K562 cells in a dose dependent manner and does not exhaust HSC function in secondary transplantation. A, Cell death was assessed by flow cytometry using annexin V (ANXA5) and 7AA D double staining after 48 hours of NR exposure. Absolute cell number was determined by flow cytometry using absolute counting beads. B, western blot quantification of NR-driven mito-nuclear protein unbalance (MTCO1/SDHA) and NR-driven induction of UPRmt chaperone HSP60. C, Mito-EGFP derived hematopoietic stem and progenitor cells were analyzed for their mitochondrial content. Confocal analysis of single cell integrated EGFP signal was used to quantify mitochondrial area (upper panel). Mitochondrial DNA content was analyzed by QPCR targeting 2 different mitochondrial genes (Cox1 and Cox3). Values are expressed as normalized ct that inversely correlated to the DNA content (lower panel). D, Analysis of radioresistant BM (recipient, CD 45.2+) of transplanted mice with BM derived from ctrl or NR diet fed mice, $n=10$. E, Secondary transplants were performed with total bone marrow from mice having received limiting-dose transplantation while treated with NR or control diet (Figure 7C-D), then analyzed at 16 weeks for persistence of donor CD45.1 stem cell function. F, Analysis of CD14+ CD16- monocytes of peripheral blood of humanized mice fed for 7 days with ctrl or NR diet (gated on hCD45), $n=5$. Student's t test $*P<0.05$, $**P<0.01$, $***P<0.001$ and Two-way ANOVA $*P<0.05$, $**P<0.01$, $***P<0.001$.

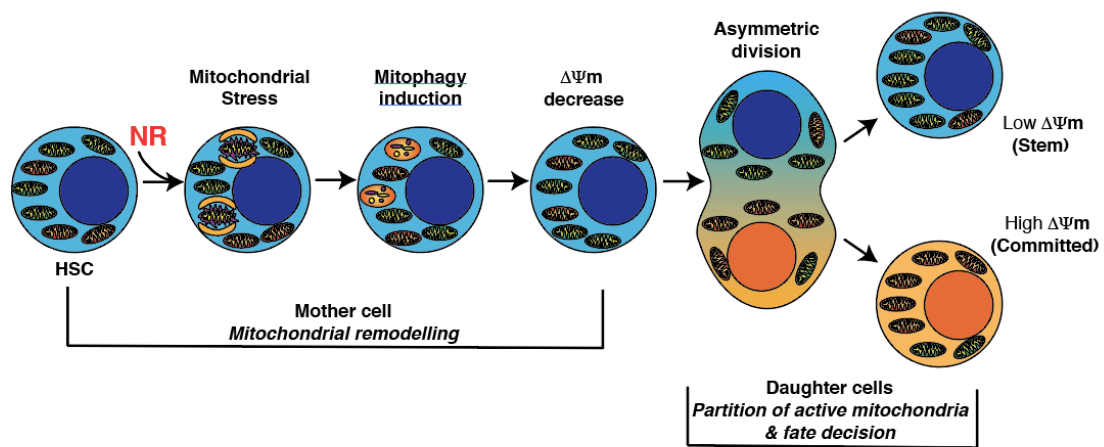


Figure S 5.8 Graphical abstract. Nicotinamide Riboside (NR) induces mitochondrial metabolic stress in hematopoietic stem cells (HSCs). NR-induced mitochondrial stress leads to induction of mitophagy, clearance of unfit high mitochondrial membrane potential ($\Delta\Psi_m$) mitochondria and thus overall reduction of $\Delta\Psi_m$. The mitochondrial remodeling triggered by NR supplementation further promotes asymmetric partitioning of active mitochondria in daughter cells, thus maintaining the output of low $\Delta\Psi_m$ HSCs, which we have previously shown to correspond to the long-term engrafting HSC population.

Chapter 6 Conclusion

The ultimate goal of this thesis was finding novel clinically compatible strategies to accelerate hematopoietic recovery in the context of bone marrow transplantation (BMT or hematopoietic stem cell transplantation, HCT). The HCT involves retrieving hematopoietic stem cells (HSC) from the donor bone marrow (or other sources, such as umbilical cord or peripheral blood) and eventually expanding the cells *in vitro* before transplanting them via the blood stream into the patient. This poses challenges at each step of the procedure, firstly because HSCs are always limited in numbers and, once outside of their native microenvironment, they tend to rapidly differentiate and ultimately exhaust their regenerative potential [228]. In addition, identified hematopoietic cell surface markers, such as the SLAM family, change upon HSC *in vitro* culture [229]. Various markers have been identified to define pure HSCs and great efforts have been invested into expanding HSCs *in vitro* without exhausting their regenerative potential [6], [18]–[20]. However, these methods have all had their success limited. Another remaining challenge is the transplantation itself, where homing of the HSC to its niche, the acceptance of the donor tissue by the recipient, and the efficient expansion of hematopoietic progenitor cells (HPCs) to functional mature blood cells of all lineages, all poses independent limitations. In this work, all transplantation experiments were done with MHC-compatible donors and recipients, therefore removing the potential variable imposed by graft-versus-host-disease. In addition, by standardizing our transplantation assay we were able to reference the hematopoietic recovery post-transplantation. However, it has to be taken into consideration that the differential pre-transplant treatments of the recipient mice used in our context may have affected the homing of donor hematopoietic stem and progenitor cells (HSPC), which we did not assess.

This work targeted two main mechanisms of maintaining HSC and progenitor function (HSPC): (i) one by directly targeting the metabolism of primitive LT-HSCs with the aim of maintaining and expanding a functional HSC pool both *in vivo* and *ex vivo*, (ii) the other one by targeting the HSPC niche, more specifically the bone marrow adipocyte, with the aim of accelerating hematopoietic production in the post-transplant period.

6.1 Kinetics of the bone marrow transplantation

In this context, we argue that it is of central important to distinguish two main hierarchies: the HSC to hematopoietic progenitor differentiation axis and the mesenchymal to adipocytic differentiation axis. The hematopoietic system is the best described stem cell system to date and the HSC is defined, as all other adult stem cells, by its function: self-renewal and giving rise to all derived mature cells of that specific organ. ‘Mesenchymal stem cells’ (MSC) constitute a still ill-defined cell population that does not behave in the typical fashion of stem cells: they trans-differentiate across lineages or de-differentiate to their previous state, depending on the shifting demands of the surrounding tissues. In addition, the newly proposed notion of location-specific skeletal stem cells (SSC) [76] and the ‘tissue-organizer’ activity of mesenchymal cells [47] have led to recent changes in the nomenclature of these cells. Rather than stem cells, they have been proposed to be simply called stromal cells [74]. Within the bone marrow, bone marrow stromal cells (BMSC) have been shown to be key player in the interaction with HSCs and progenitor cells and various markers have been proposed to define these cells including Nestin, LepR, Pdgfra, CD24 etc [52], [54], [64], [75]. Bone marrow adipocytes (BMA) are besides osteoblasts, the main cell type deriving from BMSCs, but their function towards the hematopoietic system remains highly debated, mainly because of lack of consideration to both differentiation axes: the mesenchymal to adipocytic axis and the HSC to hematopoietic progenitor axis. By submitting mice to lethal irradiation followed intra-tibial bone marrow transplants together with cells of three stages of mesenchymal to adipocyte differentiation axis, the study by Ambrosi et al most elegantly describes this phenomenon [64]. Even though these populations were identified in the context of diet induced obesity, the authors demonstrated that the most primitive multipotent cells have strong hematopoietic supportive capacities *in vivo*, which are decreased along the differentiation towards mature adipocytes.

We have in this work demonstrated that these populations also arise intrinsically in mice undergoing bone marrow transplantation and observed that pre-adipocytic cells arise in the immediate post-transplant period, which then probably differentiate towards adipocytes, filling up most of the marrow space at the peak of aplasia. Following the peak of aplasia, we observed hematopoietic-supportive multipotent stromal cells to arise, coinciding with the hematopoietic recovery. Since hematopoietic recovery post-transplant is mainly driven by proliferation and differentiation of hematopoietic progenitor cells, rather than primitive HSCs, we hypothesized that preventing adipocyte differentiation would improve HSPC function, but not necessarily HSC function. We therefore

standardized an *in vivo* bone marrow transplantation assay in which we modulated the adipocytic bone marrow content in order to better understand the interaction of bone marrow adipocytes and HSPC function. Using a modified version of the ‘Adipochaser’ lineage-tracing mouse model, we intended to assess whether adipocytes also de-differentiated to give rise to hematopoietic-supportive stromal cells, but due to leakiness of the Cre system this could not be explored. Future lineage-tracing experiments will be addressing whether this leakiness was due to high sensitivity of the Ai9 Cre mouse strain [112] or due to the increased accessibility of the TdTomato-reporter transgene. In addition, experiments will target only young mice, to reduce probabilities of non-specific labeling.

6.2 Influence of BMA on hematopoiesis

In this work, we used a pharmacological approach to modulate adipocyte differentiation, providing quantitative insight into which extent modulating adipocyte differentiation promotes hematopoiesis *in vitro*. To this end, we developed a high-throughput screening platform using Digital Holographic Microscopy (DHM), which allowed us to assess adipocytic differentiation in a non-perturbing manner, prior to co-culture with primary murine-derived HSPCs. By pre-treating the hematopoietic-supportive OP9 bone marrow-derived stromal cell line with a variety of compounds inducing or preventing adipocyte differentiation *in vitro*, we observed that high adipocytic content was always associated to a decrease in HSPC proliferation and colony-forming capacity. Untreated OP9 cells, had the strongest hematopoietic supportive capacity, while inhibition of adipocyte differentiation using newly identified inhibitors, rescued the hematopoietic supportive capacity to a certain extent. However, some compounds that prevented adipocytic differentiation negatively affected the hematopoietic supportive capacity of the OP9 stroma in other ways, which remain open to further investigation. Some suggestions include toxicity towards the OP9 stroma, reduced metabolism of OP9 cells, as could have happened with Antimycin A treatment, or induction of differentiation towards other cell fates, as suggested by the distinct cellular morphology and transcriptional profile of flavonoid-treated OP9 cells. We therefore concluded that although lower lipid content was generally associated to increased hematopoietic support, we observed an optimum along the mesenchymal-to-adipocytic axis in hematopoietic supportive capacity of OP9 cells. This is in congruence with other studies suggesting pre-adipocytes to support hematopoiesis through higher expression of Ang-1, SCF and Cxcl12, which decreases in terminally differentiated adipocytes [87].

In vivo, BMA has finally been recognized as a hematopoietic regulatory entity, although the mechanisms by which it interacts with HSPCs *in vivo*, remain largely unknown. We tested the role of bone marrow adipocytes in the context of murine hematopoietic recovery post-transplantation, therefore mostly focusing on the effect of BMA on fast proliferating and differentiating HPCs. By assessing the peripheral blood production and the colony forming capacity of HSPCs in the bone marrow of recovering mice we observed that Rosiglitazone or high fat diet-treated mice had aberrant hematopoietic recoveries. On the other hand, by inhibiting BMA formation using standard PPAR γ inhibitors we observed that GW9662 slightly improved hematopoietic recovery, therefore suggesting that BMA have a net inhibitory effect on the hematopoietic recovery of transplanted mice. Note that the main limitations posed by the *in vivo* experiments, stem from systemic changes in the metabolic state of these mice, preventing the distinction of the effects of inflammation or extramedullary adipocytes from the specific effect of bone marrow adipocytes on recovering hematopoiesis [172], [173]. Although preventing hematopoietic proliferation may be detrimental to the hematopoietic progenitor compartment, it may be of advantage for the most primitive HSC compartment. In this work, we observed that HFD-fed donor mice had decreased ST-HSCs and progenitor functionality, while the LT-HSC pool remained unchanged, as seen over 16 weeks post-transplantation. It is by now generally accepted, from both *in vitro* and *in vivo* studies, that bone marrow adipocytes maintain primitive HSCs quiescent [85], [86] and it has even been observed that extramedullary adipose tissue contains quiescent HSCs [230]. It may therefore be, that BMA act as a protective environment, maintaining the pool of the remaining most primitive HSCs in an acutely aplastic bone marrow. In this context, ours as well as others observations support our hypothesis that bone marrow adipocytes prevent HSPC proliferation and alerts to the distinction between pre-adipocytes and terminally differentiated adipocytes, as well as the distinction between primitive HSCs and HPCs.

6.3 HSC metabolism

While LT-HSCs are mostly quiescent and rarely cycle in order to give rise to their committed progeny as well as to self renew [24]–[26], HPCs are obliged to produce higher levels of ATP via mitochondrial oxidative phosphorylation in order sustain their rapid proliferation [25], [27]. Consistent with their quiescent state, most HSCs exhibit a relatively low mitochondrial potential, reflecting their glycolysis-driven metabolic profile when residing in their homeostatic niche [25], [27], [42]. Recent studies have shown that HSC also heavily rely on fatty acid oxidation [220], suggesting how adipocytes could act as a reservoir to maintain their function in acute stress. Removing HSCs from their microenvironment however, increases oxidative phosphorylation, as reflected by increased mitochondrial activity. Increased oxidative phosphorylation combined with impairment of the mitochondrial stress response can severely compromise the regenerative capacity of primitive HSCs [24]. Autophagy, the recycling mechanism of damaged intracellular

compartments (such as mitochondria), has been shown to improve HSC maintenance via FOXO3-mediation and activation of the mitochondrial stress response [38]–[40]. In this work, we reveal the ability of a different NAD⁺ boosting agents to reduce the mitochondrial membrane potential in HSCs *in vitro* and enhance self-renewing asymmetric divisions in LT-HSCs, via activation of autophagy. NAD⁺-boosters, such as the vitamin B₃-derivative Nicotinamide Riboside (NR) or Nicotinamide mononucleotide (NMN) have previously been characterized as a means of activating the NAD-dependent deacetylase sirtuin-1 (SIRT1) axis via the induction of the mitochondrial stress response in the context of aging, liver and muscle regeneration [184]–[188].

6.4 Accelerating hematopoietic recovery post-transplant

We therefore set out to test whether NAD⁺ boosters could induce the mitochondrial stress response, therefore improve HSC mitochondrial homeostasis and hematopoietic reconstitution after HSC transplantation. Supplementation of Nicotinamide Riboside (NR) to the diet of C56B6/J mice indeed resulted in a significantly enlarged pool of progenitors, without exhaustion of the LT-HSCs at homeostasis. In the context of the bone marrow transplantation, we observed NR-fed mice to accelerate hematopoietic recovery as seen by earlier exit from severe neutropenia (< 0.5 G/l) and thrombocytopenia (< 200 G/l) [225], without concomitant HSC exhaustion. In a limiting-dose bone marrow transplantation, NR treatment improved survival of mice by 80 %. Finally, using the mitophagy-reporter, mitoQC mice [211] as donors in the transplantation setting, we demonstrated LT-HSCs to display higher rates of mitophagy than progenitor cells, and that upon NR dietary supplementation mitophagy could be increased.

Our *in vitro* pharmacological modulation of the HSPC microenvironment via inhibition of adipocyte differentiation revealed us Calcipotriene, a synthetic vitamin-D₃ derivative, as a strong candidate to test *in vivo* to accelerate hematopoietic recovery post-transplantation. We observed that OP9 cells treated with calcipotriene, were prevented from DMI-induced adipocyte differentiation, maintained high expression of hematopoietic cytokines, and demonstrated enhanced lin-/cKit+/Sca1+ (LKS) progenitor cells expansion upon co-culture. Given the hormonal nature of vitamin D₃, its pleiotropic effects cover a variety of functions, most prominently in bone remodeling [231]. It has also been observed to play a direct role in developmental hematopoiesis, whereas it directly increases HSPC numbers via increased expression of hematopoietic cytokine Cxcl8 [232]. In mice, Vitamin-D receptor (VDR) deletion, leads to extensive migration of HSPCs from the bone marrow to the spleen [174]. Therefore, in addition to testing the accelerated hematopoietic recovery in mice undergoing transplantation via calcipotriene supplementation, the non-cell-autonomous effect of calcipotriene will have to be tested on HSPCs via transplantation of the bone marrow of vitamin-D receptor KO mice into wild-type mice.

6.5 Clinical perspectives

Vitamin D-deficiency affects a large percentage of the human population, especially in countries of northern latitudes, given that exposure to sunlight converts 7-dehydrocholesterol to pre-vitamin D₃, which is rapidly converted to vitamin D₃ [233]. In adults, serum Vitamin-D₃ levels are a strong predictor of bone health as well as the risk for cancer and other chronic diseases. Although supplementation of vitamin-D has not yet been associated to fat mass, an inverse relationship between serum vitamin D₃ levels and obesity has been observed, supporting evidence of the role of vitamin D₃ in reducing fat mass [234], [235]. In the setting of a bone marrow transplantation, vitamin D deficiency has been variably associated with increased complications, with a potential impact on survival outcomes [236]. The interplay between vitamin D₃ and VDR has also been implicated in modulating the immune response following BMT, therefore also possibly improving graft-versus-host disease (GvHD) in allogeneic transplants [237]. Although the mechanisms of this modulation remain largely unknown, the maintenance of multipotent stromal cells that have been shown to modulate immune responses in the setting of GvHD [238], [239], may be in part, responsible for the improved outcome post-BMT. A better understanding of how vitamin D₃ supplementation affects hematopoietic modulation in a non-cell autonomous manner could therefore prove useful for patients undergoing HCT, in particular osteoporotic patients, which have a decreased capacity of bone formation and increased marrow adiposity.

On the other hand, dietary supplementation of the vitamin-B₃ derivative, Nicotinamide Riboside (NR), in standard humanized NSG mice led to enhanced human hematopoiesis at homeostasis. It could therefore be used to reduce mortality of patients undergoing HCT, in particular elderly patients suffering from myelodysplastic syndromes where an age-dependent mitochondrial defect has already been suggested [227]. In addition, human HSCs treated *ex vivo* with NR, had increased regenerative capacity, independently from the source (fetal liver, UCB, bone marrow). This suggests that NR, and possibly other NAD⁺-boosters, such as Nicotinamide mononucleotide (NMN) could prove useful for *in vitro* HSC expansion protocols, in a variety of contexts such as the bone marrow transplantation itself, adoptive cell transfer or immunotherapy. The wide-ranging protective effects of NR on mitochondrial activity in non-hematopoietic tissues would be of additional value for HSC-ablative chemotherapy regimens, which often carry significant secondary cardiologic or neurologic toxicity due to mitochondrial impairment [193], [197].

6.6 Pharmacological perspectives

The primary chemical screening performed on the bone marrow-derived OP9 stromal cell line, led to a selection of 49 compounds that inhibited DMI-induced adipocyte differentiation, representing around 1 % of the initial compounds tested. In addition, 87 compounds increased DMI-induced adipocyte differentiation. In our setting, the search for inhibitors was motivated by a microenvironmental modulation of the HSC niche, in the context of the bone marrow transplantation. The compounds or the hereby generated knowledge could be used in other fields such as obesity. Using adipose tissue-derived cell or other pre-adipocytic cell lines, Digital holographic microscopy (DHM) could be useful to identify other molecules modulating lipid droplet accumulation. In addition, cellular morphologies, such as the alternative fibrillar phenotype observed, could be correlated to certain families of compounds, as it was the case with flavonoids. Other morphological features such as number of lipid droplets per cell could be used to identify compounds inducing adipose tissue browning. A collaboration agreement with an industrial partner has been signed in the context of our research, whereas we are in the process of applying medicinal chemistry on newly identified hits, with the aim of developing other drugs to improve hematopoietic reconstitution after bone marrow transplantation.

Appendix Standardized kinetics of murine hematopoietic recovery following chemo- and radio-ablative regimens

This work is planned for a manuscript and describes the kinetics of circulating mature blood cell types following two different methods of hematopoietic aplasia in 8- to 12-week old female C57Bl/6J mice. Sublethal 5-Fluorouracil injection was used as a model of rapid hematopoietic recovery and lethal irradiation followed by bone marrow transplantation was used as a model for slow hematopoietic recovery. The assays were standardized by pooling the results of 12 independent experiments with the aim of identifying modulators of hematopoietic recovery. The experiments were planned by Vasco Campos and executed by Aurelien Oggier and Vasco Campos. The chapter was written by Aurelien Oggier and edited by Vasco Campos.

Authors:

A. Oggier¹, V. Campos¹, Y. Yersin¹, N. Vannini^{1,2} and O. Naveiras^{1,3,4}

Affiliations:

¹Laboratory of Regenerative Hematopoiesis (GR-NAVEIRAS), Institute of Bioengineering, Ecole Polytechnique Fédérale de Lausanne (EPFL); Lausanne, Switzerland.

²Ludwig Center for Cancer Research of the University of Lausanne (UNIL), Lausanne, Switzerland.

³Swiss Institute for Experimental Cancer Research (ISREC), School of Life Sciences. Swiss Federal Institute of Technology Lausanne (EPFL), Lausanne, Switzerland.

⁴Hematology Service, Department of Oncology, Centre Hospitalier Universitaire Vaudois (CHUV); Lausanne, Switzerland.

A.1 Introduction

Haematopoiesis is defined as the production and maintenance of all blood cells through self-renewal and differentiation of haematopoietic stem cells [240]. Lymphocytes emerge from a common lymphoid progenitor (CLP) and all other cell types, including red blood cells, platelets, monocytes and granulocytes derive from a common myeloid progenitor (CMP), although recent findings question this clear separation regarding granulocytes [241], [242]. Both, total body irradiation followed by bone marrow transplantation, as well as chemotherapy treatment, have been used to study haematopoietic regeneration in a cell-autonomous, as well as micro-environment-driven manner [62], [243]–[247]. Irradiation creates DNA breaks [248] leading to cell death in proliferating cells, which in turn, leads to an inflammatory response [249]. 5-Fluorouracil (5-FU) is thought to interfere with DNA synthesis via inhibition of thymidylate synthase [250]. 5-FU has been shown to stimulate the cycling of primitive haematopoietic cells and is widely used to test hematopoietic stress response [245]. In this study, we compared the hematopoietic recovery for both irradiation-, as well as 5-FU-induced hematopoietic stress responses in C57Bl/6J animals ordered from Charles River Laboratories International. We therefore provided a standardized model of blood recovery, by gathering results from 54 control mice from 7 independent experiments for the irradiation model and 46 mice from 5 independent experiments for the chemotherapeutic model. The control mice were either not-treated or treated with intraperitoneal injections of phosphate buffer saline (PBS) or 10% dimethyl sulfoxide (DMSO) in PBS. Peripheral blood recovery curves for lymphocytes, monocytes, granulocytes ($t_{1/2}$ = 1-5 days[251]), red blood cells ($t_{1/2}$ = 23 days[252]), platelets ($t_{1/2}$ = 4-5 days [253]), haemoglobin and haematocrit were recorded, using a standard veterinarian blood counter (Scil vet abc™). Our findings highlight the differing hematopoietic stress responses between irradiation- and 5-FU-induced aplasia, as seen by a fast recovery of white blood cells and platelets following 5-FU-treatment. Red blood cell recovery was however similar in both cases.

A.2 Methods

A.2.1 Mice

C57Bl/6J 8- to 10-week old females were purchased from Charles River Laboratories International and kept at the housing facility (CONV) at the EPFL in isolated cages. Mice were fed with sterile food and water and were given sterile bedding. All the animals were left for acclimatisation for at least one week prior to experiments. All *in vivo* experiments were conducted in accordance with the Swiss law after approval by the local authorities (Service Vétérinaire de l'Etat de Vaud). Only mice in control groups were included in this study, whereas some received either PBS only (Gibco, ref: 10010015) or PBS, 10 % DMSO (Fisher Scientific, ref: BP231-100) via daily intraperitoneal injections alternating sides every day.

A.2.2 Murine bone marrow transplantation and irradiation

C57Bl/6J mice were lethally irradiated with 850 cGy split in two equal doses separated by four hours with an X-ray source (117cGy/min, Rad Source RS-2000) 24 h before transplantation. Tail vein transplantation was performed with 125×10^3 or 150×10^3 total bone marrow cells isolated from MHC-compatible donors as described in the previous chapters. An antibiotics mixture consisting of 30 mg of Enrofloxacin (300 μ L of Baytril 10% ad us. vet, 100 mg/mL, Bayer) and 5 mg of Amoxicillin (100 μ L of Amoxi-Mepha 200mg/4mL, Mepha Pharma AG) as well as 500 mg of Paracetamol (Dafalgan®) in a total of 250 mL sterile water was given for two weeks post-irradiation. The mixture was replaced once every 7 days. All mice responded to irradiation.

A.2.3 5-fluorouracil treatment

5-Fluorouracil (1000mg/20mL, Sandoz) diluted in PBS (diluted 1:1) was injected once intraperitoneally at a concentration of 250 mg/kg body weight, as previously described [254]. The above described antibiotic-paracetamol mixture (Enrofloxacin, Amoxicillin, Paracetamol) was given in 250 mL sterile water from day eight post treatment until day twenty post treatment. The mixture was replaced once every 7 days. Only mice responding to 5-FU treatment (81%), as defined by RBC count below the Charles river standards at nadir (day 10), were considered in this study [255].

A.2.4 Blood collection and analysis

Peripheral blood was collected in EDTA-coated tubes (Sartstedt, ref: 20.1278) by tail vein bleeding once or twice a week (collected blood volume per bleed: approx. 50 μ L). The blood was analysed by a standard veterinarian blood counter (Horiba, model Scil vet abc™, serial number 310AB13907).

A.3 Results

Hereafter, we describe the peripheral blood recovery curves, for both irradiation-induced-, as well as 5-FU-induced hematopoietic aplasia in C57Bl/6J mice. Of note, at homeostasis (day 0), the blood parameters exhibited the expected values, as compared to Charles River standards (Table 1). The kinetics of recovery of white blood cells (lymphocytes, monocytes and granulocytes combined) differed greatly when mice were irradiated or treated with 5-FU. Within 5-FU-treated mice, the nadir occurred on day 10 after treatment, whereas within irradiated and transplanted mice, the lowest count of white blood cells was earlier, on day 8. The number of white blood cells at nadir with 5-FU-treatment was higher than with irradiation, with $3.66 \pm 0.20 \times 10^3$ and $0.35 \pm 0.02 \times 10^3$ cells/mm³, respectively. Interestingly, both stress methods showed a peak of white blood cell count before going back to baseline values. It was earlier and more intense with 5-FU (on day 17 with $20.88 \pm 0.37 \times 10^3$ cells/mm³) than with irradiation (on day 60 with $13.29 \pm 0.72 \times 10^3$ cells/mm³). Return to baseline value of white blood cell counts occurred after day 23 for 5-FU treated mice, and after day 63 for irradiated mice.

Lymphocytes, which include natural killers, B-cells and T-cells are the main contributors to the total white blood cell count (approx. 80%), which translated into a similar to the recovery curve of white blood cells. Indeed, in 5-FU-treated mice, the lowest lymphocyte count was on day 10 after treatment, whereas within irradiated mice it was on day 8. The number of lymphocytes at nadir with 5-FU-treated mice was higher than within irradiated and transplanted mice, with respectively $3.43 \pm 0.12 \times 10^3$ versus $0.01 \pm 0.01 \times 10^3$ cells/mm³. An early and intense peak in lymphocyte count was observed within 5-FU-treated mice (on day 17 with $15.94 \pm 0.29 \times 10^3$

cells/mm³), with irradiated mice reaching $10.43 \pm 0.54 \times 10^3$ cells/mm³ on day 60 post-transplant. The recovery of lymphocytes to baseline counts occurred after day 23 for 5-FU-treated mice and after day 63 for irradiated mice.

Monocytes are part of the myeloid lineage and can give rise to macrophages and dendritic cells. The kinetics of monocytes recovery were therefore similar to the recovery kinetics of white blood cells and lymphocytes, i.e. a drop of the cell blood counts, followed by a faster recovery in 5-FU- over irradiation-treated mice. A high peak of monocyte counts also occurred in the 5-FU experiments before return baseline counts. The counts of circulating monocytes at nadir in 5-FU reached zero on day 6 and slowly recovered until day 11 ($0.05 \pm 0.01 \times 10^3$ cells/mm³), after which the counts increased fast and peaked at $0.77 \pm 0.02 \times 10^3$ cells/mm³ on day 17. In irradiated mice, the monocytes count reached 0 cells/mm³ on day 7 and stayed low until day 17, from where it slowly increased to reach a peak on day 60 ($0.47 \pm 0.03 \times 10^3$ cells/mm³). Then it decreased to baseline counts and stabilized from day 63 onward.

Granulocytes derive from the myeloid lineage and comprise neutrophils, eosinophils and basophils. The counts of circulating granulocytes at nadir following 5-FU-treatment reached $0.29 \pm 0.02 \times 10^3$ cells/mm³ on day 6 and slowly recovered until day 11 ($0.60 \pm 0.02 \times 10^3$ cells/mm³), after which the counts increased fast and peaked at $3.63 \pm 0.03 \times 10^3$ cells/mm³ on day 17. It then reached baseline counts back on day 28. For irradiated mice, the number of monocytes decreased to 0 cells/mm³ from day 7 until day 17, whereas it slowly increased to reach a peak on day 60 ($2.39 \pm 0.16 \times 10^3$ cells/mm³). Then it decreased to baseline counts and stabilized from day 63 onward.

The kinetics of red blood cells recovery was similar in both methods. Indeed, in both cases, nadir occurred on day 12 post treatment/irradiation, whereas circulating RBCs decreased to $4.41 \pm 0.16 \times 10^3$ cells/mm³ with 5-FU treatment and $3.31 \pm 0.25 \times 10^3$ cells/mm³ with irradiation. The recovery was substantially faster in 5-FU-treated mice, reaching $8.96 \pm 0.09 \times 10^3$ cells/mm³ on day 20. Whereas within irradiated and transplanted mice, the baseline-counts returned on day 28 post-transplant, with a value of $8.01 \pm 0.22 \times 10^3$ cells/mm³. Both haemoglobin and haematocrit recovery curves were similar to the RBCs recovery curves, given that haemoglobin is mainly present in RBCs and haematocrit is defined as the volume of RBCs over the total volume of blood.

Within 5-FU-treated mice, the number of platelets decreased to nadir on day 6 ($622 \pm 16 \times 10^3$ cells/mm³). Following, the number of platelets increased drastically and plateaued from day 12 to day 22 at values between $3917 \pm 311 \times 10^3$ cells/mm³ and $4998 \pm 281 \times 10^3$ cells/mm³, respectively. On day 23, the platelet count reached $1847 \pm 158 \times 10^3$ cells/mm³, until day 28 ($1877 \pm 55 \times 10^3$ cells/mm³) after which, surprisingly, increased again to reach $2842 \pm 89 \times 10^3$ cells/mm³ on day 35. In irradiation-treated mice, the level of platelets decreased dramatically to reach $104 \pm 8 \times 10^3$ cells/mm³ on day 7, recovering slowly to reach $1132 \pm 21 \times 10^3$ cells/mm³ on day 50.

A.4 Discussion

In this study, the data of 100 mice from 12 independent experiments was pooled in an effort to standardize blood recovery curves following haematopoietic stress in C57Bl/6J ordered from Charles River. Blood parameters were analysed with a Horiba Scil Vet abc machine using electrical resistance for counting and sizing (WBC, RBC, PLT) and spectrophotometry for Haemoglobin measurements. Many parameters, including strain, diet, housing of the mice as well as instrumentation for blood analysis influence on the hematologic results. We consider cytopenic, values that are two standard deviation lower than the mean of our baseline data set (Table 1). Two methods for aplasia were compared: lethal irradiation followed by transplantation and 5-Fluorouracil sublethal treatment via intraperitoneal injection. In the irradiation model, hematopoietic stress was mostly fuelled by the donor cells, which were replenishing the hematopoietic system of aplastic mice, characterized by a slow recovery curve. 5-FU-treatment on the other hand is sublethal, as the cytotoxicity it induces on hematopoietic stem and progenitor cells is not as strong as irradiation. The 5-FU induced aplasia was followed by an inflammatory response, described by the characteristic peak in white blood cell and platelet expansion [245]. All analysed white blood cells (granulocytes, lymphocytes and monocytes) followed this trend. Monocytes dropped to undetectable levels in both aplasia-inducing methods. Platelets, were depleted in both methods, though never entering thrombocytopenia ($< 200 \times 10^3$ cells/mm³) using 5-FU-treatment. The prolonged increase in platelets has previously been shown to result from a failure to downregulate megakaryocyte concentration [256]. Red blood cells however, did not react to the inflammatory response like the other cells. Red blood cell counts drop to the same level as in the irradiation-induced model and recover in a similar fashion. Altogether, these data present a standardized model of blood recovery post-aplasia in C57Bl/6J mice ordered from Charles River treated with 5-FU or lethally irradiated and transplanted, therefore allowing for a reduction in the use of animals in future studies [238]. Our results suggest that irradiation is a more suited model to study hematopoietic regeneration, since 5-FU-treatment exerted confounding inflammatory effects. Given that the regenerating donor cells are not chemically damaged in the irradiation model, suggests the kinetics of hematopoietic recovery to be mainly based on HSC self-renewal and HPC proliferation. In addition, the slow nature of the irradiation-induced hematopoietic recovery allows for more readily detection of slight improvements in hematopoietic regeneration.

A.5 Figures

Parameter	Unit	Parameter values on day 0		Charles River values	
		Mean	SD	Mean	SD
Total white blood cells	10 ³ /mm ³	8.73	2.07	8.69	2.44
Lymphocytes	10 ³ /mm ³	7.20	1.89	6.92	1.92
Monocytes	10 ³ /mm ³	0.23	0.08	0.37	0.15
Granulocytes	10 ³ /mm ³	1.49	0.94	1.41**	0.53
Red blood cells	10 ⁶ /mm ³	10.44	0.62	9.17	1.05
Platelets	10 ³ /mm ³	1512	330	1167	307
Haemoglobin	g/dL	16.53	0.86	13.72	1.59
Haematocrit	%	54.90	3.30	45.32	6.27

Table 1 Values of the different parameters measured on day 0 with standard error of the mean. Taken from the Charles River standards [255]. **eosinophils, basophils, and neutrophils combined.

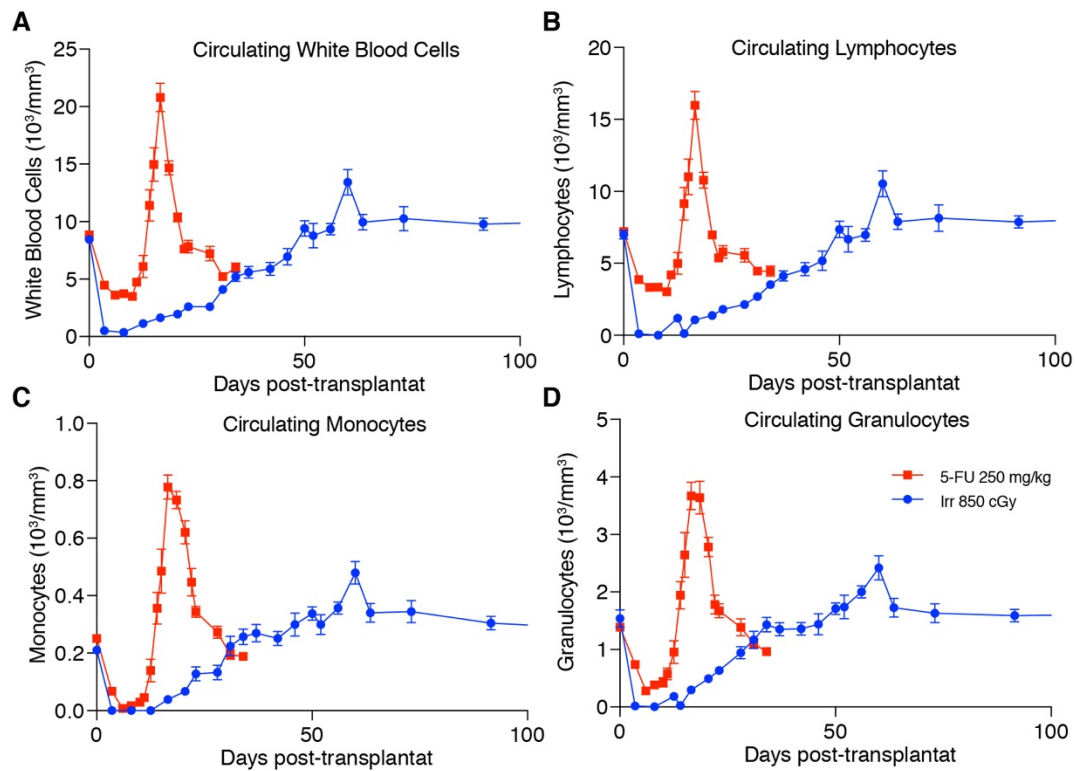


Figure A 1 Blood recovery of white blood cells following 5-FU treatment or irradiation. In red: recovery after 5-FU treatment n=46. In blue: Recovery after irradiation n=54. Recovery of A, total white blood cells. B, circulating lymphocytes. C, circulating monocytes. D, circulating granulocytes. Error bars are S.E.M.

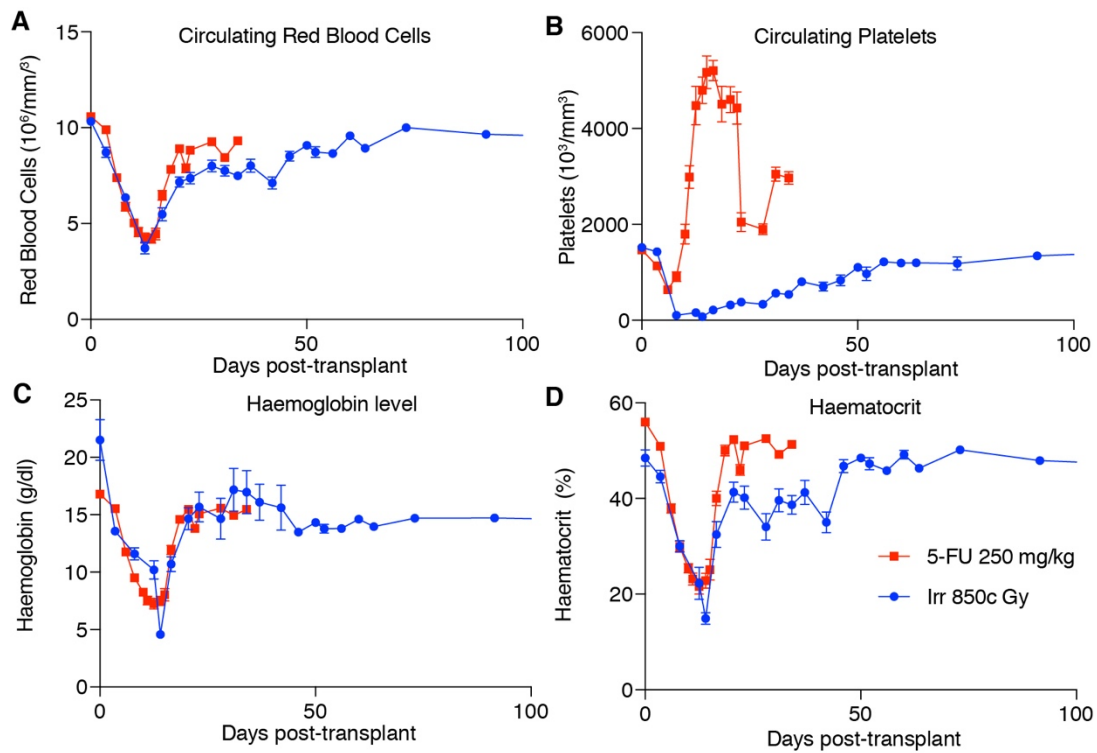


Figure A 2 Blood recovery of red blood cells, platelets, haemoglobin and haematocrit following 5-FU treatment or irradiation. In red: recovery after 5-FU treatment n=46. In blue: Recovery after irradiation n=54. Recovery of **A**, circulating red blood cells. **B**, circulating platelets. **C**, haemoglobin levels. **D**, haematocrit. Error bars are S.E.M.

References

- [1] D. Bryder, D. J. Rossi, and I. L. Weissman, "Hematopoietic Stem Cells," *Am. J. Pathol.*, vol. 169, no. 2, pp. 338–346, Aug. 2006.
- [2] J. R. Passweg *et al.*, "Impact of drug development on the use of stem cell transplantation: a report by the European Society for Blood and Marrow Transplantation (EBMT).," *Bone Marrow Transplant.*, vol. 52, no. 2, pp. 191–196, Feb. 2017.
- [3] E. A. Copelan, "Hematopoietic Stem-Cell Transplantation," *N. Engl. J. Med.*, vol. 354, no. 17, pp. 1813–1826, Apr. 2006.
- [4] R. K. Burt *et al.*, "Clinical Applications of Blood-Derived and Marrow-Derived Stem Cells for Nonmalignant Diseases," *JAMA*, vol. 299, no. 8, p. 925, Feb. 2008.
- [5] A. Tyndall *et al.*, "Autologous haematopoietic stem cell transplants for autoimmune disease – feasibility and transplant-related mortality," *Bone Marrow Transplant.*, vol. 24, no. 7, pp. 729–734, Oct. 1999.
- [6] B. Park, K. H. Yoo, and C. Kim, "Hematopoietic stem cell expansion and generation: the ways to make a breakthrough.," *Blood Res.*, vol. 50, no. 4, pp. 194–203, Dec. 2015.
- [7] D. Bhattacharya, L. I. R. Ehrlich, and I. L. Weissman, "Space-time considerations for hematopoietic stem cell transplantation," *Eur. J. Immunol.*, vol. 38, no. 8, pp. 2060–2067, Aug. 2008.
- [8] T. A. Gooley *et al.*, "Reduced Mortality after Allogeneic Hematopoietic-Cell Transplantation," *N. Engl. J. Med.*, vol. 363, no. 22, pp. 2091–2101, Nov. 2010.
- [9] C. Gisselbrecht *et al.*, "Placebo-controlled phase III trial of lenograstim in bone-marrow transplantation," *Lancet*, vol. 343, no. 8899, pp. 696–700, Mar. 1994.
- [10] D. C. Linch *et al.*, "Randomised vehicle-controlled dose-finding study of glycosylated recombinant human granulocyte colony-stimulating factor after bone marrow transplantation.," *Bone Marrow Transplant.*, vol. 11, no. 4, pp. 307–11, Apr. 1993.
- [11] R. C. Barfield, K. A. Kasow, and G. A. Hale, "Advances in pediatric hematopoietic stem cell transplantation.," *Cancer Biol. Ther.*, vol. 7, no. 10, pp. 1533–9, Oct. 2008.
- [12] C. S. Potten and M. Loeffler, "Stem cells: attributes, cycles, spirals, pitfalls and uncertainties. Lessons for and from the crypt," *Development*, vol. 110, no. 4, 1990.
- [13] M. Osawa, K. Hanada, H. Hamada, and H. Nakauchi, "Long-term lymphohematopoietic reconstitution by a single CD34-low/negative hematopoietic stem cell.," *Science*, vol. 273, no. 5272, pp. 242–5, Jul. 1996.
- [14] H. Holstege *et al.*, "Somatic mutations found in the healthy blood compartment of a 115-yr-old woman demonstrate oligoclonal hematopoiesis.," *Genome Res.*, vol. 24, no. 5, pp. 733–42, May 2014.
- [15] C. C. Hofmeister, J. Zhang, K. L. Knight, P. Le, and P. J. Stiff, "Ex vivo expansion of umbilical cord blood stem cells for transplantation: growing knowledge from the hematopoietic niche," *Bone Marrow Transplant.*, vol. 39, no. 1, pp. 11–23, Jan. 2007.
- [16] J. E. Wagner *et al.*, "Transplantation of unrelated donor umbilical cord blood in 102 patients with malignant and nonmalignant diseases: influence of CD34 cell dose and HLA disparity on treatment-related mortality and survival.," *Blood*, vol. 100, no. 5, pp. 1611–8, Sep. 2002.
- [17] K. K. Ballen, E. Gluckman, and H. E. Broxmeyer, "Umbilical cord blood transplantation: the first 25 years and beyond," *Blood*, vol. 122, no. 4, pp. 491–498, Jul. 2013.
- [18] C. C. Zhang *et al.*, "Angiopoietin-like proteins stimulate ex vivo expansion of hematopoietic stem cells," *Nat. Med.*, vol. 12, no. 2, pp. 240–245, Feb. 2006.
- [19] A. E. Boitano *et al.*, "Aryl Hydrocarbon Receptor Antagonists Promote the Expansion of Human Hematopoietic Stem Cells," *Science (80-.)*, vol. 329, no. 5997, pp. 1345–1348, Sep. 2010.
- [20] I. Fares *et al.*, "Pyrimidoindole derivatives are agonists of human hematopoietic stem cell self-renewal," *Science (80-.)*, vol. 345, no. 6203, pp. 1509–1512, Sep. 2014.
- [21] L. Shahriyari and N. L. Komarova, "Symmetric vs. Asymmetric Stem Cell Divisions: An Adaptation against Cancer?," *PLoS One*,

vol. 8, no. 10, p. e76195, Oct. 2013.

- [22] K. Ito and K. Ito, "Metabolism and the Control of Cell Fate Decisions and Stem Cell Renewal," *Annu. Rev. Cell Dev. Biol.*, vol. 32, pp. 399–409, 2016.
- [23] L. E. Purton and D. T. Scadden, "Limiting factors in murine hematopoietic stem cell assays," *Cell Stem Cell*, vol. 1, no. 3, pp. 263–70, Sep. 2007.
- [24] T. Suda, K. Takubo, and G. L. Semenza, "Metabolic Regulation of Hematopoietic Stem Cells in the Hypoxic Niche," *Cell Stem Cell*, vol. 9, no. 4, pp. 298–310, Oct. 2011.
- [25] K. Takubo *et al.*, "Regulation of Glycolysis by Pdk Functions as a Metabolic Checkpoint for Cell Cycle Quiescence in Hematopoietic Stem Cells," *Cell Stem Cell*, vol. 12, no. 1, pp. 49–61, Jan. 2013.
- [26] K. Ito and T. Suda, "Metabolic requirements for the maintenance of self-renewing stem cells," *Nat. Rev. Mol. Cell Biol.*, vol. 15, no. 4, pp. 243–56, Apr. 2014.
- [27] W.-M. Yu *et al.*, "Metabolic Regulation by the Mitochondrial Phosphatase PTPMT1 Is Required for Hematopoietic Stem Cell Differentiation," *Cell Stem Cell*, vol. 12, no. 1, pp. 62–74, Jan. 2013.
- [28] C. Chen *et al.*, "TSC–mTOR maintains quiescence and function of hematopoietic stem cells by repressing mitochondrial biogenesis and reactive oxygen species," *J. Exp. Med.*, vol. 205, no. 10, pp. 2397–2408, Sep. 2008.
- [29] Z. Tothova *et al.*, "FoxOs Are Critical Mediators of Hematopoietic Stem Cell Resistance to Physiologic Oxidative Stress," *Cell*, vol. 128, no. 2, pp. 325–339, Jan. 2007.
- [30] K. Ito *et al.*, "Reactive oxygen species act through p38 MAPK to limit the lifespan of hematopoietic stem cells," *Nat. Med.*, vol. 12, no. 4, pp. 446–451, Apr. 2006.
- [31] K. Ito *et al.*, "Regulation of oxidative stress by ATM is required for self-renewal of haematopoietic stem cells," *Nature*, vol. 431, no. 7011, pp. 997–1002, Oct. 2004.
- [32] C. R. Mantel *et al.*, "Enhancing Hematopoietic Stem Cell Transplantation Efficacy by Mitigating Oxygen Shock," *Cell*, vol. 161, no. 7, pp. 1553–1565, Jun. 2015.
- [33] N. Vannini *et al.*, "Specification of haematopoietic stem cell fate via modulation of mitochondrial activity," *Nat. Commun.*, vol. 7, no. 1, p. 13125, Dec. 2016.
- [34] D. Nakada, T. L. Saunders, and S. J. Morrison, "Lkb1 regulates cell cycle and energy metabolism in haematopoietic stem cells," *Nature*, vol. 468, no. 7324, pp. 653–658, Dec. 2010.
- [35] S. Gurumurthy *et al.*, "The Lkb1 metabolic sensor maintains haematopoietic stem cell survival," *Nature*, vol. 468, no. 7324, pp. 659–663, Dec. 2010.
- [36] B. Gan *et al.*, "Lkb1 regulates quiescence and metabolic homeostasis of haematopoietic stem cells," *Nature*, vol. 468, no. 7324, pp. 701–704, Dec. 2010.
- [37] C. Nombela-Arrieta *et al.*, "Quantitative imaging of haematopoietic stem and progenitor cell localization and hypoxic status in the bone marrow microenvironment," *Nat. Cell Biol.*, vol. 15, no. 5, pp. 533–543, May 2013.
- [38] M. Mortensen *et al.*, "The autophagy protein Atg7 is essential for hematopoietic stem cell maintenance," *J. Exp. Med.*, vol. 208, no. 3, pp. 455–467, Mar. 2011.
- [39] M. R. Warr *et al.*, "FOXO3A directs a protective autophagy program in haematopoietic stem cells," *Nature*, vol. 494, no. 7437, pp. 323–327, Feb. 2013.
- [40] M. Mohrin *et al.*, "A mitochondrial UPR-mediated metabolic checkpoint regulates hematopoietic stem cell aging," *Science (80-.)*, vol. 347, no. 6228, pp. 1374–1377, Mar. 2015.
- [41] K. Parmar, P. Mauch, J.-A. Vergilio, R. Sackstein, and J. D. Down, "Distribution of hematopoietic stem cells in the bone marrow according to regional hypoxia," *Proc. Natl. Acad. Sci.*, vol. 104, no. 13, pp. 5431–5436, Mar. 2007.
- [42] T. Simsek *et al.*, "The Distinct Metabolic Profile of Hematopoietic Stem Cells Reflects Their Location in a Hypoxic Niche," *Cell Stem Cell*, vol. 7, no. 3, pp. 380–390, Sep. 2010.

- [43] R. Schofield, "The relationship between the spleen colony-forming cell and the haematopoietic stem cell.," *Blood Cells*, vol. 4, no. 1–2, pp. 7–25, 1978.
- [44] K. A. Moore and I. R. Lemischka, "Stem Cells and Their Niches," *Science (80-.)*, vol. 311, no. 5769, pp. 1880–1885, Mar. 2006.
- [45] D. T. Scadden, "The stem-cell niche as an entity of action," *Nature*, vol. 441, no. 7097, pp. 1075–1079, Jun. 2006.
- [46] A. Wilson and A. Trumpp, "Bone-marrow haematopoietic-stem-cell niches," *Nat. Rev. Immunol.*, vol. 6, no. 2, pp. 93–106, Feb. 2006.
- [47] P. Bianco, "Bone and the hematopoietic niche: A tale of two stem cells," *Blood*, vol. 117, no. 20, pp. 5281–5288, May 2011.
- [48] J. Zhang *et al.*, "Identification of the haematopoietic stem cell niche and control of the niche size," *Nature*, vol. 425, no. 6960, pp. 836–841, Oct. 2003.
- [49] L. M. Calvi *et al.*, "Osteoblastic cells regulate the haematopoietic stem cell niche," pp. 841–846, 2003.
- [50] B. Guezguez *et al.*, "Regional Localization within the Bone Marrow Influences the Functional Capacity of Human HSCs," *Cell Stem Cell*, vol. 13, no. 2, pp. 175–189, Aug. 2013.
- [51] F. Arai *et al.*, "Tie2/Angiopoietin-1 Signaling Regulates Hematopoietic Stem Cell Quiescence in the Bone Marrow Niche," *Cell*, vol. 118, no. 2, pp. 149–161, Jul. 2004.
- [52] L. Ding, T. L. Saunders, G. Enikolopov, and S. J. Morrison, "Endothelial and perivascular cells maintain haematopoietic stem cells," *Nature*, vol. 481, no. 7382, pp. 457–462, Jan. 2012.
- [53] L. Ding and S. J. Morrison, "Haematopoietic stem cells and early lymphoid progenitors occupy distinct bone marrow niches," *Nature*, vol. 495, no. 7440, pp. 231–235, Mar. 2013.
- [54] S. Méndez-Ferrer *et al.*, "Mesenchymal and haematopoietic stem cells form a unique bone marrow niche.-supplement," *Nature*, vol. 466, no. 7308, pp. 829–834, Aug. 2010.
- [55] S. Lympéri, F. Ferraro, and D. T. Scadden, "The HSC niche concept has turned 31 Has our knowledge matured ?," vol. 1192, pp. 12–18, 2010.
- [56] S. Kumar and H. Geiger, "HSC Niche Biology and HSC Expansion Ex Vivo.," *Trends Mol. Med.*, vol. 23, no. 9, pp. 799–819, Sep. 2017.
- [57] M. E. Nuttall, A. J. Patton, D. L. Olivera, D. P. Nadeau, and M. Gowen, "Human Trabecular Bone Cells Are Able to Express Both Osteoblastic and Adipocytic Phenotype: Implications for Osteopenic Disorders," *J. Bone Miner. Res.*, vol. 13, no. 3, pp. 371–382, Mar. 1998.
- [58] M. F. Pittenger *et al.*, "Multilineage potential of adult human mesenchymal stem cells.," *Science*, vol. 284, no. 5411, pp. 143–7, Apr. 1999.
- [59] Y. Nakamura *et al.*, "Isolation and characterization of endosteal niche cell populations that regulate hematopoietic stem cells," *Blood*, vol. 116, no. 9, pp. 1422–1432, Sep. 2010.
- [60] P. Bianco, "'Mesenchymal' Stem Cells," *Annu. Rev. Cell Dev. Biol.*, vol. 30, no. 1, pp. 677–704, Oct. 2014.
- [61] B. O. Zhou *et al.*, "Bone marrow adipocytes promote the regeneration of stem cells and haematopoiesis by secreting SCF," *Nat. Cell Biol.*, vol. 19, no. 8, 2017.
- [62] O. Naveiras, V. Nardi, P. L. Wenzel, P. V Hauschka, F. Fahey, and G. Q. Daley, "Bone-marrow adipocytes as negative regulators of the haematopoietic microenvironment.," *Nature*, vol. 460, no. 7252, pp. 259–263, Jul. 2009.
- [63] Z. Belaid-Choucair *et al.*, "Human Bone Marrow Adipocytes Block Granulopoiesis Through Neuropilin-1-Induced Granulocyte Colony-Stimulating Factor Inhibition," *Stem Cells*, vol. 26, no. 6, pp. 1556–1564, Jun. 2008.
- [64] T. H. Ambrosi *et al.*, "Adipocyte Accumulation in the Bone Marrow during Obesity and Aging Impairs Stem Cell-Based Hematopoietic and Bone Regeneration," *Cell Stem Cell*, vol. 20, no. 6, pp. 1–14, Jun. 2017.
- [65] E. D. Rosen and B. M. Spiegelman, "What We Talk About When We Talk About Fat," *Cell*, vol. 156, no. 1–2, pp. 20–44, Jan. 2014.

- [66] J. M. Gimble, S. Zvonic, Z. E. Floyd, M. Kassem, and M. E. Nuttall, "Playing With Bone and Fat," *J. Cell. Biochem.*, 2006.
- [67] P. Hardouin, T. Rharass, and S. Lucas, "Bone Marrow Adipose Tissue: To Be or Not To Be a Typical Adipose Tissue?," *Front. Endocrinol. (Lausanne)*, vol. 7, p. 85, Jun. 2016.
- [68] K. J. Suchacki and W. P. Cawthorn, "Molecular Interaction of Bone Marrow Adipose Tissue with Energy Metabolism," *Curr. Mol. Biol. Reports*, vol. 4, no. 2, pp. 41–49, Jun. 2018.
- [69] M. Tavassoli, "Marrow adipose cells. Histochemical identification of labile and stable components.," *Arch. Pathol. Lab.*, 1976.
- [70] M. Tavassoli, A. Maniatis, W. C.- Blood, and undefined 1974, "Induction of sustained hemopoiesis in fatty marrow," *Am Soc Hematol.*
- [71] E. L. Scheller *et al.*, "Region-specific variation in the properties of skeletal adipocytes reveals regulated and constitutive marrow adipose tissues," *Nat. Commun.*, vol. 6, no. 1, p. 7808, Dec. 2015.
- [72] Y. Sera *et al.*, "Hematopoietic stem cell origin of adipocytes," *Exp. Hematol.*, vol. 37, no. 9, p. 1108–1120.e4, Sep. 2009.
- [73] S. M. Majka *et al.*, "De novo generation of white adipocytes from the myeloid lineage via mesenchymal intermediates is age, adipose depot, and gender specific," *Proc. Natl. Acad. Sci.*, vol. 107, no. 33, pp. 14781–14786, Aug. 2010.
- [74] P. Bianco, P. G. Robey, and P. J. Simmons, "Mesenchymal stem cells: revisiting history, concepts, and assays.," *Cell Stem Cell*, vol. 2, no. 4, pp. 313–9, Apr. 2008.
- [75] D. D. Houlihan *et al.*, "Isolation of mouse mesenchymal stem cells on the basis of expression of Sca-1 and PDGFR- α ," *Nat. Protoc.*, vol. 7, no. 12, pp. 2103–2111, Nov. 2012.
- [76] D. L. Worthley *et al.*, "Gremlin 1 identifies a skeletal stem cell with bone, cartilage, and reticular stromal potential.," *Cell*, vol. 160, no. 1–2, pp. 269–84, Jan. 2015.
- [77] T. Sugiyama, H. Kohara, M. Noda, and T. Nagasawa, "Maintenance of the Hematopoietic Stem Cell Pool by CXCL12-CXCR4 Chemokine Signaling in Bone Marrow Stromal Cell Niches," *Immunity*, vol. 25, no. 6, pp. 977–988, Dec. 2006.
- [78] B. Sacchetti *et al.*, "Self-Renewing Osteoprogenitors in Bone Marrow Sinusoids Can Organize a Hematopoietic Microenvironment," *Cell*, vol. 131, no. 2, pp. 324–336, Oct. 2007.
- [79] H. Li *et al.*, "Low/Negative Expression of PDGFR- α Identifies the Candidate Primary Mesenchymal Stromal Cells in Adult Human Bone Marrow," *Stem Cell Reports*, vol. 3, no. 6, pp. 965–974, Dec. 2014.
- [80] T. Shimozato and P. W. Kincade, "Prostaglandin E2 and Stem Cell Factor Can Deliver Opposing Signals to B Lymphocyte Precursors," *Cell. Immunol.*, vol. 198, no. 1, pp. 21–29, Nov. 1999.
- [81] P. A. Bryon, O. Gentilhomme, and D. Fiere, "[Histomorphometric analysis of bone-marrow adipose density and heterogeneity in myeloid aplasia and dysplasia (author's transl).," *Pathol. Biol. (Paris)*, vol. 27, no. 4, pp. 209–13, Apr. 1979.
- [82] A. Wilson *et al.*, "Lack of Adipocytes Alters Hematopoiesis in Lipodystrophic Mice," *Front. Immunol.*, vol. 9, p. 2573, Nov. 2018.
- [83] T.-A. Cock *et al.*, "Enhanced bone formation in lipodystrophic PPAR γ hyp/hyp mice relocates haematopoiesis to the spleen," *EMBO Rep.*, vol. 5, no. 10, pp. 1007–1012, Oct. 2004.
- [84] L. DiMascio *et al.*, "Identification of Adiponectin as a Novel Hemopoietic Stem Cell Growth Factor," *J. Immunol.*, vol. 178, no. 6, pp. 3511–3520, Mar. 2007.
- [85] D. Mattiucci *et al.*, "Bone marrow adipocytes support hematopoietic stem cell survival," *J. Cell. Physiol.*, vol. 233, no. 2, pp. 1500–1511, Feb. 2018.
- [86] T. J. Spindler, A. W. Tseng, X. Zhou, and G. B. Adams, "Adipocytic cells augment the support of primitive hematopoietic cells in vitro but have no effect in the bone marrow niche under homeostatic conditions.," *Stem Cells Dev.*, vol. 23, no. 4, pp. 434–41, Feb. 2014.
- [87] I. Oh *et al.*, "Screening of genes responsible for differentiation of mouse mesenchymal stromal cells by DNA micro-array analysis of C3H10T1/2 and C3H10T1/2-derived cell lines," *Cytotherapy*, vol. 9, no. 1, pp. 80–90, Jan. 2007.
- [88] Q. a Wang, C. Tao, R. K. Gupta, and P. E. Scherer, "Tracking adipogenesis during white adipose tissue development, expansion

and regeneration,” *Nat. Med.*, vol. 19, no. 10, pp. 1338–44, 2013.

- [89] E. Neumann, “Das Gesetz der Verbreitung des gelben und roten Markes in den Extremitätenknochen,” *Zentbl. Med. Wiss.*, vol. 18, pp. 321–323, 1882.
- [90] M. A. Bredella *et al.*, “Increased bone marrow fat in anorexia nervosa,” *J. Clin. Endocrinol. Metab.*, vol. 94, no. 6, pp. 2129–36, Jun. 2009.
- [91] M. J. Devlin *et al.*, “Caloric restriction leads to high marrow adiposity and low bone mass in growing mice,” *J. Bone Miner. Res.*, vol. 25, no. 9, pp. 2078–2088, Sep. 2010.
- [92] E. W. Yu, L. Greenblatt, A. Ejazi, M. Torriani, and M. A. Bredella, “Marrow adipose tissue composition in adults with morbid obesity,” *Bone*, vol. 97, pp. 38–42, Apr. 2017.
- [93] N. Y. Yu *et al.*, “Bone marrow fat content is correlated with hepatic fat content in paediatric non-alcoholic fatty liver disease,” *Clin. Radiol.*, vol. 72, no. 5, p. 425.e9–425.e14, May 2017.
- [94] C. M. Bastos, I. M. Araújo, M. H. Nogueira-Barbosa, C. E. G. Salmon, F. J. A. de Paula, and L. E. A. Troncon, “Reduced bone mass and preserved marrow adipose tissue in patients with inflammatory bowel diseases in long-term remission,” *Osteoporos. Int.*, vol. 28, no. 7, pp. 2167–2176, Jul. 2017.
- [95] G. R. Beck *et al.*, “The effects of thiazolidinediones on human bone marrow stromal cell differentiation in vitro and in thiazolidinedione-treated patients with type 2 diabetes,” *Transl. Res.*, vol. 161, no. 3, pp. 145–55, Mar. 2013.
- [96] J. Li *et al.*, “Dexamethasone shifts bone marrow stromal cells from osteoblasts to adipocytes by C/EBPalpha promoter methylation,” *Cell Death Dis.*, vol. 4, no. 10, pp. e832–e832, Oct. 2013.
- [97] M. E. Nuttall and J. M. Gimble, “Is there a therapeutic opportunity to either prevent or treat osteopenic disorders by inhibiting marrow adipogenesis?,” *Bone*, vol. 27, no. 2, pp. 177–84, Aug. 2000.
- [98] J. Justesen, S. B. Pedersen, K. Stenderup, and M. Kassem, “Subcutaneous Adipocytes Can Differentiate into Bone-Forming Cells *in Vitro* and *in Vivo*,” *Tissue Eng.*, vol. 10, no. 3–4, pp. 381–391, Mar. 2004.
- [99] T. Matsumoto *et al.*, “Mature adipocyte-derived dedifferentiated fat cells exhibit multilineage potential,” *J. Cell. Physiol.*, vol. 215, no. 1, pp. 210–222, Apr. 2008.
- [100] Q. A. Wang, A. Song, R. K. Gupta, B. Deplancke, and P. E. Scherer, “Reversible De-differentiation of Mature White Adipocytes into Preadipocyte-like Precursors during Lactation,” *Cell Metab.*, vol. 28, p. 282–288.e3, 2018.
- [101] E. L. Scheller and C. J. Rosen, “What’s the matter with MAT? Marrow adipose tissue, metabolism, and skeletal health,” *Ann. N. Y. Acad. Sci.*, vol. 1311, no. 1, pp. 14–30, Apr. 2014.
- [102] M. Pasquini and Z. Wang, “Current use and outcome of hematopoietic stem cell transplantation: CIBMTR Summary Slides, 2013. <http://www.cibmtr.org/ReferenceCenter/SlidesReports/SummarySlides/Documents/2013%20Summary%20Slides-%20Final%20Web%20Version%20%20V2%204.14.2014>,” 2013.
- [103] E. L. Scheller, W. P. Cawthorn, A. A. Burr, M. C. Horowitz, and O. A. MacDougald, “Marrow Adipose Tissue: Trimming the Fat,” *Trends Endocrinol. Metab.*, vol. 27, no. 6, pp. 392–403, 2016.
- [104] K. L. Spalding *et al.*, “Dynamics of fat cell turnover in humans,” *Nature*, vol. 453, no. 7196, pp. 783–787, Jun. 2008.
- [105] A. Rigamonti, K. Brennand, F. Lau, and C. A. Cowan, “Rapid Cellular Turnover in Adipose Tissue,” *PLoS One*, vol. 6, no. 3, p. e17637, Mar. 2011.
- [106] X. Fu, A. Zhao, and T. Hu, “Dedifferentiation and Adipose Tissue,” in *Cellular Dedifferentiation and Regenerative Medicine*, Berlin, Heidelberg: Springer Berlin Heidelberg, 2018, pp. 175–193.
- [107] S. Mostoufi-Moab *et al.*, “Adverse Fat Depots and Marrow Adiposity Are Associated With Skeletal Deficits and Insulin Resistance in Long-Term Survivors of Pediatric Hematopoietic Stem Cell Transplantation,” *J. Bone Miner. Res.*, vol. 30, no. 9, pp. 1657–1666, Sep. 2015.
- [108] C. Rozman, J. C. Reverter, E. Feliu, L. Berga, M. Rozman, and C. Climent, “Variations of fat tissue fraction in abnormal human bone marrow depend both on size and number of adipocytes: a stereologic study,” *Blood*, vol. 76, no. 5, pp. 892–5, Sep. 1990.

- [109] L. M. VAN PUTTEN and F. Croon, "The Life Span of Red Cells in the Rat and the Mouse as Determined by Labeling with DFP32 in Vivo," *Blood*, vol. 13, no. 8, 1958.
- [110] D. L. Coutu, K. D. Kokkalis, L. Kunz, and T. Schroeder, "Multicolor quantitative confocal imaging cytometry," *Nat. Methods*, vol. 15, no. 1, pp. 39–46, Nov. 2017.
- [111] R. Ye *et al.*, "Impact of tamoxifen on adipocyte lineage tracing: Inducer of adipogenesis and prolonged nuclear translocation of Cre recombinase," *Mol. Metab.*, vol. 4, no. 11, pp. 771–778, Nov. 2015.
- [112] T. Seime *et al.*, "Inducible cell labeling and lineage tracking during fracture repair," *Dev. Growth Differ.*, vol. 57, no. 1, pp. 10–23, Jan. 2015.
- [113] "The AdipoChaser mouse," vol. 3, no. 2, pp. 146–150, 2014.
- [114] Z. V. Wang, Y. Deng, Q. A. Wang, K. Sun, and P. E. Scherer, "Identification and Characterization of a Promoter Cassette Conferring Adipocyte-Specific Gene Expression," *Endocrinology*, vol. 151, no. 6, pp. 2933–2939, Jun. 2010.
- [115] B. O. Zhou, R. Yue, M. M. Murphy, J. G. Peyer, and S. J. Morrison, "Leptin-Receptor-Expressing Mesenchymal Stromal Cells Represent the Main Source of Bone Formed by Adult Bone Marrow," *Cell Stem Cell*, vol. 15, no. 2, pp. 154–168, Aug. 2014.
- [116] "WHO Obesity and Overweight Report 2016," <http://www.who.int/mediacentre/factsheets/fs311/en/>.
- [117] Y. Wang, M. A. Beydoun, L. Liang, B. Caballero, and S. K. Kumanyika, "Will All Americans Become Overweight or Obese? Estimating the Progression and Cost of the US Obesity Epidemic," *Obesity*, vol. 16, no. 10, pp. 2323–2330, 2008.
- [118] F. M. Gregoire, C. M. Smas, and H. S. Sul, "Understanding adipocyte differentiation," *Physiol. Rev.*, vol. 78, no. 3, pp. 783–809, 1998.
- [119] E. D. Rosen and O. MacDougald, "Adipocyte differentiation from the inside out," *Nat. Rev. Mol. Cell Biol.*, vol. 7, no. 12, pp. 885–96, 2006.
- [120] S. R. Farmer, "Transcriptional control of adipocyte formation," *Cell Metab.*, vol. 4, no. 4, pp. 263–273, 2006.
- [121] J. M. Lane, J. R. Doyle, J. P. Fortin, A. S. Kopin, and J. M. Ordovás, "Development of an OP9 derived cell line as a robust model to rapidly study adipocyte differentiation," *PLoS One*, vol. 9, no. 11, p. e112123, 2014.
- [122] J. Qin *et al.*, "A stem cell-based tool for small molecule screening in adipogenesis," *PLoS One*, vol. 5, no. 9, p. e13014, 2010.
- [123] J. F. Welter, K. J. Penick, and L. A. Solchaga, "Assessing adipogenic potential of mesenchymal stem cells: A rapid three-dimensional culture screening technique," *Stem Cells Int.*, vol. 2013, p. 806525, 2013.
- [124] G. Diaz, M. Melis, B. Batetta, F. Angius, and A. M. Falchi, "Hydrophobic characterization of intracellular lipids in situ by Nile Red red/yellow emission ratio," *Micron*, vol. 39, no. 7, pp. 819–824, 2008.
- [125] Y.-H. Lee, S.-Y. Chen, R. J. Wiesner, and Y.-F. Huang, "Simple flow cytometric method used to assess lipid accumulation in fat cells," *J. Lipid Res.*, vol. 45, no. 6, pp. 1162–1167, Jun. 2004.
- [126] M. Dragunow, R. Cameron, P. Narayan, and S. O'Carroll, "Image-Based High-Throughput Quantification of Cellular Fat Accumulation," *J. Biomol. Screen.*, vol. 12, no. 7, pp. 999–1005, 2007.
- [127] E. Gorjup, L. Peter, S. Wien, H. von Briesen, and D. Schmitt, "Automated microscopic quantification of adipogenic differentiation of human gland stem cells," *Ann. Anat.*, vol. 191, no. 1, pp. 13–22, 2009.
- [128] A. Aldridge, D. Kouroupis, S. Churchman, A. English, E. Ingham, and E. Jones, "Assay validation for the assessment of adipogenesis of multipotential stromal cells—a direct comparison of four different methods," *Cytotherapy*, vol. 15, no. 1, pp. 89–101, 2013.
- [129] R. L. B. W. C. Hyun, J. H. Davis, M. J. Fulwyler, and H. A. Pershadsingh, "Flow Cytometric Analysis of Mature Adipocytes," *Cytometry*, vol. 474, pp. 469–474, 1989.
- [130] P. Marquet *et al.*, "Digital holographic microscopy: a noninvasive contrast imaging technique allowing quantitative visualization of living cells with subwavelength axial accuracy," *Opt. Lett.*, vol. 30, no. 5, pp. 468–470, 2005.
- [131] B. Rappaz, P. Marquet, E. Cuhe, Y. Emery, C. Depeursinge, and P. Magistretti, "Measurement of the integral refractive index and dynamic cell morphometry of living cells with digital holographic microscopy," *Opt. Express*, vol. 13, no. 23, pp. 9361–

9373, 2005.

- [132] E. Cuche, P. Marquet, and C. Depeursinge, "Simultaneous amplitude-contrast and quantitative phase-contrast microscopy by numerical reconstruction of Fresnel off-axis holograms," *Appl. Opt.*, vol. 38, no. 34, pp. 6994–7001, 1999.
- [133] B. Rappaz, B. Breton, E. Shaffer, and G. Turcatti, "Digital Holographic Microscopy: A Quantitative Label-Free Microscopy Technique for Phenotypic Screening," *Comb. Chem. High Throughput Screen.*, vol. 17, no. 1, pp. 80–88, 2014.
- [134] T. Nakano, H. Kodama, and T. Honjo, "Generation of Lymphohematopoietic Cells from Embryonic Stem Cells in Culture," *Science*, vol. 265, no. 5175, pp. 1098–1101, 1994.
- [135] N. E. Wolins *et al.*, "OP9 mouse stromal cells rapidly differentiate into adipocytes: characterization of a useful new model of adipogenesis," *J. Lipid Res.*, vol. 47, no. 2, pp. 450–460, Feb. 2006.
- [136] F. J. Ruiz-Ojeda, A. I. Ruperez, C. Gomez-Llorente, A. Gil, and C. M. Aguilera, "Cell models and their application for studying adipogenic differentiation in relation to obesity: A review," *Int. J. Mol. Sci.*, vol. 17, no. 7, pp. 1–26, 2016.
- [137] R. Kong and D. J. Klemm, "Analysis and Isolation of Adipocytes by Flow Cytometry," *Methods Enzymol.*, vol. 537, pp. 281–296, 2014.
- [138] J. Kühn *et al.*, "Label-Free Cytotoxicity Screening Assay by Digital Holographic Microscopy," *Assay Drug Dev. Technol.*, vol. 11, no. 2, pp. 101–107, 2013.
- [139] B. Rappaz *et al.*, "Comparative study of human erythrocytes by digital holographic microscopy, confocal microscopy, and impedance volume analyzer," *Cytom. Part A*, vol. 73, no. 10, pp. 895–903, 2008.
- [140] A. E. Carpenter *et al.*, "CellProfiler: image analysis software for identifying and quantifying cell phenotypes," *Genome Biol.*, vol. 7, no. 10, p. R100, 2006.
- [141] J. Gao *et al.*, "Characterization of OP9 as authentic mesenchymal stem cell line," *J. Genet. Genomics*, vol. 37, no. 7, pp. 475–482, Jul. 2010.
- [142] M. Kawai and C. J. Rosen, "PPAR γ : a circadian transcription factor in adipogenesis and osteogenesis," *Nat Rev Endocrinol*, vol. 6, no. 11, pp. 629–636, Nov. 2010.
- [143] R. Z. M. W. Z. Li, "Hematopoietic recovery following chemotherapy is improved by BADGE-induced inhibition of adipogenesis," *Int. J. Hematol.*, pp. 58–72, 2013.
- [144] K. Sato *et al.*, "PPAR γ antagonist attenuates mouse immune-mediated bone marrow failure by inhibition of T cell function," *Haematologica*, vol. 101, no. 1, pp. 57–67, Jan. 2016.
- [145] D. Alpern, V. Gardeux, J. Russeil, and B. Deplancke, "Time- and cost-efficient high-throughput transcriptomics enabled by Bulk RNA Barcoding and sequencing," *bioRxiv*, p. 256594, Jan. 2018.
- [146] M. I. Love, W. Huber, and S. Anders, "Moderated estimation of fold change and dispersion for RNA-seq data with DESeq2," *Genome Biol.*, vol. 15, no. 12, p. 550, Dec. 2014.
- [147] J. Isern *et al.*, "The neural crest is a source of mesenchymal stem cells with specialized hematopoietic stem cell niche function," *Elife*, vol. 3, Sep. 2014.
- [148] A. Lagergren *et al.*, "The *Cxcl12*, *Periostin*, and *Ccl9* Genes Are Direct Targets for Early B-cell Factor in OP-9 Stroma Cells," *J. Biol. Chem.*, vol. 282, no. 19, pp. 14454–14462, May 2007.
- [149] O. Naveiras, "Novel Determinants of the Hematopoietic Microenvironment in Development and Homeostasis," *Dr. Thesis, Harvard Univ.*, 2008.
- [150] C. A. Lipinski, F. Lombardo, B. W. Dominy, and P. J. Feeney, "Experimental and computational approaches to estimate solubility and permeability in drug discovery and development settings," *Adv. Drug Deliv. Rev.*, vol. 46, no. 1–3, pp. 3–26, Mar. 2001.
- [151] M. P. Lutolf, R. Doyonnas, K. Havenstrite, K. Koleckar, and H. M. Blau, "Perturbation of single hematopoietic stem cell fates in artificial niches," *Integr. Biol. (Camb.)*, vol. 1, no. 1, pp. 59–69, Jan. 2009.
- [152] L. Dezza *et al.*, "Effects of desferrioxamine on normal and leukemic human hematopoietic cell growth: in vitro and in vivo studies," *Leukemia*, vol. 3, no. 2, pp. 104–7, Feb. 1989.

- [153] L. S. Carnevali *et al.*, "Improved HSC reconstitution and protection from inflammatory stress and chemotherapy in mice lacking granzyme B.," *J. Exp. Med.*, vol. 211, no. 5, pp. 769–79, May 2014.
- [154] K. Ito *et al.*, "Self-renewal of a purified Tie2+ hematopoietic stem cell population relies on mitochondrial clearance," *Science (80-.)*, vol. 354, no. 6316, pp. 1156–1160, Dec. 2016.
- [155] "Information professionnelle du Compendium Suisse des Médicaments," <https://compendium.ch/mpro/mnr/1183/html/fr>, no. Last access: 06.01.19, 2019.
- [156] M. Li and S. Ikehara, "Bone-marrow-derived mesenchymal stem cells for organ repair.," *Stem Cells Int.*, vol. 2013, p. 132642, Mar. 2013.
- [157] E. K. Merritt *et al.*, "Repair of Traumatic Skeletal Muscle Injury with Bone-Marrow-Derived Mesenchymal Stem Cells Seeded on Extracellular Matrix."
- [158] P. Denning-Kendall, S. Singha, B. Bradley, J. Hows, and P. O', "Cobblestone Area-Forming Cells in Human Cord Blood Are Heterogeneous and Differ from Long-Term Culture-Initiating Cells," 2003.
- [159] J. Qiao *et al.*, "Macrophages ameliorate bone marrow inflammatory injury and promote hematopoiesis in mice following hematopoietic stem cell transplantation," *Exp. Ther. Med.*, vol. 16, no. 2, pp. 567–572, May 2018.
- [160] H. Hauner, "The mode of action of thiazolidinediones.," *Diabetes. Metab. Res. Rev.*, vol. 18 Suppl 2, pp. S10-5.
- [161] R. J. Sulston *et al.*, "Increased Circulating Adiponectin in Response to Thiazolidinediones: Investigating the Role of Bone Marrow Adipose Tissue," *Front. Endocrinol. (Lausanne)*, vol. 7, p. 128, Sep. 2016.
- [162] A. V Schwartz, "TZDs and Bone: A Review of the Recent Clinical Evidence.," *PPAR Res.*, vol. 2008, p. 297893, Sep. 2008.
- [163] W. Lu, W. Wang, S. Wang, Y. Feng, and K. Liu, "Rosiglitazone Promotes Bone Marrow Adipogenesis to Impair Myelopoiesis under Stress.," *PLoS One*, vol. 11, no. 2, p. e0149543, 2016.
- [164] F. Kahles, H. M. Findeisen, and D. Bruemmer, "Osteopontin: A novel regulator at the cross roads of inflammation, obesity and diabetes.," *Mol. Metab.*, vol. 3, no. 4, pp. 384–93, Jul. 2014.
- [165] M. Yamaguchi, C. A. Baile, S. Zhu, and M. Shoji, "Bioactive flavonoid p-hydroxycinnamic acid stimulates osteoblastogenesis and suppresses adipogenesis in bone marrow culture," *Cell Tissue Res.*, vol. 354, no. 3, pp. 743–750, Dec. 2013.
- [166] Y.-R. Lou, T. C. Toh, Y. H. Tee, and H. Yu, "25-Hydroxyvitamin D3 induces osteogenic differentiation of human mesenchymal stem cells," *Sci. Rep.*, vol. 7, no. 1, p. 42816, Dec. 2017.
- [167] J. van de Peppel and J. P. T. M. van Leeuwen, "Vitamin D and gene networks in human osteoblasts," *Front. Physiol.*, vol. 5, p. 137, Apr. 2014.
- [168] J. A. Sunyecz, "The use of calcium and vitamin D in the management of osteoporosis.," *Ther. Clin. Risk Manag.*, vol. 4, no. 4, pp. 827–36, Aug. 2008.
- [169] B. Lecka-Czernik, L. A. Stechschulte, P. J. Czernik, S. B. Sherman, S. Huang, and A. Krings, "Marrow Adipose Tissue: Skeletal Location, Sexual Dimorphism, and Response to Sex Steroid Deficiency.," *Front. Endocrinol. (Lausanne)*, vol. 8, p. 188, 2017.
- [170] P. V Dlodla *et al.*, "A dose-dependent effect of dimethyl sulfoxide on lipid content, cell viability and oxidative stress in 3T3-L1 adipocytes.," *Toxicol. reports*, vol. 5, pp. 1014–1020, 2018.
- [171] H. Wang and R. E. Scott, "Inhibition of distinct steps in the adipocyte differentiation pathway in 3T3 T mesenchymal stem cells by dimethyl sulphoxide (DMSO).," *Cell Prolif.*, vol. 26, no. 1, pp. 55–66, Jan. 1993.
- [172] R. A. van der Heijden *et al.*, "High-fat diet induced obesity primes inflammation in adipose tissue prior to liver in C57BL/6j mice," *Aging (Albany. NY)*, vol. 7, no. 4, pp. 256–268, Apr. 2015.
- [173] C. Ló Pez-Otín, L. Galluzzi, J. M. P. Freije, F. Madeo, and G. Kroemer, "Leading Edge Review Metabolic Control of Longevity," *Cell*, vol. 166, pp. 802–821, 2016.
- [174] N. T. Jeanson and D. T. Scadden, "Vitamin D receptor deletion leads to increased hematopoietic stem and progenitor cells residing in the spleen.," *Blood*, vol. 116, no. 20, pp. 4126–9, Nov. 2010.
- [175] W. Beamer, L. Donahue, C. Rosen, D. B. - Bone, and undefined 1996, "Genetic variability in adult bone density among inbred

strains of mice," *Elsevier*.

- [176] M. C. Horowitz *et al.*, "Bone marrow adipocytes," *Adipocyte*, vol. 6, no. 3, pp. 193–204, Jul. 2017.
- [177] S. J. Szilvassy, R. K. Humphries, P. M. Lansdorp, A. C. Eaves, and C. J. Eaves, "Quantitative assay for totipotent reconstituting hematopoietic stem cells by a competitive repopulation strategy," *Proc. Natl. Acad. Sci.*, vol. 87, no. 22, pp. 8736–8740, Nov. 1990.
- [178] C. Taswell, "Limiting dilution assays for the determination of immunocompetent cell frequencies. I. Data analysis," *J. Immunol.*, vol. 126, no. 4, pp. 1614–9, Apr. 1981.
- [179] S. N. Catlin, L. Busque, R. E. Gale, P. Guttorp, and J. L. Abkowitz, "The replication rate of human hematopoietic stem cells in vivo," *Blood*, vol. 117, no. 17, pp. 4460–4466, Apr. 2011.
- [180] K. Busch *et al.*, "Fundamental properties of unperturbed haematopoiesis from stem cells in vivo," *Nature*, vol. 518, no. 7540, pp. 542–546, Feb. 2015.
- [181] A. Wilson *et al.*, "Hematopoietic Stem Cells Reversibly Switch from Dormancy to Self-Renewal during Homeostasis and Repair," *Cell*, vol. 135, no. 6, pp. 1118–1129, Dec. 2008.
- [182] A. Gratwohl, H. Baldomero, and J. Passweg, "Hematopoietic stem cell transplantation activity in Europe," *Curr. Opin. Hematol.*, vol. 20, no. 6, pp. 485–493, Nov. 2013.
- [183] R. H. Houtkooper *et al.*, "Mitonuclear protein imbalance as a conserved longevity mechanism," *Nature*, vol. 497, no. 7450, pp. 451–457, May 2013.
- [184] L. Mouchiroud *et al.*, "The NAD⁺/Sirtuin Pathway Modulates Longevity through Activation of Mitochondrial UPR and FOXO Signaling," *Cell*, vol. 154, no. 2, pp. 430–441, Jul. 2013.
- [185] S. Imai, C. M. Armstrong, M. Kaerberlein, and L. Guarente, "Transcriptional silencing and longevity protein Sir2 is an NAD-dependent histone deacetylase," *Nature*, vol. 403, no. 6771, pp. 795–800, Feb. 2000.
- [186] P. Belenky, F. G. Racette, K. L. Bogan, J. M. McClure, J. S. Smith, and C. Brenner, "Nicotinamide Riboside Promotes Sir2 Silencing and Extends Lifespan via Nrk and Urh1/Pnp1/Meu1 Pathways to NAD⁺," *Cell*, vol. 129, no. 3, pp. 473–484, May 2007.
- [187] C. Cantó *et al.*, "The NAD⁺ Precursor Nicotinamide Riboside Enhances Oxidative Metabolism and Protects against High-Fat Diet-Induced Obesity," *Cell Metab.*, vol. 15, no. 6, pp. 838–847, Jun. 2012.
- [188] H. Zhang *et al.*, "NAD⁺ repletion improves mitochondrial and stem cell function and enhances life span in mice," *Science (80-.)*, vol. 352, no. 6292, pp. 1436–1443, Jun. 2016.
- [189] L. M. Giammona *et al.*, "Mechanistic studies on the effects of nicotinamide on megakaryocytic polyploidization and the roles of NAD⁺ levels and SIRT inhibition," *Exp. Hematol.*, vol. 37, no. 11, p. 1340–1352.e3, Nov. 2009.
- [190] T. Peled *et al.*, "Nicotinamide, a SIRT1 inhibitor, inhibits differentiation and facilitates expansion of hematopoietic progenitor cells with enhanced bone marrow homing and engraftment," *Exp. Hematol.*, vol. 40, no. 4, p. 342–355.e1, Apr. 2012.
- [191] M. E. Horwitz *et al.*, "Umbilical cord blood expansion with nicotinamide provides long-term multilineage engraftment," *J. Clin. Invest.*, vol. 124, no. 7, pp. 3121–3128, Jul. 2014.
- [192] I. M. Konieczna, S. Panuganti, T. A. DeLuca, E. T. Papoutsakis, E. A. Eklund, and W. M. Miller, "Administration of nicotinamide does not increase platelet levels in mice," *Blood Cells, Mol. Dis.*, vol. 50, no. 3, pp. 171–176, Mar. 2013.
- [193] K. L. Bogan and C. Brenner, "Nicotinic Acid, Nicotinamide, and Nicotinamide Riboside: A Molecular Evaluation of NAD⁺ Precursor Vitamins in Human Nutrition," *Annu. Rev. Nutr.*, vol. 28, no. 1, pp. 115–130, Aug. 2008.
- [194] V. Jovaisaite and J. Auwerx, "The mitochondrial unfolded protein response—synchronizing genomes," *Curr. Opin. Cell Biol.*, vol. 33, pp. 74–81, Apr. 2015.
- [195] S. Kobel, M. Limacher, S. Gobaa, T. Laroche, and M. P. Lutolf, "Micropatterning of Hydrogels by Soft Embossing[†]," *Langmuir*, vol. 25, no. 15, pp. 8774–8779, Aug. 2009.
- [196] S. A. J. Trammell *et al.*, "Nicotinamide riboside is uniquely and orally bioavailable in mice and humans," *Nat. Commun.*, vol. 7, no. 1, p. 12948, Dec. 2016.

- [197] C. Cantó, K. J. Menzies, and J. Auwerx, "NAD⁺ Metabolism and the Control of Energy Homeostasis: A Balancing Act between Mitochondria and the Nucleus," *Cell Metab.*, vol. 22, no. 1, pp. 31–53, Jul. 2015.
- [198] J. Seita *et al.*, "Gene Expression Commons: An Open Platform for Absolute Gene Expression Profiling," *PLoS One*, vol. 7, no. 7, p. e40321, Jul. 2012.
- [199] J. Ratajczak *et al.*, "NRK1 controls nicotinamide mononucleotide and nicotinamide riboside metabolism in mammalian cells," *Nat. Commun.*, vol. 7, no. 1, p. 13103, Dec. 2016.
- [200] M. A. Goodell, K. Brose, G. Paradis, A. S. Conner, and R. C. Mulligan, "Isolation and functional properties of murine hematopoietic stem cells that are replicating in vivo," *J. Exp. Med.*, vol. 183, no. 4, pp. 1797–806, Apr. 1996.
- [201] M. J. de Almeida, L. L. Luchsinger, D. J. Corrigan, L. J. Williams, and H.-W. Snoeck, "Dye-Independent Methods Reveal Elevated Mitochondrial Mass in Hematopoietic Stem Cells," *Cell Stem Cell*, vol. 21, no. 6, p. 725–729.e4, Dec. 2017.
- [202] G. Jin *et al.*, "Atad3a suppresses Pink1-dependent mitophagy to maintain homeostasis of hematopoietic progenitor cells," *Nat. Immunol.*, vol. 19, no. 1, pp. 29–40, Jan. 2018.
- [203] C. Mantel, S. Messina-Graham, and H. E. Broxmeyer, "Upregulation of nascent mitochondrial biogenesis in mouse hematopoietic stem cells parallels upregulation of CD34 and loss of pluripotency: A potential strategy for reducing oxidative risk in stem cells," *Cell Cycle*, vol. 9, no. 10, pp. 2008–2017, May 2010.
- [204] M. Lazarou *et al.*, "The ubiquitin kinase PINK1 recruits autophagy receptors to induce mitophagy," *Nature*, vol. 524, no. 7565, pp. 309–314, Aug. 2015.
- [205] N. Mizushima, T. Yoshimori, and B. Levine, "Methods in Mammalian Autophagy Research," *Cell*, vol. 140, no. 3, pp. 313–326, Feb. 2010.
- [206] S. Park *et al.*, "Pyruvate stimulates mitophagy via PINK1 stabilization," *Cell. Signal.*, vol. 27, no. 9, pp. 1824–30, Sep. 2015.
- [207] R. A. Harris, M. M. Bowker-Kinley, B. Huang, and P. Wu, "Regulation of the activity of the pyruvate dehydrogenase complex," *Adv. Enzyme Regul.*, vol. 42, pp. 249–59, 2002.
- [208] K. Palikaras, E. Lionaki, and N. Tavernarakis, "Coordination of mitophagy and mitochondrial biogenesis during ageing in *C. elegans*," *Nature*, vol. 521, no. 7553, pp. 525–528, May 2015.
- [209] D. Ryu *et al.*, "Urolithin A induces mitophagy and prolongs lifespan in *C. elegans* and increases muscle function in rodents," *Nat. Med.*, vol. 22, no. 8, pp. 879–888, Aug. 2016.
- [210] T. G. McWilliams and I. G. Ganley, "Life in lights: Tracking mitochondrial delivery to lysosomes in vivo," *Autophagy*, vol. 12, no. 12, pp. 2506–2507, Dec. 2016.
- [211] T. G. McWilliams *et al.*, "mito-QC illuminates mitophagy and mitochondrial architecture in vivo," *J. Cell Biol.*, vol. 214, no. 3, pp. 333–345, Aug. 2016.
- [212] R. Rizzuto, M. Brini, P. Pizzo, M. Murgia, and T. Pozzan, "Chimeric green fluorescent protein as a tool for visualizing subcellular organelles in living cells," *Curr. Biol.*, vol. 5, no. 6, pp. 635–42, Jun. 1995.
- [213] R. Rizzuto *et al.*, "Double labelling of subcellular structures with organelle-targeted GFP mutants in vivo," *Curr. Biol.*, vol. 6, no. 2, pp. 183–8, Feb. 1996.
- [214] C. Yang and T. Suda, "Hyperactivated mitophagy in hematopoietic stem cells," *Nat. Immunol.*, vol. 19, no. 1, pp. 2–3, Jan. 2018.
- [215] V. Sorrentino *et al.*, "Enhancing mitochondrial proteostasis reduces amyloid- β proteotoxicity," *Nature*, vol. 552, no. 7684, pp. 187–193, Dec. 2017.
- [216] L. Leveque-El Moutte *et al.*, "Autophagy is required for stem cell mobilization by G-CSF," *Blood*, vol. 125, no. 19, pp. 2933–2936, May 2015.
- [217] N. A. Khan *et al.*, "Effective treatment of mitochondrial myopathy by nicotinamide riboside, a vitamin B3," *EMBO Mol. Med.*, vol. 6, no. 6, p. n/a-n/a, Apr. 2014.
- [218] S. J. Morrison and J. Kimble, "Asymmetric and symmetric stem-cell divisions in development and cancer," *Nature*, vol. 441, no. 7097, pp. 1068–1074, Jun. 2006.

- [219] S. B. Ting *et al.*, "Asymmetric segregation and self-renewal of hematopoietic stem and progenitor cells with endocytic Ap2a2," *Blood*, vol. 119, no. 11, pp. 2510–2522, Mar. 2012.
- [220] K. Ito *et al.*, "A PML–PPAR- δ pathway for fatty acid oxidation regulates hematopoietic stem cell maintenance," *Nat. Med.*, vol. 18, no. 9, pp. 1350–1358, Sep. 2012.
- [221] N. Vannini, A. Roch, O. Naveiras, A. Griffa, S. Kobel, and M. P. Lutolf, "Identification of in vitro HSC fate regulators by differential lipid raft clustering," *Cell Cycle*, vol. 11, no. 8, pp. 1535–1543, Apr. 2012.
- [222] H. Shitara *et al.*, "Non-invasive visualization of sperm mitochondria behavior in transgenic mice with introduced green fluorescent protein (GFP)," *FEBS Lett.*, vol. 500, no. 1–2, pp. 7–11, Jun. 2001.
- [223] H.-W. Snoeck, "Mitochondrial regulation of hematopoietic stem cells," *Curr. Opin. Cell Biol.*, vol. 49, pp. 91–98, Dec. 2017.
- [224] L. Yang *et al.*, "Identification of Lin-Sca1+kit+CD34+Flt3- short-term hematopoietic stem cells capable of rapidly reconstituting and rescuing myeloablated transplant recipients," *Blood*, vol. 105, no. 7, pp. 2717–2723, Apr. 2005.
- [225] M. Morowski, T. Vogtle, P. Kraft, C. Kleinschnitz, G. Stoll, and B. Nieswandt, "Only severe thrombocytopenia results in bleeding and defective thrombus formation in mice," *Blood*, vol. 121, no. 24, pp. 4938–4947, Jun. 2013.
- [226] A. Rongvaux *et al.*, "Development and function of human innate immune cells in a humanized mouse model," *Nat. Biotechnol.*, vol. 32, no. 4, pp. 364–372, Apr. 2014.
- [227] A. Pellagatti *et al.*, "Impact of spliceosome mutations on RNA splicing in myelodysplasia: dysregulated genes/pathways and clinical associations," *Blood*, vol. 132, no. 12, pp. 1225–1240, Sep. 2018.
- [228] N. Pineault and A. Abu-Khader, "Advances in umbilical cord blood stem cell expansion and clinical translation," *Exp. Hematol.*, vol. 43, no. 7, pp. 498–513, Jul. 2015.
- [229] C. C. Zhang and H. F. Lodish, "Murine hematopoietic stem cells change their surface phenotype during ex vivo expansion," *Blood*, vol. 105, no. 11, pp. 4314–20, Jun. 2005.
- [230] J. Han *et al.*, "Adipose tissue is an extramedullary reservoir for functional hematopoietic stem and progenitor cells," *Blood*, vol. 115, no. 5, pp. 957–964, Feb. 2010.
- [231] M. Driel van, H. Pols, and J. P. van Leeuwen, "Osteoblast Differentiation and Control by Vitamin D and Vitamin D Metabolites," *Curr. Pharm. Des.*, vol. 10, no. 21, pp. 2535–2555, Aug. 2004.
- [232] M. Cortes *et al.*, "Developmental Vitamin D Availability Impacts Hematopoietic Stem Cell Production," *Cell Rep.*, vol. 17, no. 2, pp. 458–468, 2016.
- [233] M. F. Holick, "Vitamin D Deficiency," *N. Engl. J. Med.*, vol. 357, no. 3, pp. 266–281, Jul. 2007.
- [234] K. Pathak, M. J. Soares, E. K. Calton, Y. Zhao, and J. Hallett, "Vitamin D supplementation and body weight status: a systematic review and meta-analysis of randomized controlled trials," *Obes. Rev.*, vol. 15, no. 6, pp. 528–537, Jun. 2014.
- [235] S. R. Mallard, A. S. Howe, and L. A. Houghton, "Vitamin D status and weight loss: a systematic review and meta-analysis of randomized and nonrandomized controlled weight-loss trials," *Am. J. Clin. Nutr.*, vol. 104, no. 4, pp. 1151–1159, Oct. 2016.
- [236] J. Ros-Soto, C. Anthias, A. Madrigal, and J. A. Snowden, "Vitamin D: is it important in haematopoietic stem cell transplantation? A review," *Bone Marrow Transplant.*, p. 1, Nov. 2018.
- [237] A. C. Hall and M. B. Juckett, "The role of vitamin D in hematologic disease and stem cell transplantation," *Nutrients*, vol. 5, no. 6, pp. 2206–21, Jun. 2013.
- [238] H. Yagi *et al.*, "Mesenchymal stem cells: Mechanisms of immunomodulation and homing," *Cell Transplant.*, vol. 19, no. 6, pp. 667–79, 2010.
- [239] F. Gao *et al.*, "Mesenchymal stem cells and immunomodulation: current status and future prospects," *Cell Death Dis.*, vol. 7, no. 1, p. e2062, Jan. 2016.
- [240] A. Birbrair and P. S. Frenette, "Niche heterogeneity in the bone marrow," *Ann. N. Y. Acad. Sci.*, vol. 1370, no. 1, pp. 82–96, 2016.
- [241] A. Y. Lai and M. Kondo, "T and B lymphocyte differentiation from hematopoietic stem cell," *Semin. Immunol.*, vol. 20, no. 4,

pp. 207–212, 2008.

- [242] A. Görgens *et al.*, “Revision of the Human Hematopoietic Tree: Granulocyte Subtypes Derive from Distinct Hematopoietic Lineages,” *Cell Rep.*, vol. 3, no. 5, pp. 1539–1552, 2013.
- [243] G. Doria *et al.*, “Hematopoietic reconstitution after lethal irradiation and bone marrow transplantation: effects of different hematopoietic cytokines on the recovery of thymus, spleen and blood cells,” *Bone Marrow Transplant.*, vol. 25, no. 4, pp. 427–433, 2000.
- [244] I. Rich, “The effect of 5-fluorouracil on erythropoiesis,” *Blood*, vol. 77, no. 6, pp. 1164–1170, 1991.
- [245] D. E. Harrison and C. P. Lerner, “Most primitive hematopoietic stem cells are stimulated to cycle rapidly after treatment with 5-fluorouracil,” *Blood*, vol. 78, no. 5, pp. 1237–40, 1991.
- [246] G. Poncin *et al.*, “Characterization of spontaneous bone marrow recovery after sublethal total body irradiation: Importance of the osteoblastic/adipocytic balance,” *PLoS One*, vol. 7, no. 2, 2012.
- [247] T. D. Randall and I. L. Weissman, “Hematopoietic Stem Cells After 5-Fluorouracil Treatment Phenotypic and Functional Changes Induced at the Clonal Level in,” 2007.
- [248] K. M. Prise, G. Schettino, M. Folkard, and K. D. Held, “New insights on cell death from radiation exposure,” *Lancet Oncol.*, vol. 6, no. 7, pp. 520–528, 2005.
- [249] E. K. Schulak JA, “Principles of bone marrow transplantation (BMT): providing optimal veterinary and husbandry care to irradiated mice in BMT studies,” *J Surg Res*, vol. 47, no. 1, pp. 52–58, 1989.
- [250] G. Pinedo, HM; Peters, “Fluorouracil: Biochemistry and Pharmacology,” *J. Clin. Oncol.*, vol. 6, pp. 1653–1664, 1988.
- [251] S. Bekkering, “Another look at the life of a neutrophil,” *World J. Hematol.*, vol. 2, no. 2, p. 44, 2013.
- [252] U. Dholakia, S. Bandyopadhyay, E. A. Hod, and K. A. Prestia, “Determination of RBC survival in C57BL/6 and C57BL/6-Tg(UBC-GFP) mice,” *Comp. Med.*, vol. 65, no. 3, pp. 196–201, 2015.
- [253] A. P. Bolliger and N. Everds, “Chapter 2.9 - Haematology of the Mouse A2 - Hedrich, Hans J,” *Lab. Mouse (Second Ed.)*, pp. 331–347, 2012.
- [254] M. O. Muench and M. A. S. Moore, “Accelerated Recovery of Peripheral Blood Cell Counts in Mice Transplanted with in vitro Cytokine-expanded Hematopoietic Progenitors,” *Exp. Hematol.*, 1992.
- [255] “C57BL6 Mouse Model Information Sheet,” <https://www.criver.com/sites/default/files/resources/C57BL6MouseModelInformationSheet.pdf>, no. Last access: 06.01.19, 2019.
- [256] B. P. J. Chenaille, S. A. Steward, R. A. Ashmun, and C. W. Jackson, “Prolonged Thrombocytosis in Mice After 5-Fluorouracil Results From Failure to Down-Regulate Megakaryocyte Concentration. An Experimental Model That Dissociates Regulation of Megakaryocyte Size and DNA Content From Megakaryocyte Concentration,” vol. 76, no. 3, pp. 508–515, 1990.

Curriculum Vitae

Vasco Ledebur de Antas de Campos

Institute of Bioengineering, École polytechnique fédérale de Lausanne (EPFL)

CH-1015 Lausanne

Phone: +41 21 693 72 17 | +41 76 455 18 10 (m)

Email: vasco.campos@epfl.ch

Date of Birth: 18.10.1988

Nationality: Portugal / Liechtenstein

WORK EXPERIENCE

2016-present	Research Collaboration with Endogena therapeutics, Lausanne
2011-2013	Lab Technician at the Laboratory of Stem Cell Bioengineering of Prof. Matthias Lutolf, École polytechnique fédérale de Lausanne (EPFL)
2004	Internship at r-Biopharm, Darmstadt

EDUCATION

2014-2019	PhD in Bioengineering at the Laboratory of Regenerative Hematopoiesis, École polytechnique fédérale de Lausanne (EPFL) Working title: 'Accelerating the yellow-to-red bone marrow transition'
2009-2011	MSc in Biology at the Zoological Institute, University of Basel
2006-2009	BSc in Biology , Major in Integrative Biology, University of Basel
2003-2006	Abitur at Deutsche Schule Lissabon, Portugal

SKILLS

<i>In vivo</i>	Animal handling, Bone marrow transplantation incl. single cell
<i>In vitro</i>	Mammalian cell culture, Primary stem cell culture, 3D cell culture, Flow Cytometry, Micromanipulation
Drug discovery	Small molecule screening: novel inhibitors of adipocytic differentiation
Microscopy	Confocal, Holographic, Histology, Image Analysis
Molecular Biology	Standard methods, Western Blot, qPCR, Sequencing
Data Analysis	GraphPad Prism, ImageJ, Cell Profiler, FlowJo, Metamorph, BLAST, CodonCode Aligner, MS Office, Adobe Illustrator/Photoshop
Teaching	Assistant in Cell and Molecular Biology, and Bioengineering Master courses

ORAL PRESENTATIONS

4th Swiss Image-Based Screening Conference, Zurich 2017

POSTER PRESENTATIONS

International Society for Experimental Hematology (ISEH), Los Angeles 2018
4th Bone Marrow Adiposity (BMA) Meeting, Lausanne 2017
Swiss Society of Hematology (SSGIM-SSH), Lausanne 2017
3rd Bone Marrow Adiposity (BMA) Meeting, Rotterdam 2016
International Society of Stem Cell Research (ISSCR), Stockholm 2015
Swiss Society of Hematology (SSGIM-SSH), Basel 2015
Institute of Bioengineering (IBI) Day, Lausanne 2014

PUBLICATIONS

Campos V, Rappaz B, Kuttler F, Turcatti G, Naveiras O. High-throughput, non-perturbing quantification of lipid droplets with Digital Holographic Microscopy. *J Lipid Res.* 2018 Apr 5. pii: jlr.D085217. doi: 10.1194/jlr.D085217.

Roch A, Giger S, Girotra M, **Campos V**, Vannini N, Naveiras O, Gobaa S, Lutolf MP. Single-cell analyses identify bioengineered niches for enhanced maintenance of hematopoietic stem cells. *Nature Communications.* 2017 Aug 9;8(1):221. doi: 10.1038/s41467-017-00291-3.

Tauzin L, **Campos V**, Tichet M. Cellular endogenous NAD(P)H fluorescence as a label-free method for the identification of erythrocytes and reticulocytes. *Cytometry A*. 2018 Apr;93(4):472-479. doi: 10.1002/cyto.a.23351. Epub 2018 Feb 26.

Vannini N, Girotra M, Naveiras O, Nikitin G, **Campos V**, Giger S, Roch A, Auwerx J, Lutolf MP. Specification of haematopoietic stem cell fate via modulation of mitochondrial activity. *Nature Communications*. 2016 Oct 12;7:13125. doi: 10.1038/ncomms13125.

Vannini N*, **Campos V***, Ragusa S, Stefanidis E, Ryu D, Girotra M, Semilietof A, Yersin Y, Panopoulos E, Tauzin L, Pirinen E, , Petrova PV, Vanhecke D, Coukos G, Auwerx J, Lutolf MP, Naveiras O. The NAD-booster nicotinamide riboside potently stimulates hematopoiesis through increased mitochondrial clearance. *Cell Stem Cell*. 2019 Mar 7;24(3):405-418.e7. doi: 10.1016/j.stem.2019.02.012.

* These authors contributed equally to this work

